# Naval Surface Warfare Center
**Carderock Division**
West Bethesda, MD 20817-5700

**NSWCCD-65-TR–1999/15** September 1999

Survivability, Structures, and Materials Directorate
Technical Report

# Micromechanics Based Failure Analysis of Composite Structural Laminates

by

J. Steven Mayes

20000303 043

DTIC QUALITY INSPECTED 3

# DEPARTMENT OF THE NAVY

NAVAL SURFACE WARFARE CENTER, CARDEROCK DIVISION
9500 MACARTHUR BOULEVARD
WEST BETHESDA MD 20817-5700

9078
Ser 65-106
1 Sep 99

From: Commander, Naval Surface Warfare Center, Carderock Division
To: Distribution

Subj: PROGRESSIVE FAILURE OF COMPOSITE STRUCTURAL LAMINATES

Ref: (a) NSWCCD, In-house Laboratory Independent Research Program

Encl: (1) NSWCCD-65-TR–1999/15, *Micromechanics Based Failure Analysis of Composite Structural Laminates*

1. Under reference (a), the Naval Surface Warfare Center, Carderock Division (NSWCCD) developed a constituent stress-based failure criterion and a progressive failure algorithm for investigating the material failure strengths of composite structural laminates. Enclosure (1) describes a finite element based analysis tool developed and used to predict failure of a variety of laminates under uniaxial and biaxial loads. These analytical predictions were shown to compare favorably against experimentally determined laminate failure data.

2. Comments or questions may be referred to Dr. Steven Mayes, Code 6551; telephone (301) 227-4176; e-mail, mayesjs@nswccd.navy.mil.

J. E. BEACH
By direction

1

Distribution:

COMNAVSEASYSCOM WASHINGTON DC
[SEA03P (Will), SEA03P1 (Kadala)]

CNR ARLINGTON VA [ONR 332 (Kelly), ONR 334
(Barsoum, Gagorik, Rajapakse)]

DTIC FORT BELVOIR VA

NRL [Code 6383 (Badaliance, Gause)]

Newport News Shipbuilding & Dry dock Company
Department 44
Attn: Dr. Tom Juska
4104 Washington Avenue
Newport News, VA 23607

The Boeing Company
Military Aircraft and Missile Systems Group
Attn: Ray Bohlmann
P.O. Box 516
Saint Louis, MO 63166

Structural Composites, Inc.
Attn: Dr. Ronnal Reichard
7705 Technology Drive
Melbourne, FL 32904

Virginia Polytechnical Institue & State University
Department of Engineering Science and Mechanics
Attn: Dr. Mike Hyer
Blacksburg, VA 24061

South Dakota State University
Department of Mechanical Engineering
Attn: Dr. Jeffry Welsh
Brookings, SD 57007

Pacific Northwest National Laboratory
Attn: Dr. Mark Garnich
P.O. Box 999 999 / MS K5-26
902 Battelle Boulevard
Richland, WA 99352

ANSYS, Inc.
Attn: Ray Browell
Southpointe
275 Technology Drive
Canonsburg, PA 15317

Reentry Systems Office
Naval Surface Warfare Center
Dalhgren Division Detachment, Washington D.C.
Attn: Karin Gipple
3801 Nebraska Ave.
Washington, D.C. 20393-5443

NAVSURFWARCEN CARDEROCKDIV BETHESDA
MD [Codes 011,0112 (Barkyoumb), 0115
(Messick), 3442 (TIC), 60, 64, 65, 65R
(Camponeshi, Brown), 655, 6551 (Bartlett, Garala,
Kiviat, Kuo, Macander, Mayes (3), Paraska, Potter,
Wells), 6552 (Bonanni, Charette, Cowan, Hoynes,
Loup, Miller, Palmer, Rasmussen, Telegadas), 6553
(Crane, Coffin, Williams), 654 (Conley, Hess,
Marr), 66, 67, 673, 68]

NAVSURFWARCEN DAHLGRENDIV COASTAL
SYSTEMS STATION [(Wyman)]

CONSUBLANT SHIPYARD REP, ELECTRIC BOAT
CORP., GROTON CT 06340-3000 [Dept. 46 (G.
Leon)]

Seemann Composites, Inc.
Attn: Bill Seemann
P.O. Box 3449
Gulfport, MS 39505

Mechanical Engineering Department
University of Wyoming
Laramie, WY 82071-3434
[Dr. Andy Hansen, Ms. Ronda Coguill]

John Hopkins University
Applied Physics Laboratory
Attn: Dr. Jack Roberts
Johns Hopkins Road
Laurel, MD 20707

Gibbs and Cox, Inc.
Attn: Bob Scott
1235 Jefferson Davis Hwy.
Suite 700
Arlington, VA 22202

Materials Sciences Corporation
Attn: Tom Cassin
Suite 250
500 Office Center Dr.
Fort Washington, PA 19034

NASA Langley Research Center
Hampton, VA 23681-2199
[MS188E (Dr. Damodar Ambur), MS190 (Dr. James
Starnes)]

Analyis and Technology
Attn: Bill Gregory
2341 Jefferson Davis Hwy.
Arlington, VA 22202

Northern Arizonia University
Department of Mechanical Engineering
Attn: Dr. F. E. Penado
PO Box 15600
Flagstaff, AZ 86001

Bath Iron Works
Attn: Bruce Jackson
700 Washington Street
Bath, ME 04530

Ingalls Shipbuilding
Attn: Walt Whitehead
P.O. Box 149, Mail Station 1090-11
Pascagoula, MS 39568-0149

University of Delaware
Composites Manufacturing Science Laboratory
Attn: Dr. John W. Gillespie
Newark, DE 19716

Alfred University
Mechanical Engineering Division
Attn: Dr. John Williams
One Saxon Drive
Alfred, NY 14802

# Naval Surface Warfare Center
## Carderock Division
West Bethesda, MD 20817-5700

# Micromechanics Based Failure Analysis of Composite Structural Laminates

by

J. Steven Mayes

| REPORT DOCUMENTATION PAGE | | |
|---|---|---|

Public reporting burden for this collection of information is estimated to average 1 hour per response, including the time for reviewing instructions, searching existing data sources, gathering and maintaining the data needed, and completing and reviewing the collection of information. Send comments regarding this burden estimate or any other aspect of this collection of information, including suggestions for reducing this burden, to Washington Headquarters services, Directorate for Information Operations and Reports, 1215 Jefferson Davis Highway, Suite 1204, Arlington, VA 22202-4302, and to the Office of Management and Budget, Paperwork Reduction Project (0704-0188), Washington, DC 20503.

| 1. AGENCY USE ONLY *(Leave blank)* | 2. REPORT DATE<br>September 1999 | 3. REPORT TYPE AND DATES COVERED<br>Final |
|---|---|---|

| 4. TITLE AND SUBTITLE<br>Micromechanics Based Failure Analysis of Composite Structural Laminates | 5. FUNDING NUMBERS<br>NA |
|---|---|
| **6. AUTHOR(S)**<br>J. Steven Mayes | |

| 7. PERFORMING ORGANIZATION NAME(S) AND ADDRESS(ES)<br>Naval Surface Warfare Center<br>Carderock Division<br>9500 MacArthur Boulevard<br>West Bethesda, MD 20817-5700 | 8. PERFORMING ORGANIZATION REPORT NUMBER<br>NSWCCD-65-TR–1999/15 |
|---|---|

| 9. SPONSORING/MONITORING AGENCY NAME(S) AND ADDRESS(ES)<br>Naval Surface Warfare Center<br>Carderock Division<br>9500 MacArthur Boulevard<br>West Bethesda, MD 20817-5700 | 10. SPONSORING/MONITORING AGENCY REPORT NUMBER |
|---|---|

**11. SUPPLEMENTARY NOTES**

| 12a. DISTRIBUTION/AVAILABILITY STATEMENT<br>Approved for public release; distribution is unlimited. | 12b. DISTRIBUTION CODE |
|---|---|

**13. ABSTRACT** *(Maximum 200 words)*

A micromechanics based multicontinuum theory and associated numerical algorithm was used to extract, virtually without a time penalty, the stress and strain fields for a composites' constituents during routine structural finite element analysis. Using this constituent information, a stress-based failure criterion was developed and used to construct a progressive failure algorithm for investigating the material failure strengths of composite structural laminates. The criterion is fully three-dimensional and requires a minimum number of experimentally derived constants. The failure prediction methodology attempts to maintain high computational efficiency, ease of input, and numerical accuracy. A finite element based analysis tool was developed and used to predict failure of a variety of laminates under uniaxial and biaxial loads. Two-dimensional failure surfaces for laminates under biaxial loads are generated and compared against those developed from using the Tsai-Wu failure criterion and from experimental data. The proposed failure criterion was shown to be superior to Tsai-Wu and in good agreement with experimentally determined failure loads.

| 14. SUBJECT TERMS<br>composites    micromechanics    multicontinuum<br>failure    constituent | | | 15. NUMBER OF PAGES<br>208 |
|---|---|---|---|
| | | | 16. PRICE CODE |

| 17. SECURITY CLASSIFICATION OF REPORT<br>UNCLASSIFIED | 18. SECURITY CLASSIFICATION OF THIS PAGE<br>UNCLASSIFIED | 19. SECURITY CLASSIFICATION OF ABSTRACT<br>UNCLASSIFIED | 20. LIMITATION OF ABSTRACT<br>SAR |
|---|---|---|---|

NSN 7540-01-280-5500

# TABLE OF CONTENTS

# LIST OF FIGURES

# LIST OF TABLES

# ADMINISTRATIVE INFORMATION

# ACKNOWLEDGEMENTS

# SECTION 1.

# INTRODUCTION

## *1.1. Background*

The design, analysis, and fabrication of metal naval structures has matured to the point

that fairly explicit design rules, factors of safety, and failure prediction methodology exist

in the form of handbooks and design data sheets. Application of fiber reinforced

composite materials to naval structures is considered a "new" technology, although the

aircraft and pleasure (small) boat industry have used composite structural components for

more than thirty years. Composite technologies from these industries have been slow to

transition to naval applications. Composite small boat structures are typically loaded

differently and far less severely than naval warships. Aircraft applications typically use

composite laminates much thinner than those required by naval vessels. Furthermore,

aircraft fabrication techniques for composites are economically unfeasible for large naval

components such as hulls. Decision-makers within the Navy are uncomfortable with a

general lack of and inconsistency in data associated with the design, analysis, and

fabrication of marine composite structures.

The Navy has attempted to resolve technical uncertainties considered unique to marine

applications of composites. New and much improved fabrication methods have become

available [1] reducing the variability of mechanical properties in marine composites.

Commercial finite element programs have introduced new elements and analysis

techniques aimed specifically at composite structures, facilitating more detailed and accurate structural response predictions. As these technologies advanced, naval composite structural designs moved from concept to prototype stages. Once these composite applications began to appear on naval vessels, the capability to analytically predict composite structural failure became a major issue.

The ever-growing size of many Navy composite projects such as masts, deckhouses, hangers and stacks, dictates that associated components become relatively thick. Use of fiber-reinforced plastic lamina as a basic structural material results in creation of laminates having ten or more lamina. To make matters more complex, each lamina may have a different orientation to tailor a laminate's strength, stiffness and functionality to load and service requirements. To analyze new designs, engineers compensate for this increased complexity by smearing (combining) the constituents' (fiber and matrix) mechanical properties into an assumed homogeneous lamina. They then smear the lamina's mechanical properties into an assumed homogeneous laminate to attain idealized uniform strength and stiffness throughout the structure. While this approach is fairly successful in developing global stiffness properties, it masks large internal stresses associated with fiber and matrix interactions. Thus the designer cannot accurately predict pre-, ongoing, and post-damage conditions of the laminate at the constituent level where damage occurs. At the other extreme, researchers have attempted to integrate complex micromechanics models into structural analysis. The iterative nature of this solution process results in excessive computational time and data.

Predicting failure of structural composites has been a topic of research since the mid-1960's. A review of some of that research pertinent to this dissertation is presented later. My experience has been that very few failure prediction methodologies developed in academia have been used in Navy projects developed by government and private industry. There are many possible explanations why the methods failed to make the transition: they were perceived as too complicated in view of the amount of time and funding allocated to the problem; they were formulated around plane stress assumptions and could not be applied to general three dimensional stress states; or thick laminates (typical in navy structures) simply presented too big a numerical problem.

Typically, failure analyses assume a homogeneous laminate and use the maximum attainable stress or strain values of the laminate as determined from uniaxial laboratory tests as critical failure parameters. Among the shortcomings of this method are that mitigating or exacerbating effects of interactions among the six stress components are ignored, all possible uniaxial stress states are not usually tested (typically through thickness strengths), and strength values are unique to the architecture of a particular laminate. If any of the lamina orientations, groupings, or thicknesses are changed, maximum laminate stress and strain values change also and new tests must be conducted.

When compared to the analysis of metallic structures, lack of a general failure prediction methodology for composites leads to mixed analytical results and low confidence failure predictions. Structural designers and program managers use large factors-of-safety to offset a lack of prediction accuracy. A result of this strategy is that composite structures

are heavier and cost more than necessary. In an environment in which composite structures are viewed as alternates or competitors to metal structures, over-design causes them to compare less favorably and hinders their introduction into everyday use.

### 1.2. Research Objective

The intent of this research effort is to develop a design tool for failure analysis of composite structural laminates that:

a) Conforms to analysis methods already in use,
b) Is computationally fast,
c) Produces accurate results, and
d) Requires a minimum of additional work, on the part of the user, to prepare analysis inputs.

These requirements tend to be contradictory. Computational speed is often accomplished by simplifying assumptions that reduce accuracy. Restricting analysis methods to current practice and minimizing data input also tend to oppose a goal of high accuracy. Hence, creating a design tool that balances these requirements constantly requires compromising one or the other in an attempt to arrive at some optimum solution. Such an approach will always be open to questions about the legitimacy of the methodology.

Recent introduction of Multicontinuum Theory (MCT), developed at the University of Wyoming, offers an approach to potentially meet these requirements. MCT is a theory and associated numerical algorithm for extracting, virtually without a time penalty, the stress and strain fields for a composite's constituents during a routine structural finite element analysis (FEA). Fully implemented in a FEA program, MCT provides the designer with additional insight into a composite structure's response to its load.

Ϲ

Constituent information is valuable to analysts interested in predicting composites' failure. For instance, advanced failure theories for composites may be implemented in a more straightforward and general manner at a constituent level. Damage in a composite typically begins at the constituent level and may in fact be limited to only one constituent in some situations. An accurate prediction of constituent damage at a point in a laminate provides a genesis for progressively analyzing failure of composite structure from start to finish.

## 1.3. Research Overview

The research contained herein concerns the development of a constituent-based failure criterion and its incorporation into a nonlinear finite element code to produce a design tool with progressive failure prediction capability. Progressive failure analysis in an MCT-based finite element code has opened the possibility of accurate analysis of composite structures in pre-, ongoing and post- damage conditions. Because information is developed on a level at which failure initiates, load redistribution to other parts of the structure as well as the remaining constituents can be efficiently included. This allows a designer to track failure as it occurs, region by region, and reduce the stiffness and strength of damaged areas without necessarily declaring total structural failure. Changes in the structure, to remedy weaknesses, can be concentrated to specific areas leading to a more optimized design.

Section 2 is a modest review of the published literature concerned with micromechanics-based structural failure analysis. Section 3 develops the equations of Multicontinuum Theory. Section 4 develops the constituent-based failure criteria used within this research. Section 5 discusses the importance in developing tightly bound constituent and composite properties and the often neglected influence of nonlinear shear response. Section 6 describes the MCT_77 finite element code and implementation of the mechanics issues discussed in Sections three through five. In Section 7, comparisons of analytical results against experimental data are provided to assess the validity of the methodology, which is summarized in Section 8 discussions. Stress-strain graphs and tables of important parameters for the materials used in this research are found in the Appendices.

# SECTION 2.

# LITERATURE REVIEW

Most failure criteria developed for composite structural laminates to date can be classified as macromechanical because the criteria attempt to predict failure using composite stress-strain data. A key element of macromechanics is the combining of the constituent's properties into a homogeneous set of composite lamina properties and possibly combining lamina properties in homogeneous laminate properties. Reviews of macromechanical failure criteria can be found in Tsai [2], Rowlands [3], and Nahas [4].

In contrast, micromechanical approaches retain the individual identities of each lamina and its constituents. This allows interaction among them. Composite properties are used in micromechanics analyses but failure of each constituent and its contribution to lamina and laminate failure is emphasized. All micromechanical models are predicated on a complete set of material constants for each constituent. Composite properties for a unidirectional lamina are typically synthesized from constituent properties via a finite element or closed form analytical model.

MCT is micromechanics based and routinely generates constituent level stress and strain fields during an analysis. Hence, macromechanical based failure criteria and analyses are not of primary interest in the present research. Instead, the focus is on constituent based failure approaches. Such approaches may provide higher resolution in predicting

composite material failures since failure often begins in one constituent (e.g. matrix cracking) while the other constituent remains intact.

Analysis of structural laminate failure based on micromechanics has been largely ignored in the past because constituent information was generally unavailable in standard finite element structural analysis. There were, however, notable exceptions. Aboudi [5] extended a simplified micromechanical model he developed earlier to predict failure surfaces for unidirectional fibrous composites. The micromechanics model, known as the "Method of Cells", was based on a representative unit "cell" of a composite assumed to be composed of a periodic array of square fibers embedded in a matrix (Fig. 2.1 and Fig. 2.2). The model allowed for linear variation of displacements within each of four subcells making up a representative unit cell. Continuity of average displacements and tractions was enforced between subcells. Relationships between composite stresses and those of the constituent subcells were obtained in closed-form. This closed-form relationship allowed for efficient constituent stress calculations from structural level results, thus facilitating implementation of micromechanics-based failure criteria.
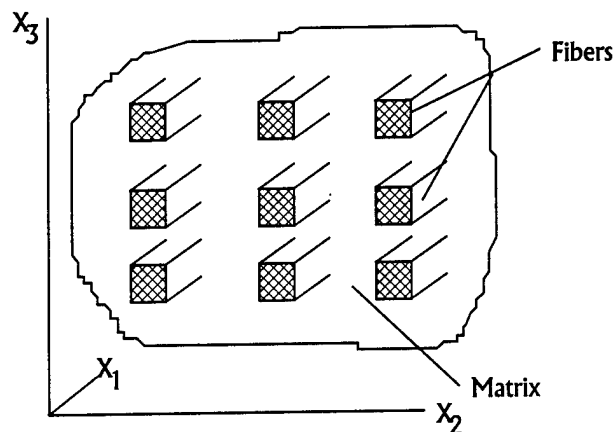


**Fig. 2.1** *Aboudi's idealized unidirectional fiber composite.*
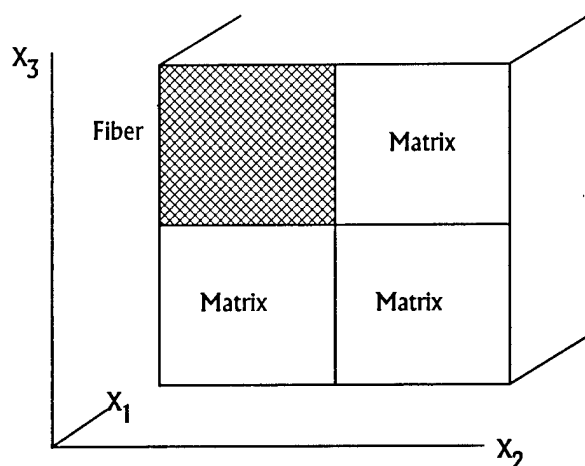
**Fig. 2.2** *Aboudi's representative unit cell.*

Three types of failures were assumed: fiber, matrix, and fiber/matrix interface. It was noted that constituent *in situ* ultimate strengths were generally different from bulk measured values and that values for constituent strengths are different in compression versus tension. Aboudi theorized that if ultimate strengths of a unidirectional composite in principal material directions could be determined, ultimate *in situ* constituent strengths could be determined by backing them out via the micromechanical model. Failure envelopes could then be generated for a composite under any complex stress state. Aboudi used this approach to implement an uncoupled (fiber from matrix) maximum stress criterion as follows. Retaining a plane stress assumption used at the lamina level, composite failure occurred when one of the following conditions was satisfied:

$$\left|\sigma_{11}^{f}\right| \geq {}^{+}S_{11}^{f} \; ; \qquad \left|\sigma_{22}^{m}\right| \geq {}^{+}S^{m} \; ; \qquad \left|\sigma_{12}^{m}\right| \geq S_{S}^{m}$$

where:

${}^{+}S_{11}^{f}$ = Fiber tensile strength,   ${}^{+}S^{m}$ = Matrix tensile strength,
$S_{S}^{m}$ = Matrix shear strength,   $\sigma_{11}^{f}$ = Axial fiber stress,
$\sigma_{22}^{m}$ = Transverse matrix stress,   $\sigma_{12}^{m}$ = Matrix in-plane shear stress.

The damage algorithm implied by the above criterion is one of catastrophic failure in both the constituent and composite when either of the constituents is damaged. This type of damage algorithm is perhaps overly simplistic in light of experimental evidence showing that matrix cracking is not necessarily catastrophic for the composite.

To verify the micromechanics model failure prediction capabilities, Aboudi made extensive comparisons of predicted off-axis tensile strengths of various unidirectional lamina with experimental data from six composites: boron/epoxy, graphite/polyimide, AS4/3501 graphite/epoxy, aramid/epoxy, glass/epoxy, and boron/aluminum. There was good agreement between predicted and measured strengths. Fig. 2.3 shows a typical result. Failures in these composites were catastrophic when either constituent was damaged so Aboudi's failure criterion worked well in these cases.

Pecknold [6] and Rahman [7] extended a micromechanical model developed earlier by Pecknold to predict composite structural failure within the framework of a finite element program. Their micromechanical model, like that of Aboudi, assumes a composite microstructure composed of square fibers arranged in a doubly periodic array (Fig. 2.1). The model, referred to as a "Combination Type", was based on a mechanics of materials approach and recognized the restraining effect of the fibers on the matrix. The model used a representative unit cell similar to that used by Aboudi (Fig. 2.2), except two matrix subcells were combined for a total of three instead of four subcells. Effective elastic constants for the composite unit cell were developed by use of spring analogies representing a subcells' stiffness. Constant stress or constant strain was assumed within

each constituent, depending on load direction. This approach led to a simpler formulation of composite properties than the Method of Cells, but with comparable accuracy. The micromechanics model was linked to and drove the composite material response of the finite element analysis at each material (Gauss) point.
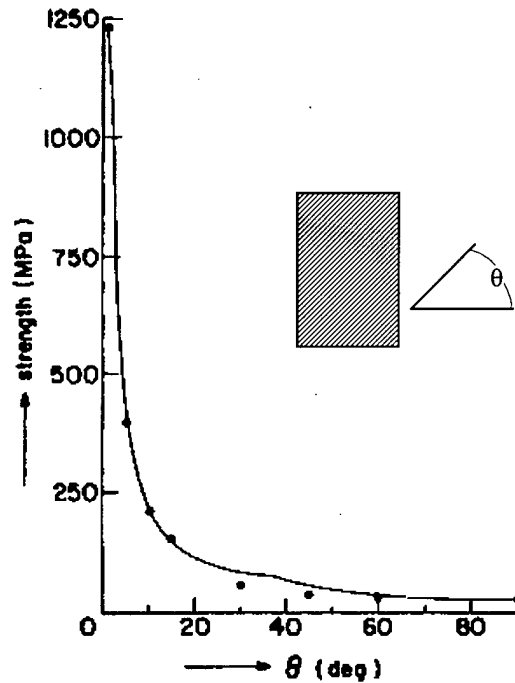


**Fig. 2.3** *Aboudi's method-of cells comparison between predicted and measured off-axis strength of a glass/epoxy composite [5].*

Rahman recognized six failure criteria: five uncoupled, in-plane only, maximum stress micromechanical criteria and one macromechanical criterion. Failure occurred when one of the conditions listed in Table 2.1 was satisfied. Implied in the criteria was directionality (orientation) of the failure, e.g., matrix cracks along the fiber axis when transverse tensile failure occurred.

**Table 2.1** *Failure criteria used in the Combination Type micromechanical model.*

| Failure Type | Condition |
|---|---|
| Fiber fracture | $^+\sigma_{11}^f \geq {}^+S_{11}^f$ |
| Matrix shearing | $\sigma_{12}^m \geq S_{12}^m$ |
| Transverse matrix cracking in tension | $^+\sigma_{22}^m \geq {}^+S_{22}^m$ |
| Transverse matrix crushing | $\left| {}^-\sigma_{22}^m \right| \geq \left| {}^-S_{22}^m \right|$ |
| Axial matrix cracking in tension | $^+\sigma_{11}^m \geq {}^+S_{11}^m$ |
| Lamina kink banding (fiber micro-buckling) | $\left| {}^-\sigma_{11} \right| \geq (FVF)G_{12}$ |

In Table 2.1:

- $FVF$ = Composite fiber volume fraction,
- $G_{12}$ = Composite in-plane shear modulus,
- $^-S_{22}{}^m$ = Matrix *in situ* compression strength,
- $^-\sigma_{11}$ = Compressive stress in the lamina,
- $^+\sigma_{11}{}^m$ = Axial tensile stress in the matrix.

Once constituent damage was detected, constituent material stiffnesses were gradually degraded and relevant stress components were either fully relieved (fiber fracture or matrix cracking) or held constant (matrix shearing, crushing or lamina kink banding) at the Gauss point being evaluated. The material softening and stress release allowed the load to be redistributed within the composite to surrounding undamaged areas. A stiffness degradation algorithm uncoupled failure direction response from other stress and strain components within the compliance matrix. This was accomplished by setting off-diagonal terms to zero and increasing the diagonal term compliance by the inverse of a specified stiffness reduction factor. As an example, Fig. 2.4 shows a fiber compliance matrix after axial failure.

The stiffness reduction factor, $D_{ij}$, controlled how rapidly the load redistribution occurred and its value, empirically determined, was chosen to improve solution convergence. Rahman [7] noted that solutions appeared insensitive to a wide range of stiffness

reduction factors and included examples such as 0.25 for shear modulus and 0.01 to 0.001 for Young's modulus.

$$[S^f] = \begin{bmatrix} D_{11}^{-1}s_{11} & 0 & 0 & 0 & 0 & 0 \\ & s_{22} & s_{23} & s_{24} & s_{25} & s_{26} \\ & & s_{33} & s_{34} & s_{35} & s_{36} \\ & & & s_{44} & s_{45} & s_{46} \\ & Sym & & & s_{55} & s_{56} \\ & & & & & s_{66} \end{bmatrix}$$

**Fig. 2.4** *Rahman's fiber compliance matrix after tensile failure [7].*

Rahman used the Combination Type micromechanics model and associated failure criteria to predict and compare off-axis lamina strengths of the same experimental data sets used by Aboudi. Results were in excellent agreement with experimental data and virtually identical to those from Method of Cells. Rahman went on to analyze more complex laminates and incorporated nonlinear shear modulus behavior in the micromechanical model. Excellent agreement between analytical results and experimental data of composite failure strengths was achieved in four tensile-loaded, boron/epoxy laminate configurations ([0/90]$_S$, [±30]$_S$, [±60]$_S$, [±45/90$_3$]$_S$). Good agreement in composite failure strength and correct identification of failure type was achieved in the analysis of four compressive-loaded, boron/epoxy laminates ([0/90]$_S$, [±30]$_S$, [±60]$_S$, [±20]$_S$).

Rahman used the failure criteria in a progressive failure algorithm within the finite element framework. The algorithm was used to simulate the compressive behavior of a notched (open hole), [±45]$_{6S}$, T300/BP976 laminate to failure. The algorithm indicated

13

that initial damage was fiber micro-buckling around the hole's edge, which precipitated local matrix shear failure. A reduction in shear stiffness followed which precipitated additional fiber micro-buckling cascading into laminate failure. Analytical results were in good agreement with experimental data predicting a failure load 11% higher than actual. Rahman noted in his conclusions that a possible improvement in his results, especially in predicting compressive failure, may have been achieved by using interactive failure criteria that account for mitigating and exacerbating reactions between the stresses rather than simple maximum-stress criteria.

Kwon [8] also developed a micromechanics model to describe failure and damage progress in laminated fibrous composite structures. Kwon's model assumed the same periodic composite microstructure and unit cell geometry as Aboudi (Fig. 2.1 and Fig. 2.2). Like Aboudi, constant stress and strain is assumed within each subcell, which simplifies determination of constituent (subcell) stresses from those of the composite (closed-form equations). The model was incorporated into a finite element program but, unlike Pecknold and Rahman, it does not drive the composite material response of the structure. Instead, the model uses composite strains computed in the course of normal structural analysis (assuming pseudo-homogenous material properties) to derive constituent strains and stresses.

Kwon's micromechanical failure criteria, like that of Aboudi, Pecknold, and Rahman, was based on fiber and matrix stresses. Assuming plane stress, failure occurred when one of four conditions was satisfied in a local material coordinate system. For fiber breakage

$$\left| \frac{\sigma_{11}^{f}}{^{+}S_{11}^{f}} \right| = 1 \quad if \, \sigma_{11}^{f} > 0 \qquad \text{or} \qquad \left| \frac{\sigma_{11}^{f}}{^{-}S_{11}^{f}} \right| = 1 \quad if \, \sigma_{11}^{f} < 0 \, .$$

For matrix cracking a quadratic interactive failure criterion (the form noted to be similar to those proposed by Hashin and Rotem, [9] and Yamada and Sun [10]) was used:

$$\left( \frac{\sigma_{22}^{m}}{^{+}S_{22}^{m}} \right)^{2} + \left( \frac{\sigma_{12}^{m}}{S_{S}^{m}} \right)^{2} = 1 \quad if \, \sigma_{22}^{m} \geq 0 \qquad \text{or} \qquad \left( \frac{\sigma_{22}^{m}}{^{-}S_{22}^{m}} \right)^{2} + \left( \frac{\sigma_{12}^{m}}{S_{S}^{m}} \right)^{2} = 1 \quad if \, \sigma_{22}^{m} < 0$$

Once constituent failure was detected, the damage algorithm degraded appropriate constituent material properties by setting normal and shear moduli to near zero values. Near zero values, rather than zero, were necessary to avoid numerical difficulties associated with matrix singularities.

Kwon's analytical predictions of off-axis lamina strength were in excellent agreement with the same experimental data sets used by Aboudi and Pecknold. Kwon extended his damage algorithm to analyze progressive damage in a [(0/90)$_6$]$_s$, graphite/epoxy, cross-ply, composite laminate containing a hole under a tensile load. Analysis was in excellent agreement with experimental data for ultimate failure strength (345 MPa versus 360 MPa experimental) as well as type, location and failure path direction (66°-78.5° analytical versus 75° experimental off the applied load axis).

Micromechanics-based analysis of fibrous composites is not limited to unidirectional lamina. Blackketter [11] developed a finite element based, three-dimensional micromechanics model for describing damage propagation in a plain weave

graphite/epoxy (AS4/3501) composite (Fig. 2.5). Constituents of a unit cell were identified as matrix or yarn. A separate two-dimensional finite element micromechanics model (single fiber in a matrix) was used to generate material properties of yarn from fiber and matrix properties.
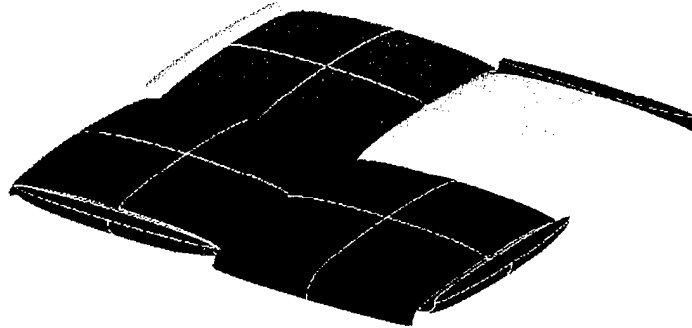


**Fig. 2.5** *Plain weave fabric idealization showing yarn pattern.*

Like Rahman, Blackketter used stiffness reduction factors to control load redistribution to undamaged areas and to account for both the type and direction (orientation) of the failure. Table 2.2 shows, for example, a transverse tension failure would result in a near zero value for the transverse modulus, an 80% reduction to the in-plane shear moduli, while the remaining moduli keep their original value.

**Table 2.2** *Blackketter's failure modes and degradation values of elastic properties.*

| Failure Mode | Stiffness Reduction Factors | | | | | |
|---|---|---|---|---|---|---|
| | $E_{11}$ | $E_{22}$ | $E_{33}$ | $G_{23}$ | $G_{13}$ | $G_{12}$ |
| Longitudinal tension ($^{+}S_{11}$) | 0.01 | 0.01 | 0.01 | 0.01 | 0.01 | 0.01 |
| Transverse tension ($^{+}S_{22}$) | 1.0 | 0.01 | 1.0 | 1.0 | 0.2 | 0.2 |
| Transverse tension ($^{+}S_{33}$) | 1.0 | 1.0 | 0.01 | 1.0 | 0.2 | 0.2 |
| Transverse shear ($S_{23}$) | 1.0 | 0.01 | 0.01 | 0.01 | 0.01 | 0.01 |
| Longitudinal shear ($S_{13}$) | 1.0 | 1.0 | 0.01 | 1.0 | 0.01 | 1.0 |
| Longitudinal shear ($S_{12}$) | 1.0 | 0.01 | 1.0 | 1.0 | 1.0 | 0.01 |

A significant conclusion appearing in Blackketter's work noted that nonlinear shear stress-strain behavior was caused principally by damage propagation rather than nonlinear matrix material behavior.

The research cited above represents significant achievements in constituent-based structural analysis but further improvements can be made. Driving composite response from a constituent level, as in the research of Rahman and Pecknold, must be done efficiently or computational time penalties could become significant. Extensions of a finite element failure code to other constitutive models, such as viscoelasticity, could impose severe computational penalties that would render the method a less desirable analysis alternative to mainstream users. Rahman and Pecknold note that using a stress-interactive failure criterion rather than a simple maximum stress (local material coordinate system) criterion may further improve failure predictions. But using a stress-interactive constituent failure criterion, assuming plane stress in the constituents such as that used by Kwon, does not address the general load case. Although a composite laminate or lamina may be in a state of plane stress, its constituents are generally in a fully three-dimensional stress state.

Approaches such as Method of Cells are restricted by geometrical considerations. For example, the continuous fiber composite model assumes a square packing array with square fibers. Brockenbrough *et al.* [12] have shown that packing arrangements have a pronounced effect on inelastic behavior in composites. One of virtues of MCT is a model geometry may be developed for any microstructure, including random distributions of

reinforcement. This capability may be critical when attentions are turned to analyses of other composite material architectures such as woven fabrics, particulate, and short (chopped) fiber.

Interestingly, in the literature reviewed, no attempts were made to compare the relative accuracy between micromechanics-based failure predictions and macromechanics failure predictions. This comparison would seem important in assessing the net benefits gained from the additional work required to implement micromechanics based failure analysis methods.

# SECTION 3.

# MULTICONTINUUM THEORY

## 3.1. Continuum Definition of Stress

Multicontinuum theory (MCT) development is presented in detail in papers by Garnich [13] and Garnich and Hansen [14,15]. It is summarized here as a convenience and to emphasize concepts important to implementing a constituent-based failure analysis.

MCT begins with a continuum definition of stress at a point. The concept of stress in homogeneous materials, such as steel, is a familiar one to most engineers. Yet, if looked at on a micro-scale, Fig. 3.1, one sees that the "homogeneous" material is hardly homogeneous. It is obvious that stresses will vary significantly from point to point across the material [16].



**Fig. 3.1** *Photomicrograph of construction grade steel.*

The homogenized value used to characterize the stress tensor at this point is derived by taking a volume average of all stresses in the region:

$$\underset{\sim}{\sigma} = \frac{1}{V} \int_D \underset{\sim}{\sigma}(\mathbf{x}) \, dV ,$$
(3.1)

where $D$ is the region representing the continuum point. The concept of a multicontinuum simply extends this concept to reflect coexisting materials within a continuum point. Consider a composite material with two clearly identifiable constituents as shown in Fig. 3.2.
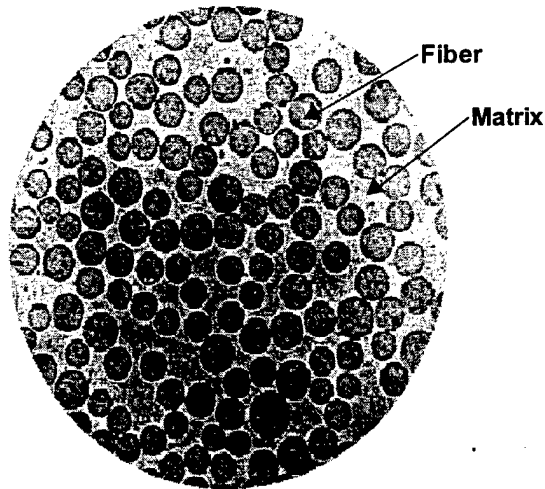


**Fig. 3.2** *Composite lamina as a multicontinuum.*

Using equation (3.1) for each constituent

$$\underset{\sim}{\sigma}_f = \frac{1}{V_f} \int_{D_f} \underset{\sim}{\sigma}(\mathbf{x}) \, dV ,$$
(3.2)

and

$$\underset{\sim}{\sigma}_m = \frac{1}{V_m} \int_{D_m} \underset{\sim}{\sigma}(\mathbf{x}) \, dV ,$$
(3.3)

where

$$D = D_f \cup D_m. \tag{3.4}$$

Combining equations (3.1), (3.2), and (3.3) leads to

$$\underset{\sim}{\sigma} = \phi_f \, \underset{\sim}{\sigma}_f + \phi_m \, \underset{\sim}{\sigma}_m, \tag{3.5}$$

where $\phi_f$ and $\phi_m$ are the volume fractions of fiber and matrix respectively.

Likewise, for strains we have:

$$\underset{\sim}{\varepsilon} = \phi_f \, \underset{\sim}{\varepsilon}_f + \phi_m \, \underset{\sim}{\varepsilon}_m. \tag{3.6}$$

It is important to note the averaging process that results in these equations. That is, we are not concerned with stress and strain variations through individual constituents within $D$ but only with their average values. This is an information compromise that separates structural analysis from micromechanical analysis. Accounting for stress variations throughout every fiber at every material point in even a modest structure is simply not possible or desirable. In contrast, providing constituent average stress and strain fields opens a new and manageable information window on a composite material's response to a load as compared to a classic single continuum approach.

### 3.2. Determining Constituent Stresses and Strains

Finite element solutions of structural problems produce stress and strain fields of the composite thereby providing two of the four unknowns in equations (3.5) and (3.6). To

provide closure of the equations, constitutive relations are required for the composite as well as the constituents. Here we change from direct tensor to contracted matrix notation and write

$$
\begin{Bmatrix} \sigma_{11} \\ \sigma_{22} \\ \sigma_{33} \\ \sigma_{12} \\ \sigma_{13} \\ \sigma_{23} \end{Bmatrix} = \begin{bmatrix} c_{11} & c_{12} & c_{13} & c_{14} & c_{15} & c_{16} \\ & c_{22} & c_{23} & c_{24} & c_{25} & c_{26} \\ & & c_{33} & c_{34} & c_{35} & c_{36} \\ & & & c_{44} & c_{45} & c_{46} \\ & SYM & & & c_{55} & c_{56} \\ & & & & & c_{66} \end{bmatrix} \begin{Bmatrix} \varepsilon_{11} \\ \varepsilon_{22} \\ \varepsilon_{33} \\ \gamma_{12} \\ \gamma_{13} \\ \gamma_{23} \end{Bmatrix}.
\tag{3.7}
$$

For composite and constituents there follows:

$$
\{\sigma\} = [C](\{\varepsilon\} - \{\varepsilon_o\}),
\tag{3.8}
$$

$$
\{\sigma_f\} = [C_f](\{\varepsilon_f\} - \{\varepsilon_{fo}\}),
\tag{3.9}
$$

$$
\{\sigma_m\} = [C_m](\{\varepsilon_m\} - \{\varepsilon_{mo}\}),
\tag{3.10}
$$

where $[C]$ and $[C_\beta]$ represents material stiffness matrices and $\{\varepsilon_o\}$ and $\{\varepsilon_{\beta o}\}$ are thermal strains. Substituting equations (3.8), (3.9), and (3.10) into (3.5) and using (3.6) gives

$$
\phi_f [C_f](\{\varepsilon_f\} - \{\varepsilon_{fo}\}) + \phi_m [C_m](\{\varepsilon_m\} - \{\varepsilon_{mo}\}) = [C](\phi_f \{\varepsilon_f\} + \phi_m \{\varepsilon_m\} - \varepsilon_o).
\tag{3.11}
$$

Solving for $\{\varepsilon_f\}$ gives

$$
\begin{aligned}
\{\varepsilon_f\} = &-\frac{\phi_m}{\phi_f}([C] - [C_f])^{-1}([C] - [C_m])\{\varepsilon_m\} \\
&+ \frac{\theta}{\phi_f}([C] - [C_f])^{-1}([C]\{\alpha\} - \phi_f [C_f]\{\alpha_f\} - \phi_m [C_m]\{\alpha_m\}),
\end{aligned}
\tag{3.12}
$$

where

$$\{\varepsilon_o\} = \theta \{\alpha\}, \qquad \{\varepsilon_{fo}\} = \theta \{\alpha_f\}, \qquad \{\varepsilon_{mo}\} = \theta \{\alpha_m\}.$$

In the above, $\alpha$ represents the coefficient of thermal expansion and $\theta$ is the relative temperature. Equation (3.12) may be rewritten as

$$\{\varepsilon_f\} = [A]\{\varepsilon_m\} + \frac{\theta}{\phi_f}\{a\}, \qquad (3.13)$$

where

$$[A] = -\frac{\phi_m}{\phi_f}\left([C]-[C_f]\right)^{-1}\left([C]-[C_m]\right),$$

and

$$\{a\} = \left([C]-[C_f]\right)^{-1}\left([C]\{\alpha\} - \phi_f[C_f]\{\alpha_f\} - \phi_m[C_m]\{\alpha_m\}\right).$$

Note that $[A]$ is a matrix relating mechanical constituent strains, while the vector $\{a\}$ relates constituent thermal strains. Typically $[C_f]$, $[C_m]$, $\{\alpha_f\}$, and $\{\alpha_m\}$, are known material properties of the constituents. $[C]$ and $\{\alpha\}$ of the composite are developed from micromechanical modeling. Hence, $[A]$ and $\{a\}$ are known *a priori* and could be calculated independent of the finite element program.

Determining constituent strains from composite strains requires substituting equation (3.13), into (3.6) and solving for $\{\varepsilon_m\}$ as

$$\{\varepsilon_m\} = \left(\phi_m[\text{I}] + \phi_f[A]\right)^{-1}\left(\{\varepsilon\} - \theta\{a\}\right). \qquad (3.14)$$

where [I] is the identity matrix. Substituting (3.14) back into (3.6) yields an expression for $\{\varepsilon_f\}$ as

$$\{\varepsilon_f\} = \frac{1}{\phi_f} \left( \{\varepsilon\} - \phi_m \{\varepsilon_m\} \right). \tag{3.15}$$

Equations (3.14) and (3.15) allow constituent strains to be to be calculated from composite strains at any point in the finite element model. Using equations (3.9) and (3.10), constituent stresses can be calculated.

### 3.3. MCT and Material Failure

Clearly, the composite and constituent stresses and strains developed previously are based on average values at a continuum point. In the finite element method, numerical integration samples stress, strain, and material continuum values at Gauss quadrature or "material" points. Implied in the derivation of MCT and its finite element implementation is that both fiber and matrix exist at every point in the composite. The concept of average values at a continuum point applies to material properties also, i.e.; there is no variation across that point in either constituent. Therefore, when a constituent material fails at a Gauss (continuum) point it fails absolutely without directionality and only the other constituent remains. This is in sharp contrast to some of the work discussed previously in the literature review, which incorporate failure models that attempt to include directional dependence.

# SECTION 4.

# FAILURE CRITERIA

## *4.1. Overview of Quadratic Failure Criteria*

A general overview of current failure criteria is given in Appendix G. Here we are only concerned with failure criteria that account for the interaction effect of the various stresses on a material's strength.

The Maximum Distortional Energy, or von Mises, criterion is the most widely used criterion for predicting yield points in isotropic metals. This criterion has also been used to predict brittle failure in isotropic materials. The isotropic von Mises failure criterion is a special case of a general form called quadratic interaction criterion, so named because it includes terms to account for interaction between the stress components. Hill [17] generalized the von Mises criterion to include the effects of orthotropic behavior. The Hill criterion is given by

$$
\begin{aligned}
&F_1(\sigma_1 - \sigma_2)^2 + F_2(\sigma_2 - \sigma_3)^2 + F_3(\sigma_3 - \sigma_1)^2 \\
&+ F_{23}(\sigma_{23} + \sigma_{32})^2 + F_{13}(\sigma_{13} + \sigma_{31})^2 + F_{12}(\sigma_{12} + \sigma_{21})^2 = 1,
\end{aligned}
\tag{4.1}
$$

where

$$
2F_1 = \frac{1}{S_{11}^2} + \frac{1}{S_{22}^2} - \frac{1}{S_{33}^2}, \qquad 2F_2 = \frac{1}{S_{22}^2} + \frac{1}{S_{33}^2} - \frac{1}{S_{11}^2}, \qquad 2F_3 = \frac{1}{S_{33}^2} + \frac{1}{S_{11}^2} - \frac{1}{S_{22}^2}
$$

$$
2F_{12} = \frac{1}{S_{12}^2}, \qquad 2F_{13} = \frac{1}{S_{13}^2}, \qquad 2F_{23} = \frac{1}{S_{23}^2}.
$$

In the above, $\sigma_{ij}$ are stresses referenced to the principal axes of orthotropy (principal material directions), while $S_{ij}$ represent failure strengths. As presented, Hill's criterion assumes no difference between tensile and compressive yield strengths.

A generalized quadratic interaction criterion form, suggested by Gol'denblat and Kopnov [18] and proposed by Tsai and Wu [19], is given as

$$F_i\sigma_i + F_{ij}\sigma_i\sigma_j = 1, \tag{4.2}$$

where $F_i$ and $F_{ij}$ are experimentally determined strength tensors and contracted tensor notation is used ($i,j$ = 1 to 6). Hoffman [20] has suggested that the linear terms, $F_i$, are necessary to account for differences in tensile and compressive strengths, whereas Tsai and Wu state that they are necessary to account for internal stresses. Expanding equation (4.2) for an orthotropic material, using symmetry of the strength tensors, assuming no interaction between normal and shear stresses, and assuming negative and positive shears are equal gives

$$F_1\sigma_1 + F_2\sigma_2 + F_3\sigma_3 + F_{11}\sigma_1^2 + F_{22}\sigma_2^2 + F_{33}\sigma_3^2 + F_{44}\sigma_4^2$$
$$+ F_{55}\sigma_5^2 + F_{66}\sigma_6^2 + 2F_{12}\sigma_1\sigma_2 + 2F_{13}\sigma_1\sigma_3 + 2F_{23}\sigma_2\sigma_3 = 1, \tag{4.3}$$

where

$$F_1 = \frac{1}{{}^+S_{11}} + \frac{1}{{}^-S_{11}}, \qquad F_2 = \frac{1}{{}^+S_{22}} + \frac{1}{{}^-S_{22}} \qquad F_3 = \frac{1}{{}^+S_{33}} + \frac{1}{{}^-S_{33}}$$

$$F_{11} = \frac{1}{{}^+S_{11}{}^-S_{11}} \qquad F_{22} = \frac{1}{{}^+S_{22}{}^-S_{22}} \qquad F_{33} = \frac{1}{{}^+S_{33}{}^-S_{33}}$$

$$F_{44} = \frac{1}{S_{12}^2}, \qquad F_{55} = \frac{1}{S_{13}^2}, \qquad F_{66} = \frac{1}{S_{23}^2},$$

$$F_{12} = \frac{1}{2P^2}\left[1 - P(F_1 + F_2) - P^2(F_{11} + F_{22})\right],$$

$$F_{13} = \frac{1}{2Q^2}\left[1 - Q(F_1 + F_3) - Q^2(F_{11} + F_{33})\right],$$

$$F_{23} = \frac{1}{2R^2}\left[1 - R(F_2 + F_3) - R^2(F_{22} + F_{33})\right].$$

The terms accounting for coupling effects between normal stresses, $F_{12}$, $F_{13}$, and $F_{23}$, require experimental determination using biaxial tests. For example, using biaxial tension failure loads $P$, $Q$, and $R$, $\sigma_1=\sigma_2=P$, $\sigma_1=\sigma_3=Q$ and $\sigma_2=\sigma_3=R$. The remaining coefficients can be experimentally determined from simple uniaxial or shear tests. The Tsai-Wu criterion appears to be the most widely used quadratic stress-interaction criterion for predicting macro failure in composite materials.

Hashin [21] developed a three-dimensional, stress interactive, failure criterion for unidirectional lamina that recognized two distinct and uncoupled failure modes. While the failure criterion itself is based on composite stresses, it constructs a piecewise continuous failure form based on constituent failure modes.

Hashin states that most failure criteria that account for stress interaction are quadratic in stress and that choice of a quadratic polynomial is based solely on curve fitting considerations. Quadratic criteria are third in a hierarchy of potential approximations of failure surfaces (constant or maximum stress, linearly varying stress and quadratic). A quadratic approximation, he notes, "is the simplest presentation which can fit the data reasonably well and in view of the significant scatter of failure test data it hardly seems worthwhile to employ cubic or higher approximations."

A unidirectional, fiber reinforced composite is assumed to be transversely isotropic. A local orthogonal coordinate system is defined in which the fiber axis serves as the principal, $x_1$, material direction, and $x_2$, $x_3$ the transverse directions. Since material constants assume transverse isotropy, stresses can be expressed as values invariant under rotations about the principal material direction. The failure state of either constituent material can be expressed in terms of these transversely isotropic stress invariants. Although Hashin derived the invariants, Hansen [22], in development of an anisotropic flow rule for plastic behavior in composite materials, presented a different form (both forms attributed to Spencer) used here. The five transversely isotropic stress invariants are:

$$
\begin{aligned}
I_1 &= \sigma_{11}, \\
I_2 &= \sigma_{22} + \sigma_{33}, \\
I_3 &= \sigma_{22}^2 + \sigma_{33}^2 + 2\sigma_{23}^2, \\
I_4 &= \sigma_{12}^2 + \sigma_{13}^2, \\
I_5 &= \sigma_{22}\sigma_{12}^2 + \sigma_{33}\sigma_{13}^2 + 2\sigma_{12}\sigma_{13}\sigma_{23}.
\end{aligned}
\tag{4.4}
$$

Hashin's choice of a quadratic form eliminates $I_5$ from appearing in the failure criteria. Therefore the most general form for a quadratic criterion is

$$
A_1 I_1 + B_1 I_1^2 + A_2 I_2 + B_2 I_2^2 + C_{12} I_1 I_2 + A_3 I_3 + A_4 I_4 = 1.
\tag{4.5}
$$

Feng [23], in an analogous manner, developed a quadratic interaction failure criteria based on transversely isotropic strain invariants.

At this point, it is instructive to compare the criterion of Tsai and Wu with that of Hashin. Tsai and Wu, in reference [19] presented a form of equation (4.3) for transversely isotropic composites as

$$
\begin{aligned}
F_1\sigma_{11} + F_2(\sigma_{22} + \sigma_{33}) &+ F_{11}\sigma_{11}^2 + F_{22}(\sigma_{22}^2 + \sigma_{33}^2 + 2\sigma_{23}^2) + F_{44}(\sigma_{12}^2 + \sigma_{13}^2) \\
&+ 2F_{12}(\sigma_{11}\sigma_{22} + \sigma_{11}\sigma_{33}) + 2F_{23}(\sigma_{22}\sigma_{33} + \sigma_{23}^2) = 1.
\end{aligned}
\tag{4.6}
$$

Rewriting equation (4.6) in terms of the transversely isotropic stress invariants gives

$$
F_1 I_1 + F_2 I_2 + F_{11} I_1^2 + F_{22} I_3 + F_4 I_4 + 2F_{12} I_1 I_2 + 2F_{23}(I_2^2 - I_3) = 1,
$$

or,

$$
F_1 I_1 + F_{11} I_1^2 + F_2 I_2 + 2F_{23} I_2^2 + 2F_{12} I_1 I_2 + (F_{22} - 2F_{23})I_3 + F_4 I_4 = 1.
\tag{4.7}
$$

Comparing equation (4.7) to equation (4.5), shows that the Tsai-Wu criterion for transversely isotropic materials and the Hashin failure criterion have the same functional form. Their difference is in defining the coefficients of the stress terms. The Tsai-Wu equation is used to define a smooth and continuous failure surface in both the tension and compression regions of space. As a result, the stress tensors are functions of both tensile and compressive composite strengths. Hashin identified two composite failure modes; fiber versus matrix influenced, and develops separate equations based on the failure mode to determine a failure state. Hashin further recognized that a composite typically has different ultimate strengths in tension and compression, so both fiber and matrix failure criteria have tensile and compressive subforms. Hence, the coefficients of the stress terms are functions of only tension or compression strengths resulting in a continuous but not smooth stress space failure surface.

## 4.2. MCT Failure Criterion

In a major departure from Hashin's failure criterion, a failure criterion was developed for each constituent rather than the composite. The criterion is in the form of equation (4.5) and uses constituent stress information produced by MCT. As a consequence, the transversely isotropic stress invariants, defined in equation (4.4), were used for each constituent of the microstructure under consideration. This approach is unique in that an anisotropic failure theory is used on an isotropic matrix material. This complexity is necessitated by the fact that the matrix failure behavior will be anisotropic due to microstructural geometry. Consider a transversely isotropic unidirectional composite. If all fibers were removed, leaving their holes, only a matrix of "Swiss cheese" would remain. Because of the remaining microstructure, macroscopic failure of the material will be fundamentally different in axial versus transverse directions. This results in a transversely isotropic failure envelope.

Anisotropic failure behavior of *in situ* matrix material precludes using a simple isotropic failure criterion such as maximum principal stress. Also, recognizing that constituents typically have different ultimate strengths in tension and compression, each constituent failure criterion has a tensile and compressive subform.

As a first approximation, we would like to simplify equation (4.5) . Pipes and Cole [24] demonstrated some of the difficulties in experimentally determining stress interaction terms such as $F_{12}$. Further, Narayanaswami [25] demonstrated numerically that setting

the stress interaction term $F_{12}$ to zero in the Tsai-Wu quadratic failure criterion (analogous to $C_{12}$ in equation (4.5)) in plane stress analyses, resulted in less than 10% error for all the load cases and materials considered. Hence, we set $C_{12}$ equal to zero. Tsai and Wu identify the linear terms in equation (4.7) as necessary to account for internal stresses. Internal stresses are accounted for in the formulation of Multicontinuum Theory so the linear terms are eliminated from equation (4.5). If later analytical comparisons against experimental results do not provide a satisfactory correlation, these terms, along with the term $C_{12}$, will be reexamined for their potential contributions.

Noting the above, the general form for a stress interactive failure criterion, after changing to a consistent coefficient notation, is given by

$$A_1 I_1^2 + A_2 I_2^2 + A_3 I_3 + A_4 I_4 = 1. \tag{4.8}$$

### 4.2.1. Fiber Failure

Most fibers used for composite reinforcement have greater transverse strengths than the matrices commonly used with them. Hence, we assume that transverse failure of these composites is matrix dominated. Based on this assumption, we set $A_2$ and $A_3$ equal to zero in equation (4.8) as their associated stress invariants involve transverse normal stresses. The fiber failure criterion reduces to:

$$A_1^f \left( I_1^f \right)^2 + A_4^f I_4^f = 1. \tag{4.9}$$

To determine coefficients for each stress term, we solve equation (4.9) considering individual load cases of pure in-plane shear, tension, and compression. For the case of in-plane shear load only ($\sigma_{11}{}^f = 0$), we find

$$A_4^f = \frac{1}{\left(S_{12}^f\right)^2}.$$

For the case of tensile load only ($\sigma_{11}{}^f > 0$; $\sigma_{12}{}^f = 0$), we find

$$^+A_1^f = \frac{1}{\left(^+S_{11}^f\right)^2}.$$

For the case of compression load only ($\sigma_{11}{}^f < 0$; $\sigma_{12}{}^f = 0$), we find

$$^-A_1^f = \frac{1}{\left(^-S_{11}^f\right)^2}.$$

The criterion for fiber failure can now be expressed as:

$$^{\pm}A_1^f \left(I_1^f\right)^2 + A_4^f I_4^f = 1. \tag{4.10}$$

The $\pm$ symbol indicates that the appropriate tensile or compressive ultimate strength value is used depending on the constituent's stress state. All of the fiber failure parameters can be experimentally determined using simple uniaxial or shear tests.

### 4.2.2. Matrix Failure

To determine the coefficients of equation (4.8) for matrix failure, we first solve the equation considering load cases of pure in-plane and transverse shear. For the case of transverse shear only ($\sigma_{11}{}^m = \sigma_{22}{}^m = \sigma_{33}{}^m = \sigma_{12}{}^m = 0$), we find

$$A_3^m = \frac{1}{2\left(S_{23}^m\right)^2}.$$

For the case of in-plane shear only ($\sigma_{11}{}^m = \sigma_{22}{}^m = \sigma_{33}{}^m = \sigma_{23}{}^m = 0$), we find

$$A_4^m = \frac{1}{\left(S_{12}^m\right)^2}.$$

Since most fibers used for composite reinforcement have greater longitudinal strengths than the matrices commonly used in conjunction with them, we assume that the longitudinal failure of these composites is fiber dominated. Based on this assumption (and some numerical sensitivity studies), we set $A_1$ equal to zero. Incorporating these results into (4.8) gives

$$A_2^m \left(I_2^m\right)^2 + \frac{1}{2\left(S_{23}^m\right)^2} I_3^m + \frac{1}{\left(S_{12}^m\right)^2} I_4^m = 1. \tag{4.11}$$

To determine $A_2{}^m$, we consider the case of transverse tensile load only ($\sigma_{23}{}^m = \sigma_{12}{}^m = 0$; $(\sigma_{22}{}^m + \sigma_{33}{}^m) > 0$) and find

$${}^+A_2^m = \frac{1}{\left({}^+S_{22}^{22m} + {}^+S_{33}^{22m}\right)^2} \left(1 - \frac{\left({}^+S_{22}^{22m}\right)^2 + \left({}^+S_{33}^{22m}\right)^2}{2\left(S_{23}^m\right)^2}\right).$$

Note that, while a pure transverse (one-dimensional) load on a composite lamina results in

$$\sigma_{11} = \sigma_{33} = 0,$$

the constituents experience a fully three-dimensional stress state. Likewise, for the case of a pure transverse compressive load ($\sigma_{23}{}^m = \sigma_{12}{}^m = 0$; $(\sigma_{22}{}^m + \sigma_{33}{}^m) < 0$)

$$^-A_2^m = \frac{1}{\left(^-S_{22}^{22m} + {}^-S_{33}^{22m}\right)^2}\left(1 - \frac{\left(^-S_{22}^{22m}\right)^2 + \left(^-S_{33}^{22m}\right)^2}{2\left(S_{23}^m\right)^2}\right).$$

The criterion for matrix failure can now be expressed as

$$^{\pm}A_2^m\left(I_2^m\right)^2 + A_3^m I_3^m + A_4^m I_4^m = 1. \tag{4.12}$$

All of the matrix failure parameters can be experimentally determined using simple uniaxial or shear tests.

### 4.3. Material Point Failure

MCT's fundamental concept of average field values at a continuum point is also applied to material properties. There is no variation in material properties across a constituent at a continuum point. Therefore, when a constituent material fails, it fails absolutely within the point, without directionality, and loses the ability to sustain any load. Furthermore, at every point in the composite, both fiber and matrix are assumed to exist. Therefore, when one constituent fails the other constituent remains.

As discussed previously, an interesting ramification of this type of constituent based failure is that even though the matrix material is isotropic (Table 4.1) in a neat or bulk resin form, its *in situ* failure properties will be anisotropic. Take for example the E-glass/vinylester composite used in this research. From an MCT perspective, a composite with failed fibers is composed of only matrix. Yet the "composite", composed of matrix only results in transversely isotropic properties as determined by micromechanics (Table 4.2).

**Table 4.1** *Vinylester matrix properties.*

| E (GPa) | $\nu$ |
|---------|-------|
| 4.66 | 0.292 |

**Table 4.2** *E-glass/vinylester composite properties with fiber failure.*

| $E_{11}$ (GPa) | $E_{22}$ (GPa) | $G_{12}$ (GPa) | $G_{23}$ (GPa) | $\nu_{12}$ | FVF |
|---------------|---------------|---------------|---------------|-----------|-----|
| 2.32 | 1.11 | 0.610 | 0.403 | 0.290 | 51% |

# SECTION 5.

# DEVELOPING MATERIAL PROPERTIES

## 5.1. Experimental Determination of Composite Material Properties

The MCT_77 finite element program is capable of modeling nonlinear-elastic composite laminates formed by stacking lamina composed of unidirectional reinforcing fibers in a polymer matrix. Theory and software assume transversely isotropic lamina.

The key philosophy in conducting a MCT_77 failure analysis is to "tune" the finite element code to materials composing the structure. Definition of a "new" material requiring its own characterization must include not only a composite with different constituents but also composites formed with different fiber volume fractions and manufacturing processes. Stress-strain curves, especially those with significant non-linear behavior, the moduli derived from them, and ultimate failure strengths are all important parameters in characterizing material behavior.

A suite of six tests conducted for the most part on unidirectional laminates is necessary to fully characterize a material for failure analysis. These tests are used to:

1) Determine nonlinear stress-strain parameters.
2) Determine five independent composite elastic constants: $E_{11}$, $E_{22}$, $G_{12}$, $G_{23}$, and $v_{12}$.
3) Determine six ultimate composite strengths: ${}^{+}S_{11}$, ${}^{+}S_{22}$, ${}^{-}S_{11}$, ${}^{-}S_{22}$, $S_{12}$, and $S_{23}$.

The suite of material tests used in this research and their relevant ASTM standards are listed in Table 5.1. It should be noted that ASTM test methods recommend a minimum

of five specimens be tested for statistical significance [26,27]. MCT_77 software does not differentiate between tensile and compressive elastic constants. Arbitrarily, tensile elastic constants were used in all MCT_77 analyses contained within this research.

**Table 5.1** *ASTM test suite for characterizing composite (lamina) materials.*

| ASTM STANDARD | TYPE OF TEST | CONSTANTS DETERMINED |
|---|---|---|
| D3039 | Longitudinal Tension | $^{+}E_{11}, {}^{+}v_{12}, {}^{+}S_{11}$ |
| " | Transverse Tension | $^{+}E_{22}, {}^{+}v_{21}, {}^{+}S_{22}$ |
| D3410 | Longitudinal Compression | $^{-}E_{11}, {}^{-}v_{12}, {}^{-}S_{11}$ |
| " | Transverse Compression | $^{-}E_{22}, {}^{-}v_{21}, {}^{-}S_{22}$ |
| D3518 | Longitudinal Shear | $G_{12}, S_{12}$ |
| D5379 | Transverse Shear | $G_{23}, S_{23}$ |

## 5.2. Determining Constituent Material Properties

MCT_77's ability to calculate accurate constituent stress and strain fields is dependent on constituent elastic constants derived from experimentally determined composite values. Further, MCT_77's ability to execute realistic failure analysis is dependent on accurate values for constituent strengths also derived from experimentally determined composite values. The relationship between composite (macro) and constituent (micro) elastic constants is developed using a finite element idealization of a fiber imbedded in a matrix known as a micromechanics model. The finite element micromechanics model used in this research was advanced by Garnich [13] which contains discussion of its development. Only major components of the model will be summarized here.

The micromechanics model is based on an assumption of uniform hexagonal fiber packing within the lamina's matrix (Fig. 5.1). A unit cell, representative of the repeating microstructure, is extracted from a region bounded by symmetry lines. Unit cell

geometry, fiber volume fraction, and boundary conditions are used to define the finite element model (Fig. 5.2).

Matrix

Symmetry
Lines
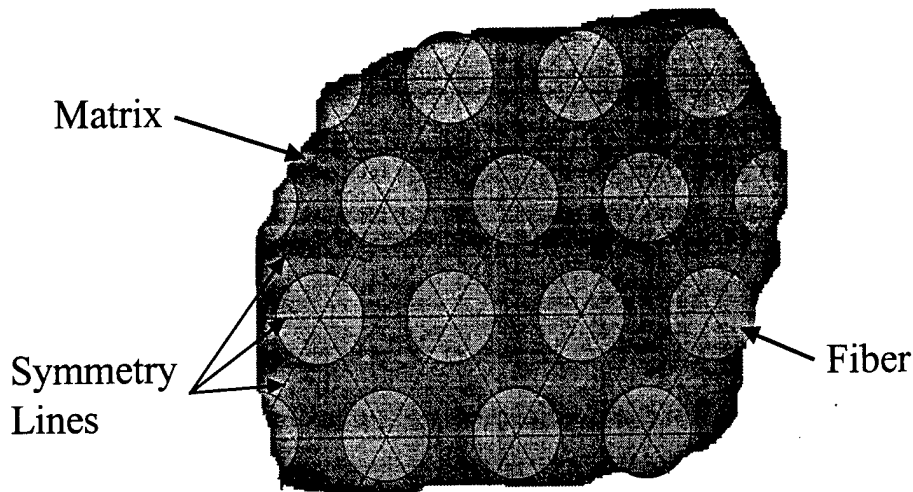
Fiber

Fig. 5.1 *Idealized lamina microstructure.*

The unit cell is based on a generalized plane strain assumption in the fiber direction but is fully three-dimensional. The cell is modeled with ANSYS® finite element software using an ANSYS® scripting language that allows material properties and fiber volume fraction to be varied as required. The model uses 528 eight-node brick (SOLID45) elements for a total of 3444 degrees of freedom. Boundary conditions necessary to enforce compatibility of unit cell boundaries with adjacent unit cells are generated automatically. Four linear elastic load cases are solved (longitudinal tension, transverse tension, transverse shear and longitudinal shear) to determine and verify five independent elastic constants ($E_{11}$, $E_{22}$, $G_{12}$, $G_{23}$, $\nu_{12}$) for transversely isotropic composite lamina.

ANSYS
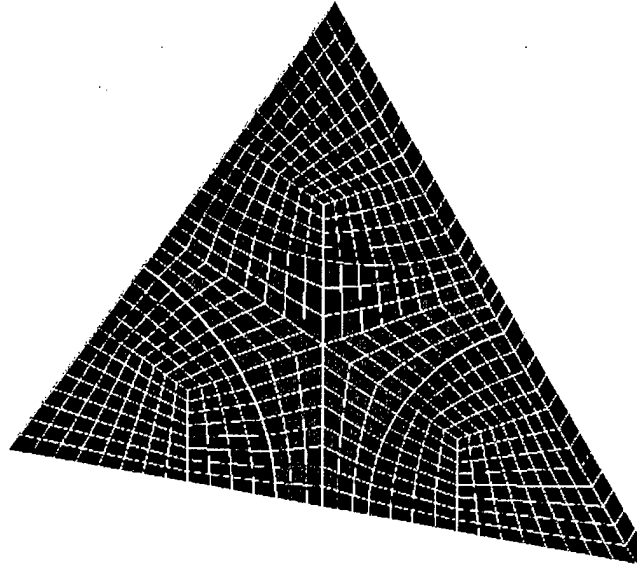


**Fig. 5.2** *Finite element model of a unit cell.*

Ideally, development of a consistent set of composite elastic constants would begin by acquiring elastic constants for each constituent. Bulk matrix material properties are typically isotropic and could be determined directly by standard (ASTM) material testing methods. Reinforcement properties are more difficult to determine directly using standard testing techniques due to their small diameters and fibrous nature. Generally, fiber properties are inferred or "backed out" from results of composite lamina tests. *In situ* material constants for commonly used reinforcing fibers and polymer matrices are available in published literature [28].

As reported elsewhere [7,5], the *in situ* constituent material constants are generally different than those for the bulk materials. These differences can be illustrated by examining matrix *in situ* and bulk shear behavior. For example, a composite lamina's response to a shear load, whether in- or out-of-plane, is dominated by load transfer within the matrix. The experimentally determined shear stress-strain curves for bulk vinylester

resin and a E-glass/vinylester lamina in Fig. 5.3 not only have different magnitudes but also different shapes. The neat resin curve is nearly linear where composite curves show significant nonlinearity.
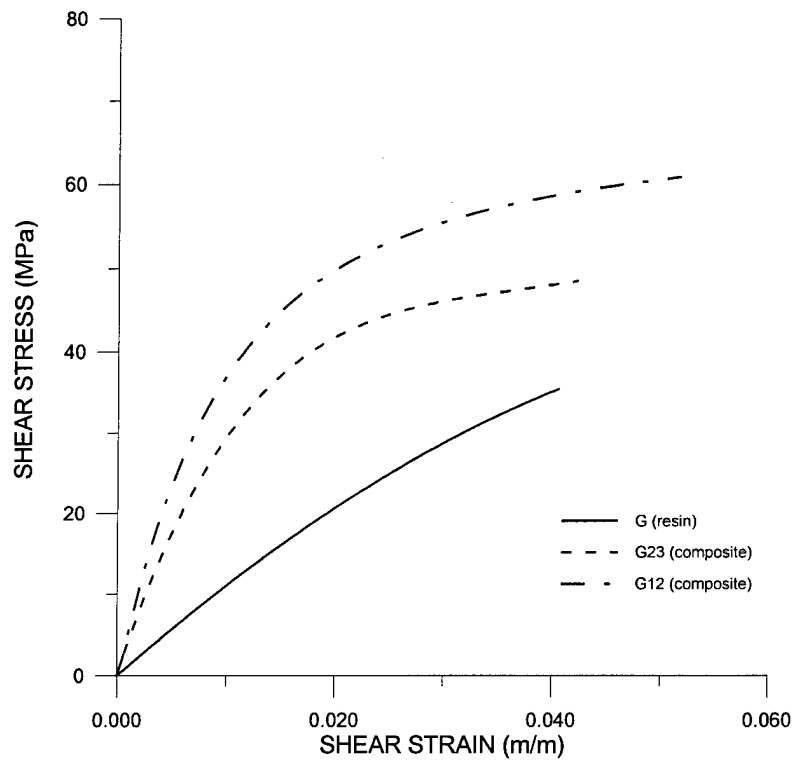


**Fig. 5.3** *Comparison of composite/matrix shear behavior.*

As a result of differing bulk versus *in situ* behavior, all constituent material constants for MCT_77 analyses were backed out from experimentally determined composite values via the micromechanics model. Bulk constituent material properties provided good starting values for the micromechanics model in an iterative approach to determine *in situ* properties. MCT_77, in conjunction with the ANSYS® pre-processor, can run the micromechanics model in reverse so that constituent properties consistent with experimentally determined composite properties can be determined in an automated fashion.

### 5.3. Constitutive Model for Changing Shear Properties

A majority of composite materials in use today have organic matrices that produce significant nonlinear shear stress-strain behavior (see for example Fig. 5.3). Failure of a structure can be defined in terms of strain, displacement, or stress. Hence, to completely capture the response of a structure to a generally applied load, both the stress and strain states need to be determined. Failure to model nonlinear shear behavior can lead to poor approximations of a composite's response to load as shown Fig. 5.4. Nonlinear behavior can also be found in transversely loaded lamina. However, transverse nonlinearity occurs over a much smaller strain range due to low ultimate strength in that direction and thus can be neglected in most structural analyses.

As previously mentioned, the success of an MCT-based analysis depends in large part on a consistent relationship between composite and constituent material properties. Analyses having significant shear require incremental application of the load and a corresponding application of an appropriate tangent shear modulus to account for nonlinear structural response over the entire load range. Micromechanics arguments suggest that maintaining consistent composite-constituent material relationships when nonlinear composite shear moduli exists also requires the constituents' shear moduli to change. Changes to constituent properties, in turn, affect other composite elastic constants besides shear modulus since they are linked through common constituents. Assuming shear behavior of the fiber remains linear elastic, the matrix shear modulus must be adjusted to maintain consistency with the composite elastic constants.
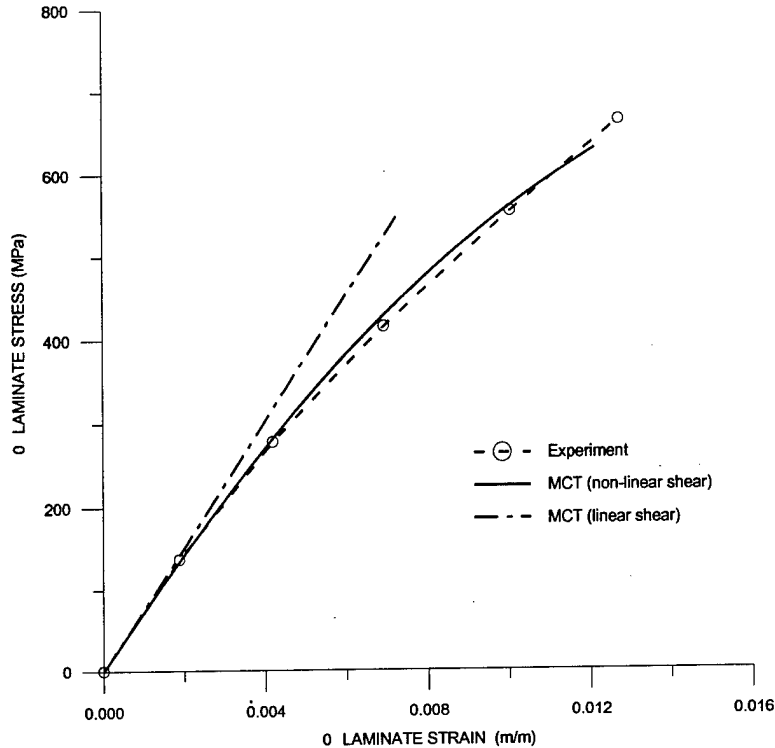
**Fig. 5.4** *MCT_77 laminate analysis of boron/5505 [±30]s with and without nonlinear shear effects.*

Researchers have applied many different constitutive models to address changing material constants under shear and combined load states. Most appear to rely on plasticity [7,29,30,31] or nonlinear-elasticity [32,33,34] theories. While these constitutive models have resulted in good approximations to composite nonlinear shear behavior, others [13,35,36] have shown that nonlinear polymeric behavior is viscoelastic in nature.

Figures 5.5-5.7 present hypothetical stress-strain curves for elastic-plastic, viscoelastic, and nonlinear-elastic behaviors. A linear region terminated by a transition, or yield point, to nonlinear behavior characterizes the elastic-plastic curve, shown in Fig. 5.5.
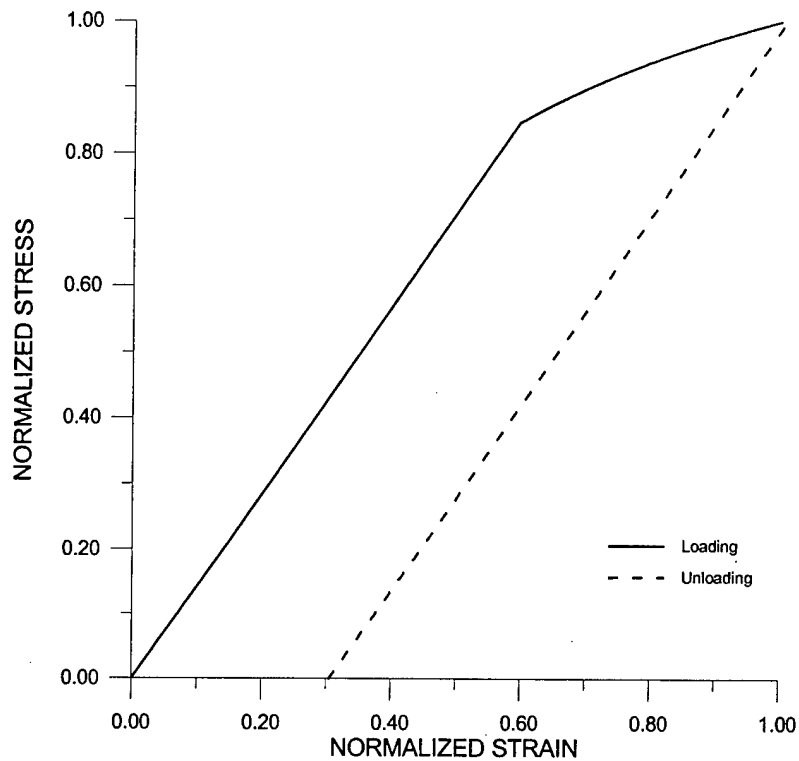
**Fig. 5.5** *Elastic-plastic stress-strain curve for a hypothetical material.*

Upon unloading, the elastic-plastic curve reverts to its previous linear behavior but does not return to zero strain. The residual strain is the result of inelastic plastic flow.

The nonlinear-elastic curve, shown in Fig. 5.6, is nonlinear throughout its load history and unloads back down the loading path to zero strain if no damage in the material has occurred. The unloading path shown in Fig. 5.6 is offset slightly from the loading path for clarity.
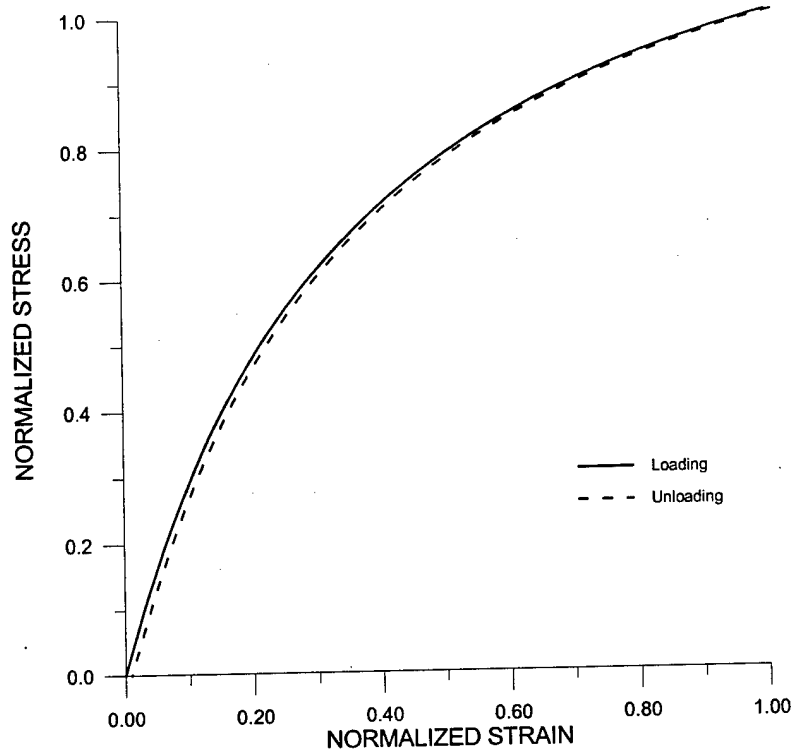
**Fig. 5.6** *Nonlinear-elastic stress-strain curve for a hypothetical material.*
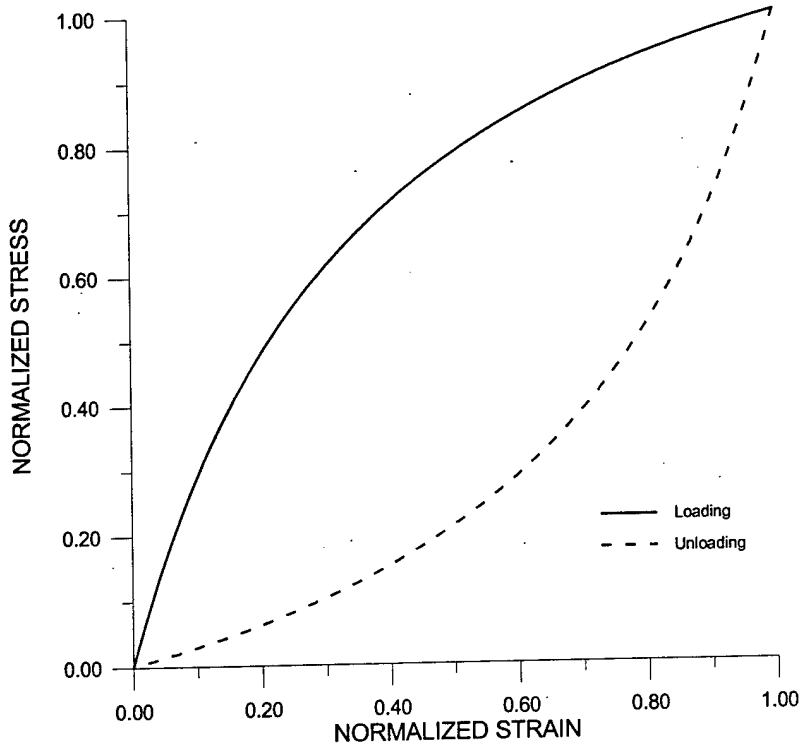


**Fig. 5.7** *Viscoelastic stress-strain curve for a hypothetical material.*

Viscoelastic behavior, shown in Fig. 5.7, is time dependent, whereas elastic-plastic and nonlinear-elastic behaviors are not. The stress-strain curve is nonlinear throughout its load history and returns to zero strain at zero load if no damage in the material has occurred.

Figures 5.8 and 5.9 show experimental stress-strain curves for two different composite materials. The shape of these curves support the supposition that composite material behavior is viscoelastic. However, from Figures 5.5-5.7 it is apparent that the three constitutive models, elastic-plastic, viscoelastic, and nonlinear-elastic, will produce similar stress-strain curves for monotonic loading. Hence, for the purpose of a failure analysis using stress-based failure criteria, each of the constituent models would produce essentially identical failure results under quasi-static loading conditions. Application of Multicontinuum Theory using viscoelasticity (or plasticity) constitutive models would be far more complex than using a nonlinear-elastic model. Further, for the research considered herein, unloading of the composite was not a consideration. Hence, a nonlinear-elastic constitutive model relating changes in elastic constants due to changing composite shear modulus was developed. Linear elasticity was used to model pure tension and compression behavior.
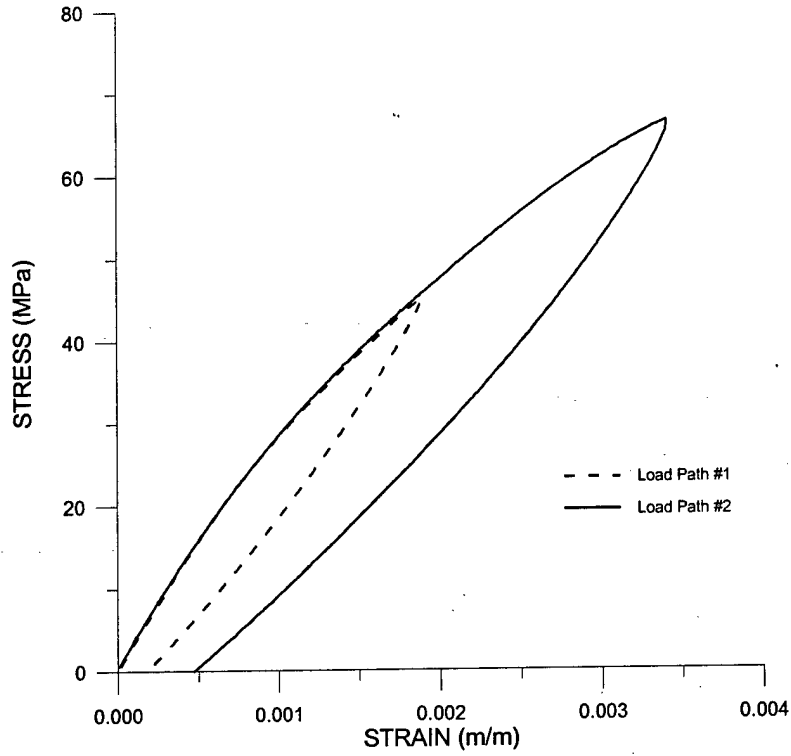
**Fig. 5.8** *E-glass/8084 [±45]$_S$ tensile behavior for load-unload.*
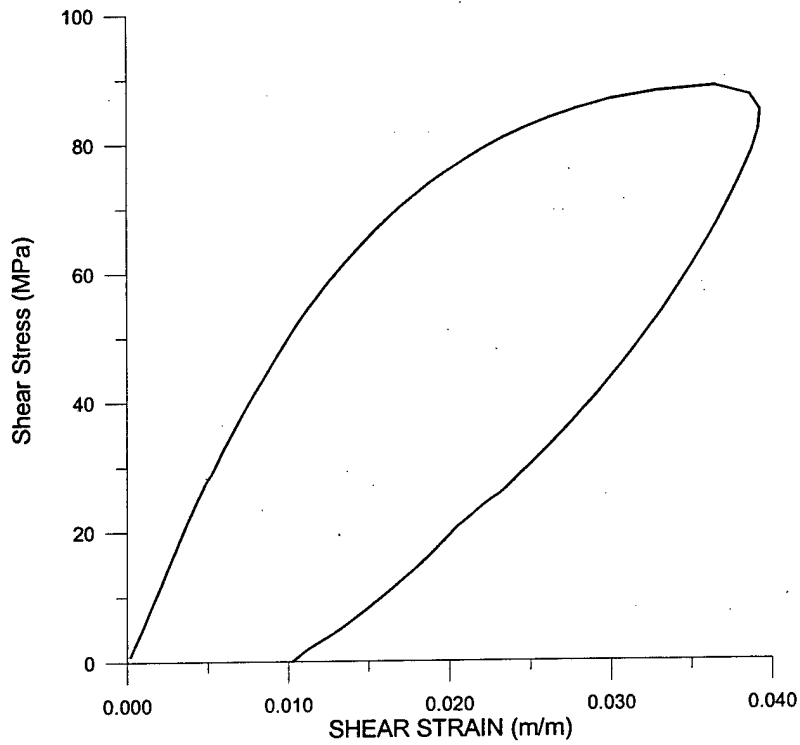


**Fig. 5.9** *AS4/3501 [0] V-notched shear behavior for load-unload.*

MCT_77's nonlinear-elastic constitutive model was predicated on the following:

1. Matrix compressibility does not change with stress state (constant bulk modulus).
2. Fiber elastic constants do not change with stress state.
3. To correctly respond to the known and limiting cases of pure in-plane and pure out-of-plane shear loads, shear moduli derived from curve fits of experimentally determined composite shear stress-strain curves were used to define nonlinear behavior.
4. In cases where two in-plane or in-plane and out-of-plane shear loads are present, the shear contributing the largest amount of deviatoric strain energy determines the value of the composite tangent shear modulus used in the constitutive model.

MCT_77 uses a three-term exponential series to fit both in- and out-of-plane experimental shear stress-strain curves. Curve fits of shear stress-strain data have the form

$$\tau = C_0 + C_1 e^{(a_1\gamma)} + C_2 e^{(a_2\gamma)}, \tag{5.1}$$

where $C_i$ and $a_i$ are curve fit parameters and $\gamma$ is engineering shear strain. Nonlinear regression is used to fit the five equation parameters to data generated by experimental tests. Strain dependent, tangent shear moduli are computed from the first derivative of equation (5.1) for use during a finite element analysis. Appendix D provides a detailed discussion of the nonlinear regression procedure used.

During an MCT_77 analysis, recalculation of all composite and matrix material constants is initiated by changes in composite shear strain values. The relationships between composite and matrix material constants are developed in an unconnected pre-processing procedure by varying matrix properties in a prescribed manner and using micromechanics to derive new composite properties. The procedure varies the matrix shear modulus from 0%-100% (usually in increments of 10%) of its initial *in situ* value as determined from

material tests.  An assumption of a constant bulk modulus provides the second

independent elastic constant.  Discrete increments in matrix elastic constants and constant

fiber elastic constants form input to the micromechanics model for calculating

corresponding composite constants.  A curve for each elastic constant, normalized with

respect to the composite tangent shear modulus, was fitted through the values determined

at each data point.  Quadratic equations for four curves, $E_{22}$, $v_{12}$, $G_{23}$, and $G^m$, referenced

to changes in composite $G_{12}$ and four curves, $E_{22}$, $v_{12}$, $G_{12}$, and $G^m$, referenced to changes

in composite $G_{23}$ were incorporated into the MCT_77 program.  An example of a

quadratic shear relationship is shown in Fig. 5.10.



$$y = -1.111E+00x^2 + 3.479E+00x + 5.915E-02$$
$$R^2 = 9.983E-01$$
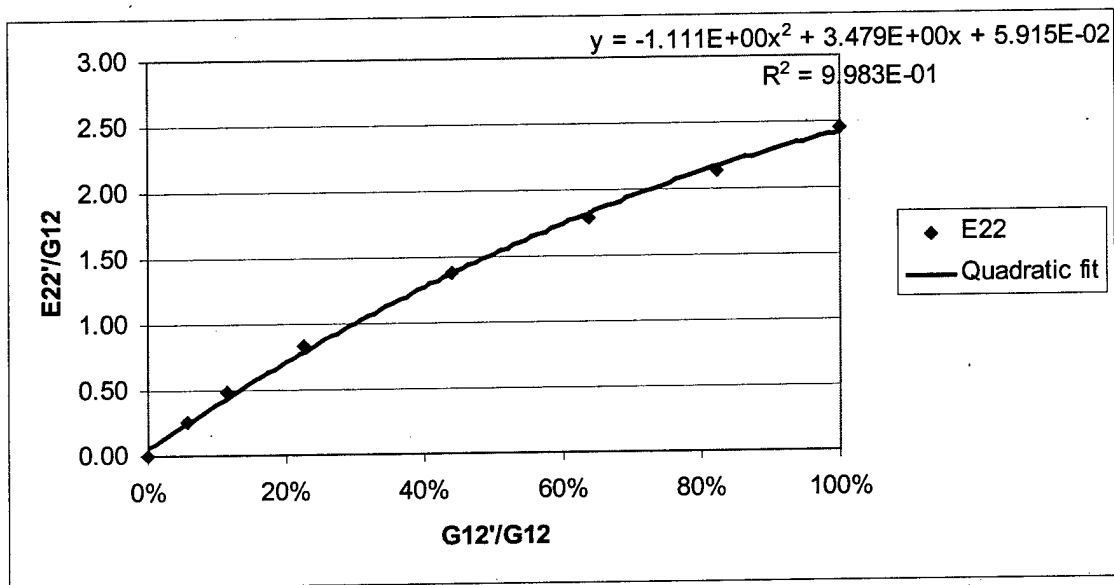
**Fig. 5.10** *$E_{22}$ as a function of change in $G_{12}$ for E-glass/8084.*

All quadratic curve fits of the micromechanical data were excellent, resulting in $R^2$ values

of 0.97 or better.  Appendix A contains the complete set of quadratic curve fits for

boron/epoxy, Appendix B for E-glass/vinylester, and Appendix C for carbon/epoxy composites used in this research.

### 5.4. Determining Constituent Ultimate Strengths

The MCT failure criterion developed previously required determining five failure parameters, $A_1{}^f$, $A_4{}^f$, $A_2{}^m$, $A_3{}^m$, and $A_4{}^m$. These parameters are functions of ultimate constituent strengths, $^{\pm}S_{11}{}^f$, $S_{12}{}^f$, $^{\pm}S_{22}{}^m$, $^{\pm}S_{33}{}^m$, $S_{12}{}^m$, and $S_{23}{}^m$. Constituent strengths were derived from experimentally determined composite lamina ultimate strengths. Determining which constituent precipitates composite failure is necessary for establishing accurate constituent failure values. Identifying the constituent that precipitates failure in longitudinal and transverse lamina tension and compression tests is intuitive and straightforward, i.e., fiber failure for longitudinal loads and matrix failure for transverse loads. Identifying the constituent leading to shear failure is more problematic, as non-catastrophic matrix and fiber damage begins well before ultimate composite strength is achieved [37]. Good initial values for constituent shear strengths could be obtained from an MCT analysis of experimentally determined ultimate composite shear strengths.

In an effort to more rigorously determine the ultimate constituent shear strengths, a procedure using nonlinear regression analysis of load cases involving shear was developed. Data from off-angle, balanced, symmetric laminates, $[\pm\theta]_s$, provided an excellent basis for determining optimized constituent failure parameters. These laminates produced varying degrees of combined shear and normal stresses and tended to fail in modes that allowed analytical identification of the constituent precipitating laminate

failure. Off-angle, unbalanced, laminates, $[+\theta]_n$ or $[-\theta]_n$ also produced varying shear and normal stresses but had to be used with caution because of non-uniform stress states caused by warping of the test specimen [24].

Using ultimate composite failure strengths for each off-angle laminate, MCT_77 calculated the constituents' transversely isotropic stress invariants at the experimentally determined point of composite failure. Next, the failure mode for each laminate tested was tentatively identified. As a general rule, composite failure is fiber dominated at lower fiber orientation angles (approximately 20° and less) and matrix dominated at higher fiber angles. Visually determining failure modes from test specimens is difficult, so it becomes more convenient to do analytically. As mentioned previously, good initial guesses for constituent ultimate shear strengths using MCT_77 can be derived from experimentally determined unidirectional lamina ultimate shear strengths or taken from the available literature. The data were sorted by failure mode (fiber or matrix). Using the failure criterion and nonlinear regression analysis, a best fit was determined for the failure parameter $A_3{}^m$ and $A_4{}^m$ for the matrix and $A_4{}^f$ for the fiber. After the first trial optimization, updated values for $A_3{}^m$, $A_4{}^m$, and $A_4{}^f$ were used to recheck the failure modes. If modes changed, another iteration was required. Once failure parameters were "tuned" to off-angle laminate results, MCT_77 failure analyses on more complicated composite structural laminates were conducted. Appendix E provides a detailed discussion of the optimization procedure used.

# SECTION 6.

# MCT_77 FINITE ELEMENT CODE

## *6.1. General Capabilities of MCT_77*

The goal of the research contained within this dissertation was to develop a finite-element-based tool for the failure analysis of practical composite structural laminates. To that end, a "building block" philosophy was used to develop the finite element software:

1.  Discretize ("mesh") the structure using standard FEA techniques and commonly available graphical software.
2.  Exercise judicious element choices. Three-dimensional solid elements are preferred in most cases because they produce a complete stress tensor. The three-dimensional capability penalizes the designer by requiring re-meshing of the structure with any changes in laminate thickness. Shell elements are overwhelming favored by designers because they allow element thickness to be specified without changing the original structural element mesh. Shell elements provide only five out of the six stress tensor components because they are formulated on a modified plane-stress assumption. The normal through-thickness stress, important in delamination, is assumed to be zero.
3.  Use a layering capability in each element to breakdown the composite laminate into individual lamina.
4.  Breakdown the lamina into constituents (fiber and matrix) using MCT.
5.  Conduct failure analysis at the constituent level where structural damage initiates.

MCT_77 is a conventional displacement-based, finite element code. What sets MCT_77 apart from other finite element codes is an implementation of Multicontinuum Theory allowing constituent stress and strain fields to be extracted from those of the composite material. Material behavior is limited to nonlinear elastic. Inelastic behavior due to damage is accommodated through a progressive failure algorithm. MCT_77 was written in FORTRAN 77 for maximum portability between computer platforms. The code was extensively commented and written in a modular fashion for readability and to facilitate

upgrades. Appendix F provides a detailed explanation of the MCT_77 program and its inputs.

6.1.1. Element Library

MCT_77 currently has a four-element library consisting of the following:

1. QUAD4: Four-node, two-dimensional, 2 degree-of-freedom (DOF), plane stress/strain, bilinear, isoparametric, quadrilateral element.
2. QUAD8: Eight-node, two-dimensional, 2 DOF, plane stress/strain, quadratic (serendipity) isoparametric, quadrilateral element.
3. BRICK8: Eight-node, three-dimensional, 3 DOF, trilinear, isoparametric hexahedral element.
4. SHELL8: Eight-node, two-dimensional, 5 DOF, modified plane stress, quadratic (serendipity), isoparametric shell element.

Currently, elements cannot be mixed within a MCT_77 analysis nor can they be degenerated to triangular or wedge shapes.

The linear elements, QUAD4 and BRICK8, have the option of "incompatible" (or "nonconforming") element formulations [38]. This formulation uses shape functions incorporating internal degrees-of-freedom permitting displacements to be discontinuous across adjacent element boundaries, hence, "incompatible". The formulation allows element boundaries to assume curved shapes in a manner similar to higher order quadratic elements but without the additional nodes and associated increase in computational and storage requirements. In the presence of shear, incompatible element formulation results in more stable element behavior and greater accuracy than regular linear elements.

All MCT_77 elements have the ability to model lamina layering. The user specifies total laminate thickness and number of lamina. Currently, MCT_77 assumes a constant lamina thickness. Formulation of lamina layer stiffness is the same as the element that contains it. SHELL8 element layers are under a modified plane stress assumption ($\sigma_{33}=0$) and use 2×2×2 (in-plane element $x$ direction by in-plane element $y$ direction by out-of-plane element $z$ direction) Gauss integration within each layer. QUAD4 and QUAD8 layers are under full plane stress assumption ($\sigma_{33}=\sigma_{13}=\sigma_{23}=0$) and use 2×2×1 Gauss integration within each layer. BRICK8 layers produce a full stress tensor and use 2×2×2 Gauss integration within each layer.

### 6.1.2. Boundary Conditions

MCT_77 is specifically designed to support boundary conditions that typically arise in structural analysis. MCT_77 supports any admissible combination of the following prescribed loads:

a) Nodal forces.
b) Uniform temperature.
c) Nodal temperatures.
d) Element pressures.
e) Body forces arising from translational or rotational accelerations.

MCT_77 supports any admissible combination of the following prescribed displacements:

a) Homogeneous nodal displacements.
b) Non-homogeneous nodal displacements.
c) Nodal constraint equations.

MCT_77 can apply loads and non-homogeneous nodal displacements as a single step or arbitrary ramp function. The incremental nature of ramping loads from zero to a target value lends itself to the nonlinear behavior characteristic of structural failure analysis.

Constraint equations implemented in MCT_77 allow the user to define complex relationships between degrees-of-freedom of different nodes. For example, constraint equations are useful in applying boundary conditions representing planes of symmetry. Constraint equations have the form:

$$C_1 * DOF_i^1 + C_2 * DOF_j^2 + \ldots + C_n * DOF_k^n = C$$

where $C_i$ are constants and $DOF_i^n$ are degree of freedom $i$ of node $n$. A simple constraint equation coupling the $x$ degrees-of-freedom of nodes 1 and 2 so they move together (equal magnitude) would look like

$$(1) * DOF_1^1 + (-1) * DOF_1^2 = 0.$$

## 6.2. ANSYS® Interfacing

A key component to a successful finite element analysis is the assimilation and interpretation of results by the user. Even a modest size analysis can result in a voluminous amount of data describing the distribution and intensity of field variables over the structural domain. Further, inputting a structure's geometry and developing a finite element mesh as a sequence of formatted numbers within a text file can be tedious and error prone.

It is beyond the scope of this, or perhaps any, structural research effort to attempt independent development of a visual simulation program when so many are commercially available. A more efficient approach is to write computer programs that function as an interface between finite element input and output information with that required by a commercially available visual simulation program.

To facilitate construction of finite element models for MCT_77 analyses, a translator, ANS2MCT, has been written allowing the designer to use pre-processing capabilities of the ANSYS® [39] finite element program to create the geometry and finite element mesh of the structure being analyzed. ANS2MCT converts ANSYS® database information to MCT_77 readable format. If requested, the MCT_77 code writes results files that can be read by ANSYS® for post-processing.

As shown in Figures 6.1-6.6, visualization can be especially useful in progressive failure analyses when specific color-coding designates damaged regions within a laminate. This allows the user to step through the load history and watch material failure initiate and propagate throughout the laminate. A user/designer can then modify the material architecture of the structure in a more precise manner tending to optimize the design goals of maximum structural strength or stiffness at minimum weight and cost. The color codes in Figures 6.2-6.6 use blue to indicate undamaged composite material, green to indicate composite damage due to matrix failure, and red to indicate composite damage due to fiber failure. Section 6.5 discusses an MCT based progressive failure analysis approach in detail.
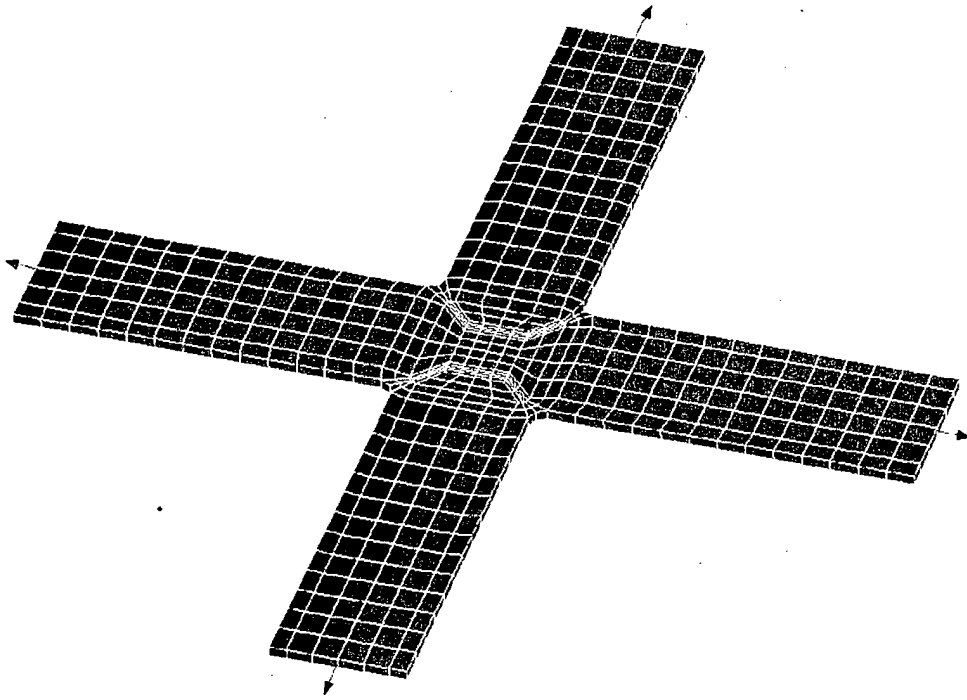
**Fig. 6.1** *FE idealization of a cruciform specimen under biaxial tension-tension load.*
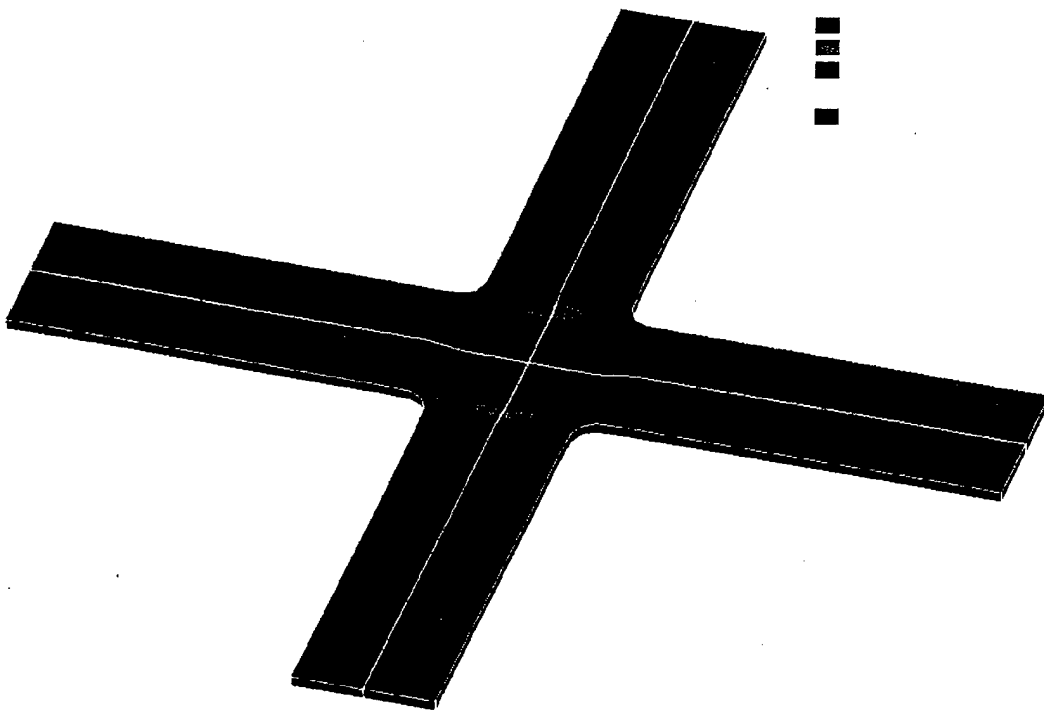


**Fig. 6.2** *Composite damage in the cruciform specimen at load step 9.*
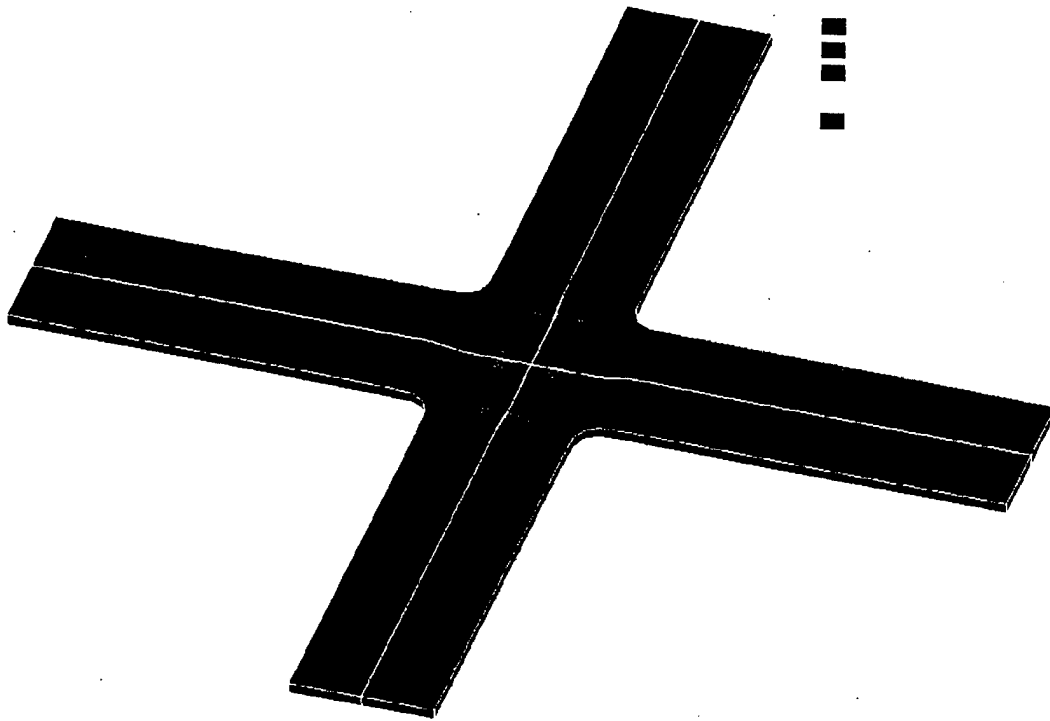
**Fig. 6.3** *Composite damage in the cruciform specimen at load step 10.*
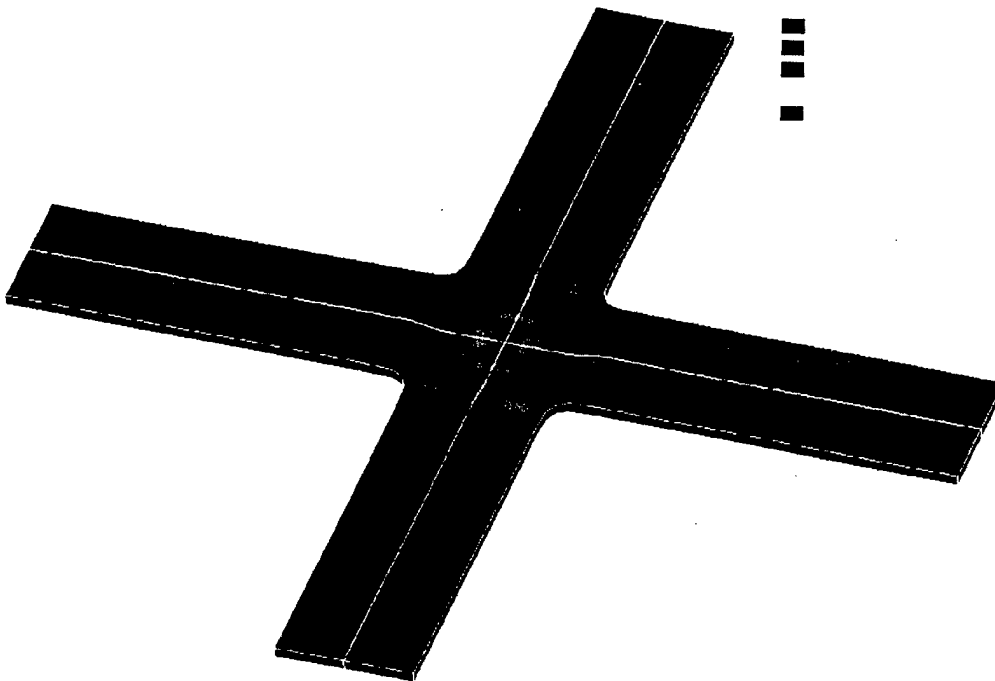


**Fig. 6.4** *Composite damage in the cruciform specimen at load step 22.*
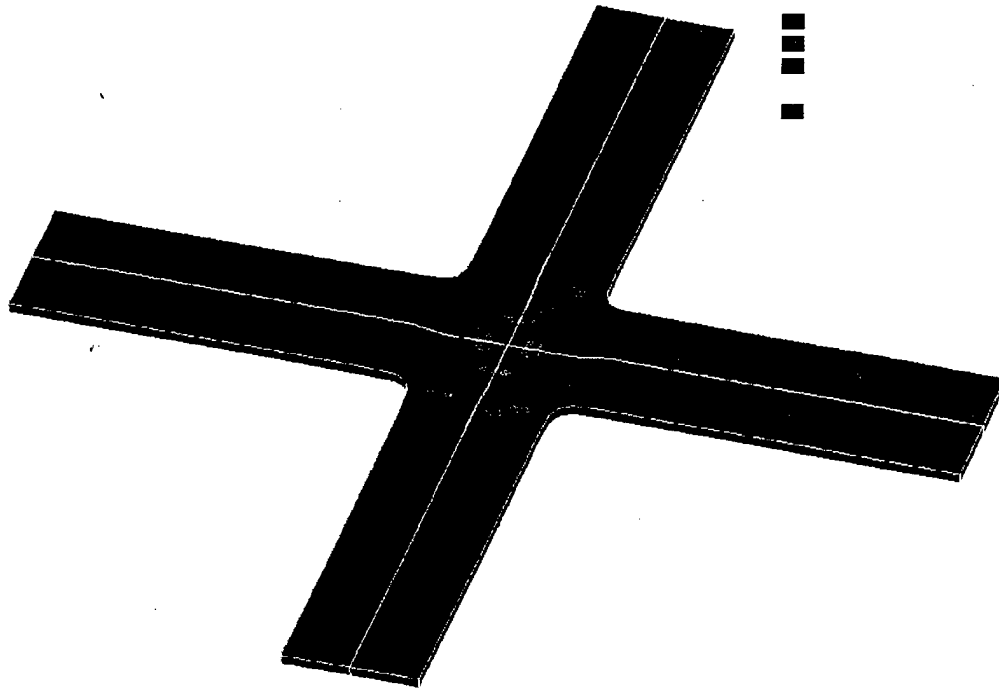
**Fig. 6.5** *Composite damage in the cruciform specimen at load step 23.*
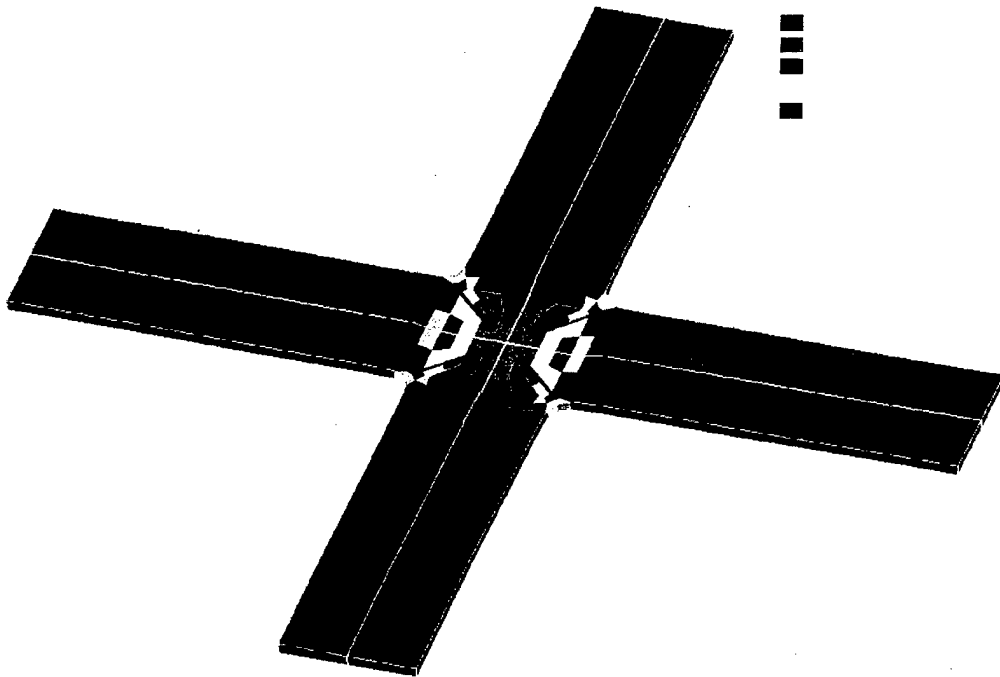


**Fig. 6.6** *Composite damage in the cruciform specimen at load step 24.*

## 6.3. Incorporation of Multicontinuum Theory

MCT equations, developed in Section 3, are implemented within the MCT_77 code in two subroutines. The first subroutine calculates the $[A]$ and $\{a\}$ (see equation 3.13) matrices for all composite materials defined by the user. The second subroutine extracts constituent strains from composite values and computes constituent stresses. Calculations within these routines follow their derivation and are applied in a straightforward manner.

For a linear elastic analysis in which material properties do not change, an MCT decomposition of composite strains and stresses could be accomplished in a single post-processing step. The brevity and simplistic character of the MCT specific subroutines offers the potential for a relatively quick and trouble-free incorporation as user-defined subroutines available as part of most commercial finite element codes. However, for nonlinear progressive failure analysis, complete integration of these subroutines with the bulk FEA code is computationally advantageous.

## 6.4. Nonlinear Constitutive Model for Changing Shear Properties

MCT_77 execution of the constitutive model developed in Section 5 requires the load to be applied as a step-wise ramp. When shear stresses are present, MCT_77 computes a composite tangent modulus from the appropriate shear stress–strain curve fit information. Using the tangent shear modulus, the remaining elastic constants for both composite and constituents are calculated from equations relating them to change in shear modulus (See

Figures A.6-A.9, B.7-B.14, and C.7-C.14). Element stiffness is recalculated based on updated material properties. A gradual softening of the structure causes a load equilibrium imbalance which is resolved by Newton-Raphson iterations as described in section 6.5. Once equilibrium is achieved, the process is repeated for subsequent load steps until the maximum load is reached.

Most of the nonlinear constitutive model is incorporated as an algorithm within a single MCT_77 subroutine. When an analysis incorporating nonlinear shear is requested, the algorithm is executed at every Gauss point within the structure. Executing a small collection of algebraic equations to produce macro- and micromechanical material data is several orders of magnitude faster than executing the micromechanics finite element model itself and produces virtually identical results.

## 6.5. Progressive Failure Analysis

In the finite element method, numerical integration samples stress, strain, and material values at Gauss quadrature or "material" points. There is a hierarchy to the material numbering in the MCT_77 finite element code that corresponds to severity of composite damage at a material point. Three composite material conditions or states, listed in increasing severity, are defined as:

1. Undamaged composite,
2. Composite damaged by matrix failure, and
3. Composite damaged by fiber failure.

There are four constituent states corresponding to the three composite damage states:

1. Intact fiber (composite states 1 and 2),
2. Failed fiber (composite state 3),
3. Intact matrix (composite states 1 and 3), and
4. Failed matrix. (composite state 2 and 3).

When either constituent fails, its moduli is reduced to a near zero value. Near zero values are used rather than zero to avoid numerical difficulties. Matrix moduli are reduced to 1% of their original value. Fiber moduli, which are typically one to two orders of magnitude larger than matrix moduli, are reduced by whatever percentage is required to bring damaged fiber values to the same magnitude as damaged matrix so that near zero stiffness values are the same for both constituents. In practice, a failed fiber constituent reduces the load carrying capacity of the composite so severely that it can be assumed that both constituents have failed. Since all constituent properties, both intact and failed, are known *a priori,* micromechanics can be used to determine damaged composite properties due to a failed constituent outside the MCT_77 program. Files defining damaged and intact composite and constituent elastic constants form input to the MCT_77 program as seven different material types: three composite and four constituent damage states.

A MCT_77 failure analysis requires the load to be incrementally applied. The composite material damage state at every Gauss point is stored for the entire analysis. Initially, composite material properties are set to a state 1 (undamaged) condition. At each load step, a damage algorithm, using the failure criteria formulated in Section 4, checks each Gauss point for constituent failure based on accumulative stresses. If constituent failure is detected, composite material properties are set to either state 2 or 3 and all stresses

(composite and constituent) at that Gauss point are set to zero. Gauss point stresses are recalculated using accumulated strains and updated material properties.

Implementation of the Tsai-Wu failure criterion within MCT_77 is a straightforward duplication of the MCT failure criterion implementation. Instead of examining constituent stress states, the program uses the composite stress state at each material point. If Tsai-Wu indicates composite failure, the material properties at that point are set to the most severe damage state (number 3).

After all Gauss points in the model have been checked for material failure and modified (if necessary), an internal (resisting) load vector is calculated. Gradual softening of the structure due to Gauss point material failures will cause an equilibrium imbalance between the applied (external) and internal load vectors. An iterative procedure within each load step calculates differences between external and internal load vectors, called the residual load vector, and applies it to the structure as a "virtual" load. The net effect is to increase nodal displacements. Hence, Gauss point strains and stresses increase until equilibrium is restored and the next load step is applied.

The general process outlined above is standard procedure for nonlinear finite element problems. Particular solution methods can be found in the literature [40] but the most common methods are the Newton-Raphson and Modified Newton-Raphson. The Newton-Raphson method recalculates the global stiffness matrix each time there is a change in material properties of the structure. Formulating the global stiffness matrix is

the single most time consuming task within the finite element method. MCT_77 uses the Modified Newton-Raphson method which recalculates the global stiffness matrix only at the beginning of a load step and reuses it during subsequent equilibrium iterations. Reusing the global stiffness matrix requires more iteration for equilibrium but results in significant timesaving.

Equilibrium is achieved when a ratio of the Euclidean ($L^2$) norms of the residual-to-accumulated external load vectors is less than a prescribed tolerance

$$\frac{\left(\sum R_i^2\right)^{\frac{1}{2}}}{\left(\sum P_i^2\right)^{\frac{1}{2}}} \leq \text{FTOL} \quad i = 1, \text{total DOF}. \tag{6.1}$$

MCT_77 allows user specified FTOL values but typically values on the order of $10^{-3}$ ($10^{-4}$ is default) provide sufficient accuracy.

Structural failure is defined as that point in the load history when the structure can no longer support the accumulated load and deflections begin to grow without bound. Unbounded growth is detected during equilibrium iterations by measuring the percentage change in the Euclidean norm of subsequent displacement vectors referenced to the norm of the first iteration displacement vector. The measure, taken within a load step, is given by

$$\left|\frac{\left(\sum \Delta D_1^2\right)^{\frac{1}{2}} - \left(\sum \Delta D_i^2\right)^{\frac{1}{2}}}{\left(\sum \Delta D_1^2\right)^{\frac{1}{2}}}\right| \leq \text{DTOL}, \tag{6.2}$$

where *i* varies from two to the maximum number of iterations. MCT_77 allows user-specified DTOL values but typically values around 7.0 (the default) stop the program before numeric singularities generate fatal execution errors.

A flow chart for an MCT_77 progressive failure analysis is shown in Fig. 6.7.
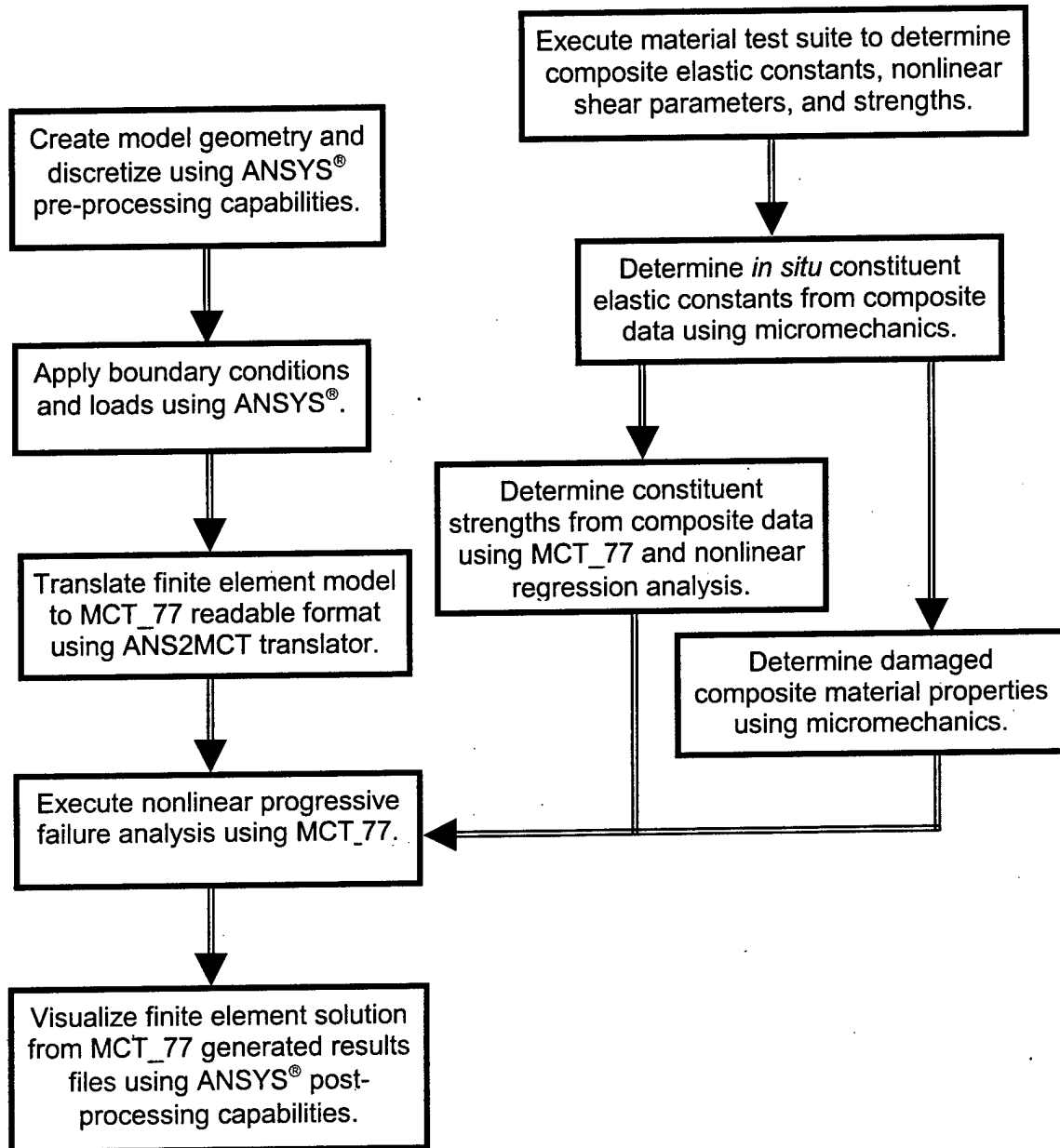


**Fig 6.7** *Flow chart for an MCT_77 Progressive failure analysis.*

# SECTION 7.

# COMPARISON OF ANALYSIS VERSUS EXPERIMENT

## *7.1. Overview*

In this section, results from MCT_77 failure analyses are compared against experimental data of laminates fabricated from three different materials and tested under uniaxial or biaxial load conditions. Stress-strain curves are used to qualify MCT_77's ability to simulate laminate structural behavior. As mentioned in Section 4, the Tsai-Wu criterion is the most widely used stress-interactive failure prediction methodology. Hence, it was considered in this research as state-of-the-practice and used in conjunction with experimental data to benchmark the accuracy of MCT failure predictions.

## *7.2. Uniaxial Loading*

### 7.2.1. Boron/5505 Composite

Experimental stress-strain curves for laminate specimens fabricated from boron/5505 (boron/epoxy) composites were digitized from figures published by Petit and Waddoups [41]. The authors note that the stress-strain curves presented were based on a single test; hence, there was no statistical basis for the results. MCT_77 results are based on constitutive material properties backed out via micromechanics from experimental data as reported in Appendix A.

Ten laminates of different architectures were tested under uniaxial tension, uniaxial compression, or both. Stress-strain graphs for all laminates tested by Petit and Waddoups are included in Appendix A. Only a few of the more interesting results are discussed here.
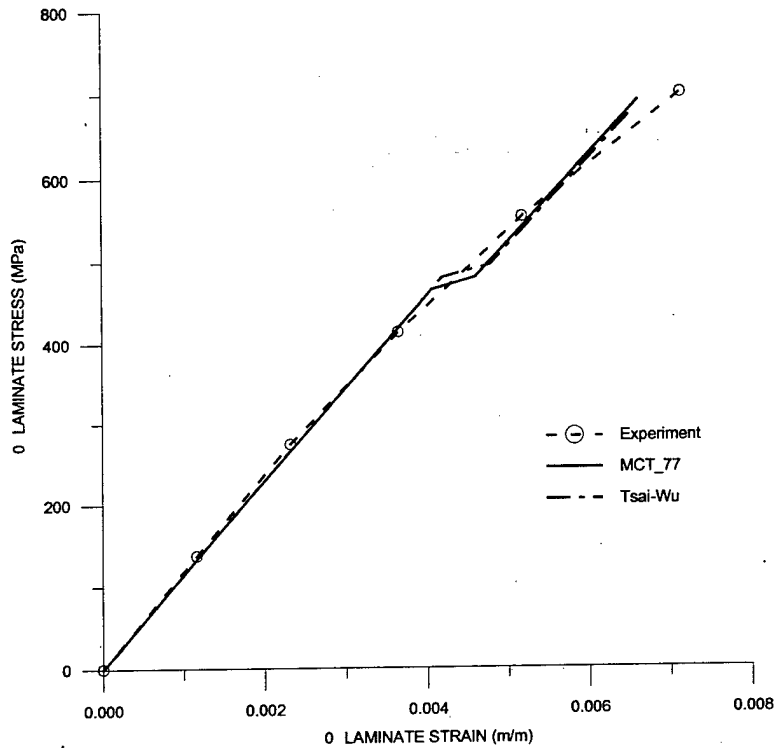


**Fig. 7.1** *Boron/5505 [0/90]$_S$ laminate under uniaxial tension.*

Fig. 7.1 presents the experimentally and analytically simulated stress-strain behavior of a [0/90]$_S$ laminate. Analytically, the matrix in the laminate's 90° plies experienced tensile failure at approximately 500 MPa but the laminate continued to load without significant loss in stiffness to approximately 700 MPa. The experimental data appear to support this scenario with initially linear behavior transitioning to nonlinear behavior at approximately 400 MPa due conceivably to matrix damage. MCT and Tsai-Wu laminate strength predictions were almost identical and within 1% of the experimental value.
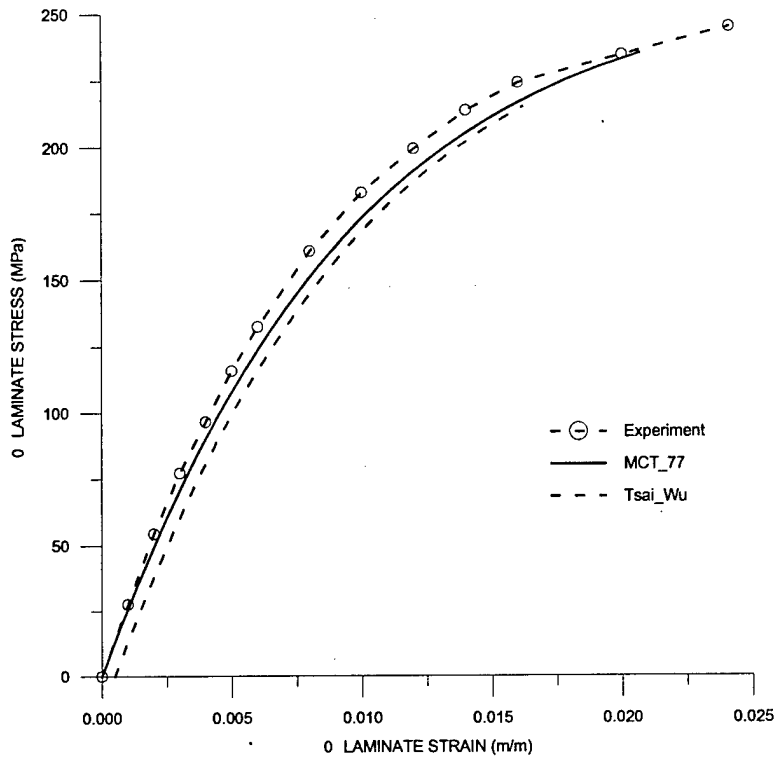
**Fig. 7.2** *Boron/5505 [±45]_S laminate under uniaxial tension.*

In Fig. 7.2, MCT_77 captured the highly non-linear response of a [±45]_S laminate and predicted an ultimate failure load within 1% of the experimental value. Tsai-Wu failure prediction was within 10%. The Tsai-Wu curve follows the MCT curve identically up to failure and is offset for clarity. MCT analysis indicated laminate failure was precipitated by matrix tensile failure.

Currently, MCT_77 can accommodate only one modulus per direction, i.e.; it cannot differentiate between tensile and compressive moduli. The boron/5505 lamina compressive Young's modulus (227 GPa) was approximately 10% higher than the tensile Young's modulus (207 GPa). MCT_77 material behavior was based on the tensile Young's modulus hence the stress-strain curves in analyses of all compressive tests were

more compliant than those of the experimental data. In practice, an average of the tensile

and compressive moduli values could be used without a significant decrease in analysis

accuracy.
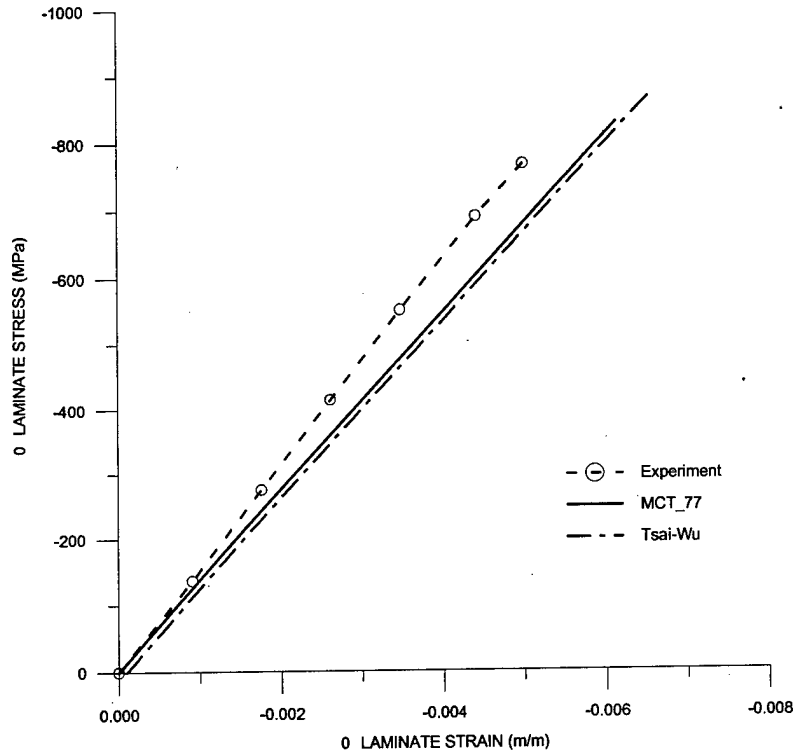


**Fig. 7.3** *Boron/5505 [±20]ₛ laminate under uniaxial compression.*

The [±20]ₛ laminate, shown in Fig. 7.3, experienced a linear response throughout the

compressive load. Analytically, MCT predicted laminate failure due to matrix *tensile*

rupture. MCT predicted a laminate failure load within 12% and Tsai-Wu within 17% of

the experimental result. Again, the Tsai-Wu curve is offset for clarity.
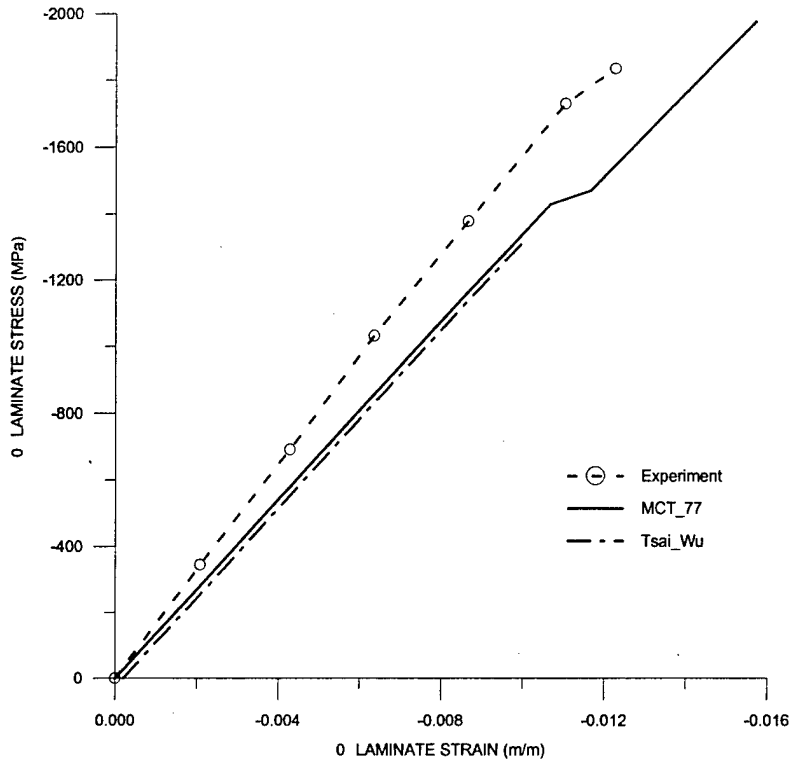
**Fig. 7.4** *Boron/5505 [(0)₃/±45]ₛ laminate under uniaxial compression.*

The [(0)₃/±45]ₛ laminate, shown in Fig. 7.4, experienced linear response throughout the load. The MCT matrix failure criterion does not allow for matrix failure in the fiber direction but the analysis indicated transverse tensile matrix failure in the 0° plies at approximately 75% of the ultimate load due to a Poisson effect. Any indication of matrix failure in the experimental data appeared near ultimate load. Ultimate laminate failure occurred when fibers in the 0° plies ruptured. MCT ultimate failure load prediction was within 10% of the experimental value. The Tsai-Wu prediction was off by 26% of the experimental value because it coincides with transverse lamina (matrix) failure in the 0° plys. The Tsai-Wu curve is offset from the MCT curve for clarity.

A summary of MCT and Tsai-Wu failure predictions for the boron/5505 laminates considered is presented in Table 7.1. A measure of predictive accuracy or "modeling bias" is calculated as (predicted failure value/experimentally determined value). Scatter in the data is measured as the coefficient-of-variation (COV) about a mean value and is calculated as ((mean value/standard deviation) × 100).

**Table 7.1** *Summary of failure loads for boron/5505 laminates.*

| Laminate | Exp | MCT/Exp | Tsai-Wu/Exp |
|----------|-----|---------|-------------|
| [0/90]s C | -1814 | 0.92 | 0.92 |
| [0/90]s T | 699 | 1.01 | 0.99 |
| [±20]s C | -766 | 1.12 | 1.17 |
| [±20]s T | 927 | 1.16 | 1.32 |
| [±30]s C | -307 | 1.32 | 1.32 |
| [±30]s T | 664 | 0.97 | 0.99 |
| [±45]s T | 245 | 1.00 | 0.90 |
| [±60]s C | -397 | 0.63 | 0.66 |
| [±60]s T | 122 | 0.93 | 0.86 |
| [0₃/±45]s C | -1833 | 1.10 | 0.74 |
| [0₃/±45]s T | 941 | 0.98 | 1.20 |
| [0/90/±45]s T | 497 | 1.02 | 0.82 |
| [0/±60]s T | 499 | 1.04 | 0.97 |
| [65₃/20/-70]s T | 136 | 1.47 | 1.47 |
| [90₃/±45]s T | 138 | 1.13 | 1.19 |
| | Avg = | 1.05 | 1.03 |
| | COV = | 17.9% | 22.6% |

Table 7.1 shows there is a significant amount of scatter in both failure predictions for the boron/5505 uniaxial load cases. This scatter prevents a statistically meaningful comparison between MCT and Tsai-Wu criterion for failure prediction accuracy. The large COVs result from both the lack of an experimentally determined failure value representative of the data sets due to using only one data point per test and inaccuracies in

the failure criteria. It is statistically significant, however, that the Tsai-Wu criterion produced greater scatter about the mean average value than MCT.

## 7.2.2. E-glass/8084 Composite

Stress-strain curves for laminate specimens fabricated from E-glass/8084 (glass/vinylester) composites were experimentally determined by the University of Wyoming's Composite Materials Research Group from laminates provided by Seemann Composites Inc.

MCT_77 results were based on constitutive material properties backed out via micromechanics from experimental data based on at least five samples per test. Material properties used in the analysis are discussed in Appendix B. E-glass/8084 lamina had essentially the same modulus values in tension and compression. Ten laminates of different architectures were tested under uniaxial tension, uniaxial compression or both. Stress-strain graphs for all the E-glass/8084 laminates tested are included in Appendix B. A limited number of results are discussed here.

Seven unidirectional lamina with increasing fiber angle, relative to the direction of the applied tensile load, were tested to develop data for failure criteria optimization. Agreement between MCT failure predictions and off-angle tension test results, shown in Fig. 7.5, was excellent and can be attributed to self-consistency of failure parameters generated by the optimization procedure discussed in Section 5. Agreement between Tsai-Wu predictions and test results was also excellent and can be attributed to the nature

of the off-axis test in which any failure, matrix or fiber, results in catastrophic failure of the composite.
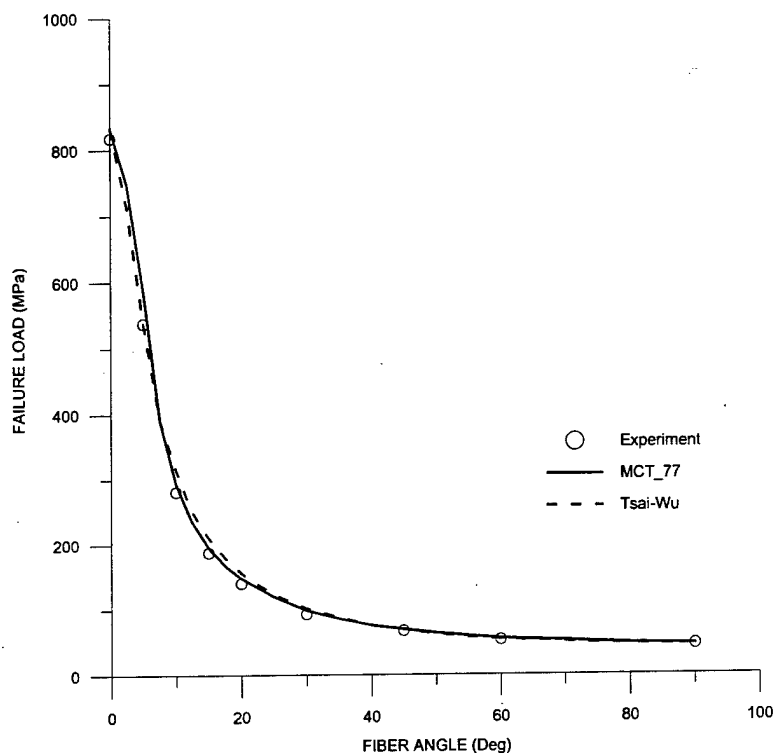


**Fig. 7.5** *Off-angle E-glass/8084 lamina under uniaxial tension.*

Fig. 7.6 shows the stress-strain response for a [0/90]$_s$ laminate. Analytically, both MCT and Tsai-Wu indicated tensile failure in the 90° plies at approximately 100 MPa. The laminate continued to load without a significant loss in stiffness to approximately 350 MPa. As with the boron/5505 [0/90] laminate, the MCT analysis indicated transverse tensile matrix failure in the 0° plies near the ultimate load due to a Poisson effect. Both MCT and Tsai-Wu predict catastrophic laminate failure after tensile rupture of the 0° plies. MCT under-predicted laminate strength by 3% and Tsai-Wu over-predicted laminate strength by 11% of the experimental value.
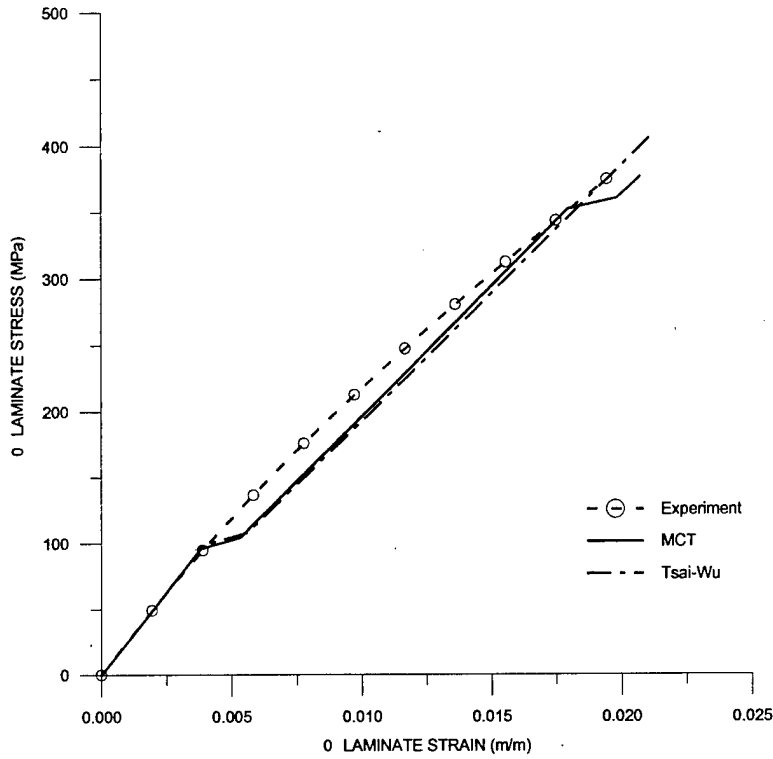
**Fig. 7.6** *E-glass/8084 [0/90]$_S$ laminate under uniaxial tension.*
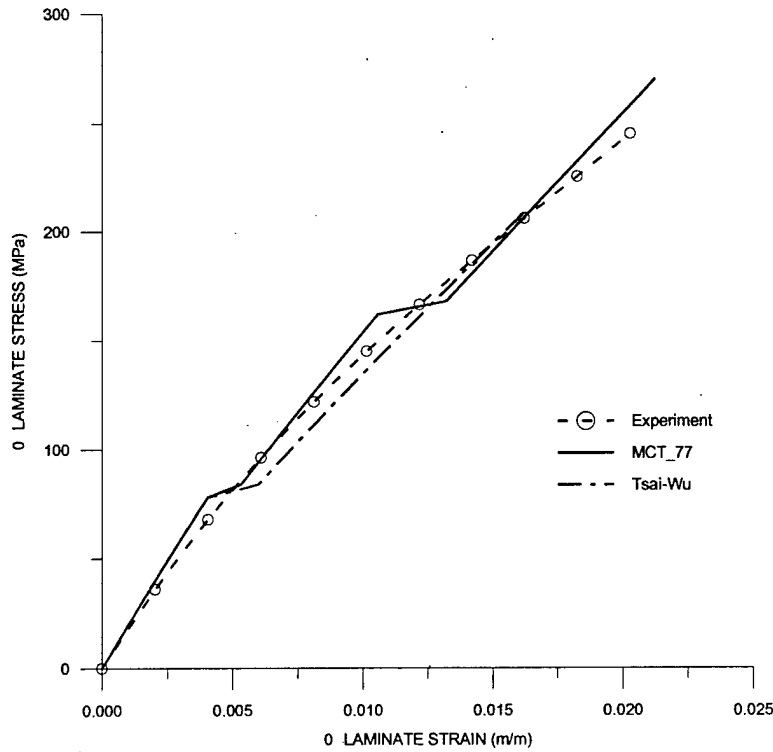


**Fig. 7.7** *E-glass/8084 [0/90/±45]$_S$ laminate under uniaxial tension.*

The quasi-isotropic [0/±45/90]s laminate, shown in Fig. 7.7, had a tensile load response reminiscent of that seen in the [0/90]s laminate as matrix tensile failure occurred analytically in the 90° plies at approximately 80 MPa. Additional matrix tensile failure in the ±45° plies was predicted prior to catastrophic tensile fiber failure in the 0° plies. Tsai-Wu predicted only tensile failure in the 90° plies. MCT and Tsai-Wu stress-strain results were in excellent agreement with experimental data and predicted ultimate failure loads within 13% of the experimental value.
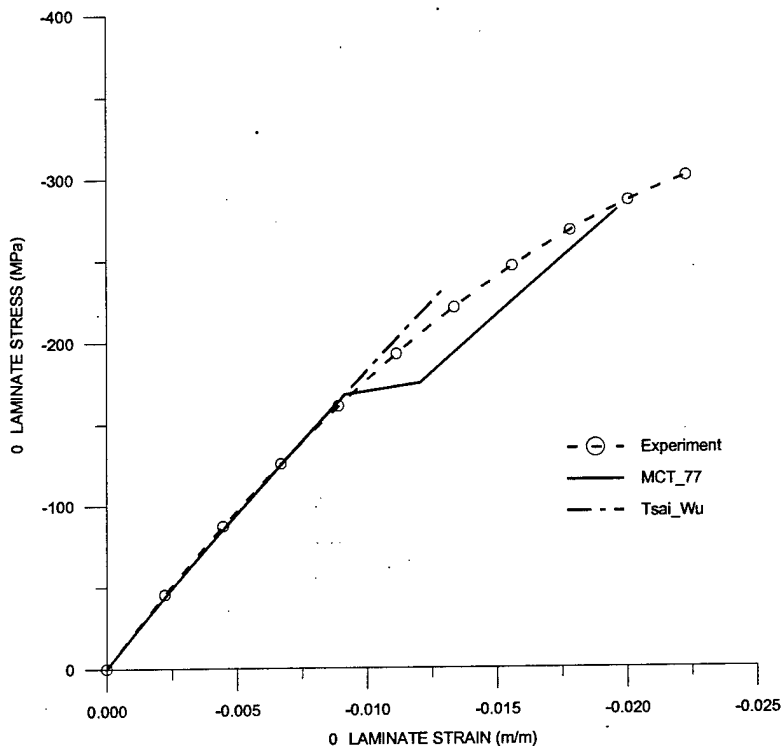


**Fig. 7.8** *E-glass/8084 [0/90/±45]s laminate under uniaxial compression.*

The quasi-isotropic [0/±45/90]s laminate, shown in Fig. 7.8, had a linear compressive load response to about -180 MPa. At that point both the MCT analysis and the nonlinear behavior of the experimental data suggested matrix compressive failure initiated in the

90° plies. The Tsai-Wu prediction was linear to a failure load 21% below the experimental value. MCT predicted an ultimate load 5% below the experimental value.

A summary of MCT and Tsai-Wu failure predictions for the E-glass/8084 laminates analyzed is presented in Table 7.1. There is significantly less scatter in the failure predictions than those seen in the boron/5505 results. This difference can be partly attributed to the improved statistical representation of the experimental failure loads achieved by averaging five data points per case. MCT and Tsai-Wu produced the same mean values for the E-glass/8084 uniaxial load cases with Tsai-Wu again producing significantly more scatter in failure prediction accuracy.

**Table 7.2** *Summary of failure loads for E-glass/8084 laminates.*

| Laminate | Exp | MCT/Exp | Tsai-Wu/Exp |
|---|---|---|---|
| [0/90]$_S$ C | -381 | 1.01 | 1.01 |
| [0/90]$_S$ T | 374 | 1.03 | 1.11 |
| [0/90/±45]$_S$ C | -301 | 0.95 | 0.79 |
| [0/90/±45]$_S$ T | 245 | 1.13 | 0.88 |
| [±45]$_S$ C | -110 | 0.95 | 0.98 |
| [±45]$_S$ T | 100 | 0.96 | 1.05 |
| [5]$_N$ T | 537 | 1.09 | 1.01 |
| [10]$_N$ T | 281 | 1.05 | 1.12 |
| [15]$_N$ T | 187 | 1.04 | 1.12 |
| [20]$_N$ T | 140 | 1.06 | 1.11 |
| [30]$_N$ T | 93 | 1.06 | 1.10 |
| [45]$_N$ T | 67 | 1.04 | 1.04 |
| [60]$_N$ T | 53 | 1.06 | 1.02 |
| | Avg = | 1.03 | 1.03 |
| | COV = | 5.1% | 9.6% |

### 7.2.3. AS4/3501 Composite

Failure data for laminate specimens fabricated from AS4/3501 (carbon/epoxy) composites were experimentally determined in previous research projects conducted by the Composite Materials Research Group. Fourteen laminates of different architectures were tested under either uniaxial tension or compression. Stress-strain curves were not available for most of the AS4/3501 laminates tested. The two curves that were available were digitized and presented here. MCT_77 results were based on constitutive material properties backed out via micromechanics from experimental data based on at least five samples per test. Material properties used in the analysis are discussed in Appendix C. AS4/3501 lamina have essentially the same modulus values in tension and compression.
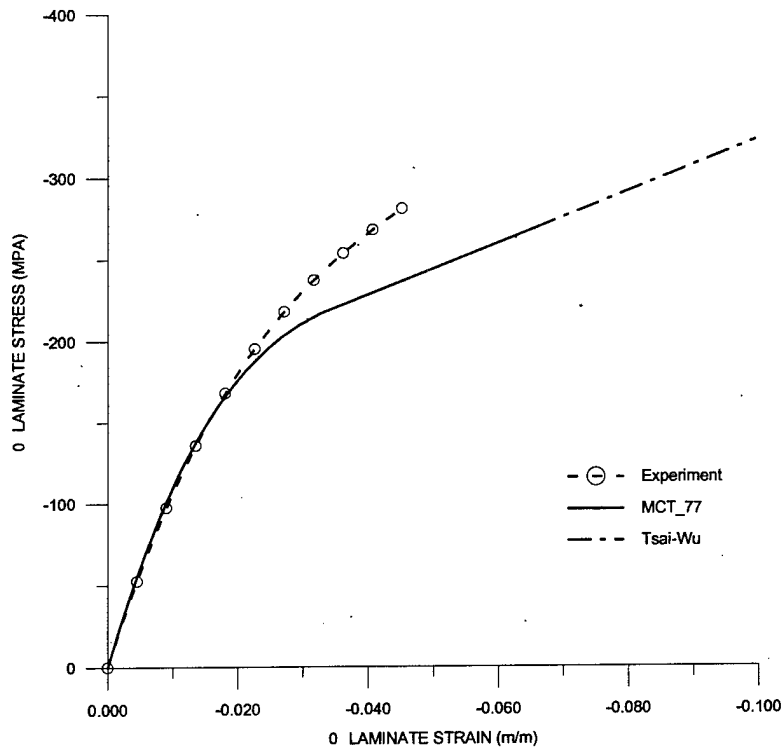


**Fig. 7.9** *AS4/3501 [±60]ₛ laminate under uniaxial compression.*

The [±60]$_S$ laminate, shown in Fig. 7.9, initially had a near linear load response to the applied compressive load. At approximately -175 MPa, the analytical simulation went nonlinear due to significant levels of shear stress which appear to be supported by the experimental data. The MCT curve assumed a linear stress-strain response above –0.04 shear strain because shear strain levels exceeded the stored shear stress strain curve data. MCT used the last positive tangent shear modulus calculated from the stored shear stress-strain curve to complete the applied load. MCT over-estimated the strain response by over 70% but estimated the failure load within 3% of the experimental data. Tsai-Wu was within 14%. No composite damage was detected until compressive failure of the fibers precipitated ultimate laminate failure.
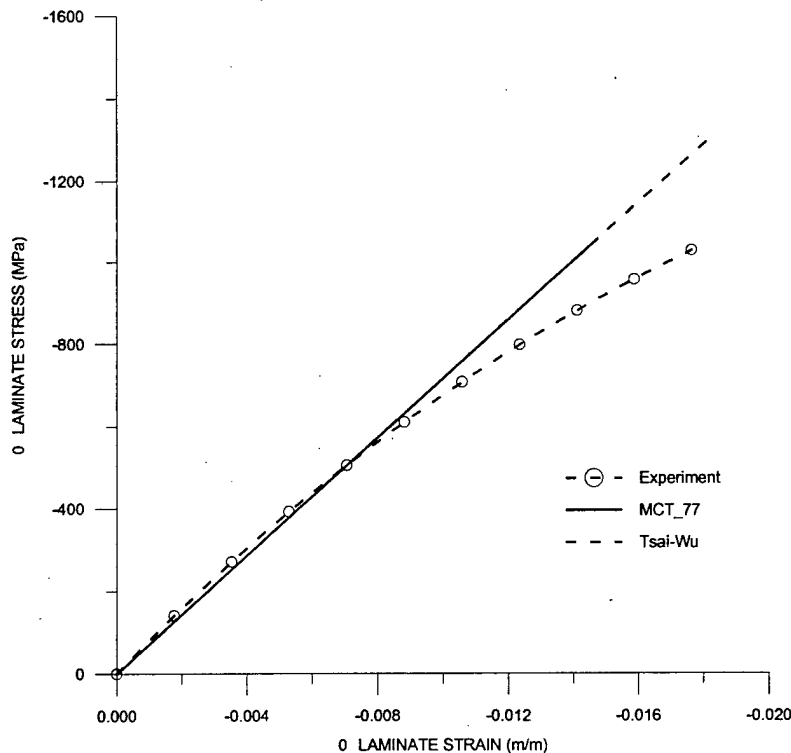


**Fig. 7.10** *AS4/3501 [0/90]$_S$ laminate under uniaxial compression.*

The experimental $[0/90]_S$ cross-ply laminate data, shown in Fig. 7.10, was slightly nonlinear because high matrix compressive strength allowed nonlinear matrix behavior to manifest itself in the 90 plies (see lamina transverse compression stress-strain curve in Fig. C.4). MCT_77 assumed linear transverse compression behavior but still predicted a failure load within 1% of the experimentally determined value. The Tsai-Wu failure prediction was off by 26%.

**Table 7.3** *Summary of failure loads for AS4/3501 laminates.*

| Laminate | Exp | MCT/Exp | Tsai-Wu/Exp |
|---|---|---|---|
| $[\pm 15]_S$ T | 786 | 1.40 | 2.80 |
| $[\pm 22]_S^*$ T | 786 | 1.01 | 2.02 |
| $[\pm 30]_S$ T | 455 | 1.00 | 2.05 |
| $[\pm 45]_S$ T | 155 | 0.95 | 1.08 |
| $[\pm 60]_S$ C | -288 | 0.97 | 1.14 |
| $[\pm 60]_S$ T | 74 | 1.16 | 0.73 |
| $[\pm 75]_S$ T | 43 | 1.02 | 0.77 |
| $[90/0]_{3S}$ C | -1074 | 1.01 | 1.26 |
| $[(\pm 45/0_2)_2/90]_S$ C | -1074 | 1.03 | 0.67 |
| $[\pm 45/0/90]_{2S}$ C | -855 | 0.91 | 0.69 |
| $[\pm 45_2/0_3/\pm 45]_S$ C | -827 | 0.94 | 0.44 |
| $[\pm 45_2/0_3/90_2]s$ C | -746 | 1.22 | 0.97 |
| $[\pm 45_2/90/0]s$ C | -753 | 0.83 | 0.53 |
| $[\pm 45_2/90_3/0_2]s$ C | -599 | 1.20 | 1.02 |
| Avg = | | 1.05 | 1.15 |
| COV = | | 14.3% | 58.8% |

A summary of MCT and Tsai-Wu failure predictions for the AS4/3501 laminates analyzed is presented in Table 7.3. The table shows MCT produced a 78% improvement in failure prediction accuracy over Tsai-Wu in average absolute differences. This was a much greater accuracy improvement than that seen for boron/5505 (32%) or E-glass/8084 (38%). The source of this difference is not clear, but it should be noted that both boron

and E-glass are isotropic fibers whereas AS4 carbon is anisotropic. Further, the boron/5505 and E-glass laminates had low fiber volume fractions (~50%), whereas the AS4/3501 laminates had a significantly higher fiber volume fraction (~67%).

## 7.3. Biaxial Loading

Arguments can be made that most composite structures typically operate under multi-axial load states, hence testing composite laminates under such conditions would be the prudent course of action. Unfortunately, triaxial or biaxial load tests of composite laminates are considerably more difficult to accomplish than uniaxial load tests. There is an order-of-magnitude increase in the complexity of both the test frames which apply the load and the design and fabrication of laminate test specimens. As a result, there is a paucity of multi-axial experimental failure data to verify analysis. Welsh [42] designed and fabricated a next-generation triaxial test frame and experimentally developed biaxial (tension-tension and tension-compression) failure surfaces for AS4/3501 [0/90]$_s$ laminates. The experimentally determined biaxial failure data along with two dimensional failure surfaces developed using MCT and Tsai-Wu failure criteria are shown in Fig. 7.11. The failure surface generated by the MCT failure criterion and the experimental data were in excellent agreement. The failure surface generated by the Tsai-Wu failure criteria was not.
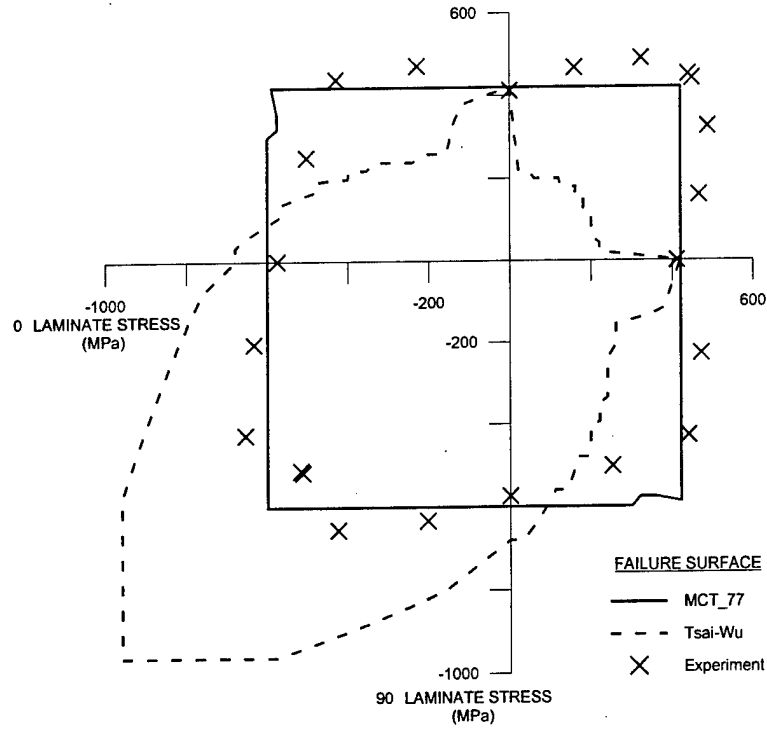
**Fig. 7.11** *AS4/3501 [0/90]$_S$ laminate biaxial failure envelopes for combined 0-90 loading.*
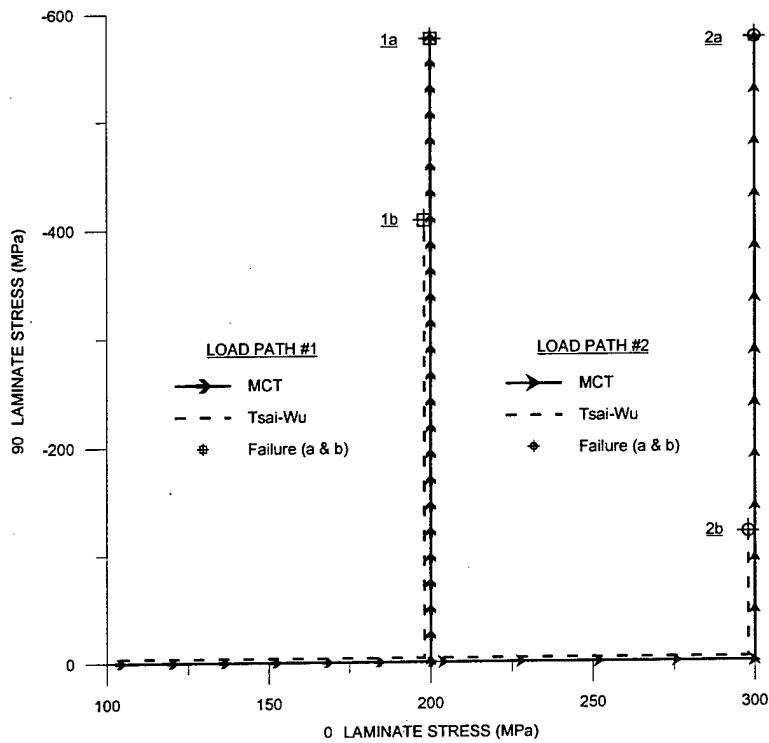


**Fig. 7.12** *Two load paths for a AS4/3501 [0/90]$_S$ laminate in quadrant IV of Fig. 7.11*

Lack of accuracy in Tsai-Wu predictions can be attributed to two fundamental problems. The first can be illustrated by examining two load paths, shown in Fig. 7.12 occurring in quadrant IV of two-dimensional stress space. On leg one of load path #1, a 200 MPa tensile load is applied to the laminate in the 0° direction. Holding the 200 MPa load constant, the second leg of the load path applies a 600 MPa compressive load in the 90° direction until compressive fiber failure occurs. Load path #2 is identical to #1 except the magnitude of the first leg is increase from 200 MPa to 300 MPa. Tsai-Wu now detects tensile failure of the 90° plies and reduces the composite material stiffness and subsequent load carry capability to near zero. When leg two of load path #2 is applied to the 90° plies, for the Tsai-Wu case there is no structural resistance, displacements grow without bound, and failure is declared.

The MCT failure criterion also detects tensile failure in the 90° plies during the first leg of path #2, but determines only matrix failure has occurred. Composite material properties are reduced to account for macro-damage due to matrix failure. However, the reduced composite properties retain the undamaged fiber's ability to sustain load. When leg two load is applied, the laminate continues to load, in a manner almost identical to path #1, until compressive fiber failure occurs. An inability of the Tsai-Wu criterion to differentiate between minor (matrix) and major (fiber) constituent damage overly penalizes any simulation of a laminate's load carrying capability.

A second shortcoming in the Tsai-Wu criterion is found in the failure parameters $F_1$-$F_3$ and $F_{11}$-$F_{33}$ (see Section 4.1). Their development results in an questionable dependence

of failure predictions in the purely compressive quadrant III region of stress space on *tensile* strength properties and vise-versa for the purely tensile quadrant II. Lamina strengths are clearly dependent on the tensile or compressive nature of the applied load and its orientation relative to the composite's constituents. The effort to develop a single smooth and continuous failure surface, while convenient, is simply too constraining. A single, smooth curve cannot adequately account for the variety of failure modes arising from radical strength differences between constituents and significant tension and compression strength differences within each constituent.

Significant differences in tensile and compressive longitudinal and transverse strengths (831 and −1079 longitudinal and 28 MPa and −282 MPa transverse respectively) for AS4/3501 lamina and the assumption of developing a smooth surface result in the skewed Tsai-Wu failure surface of quadrants I and III. This effect is somewhat mitigated for [0/90]$_S$ E-glass/8084 laminates, shown in Fig. 7.13, where tensile and compressive longitudinal and transverse strengths (818 and −759 longitudinal and 45 MPa and −144 MPa transverse respectively) are closer together. Interestingly, Tsai-Wu and MCT failure surfaces for a [0/90]$_S$ laminate under combined in-plane shear and normal loading, shown in Fig. 7.14, are virtually identical.

Failure surfaces for quasi-isotropic, [0/90/±45]$_S$, E-glass/8084 laminates under normal-normal and normal-shear loading are shown in Fig. 7.15 and Fig. 7.16 respectively. Currently there are no experimental data to verify these surfaces.
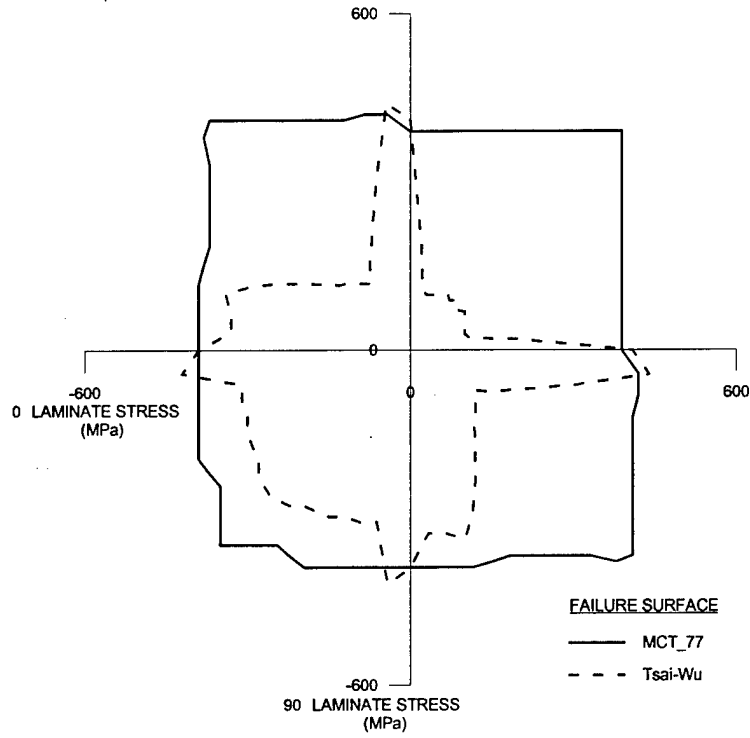
**Fig. 7.13** *E-glass/8084 [0/90]ₛ laminate biaxial failure envelopes for combined 0-90 loading.*
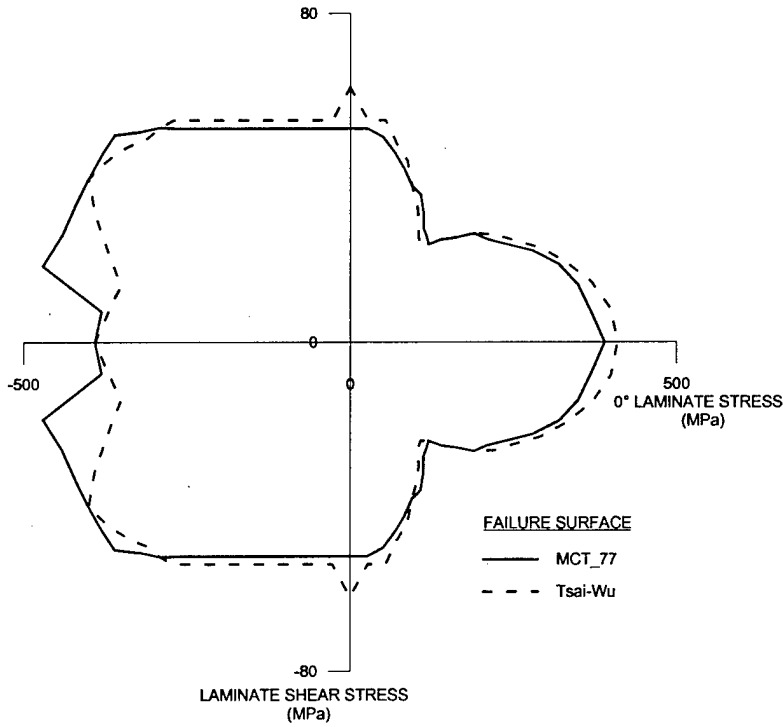


**Fig. 7.14** *E-glass/8084 [0/90]ₛ laminate biaxial failure envelopes for combined 0-Shear loading.*
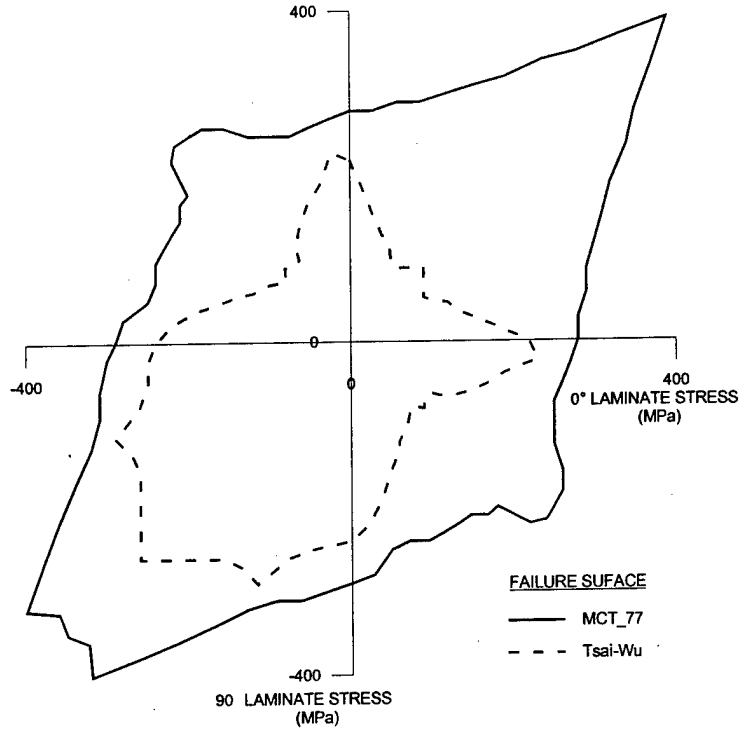
**Fig. 7.15** *E-glass/8084 [0/90/±45]s laminate biaxial failure envelopes for combined 0-90 loading.*
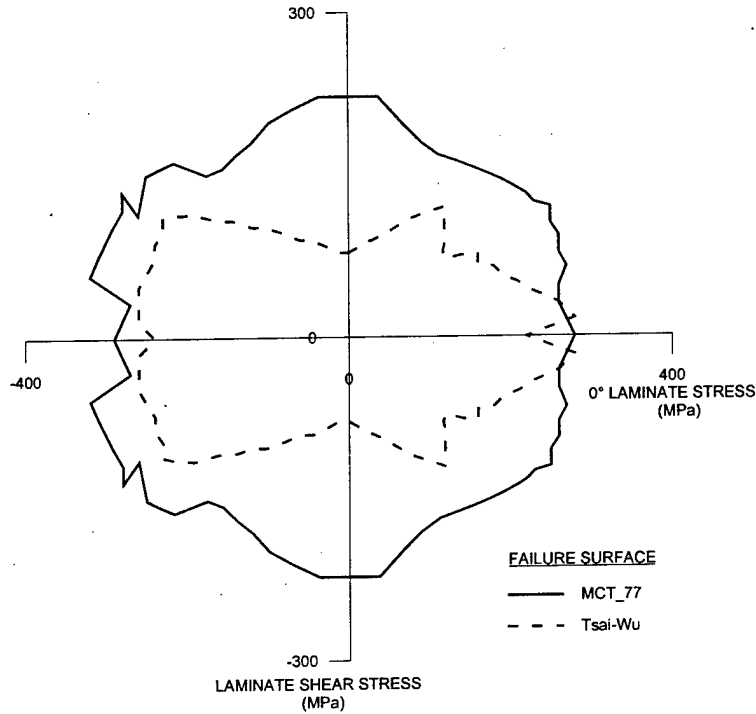


**Fig. 7.16** *E-glass/8084 [0/90/±45]s laminate biaxial failure envelopes for combined 0-Shear loading.*

# SECTION 8.

# SUMMARY AND RECOMMENDATIONS

## 8.1. Summary

The purpose of the research documented herein was to develop a finite element based analysis tool for predicting failure in composite structural laminates. Multicontinuum Theory provided the theoretical framework with which to accomplish this goal. Using constituent stress information provided by MCT, a constituent-based stress-interactive failure criterion was proposed. The failure criterion, functionally identical to the Tsai-Wu and Hashin criteria, results in a continuous but not smooth failure surface for a composite laminate by recognizing tensile and compressive failure modes unique to each constituent.

When benchmarking the MCT failure criterion against the Tsai-Wu criterion and experimental data, MCT resulted in a significant improvement in average absolute differences between predicted and experimentally determined laminate failure strengths for all the uniaxial load cases considered. There were large standard deviations in the results which are characteristic of composite failure phenomena. Although using MCT resulted in significant improvements in prediction precision over Tsai-Wu in uniaxial load cases, their differences became even more apparent in the analysis of biaxial load cases. For the single set of experimental biaxial data available, the MCT-generated failure surface was in excellent agreement while the Tsai-Wu generated surface was not. Further, the Tsai-Wu failure surface was neither consistently conservative nor un-

conservative when compared to the experimental data, which is unacceptable in structural design. Since MCT failure methodology has been shown to be successful using three dimensional constituent stress fields derived from uniaxial and biaxial tests, there is good reason to believe that it will also be successful in failure predictions involving three-dimensional load cases. Increased failure prediction confidence, provided by MCT, requires a few more material tests ($[\pm\theta]_s$ to optimize constituent shear strengths) than those necessary to determine the failure tensors for an analogous Tsai-Wu analysis.

### 8.2. Recommendations for Future Research

Experimentally generated stress-strain curves clearly show that composite behavior is viscoelastic. The nonlinear elastic constituent model used in this research should be replaced with a viscoelastic one. Because the source of nonlinearity in organic composites is rooted in the matrix, a viscoelastic model should address all potential sources of nonlinearity (e.g. shear and transverse compression). Should research emphasis turn to metal matrix composites, an elastic-plastic constitutive model should also be available.

Multicontinuum theory is not restricted by the geometry of underlying microstructure. In this research, only lamina based on hexagonal fiber packing were considered. A library of micromechanics models should be developed to broaden MCT_77's analytical scope. The library could include microstructures for the following:

    a. Random fiber packing of unidirectional lamina,
    b. Woven fabrics,
    c. Stitched fabrics,

d.  Randomly distributed short (chopped) fiber reinforcement, and

e.  Randomly distributed particulate reinforcement.

Further, Multicontinuum Theory could be extended to a third constituent to account for interfacial phases between the matrix and reinforcement or the warp, weft, and matrix components of a woven fabric composite.

Upgrading MCT_77 software to bring it more inline with commercial finite element codes would be a worthwhile endeavor. Without comment, the follow upgrades could enhance MCT_77's analysis capabilities

a.  Ability to degenerate elements to a lower number of nodes;

b.  Ability to mix element types within a single analysis;

c.  Parse a single user input file to determine quantities to be read and conduct error checking;

d.  A computationally more efficient method for solving matrix equations, such as Inverse-Broyden, should be incorporated for incremental analyses;

e.  General improvements in the ANSYS to MCT_77 translator;

f.  Expand element library (twenty-node BRICK and improved SHELL elements); and

g.  Port MCT_77 code to FORTRAN 90 to take advantage of dynamic memory allocation.

Development of the MCT failure criteria is not complete. The criteria could be expanded to included fiber buckling which is especially significant in carbon/epoxy laminates. Fiber-matrix debonding could also be incorporated as a failure mode. The nonlinear regression optimization procedure for determining constituent shear strengths typically has poor convergence. Improved optimization techniques should be available.

M.J. Hinton, P.Soden, and S. Kaddour [43] are conducting a "World Wide Exercise" to determine the status of methods for predicting the strength of organic composite

laminates. Proponents of approximately a dozen different failure theories were given identical material data and asked to predict failure for a given set of laminates under biaxial load. The exercise is ongoing and is scheduled for completion in 1999. The experimental data and analytical results from this study should provide invaluable insight into the phenomena of composite failure.

The ultimate verification of MCT or any other structural failure criteria is found in the analysis of actual in-service structures. Verification of this sort will require acceptance of the criterion by a number of working engineers, a time frame measured in decades, and funding in the tens of millions of dollars.

# REFERENCES

1 Lazarus, P. ,"Competing Composites", *Professional BoatBuilder*, August/September (1997)

2 Tsai, S.W., "A Survey of Macroscopic Failure Criteria for Composite Materials," *Journal of Reinforced Plastics and Composites,* Vol. 3, 1984, pp. 40-62

3 Rowlands, R.E., "Strength (failure) Theories and Their Experimental Correlation", *Handbook of Composites,* Vol.3—*Failure Mechanics of Composites,* Ed. G.C. Sih and A.M. Skudra, pp. 71-125. Elsevier Science Publishers, North Holland (1985)

4 Nahas, M. N., "Survey of Failure and Post-Failure Theories of Laminated Fiber-Reinforced Composites," *Journal of Composites Technology and Research,* Vol. 8, 1986, pp. 138-153.

5 Aboudi, J., "Micromechanical Analysis of the Strength of Unidirectional Fiber Composites," *Composites Science and Technology,* Vol. 33, 1988, pp.79-96

6 Pecknold, D.A. and S. Rahman, "Application of a New Micromechanics-Based Homogenization Technique for Nonlinear Compression of Thick-Section Laminates," *Compression Response of Composite Structures, ASTM STP 1185,* S.E. Groves and A.L. Highsmith, Eds., American Society for Testing and Materials, Philadelphia, 1994, pp. 34-54.

7 Rahman, S., and D.A. Pecknold, Micromechanics-Based Analysis of Fiber-Reinforced Laminated Composites, Civil Engineering Studies, UILU-ENG-92-2012, Department of Civil Engineering , University of Illinois, Urbana-Champaign, Sept 1992

8 Kwon, Y.W., and J.M. Berner, "Micromechanics model for Damage and Failure Analyses of Laminated Fibrous Composites", *Engineering Fracture Mechanics,* Vol. 52, No. 2, 1995, pp. 231-242

9 Z. Hashin and A. Rotem, "A Fatigue Failure Criterion for Fiber Reinforced Materials," *Journal of Composite Materials,* Vol. 7 (1973), pp. 448-464

10 S.E. Yamada and C.T. Sun, "Analysis of Laminate Strength and its Distribution," *Journal of Composite Materials,* Vol. 12 (1978), pp. 275-284

11 Blackketter, D.M., D.E Walrath, and A.C. Hansen, "Modeling Damage in a Plain Weave Fabric-Reinforced Composite Material," *Journal of Composites Technology & Research,* Vol. 15, No. 2, Summer 1993, pp. 136-142

12 Brockenbrough, J.R., S. Suresh, & H.A. Wienecke, "Deformation of Metal Matrix Composites with Continuous Fibers: Geometrical Effects of Fiber Distribution and Shape, *Acta Metall. Mater.*, Vol. 39, No. 5, pp. 735-752.

13 Garnich, M. R., A Multicontinuum Theory for Structural Analysis of Composite Materials, Ph.D. Dissertation, University of Wyoming, Department of Mechanical Engineering, August, 1996

14 Garnich M.R. and A.C. Hansen, "A Multicontinuum Theory for Thermal-Elastic Finite Element Analysis of Composite Materials, *Journal of Composite Materials*, Vol. 31, No. 1, 1997.

15 M.R. Garnich and A.C. Hansen, "A Multicontinuum Approach to Structural Analysis of Linear Viscoelastic Composite Materials, *Journal of Applied Mechanics*, Vol. 64, pp. 795-803, December, 1997

16 Commission of the European Communities, De Ferri Metallographia IV, Verlag Stahleisen m.b.H., Dusseldorf. Germany, 1983

17 Hill, R., The Mathematical Theory of Plasticity, New York, Oxford University Press (1950)

18 Gol'denblat, I. and Kopnov, V.A., "Strength of Glass Reinforced Plastics in the Complex Stress State," Mekhanika Polimerov, Vol. 1, pp. 70-78, (1965), English translation: Polymer Mechanics, Vol. 1, pp. 54-60, (1966)

19 Tsai, S.W. and Wu, E.M., "A General Theory of Strength for Anisotropic Materials," *Journal of Composite Materials*, Vol. 5, pp. 58-80 (1971)

20 Hoffman, O., "The Brittle Strength of Orthotropic Materials," *Journal of Composite Materials*, Vol. 1, pp. 200-206 (1967)

21 Hashin, Z., "Failure Criteria for Unidirectional Fiber Composites," *Journal of Applied Mechanics*, Vol. 47, pp. 329-334, June 1980

22 Hansen, A.C., D.M. Blackketter, and D.E. Walrath, "An Invariant-Based Flow Rule for Anisotropic Plasticity Applied to Composite Materials," *Journal of Applied Mechanics*, Vol. 58, December 1991, pp. 881-888

23 Feng, W.W., "A Failure Criterion for Composite Materials," *Journal of Composite Materials*, Vol. 25, January 1991, pp. 88-100

24 Pipes, R.B., and B.W. Cole, "On the Off-Axis Strength Test for Anisotropic Materials," *Journal of Composite Materials*, Vol. 7, April 1973, pp. 246-256

25 Narayanaswami, R., and H.M. Adelman, "Evaluation of the Tensor Polynomial and Hoffman Strength Theories for Composite Materials," *Journal of Composite Materials*, Vol. 11, October 1977, pp. 366-377

26 Test Method D3410/3410M –94, "Standard Test Method for Compressive Properties of Polymer Matrix Composite Materials with Unsupported Gage Section," in Annual Book of ASTM Standards Vol. 15.03, Philadelphia, PA

27 Test Method D3039/3039M –95, "Standard Test Method for Tensile Properties of Polymer Matrix Composite Materials," in Annual Book of ASTM Standards Vol. 15.03, Philadelphia, PA

28 Chamis, C.C, Simplified Composite Micromechanics Equations for Hygral, Thermal and Mechanical Properties, NASA Technical Memorandum 83320, February 1983

29 Adams, D.F. and D.A.Crane, "Combined Loading Micromechanical Analysis of a Unidirectional Composite," *Composites*, Vol. 15, No. 3, July 1984, page 182

30 Hashin, Z., D. Bagchi, and B.W. Rosen, Nonlinear behavior of Fiber Composite Laminates, NASA Contractor Report, NASA-CR-2313, April 1974, pp. 12-14

31 Vaziri, R., M.D. Olson, and D.L. Anderson, "A Plasticity-Based constitutive Model for fibre-Reinforced composite Laminates, *Journal of Composite Materials*, Vol. 25, May 1991, pp. 512-535

32 Hahn, H.T., S.W. Tsai, "Nonlinear Elastic Behavior of Unidirectional Composite Laminae," *Journal of Composite Materials*," Vol. 7, April 1973, p. 102

33 Hahn, H. T. "Nonlinear Behavior of Laminated Composites," *Journal of Composite Materials*, Vol. 7, April 1973, pp. 257-271

34 Chang, F.K., L.B. Lessard, "Damage Tolerance of Laminated Composites Containing and Open Hole and Subjected to Compressive Loadings: Part I-Analysis," *Journal of Composite Materials*, Vol. 25, January 1991, pp. 6-8

35 Frank, L.E. Constitutive Modeling of Polymers Using Submicrocrack Concentration as an Internal State Variable, Masters Thesis, University of Wyoming, Department of Mechanical Engineering, December 1990, pp. 65-91, 106-107

36 Gibson, R.F. "Analysis of Viscoelastic and Dynamic Behavior," in Principles of Composite Material Mechanics, McGraw-Hill, New York, 1994

37 Gipple, K. and E.T. Camponeschi, "The Influence of Material Nonlinearity and Microstructural Damage on the Inplane Shear Response of Carbon/Epoxy composites," *Composite Letters*, Vol. , pp.9-11

38 Hughes, T.J.R., <u>The Finite Element Method: Linear Static and Dynamic Analysis</u>, Prentice-Hall. 1987, pp. 242-254.

39 ANSYS®, Inc., 201 Johnson Road, Houston, PA 15342-1300

40 Cook, R.D., D.S. Malkus, and M. E. Plesha, <u>Concepts and Applications of Finite Element Analysis</u>: Chapter 17, "An Introduction to Some Nonlinear Problems", 3.ed. John Wiley & Sons, New York, 1989

41 Pettit, P.H., M.E. Waddoups, "A Method of Prediction the Nonlinear Behavior of Laminated Composites," *Journal of Composite Materials*, Vol. 3, 1969, pp. 2-19

42 Welsh, J.S., and Adams, D.F., "Development of a True Triaxial Testing Facility for Composite Materials," Report No. UW-CMRG-R-99-102, Composite Materials Research Group, University of Wyoming, Laramie, WY, May 1999.

43 Hinton, M., P.Soden and S. Kaddour, "Comparison of Failure Prediction Methods for Glass/Epoxy and Carbon/Epoxy Laminates under Biaxial Stress," Presentation to the MIL Handbook 17 Meeting, 30 March – 2 April 1998, San Diego, CA.

# APPENDIX A

# BORON/5505 LAMINA PROPERTIES

## A.1. Material Test Suite

The composite material properties presented in this appendix are from lamina composed of boron reinforcing fibers in a Narmco 5505 epoxy matrix. The fiber volume fraction was given as 50%. Experimental stress-strain curves for five of the tests making up the material test suite (longitudinal and transverse tension and compression, and longitudinal shear) were digitized from figures published by Petit and Waddoups [1] and are presented in Fig. A.1 - Fig. A.5. Only five tests of the material test suite were conducted on this composite. No out-of-plane shear response was recorded. Only in-plane load cases were considered. The authors note that the stress-strain curves presented are based on a single test, hence there is no statistical basis for the results. No curve fits were used to plot the experimental data, i.e., the lines are linear between the digitized points.

MCT_77 results, based on constitutive material properties backed out via micromechanics from the experimental data, are also plotted. Boron/5505 lamina had different tension and compression modulus values. MCT_77 currently supports only one modulus value per direction, so tensile modulus values were used in all analyses.

Table A.1 presents experimentally determined initial composite elastic constants. Table A.2 presents *in situ* constituent elastic constants backed out from composite values. Table A.3 presents curve fit parameters for the nonlinear composite shear stress-strain curve.

**Table A.1** *Boron/5505 composite elastic constants derived from experimental data.*

| $E_{11}$ (Gpa) | $E_{22}$ (GPa) | $G_{12}$ (GPa) | $G_{23}$ (GPa) | $\nu_{12}$ | FVF |
|---|---|---|---|---|---|
| 207.0 | 21.0 | 7.71 | 7.23 | 0.294 | 0.50 |

**Table A.2** In situ *elastic constants for boron/5505 constituents.*

| Constituent | E (GPa) | $\nu$ |
|---|---|---|
| Boron | 407 | 0.25 |
| 5505 epoxy | 7.24 | 0.35 |

**Table A.3** *Nonlinear shear-12 curve fit parameters for boron/5505.*

| $C_0$ (MPa) | $C_1$ (MPa) | $C_2$ (MPa) | $a_1$ | $a_2$ |
|---|---|---|---|---|
| 138.6 | -136.9 | -1.726 | -45.23 | -881.8 |
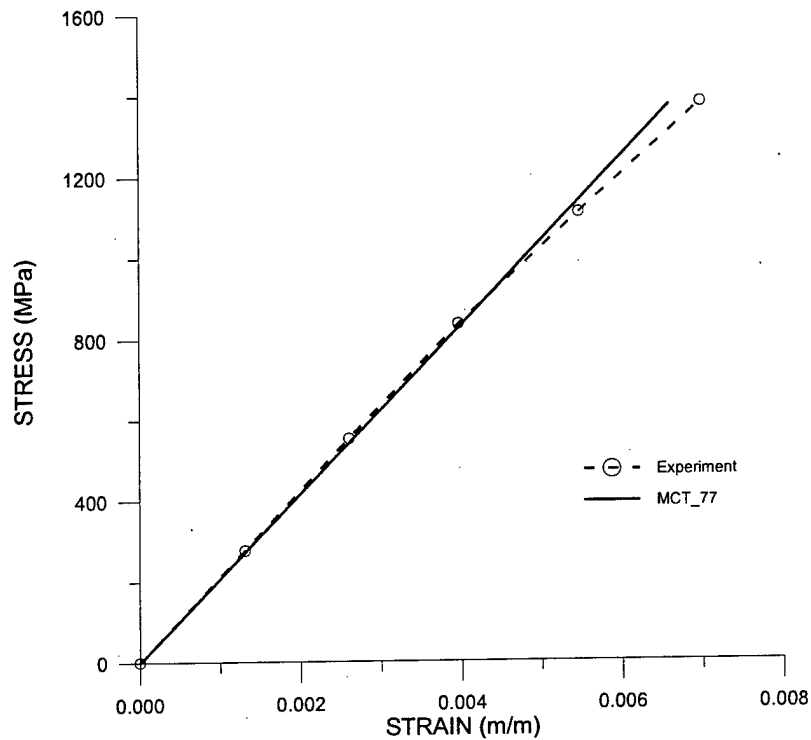


**Fig. A.1** *Boron/5505 lamina under longitudinal tension.*
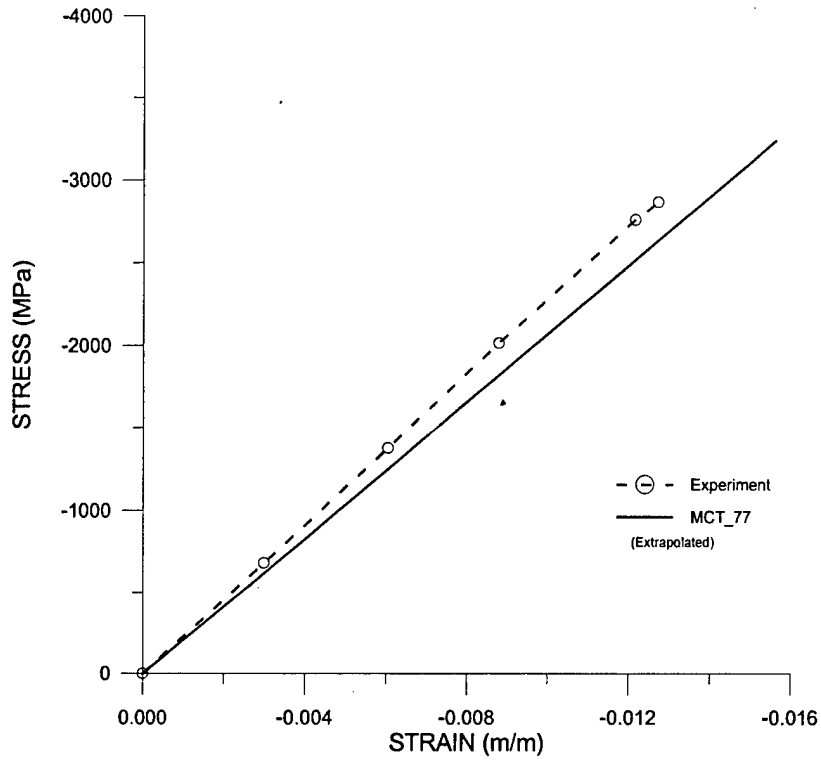
**Fig. A.2** *Boron/5505 lamina under longitudinal compression.*
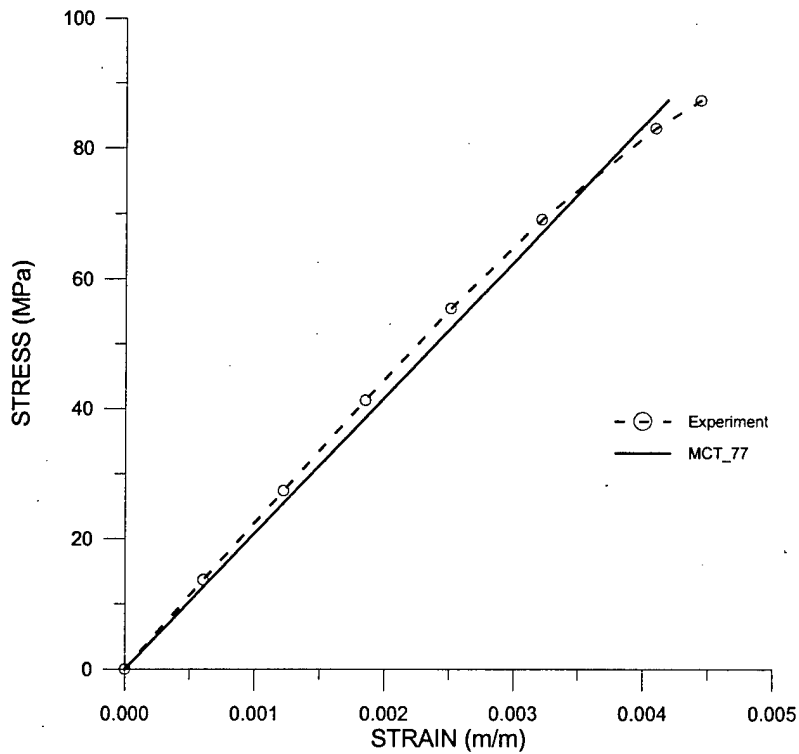


**Fig. A.3** *Boron/5505 lamina under transverse tension.*
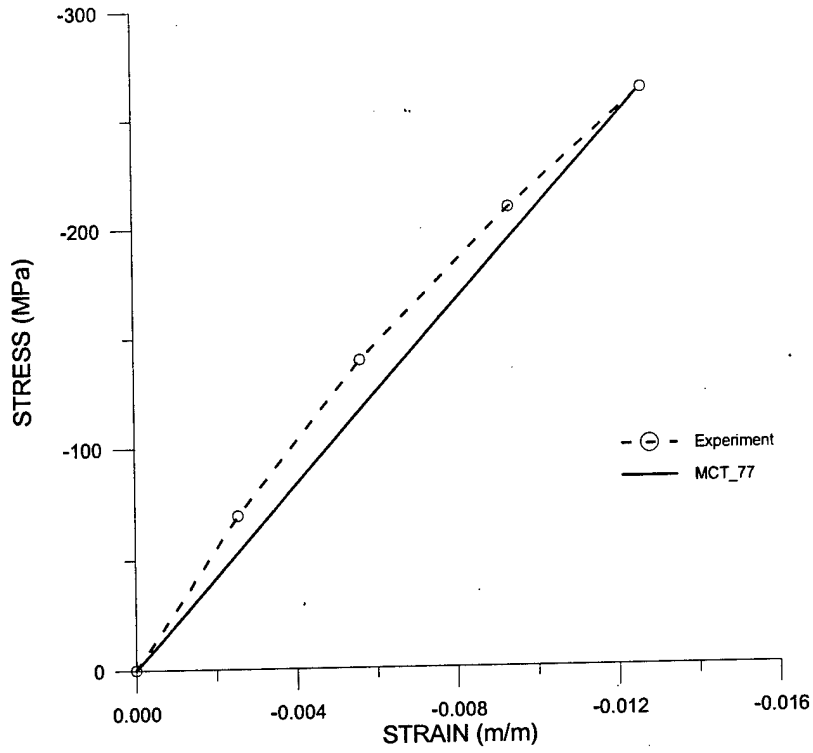
**Fig. A.4** *Boron/5505 lamina under transverse compression.*
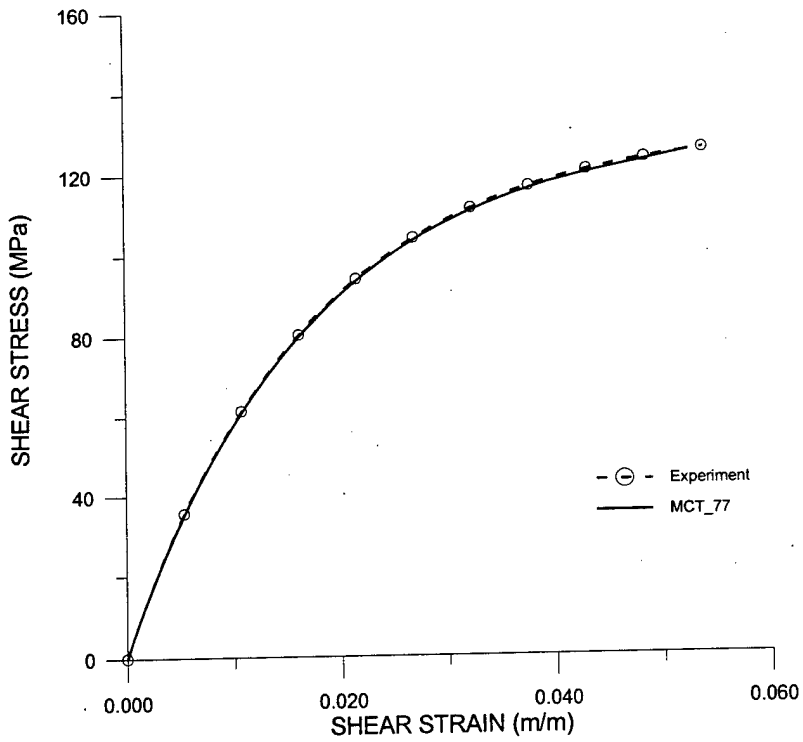


**Fig. A.5** *Boron/5505 lamina under longitudinal shear.*

Note that the shear stress/strain results were taken from the results of a $[\pm45]_s$ tension test. The curve is a combination of digitized results taken from the graphs of Petit and Waddoups and tabular stress/strain results published by Rosen [2] based on additional work published by Petit [3].

### A.2. Micromechanics Results: Referenced to Changing $G_{12}$

Changes in composite and matrix elastic constants with respect to change in the composite shear modulus were determined by invoking the constitutive model described in section 5.3. Although it is the composite shear strain that initiates recalculation of all material constants within the MCT_77 code, the composite-constituent relationships were developed by varying the matrix shear modulus from 0% to 100% of its initial *in situ* value and using micromechanics to derive new composite properties. Once a set of constituent-composite properties are developed, the relationships are redefined in terms of change in shear modulus. A curve for each elastic constant, normalized with respect to the tangent composite shear modulus, was fitted through the values determined at each data point. Quadratic equations for four curves, $E_{22}$, $v_{12}$, $G_{23}$, and $G^m$, referenced to changes in composite $G_{12}$ are presented in Fig. A.6 through Fig. A.9. Numerical results are available in Table A.4.

$$y = -1.201E+00x^2 + 3.853E+00x + 4.270E-02$$
$$R^2 = 9.992E-01$$
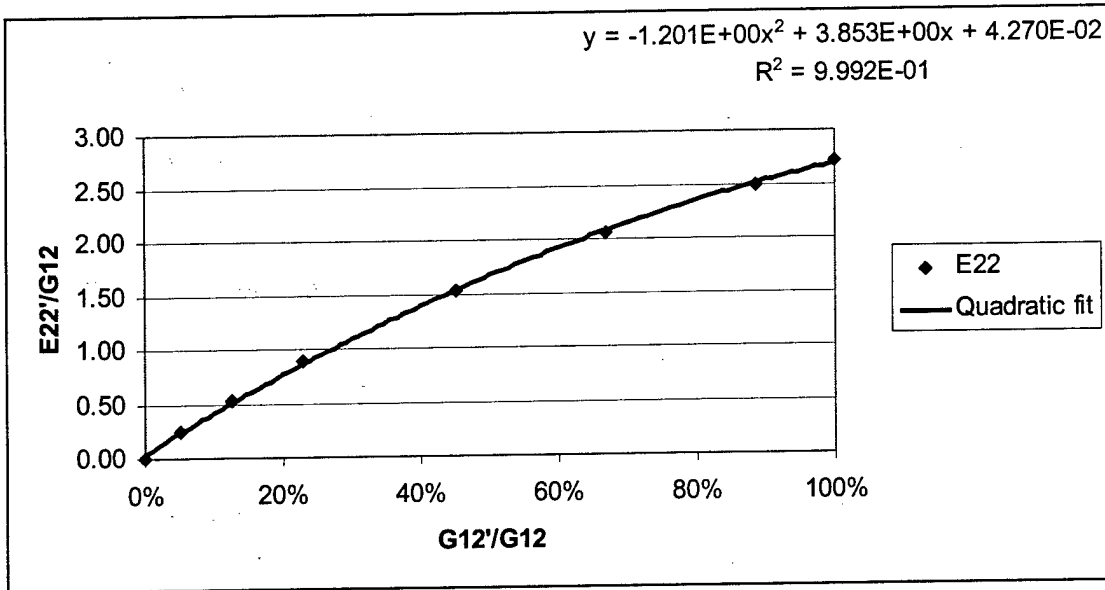
**Fig. A.6** *Boron/5505: $E_{22}$ as a function of change in $G_{12}$.*



$$y = 2.374E-03x^2 - 1.290E-02x + 4.861E-02$$
$$R^2 = 9.999E-01$$
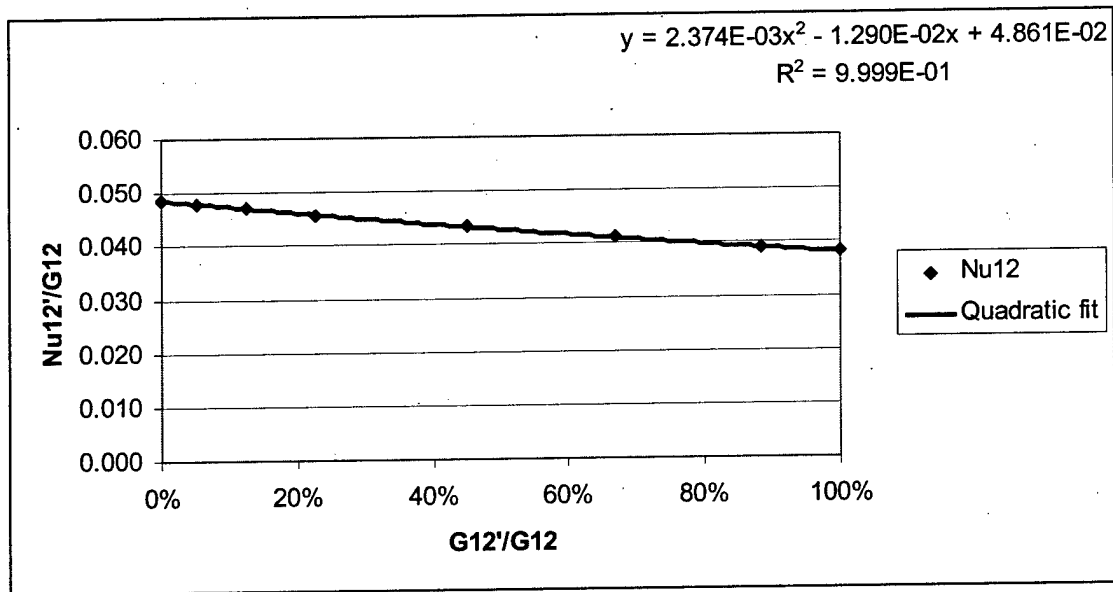
**Fig. A.7** *Boron/5505: $\nu_{12}$ as a function of change in $G_{12}$.*

$$y = -1.674\text{E-}01x^2 + 1.095\text{E+}00x + 5.497\text{E-}03$$
$$R^2 = 9.999\text{E-}01$$
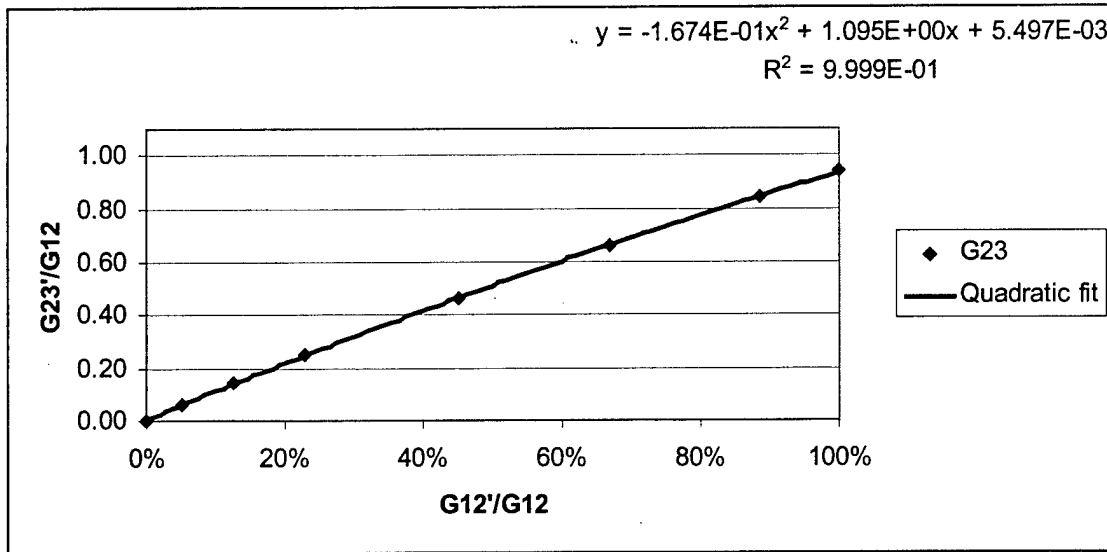
**Fig. A.8** *Boron/5505: $G_{23}$ as a function of change in $G_{12}$.*

$$y = 1.474\text{E-}02x^2 + 3.327\text{E-}01x + 1.234\text{E-}05$$
$$R^2 = 1.000\text{E+}00$$
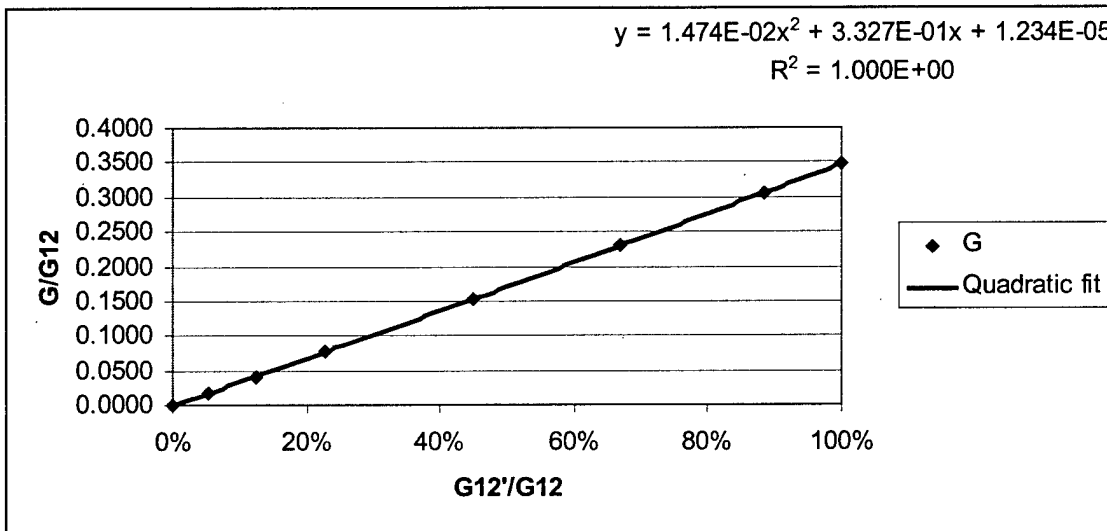
**Fig. A.9** *Boron/5505: G as a function of change in $G_{12}$.*

**Table A.4** *Micromechanics results for boron/5505 lamina properties referenced to changing $G_{12}$ shear modulus.*

| Matrix | Value | Value/G12 | Composite | Value | Value/G12 |
|---|---|---|---|---|---|
| **100%** | | | | | |
| E (GPa) | 7.239 | | E11 (GPa) | 206.9 | 26.82 |
| G (GPa) | 2.681 | 0.3475 | E22 (GPa) | 21.00 | 2.722 |
| Nu | 0.350 | | G12 (GPa) | 7.715 | 1.000 |
| K (GPa) | 8.046 | | G23 (GPa) | 7.229 | 0.9370 |
| | | | Nu12 | 0.294 | 0.0381 |
| **88%** | | | | | |
| E (GPa) | 6.448 | | E11 (GPa) | 206.5 | 26.77 |
| G (GPa) | 2.359 | 0.3058 | E22 (GPa) | 19.24 | 2.494 |
| Nu | 0.366 | | G12 (GPa) | 6.825 | 0.885 |
| K (GPa) | 8.046 | | G23 (GPa) | 6.489 | 0.8411 |
| | | | Nu12 | 0.301 | 0.0390 |
| **66%** | | | | | |
| E (GPa) | 4.946 | | E11 (GPa) | 205.7 | 26.66 |
| G (GPa) | 1.769 | 0.2294 | E22 (GPa) | 15.82 | 2.051 |
| Nu | 0.398 | | G12 (GPa) | 5.164 | 0.669 |
| K (GPa) | 8.046 | | G23 (GPa) | 5.085 | 0.6591 |
| | | | Nu12 | 0.317 | 0.0411 |
| **44%** | | | | | |
| E (GPa) | 3.374 | | E11 (GPa) | 204.9 | 26.56 |
| G (GPa) | 1.180 | 0.1529 | E22 (GPa) | 11.820 | 1.532 |
| Nu | 0.430 | | G12 (GPa) | 3.476 | 0.4506 |
| K (GPa) | 8.046 | | G23 (GPa) | 3.586 | 0.4648 |
| | | | Nu12 | 0.334 | 0.0433 |
| **22%** | | | | | |
| E (GPa) | 1.727 | | E11 (GPa) | 204.100 | 26.45 |
| G (GPa) | 0.590 | 0.0765 | E22 (GPa) | 6.901 | 0.8945 |
| Nu | 0.464 | | G12 (GPa) | 1.755 | 0.227 |
| K (GPa) | 8.046 | | G23 (GPa) | 1.936 | 0.2509 |
| | | | Nu12 | 0.353 | 0.0458 |
| **12%** | | | | | |
| E (GPa) | 0.952 | | E11 (GPa) | 203.7 | 26.40 |
| G (GPa) | 0.322 | 0.0417 | E22 (GPa) | 4.122 | 0.5343 |
| Nu | 0.480 | | G12 (GPa) | 0.9610 | 0.125 |
| K (GPa) | 8.046 | | G23 (GPa) | 1.1050 | 0.1432 |
| | | | Nu12 | 0.363 | 0.0471 |
| **5%** | | | | | |
| E (GPa) | 0.3999 | | E11 (GPa) | 203.4 | 26.36 |
| G (GPa) | 0.1341 | 0.0174 | E22 (GPa) | 1.858 | 0.2408 |
| Nu | 0.492 | | G12 (GPa) | 0.4016 | 0.052 |
| K (GPa) | 8.046 | | G23 (GPa) | 0.4787 | 0.0620 |
| | | | Nu12 | 0.370 | 0.0480 |
| **0.1%** | | | | | |
| E (GPa) | 0.008042 | | E11 (GPa) | 203.2 | 26.34 |
| G (GPa) | 0.002681 | 0.0003 | E22 (GPa) | 0.039 | 0.0051 |
| Nu | 0.4998 | | G12 (GPa) | 0.0081 | 0.001 |
| K (GPa) | 8.046 | | G23 (GPa) | 0.0099 | 0.0013 |
| | | | Nu12 | 0.375 | 0.0486 |

## A.3. Micromechanics Results: Referenced to Changing $G_{23}$

Petit and Waddoups did not publish transverse shear data. All load cases published within the paper were in-plane loading only, precluding the necessity of out-of-plane data. MCT_77 analysis conducted on these load cases assumed in-plane and out-of-plane shear stress-strain curves to be identical in shape. Ultimate constituent shear strengths, both in- and out-of-plane are determined analytically using the optimization procedure outlined in section 5.4.

## A.4. Failure Data: Elastic Constants

Failure of a constituent is assumed absolute without directionality. Moduli for the failed constituent are set at near zero values, rather than zero, to avoid numerical difficulties within the MCT_77 code. As shown in Table A.5, matrix moduli are reduced to 1% of original value. Failed fiber moduli, which are initially one to two orders of magnitude larger than those of the matrix, are reduced such that their magnitudes are of the same order as that of failed matrix to avoid any artificial stiffness in failed regions. Damaged composite properties that reflect failed constituents, shown in Table A.6 and Table A.7, are calculated via the micromechanics model. A complete input file of material properties for a MCT_77 failure analysis consist of seven materials: undamaged composite, intact fiber, intact matrix, fiber-failed composite, matrix-failed composite, failed fiber, and failed matrix. A fiber-failed composite assumes simultaneous matrix failure also.

**Table A.5** *Elastic constants for boron/5505 constituents assuming failure.*

| Constituent | E (GPa) | % of Original Value | $\nu$ |
|---|---|---|---|
| Boron | 0.0407 | 0.01 | 0.25 |
| 5505 epoxy | 0.0724 | 1.0 | 0.35 |

**Table A.6** *Boron/5505 composite elastic constants with failed fiber/matrix.*

| $E_{11}$ (GPa) | $E_{22}$ (GPa) | $G_{12}$ (GPa) | $G_{23}$ (GPa) | $\nu_{12}$ | FVF |
|---|---|---|---|---|---|
| 0.0567 | 0.0540 | 0.0210 | 0.0208 | 0.308 | 0.50 |

**Table A.7** *Boron/5505 composite elastic constants with failed matrix.*

| $E_{11}$ (GPa) | $E_{22}$ (GPa) | $G_{12}$ (GPa) | $G_{23}$ (GPa) | $\nu_{12}$ | FVF |
|---|---|---|---|---|---|
| 203.0 | 0.220 | 0.0805 | 0.00752 | 0.293 | 0.50 |

## A.5. Failure Data: Ultimate Strengths

The ultimate strengths of the composite are taken from material test suit results. Ultimate strengths of fiber and matrix are backed out of composite results via a MCT_77 analysis using material constants listed in Table A.1 through Table A.3 and the composite strengths listed in Table A.8. Determination of constituent shear strengths are further refined by nonlinear regression optimization of experimental results from [±θ] tests as discussed in section 5.4. Composite ultimate strengths are not used directly in the failure criterion implemented in MCT_77.

**Table A.8** *Boron/5505 composite ultimate strengths.*

| $^{+}S_{11}$ (MPa) | $^{-}S_{11}$ (MPa) | $^{+}S_{22}$ (MPa) | $^{-}S_{22}$ (MPa) | $S_{12}$ (MPa) | $S_{23}$ (MPa) |
|---|---|---|---|---|---|
| 1379.0 | 2864.0 | 87.6 | 262.0 | 125.5 | 95.52* |

*$S_{23}$ determined analytically by nonlinear regression.

**Table A.9** In situ *boron fiber strengths.*

| $^{+}S_{11}^{11f}$ (MPa) | $^{-}S_{11}^{11f}$ (MPa) | $S_{12}^{12f}$ (MPa) |
|---|---|---|
| 2709 | -6454 | 180 |

**Table A.10** In situ *5505 matrix strengths.*

| $^{+}S_{22}^{22m}$ (MPa) | $^{-}S_{22}^{22m}$ (MPa) | $^{+}S_{33}^{22m}$ (MPa) | $^{-}S_{33}^{22m}$ (MPa) | $S_{12}^{12m}$ (MPa) | $S_{23}^{23m}$ (MPa) |
|---|---|---|---|---|---|
| 70.9 | -212 | 7.53 | -22.5 | 83.2 | 64.2 |

Constituent ultimate strengths are listed in Table A.9 and Table A.10. The subscript is the component of ultimate strength and the superscript is the direction of ultimate applied load, e.g., $^{+}S_{33}^{22}$ is the strength (max stress) in the *33* direction when an ultimate *22* tensile load is applied. All constituent ultimate strengths listed are required input to the failure criterion implemented in MCT_77.

### A.6. Uniaxial Laminate Tests

Experimental stress-strain curves for laminate specimens fabricated from boron/5505 (boron/epoxy), shown in Fig. A.10 - Fig. A.24, were digitized from figures published by Petit and Waddoups. The authors note that the stress-strain curves presented are based on a single test, hence there is no statistical basis for the results. No curve fits were used to

plot the experimental data against MCT_77 results, i.e., the lines are linear between digitized points.

Analytical results based on a non-finite element program developed by Petit and Waddoups are also presented. Their program calculated laminate stress at a point based on tangent moduli from five lamina curves (longitudinal and transverse lamina tension and compression, and in-plane shear) at each step of an incrementally applied load. Their approach is remarkably accurate, especially considering the work was conducted in the late 1960's.
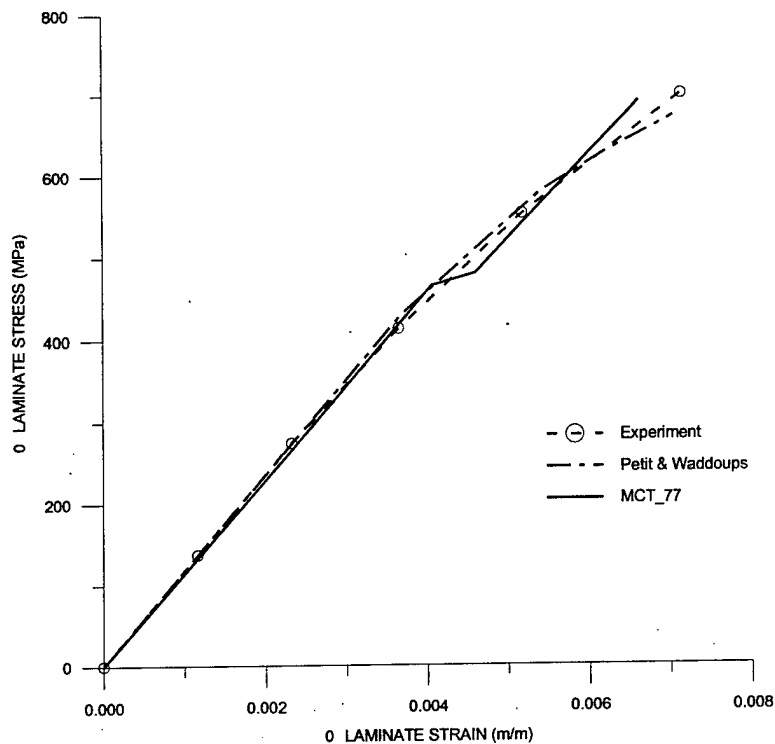


**Fig. A.10** *Boron/5505 [0/90]$_S$ laminate under uniaxial tension.*
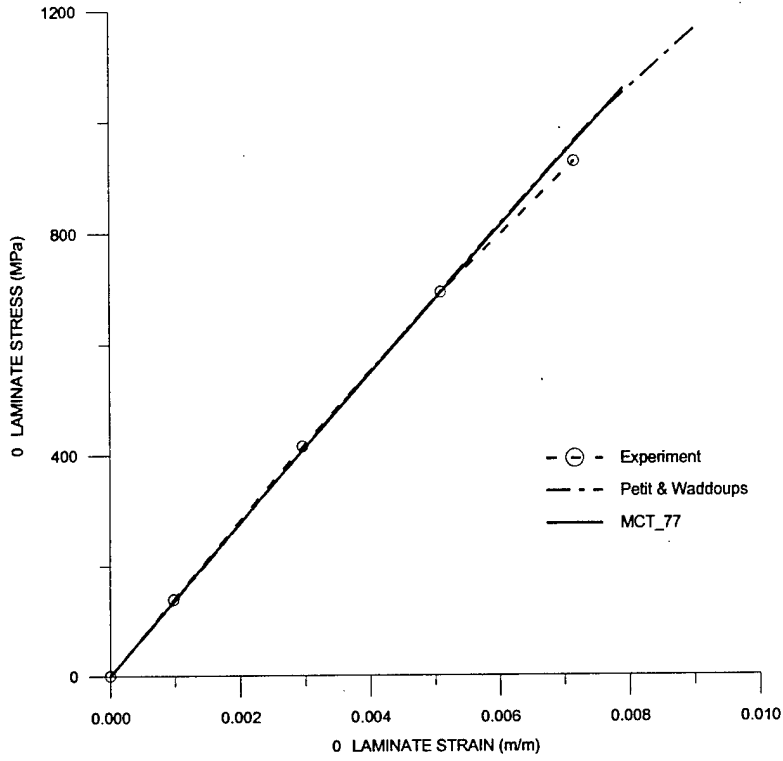
**Fig. A.11** *Boron/5505 [±20]ₛ laminate under uniaxial tension.*
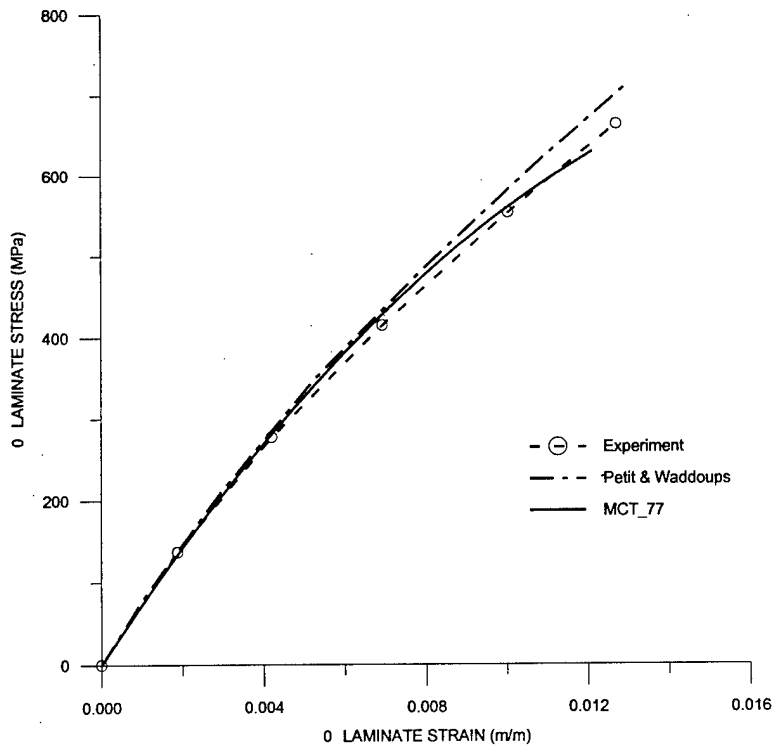


**Fig. A.12** *Boron/5505 [±30]ₛ laminate under uniaxial tension.*
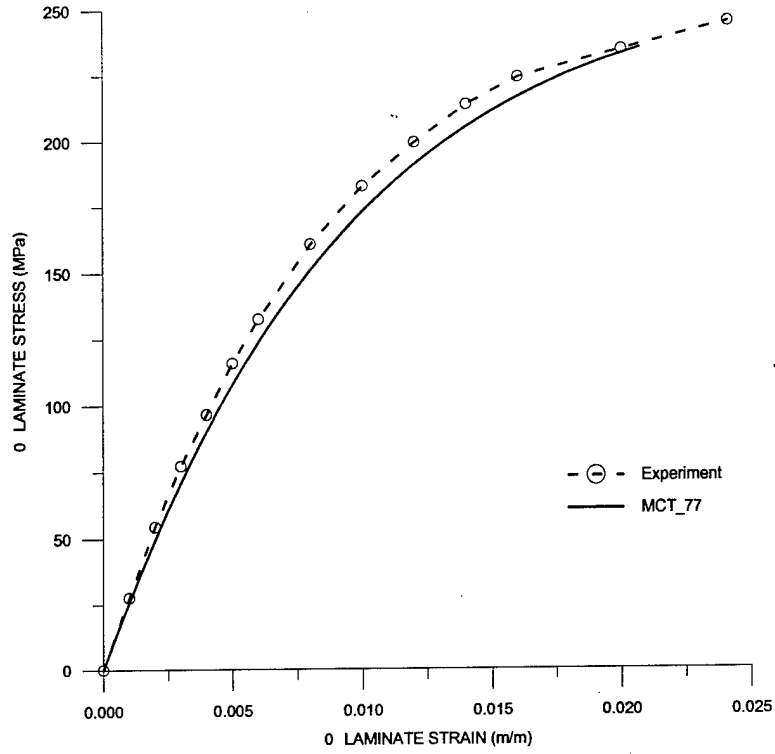
**Fig. A.13** *Boron/5505 [±45]*$_S$ *laminate under uniaxial tension.*
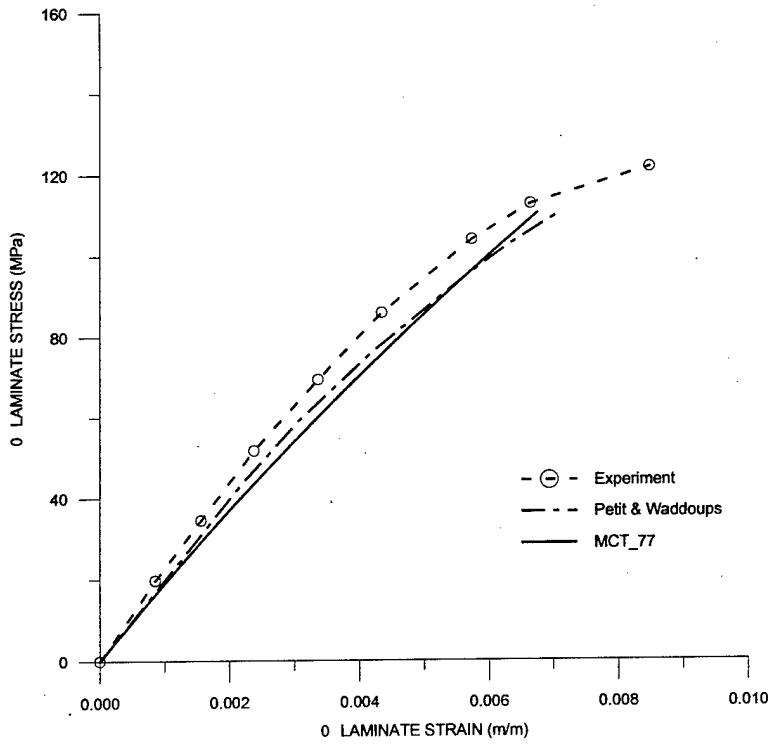


**Fig. A.14** *Boron/5505 [±60]*$_S$ *laminate under uniaxial tension.*
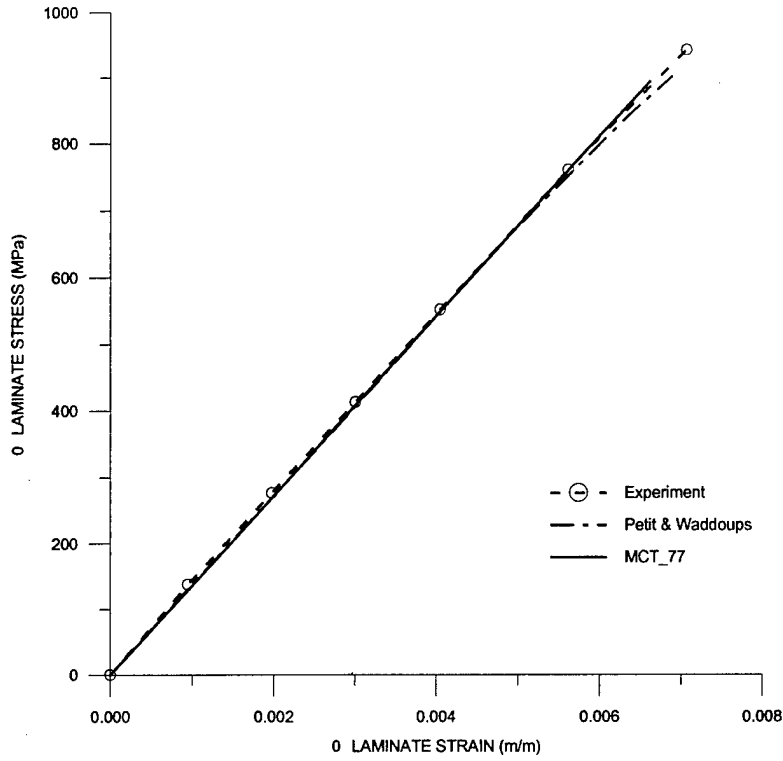
**Fig. A.15** *Boron/5505 [(0)₃/±45]ₛ laminate under uniaxial tension.*
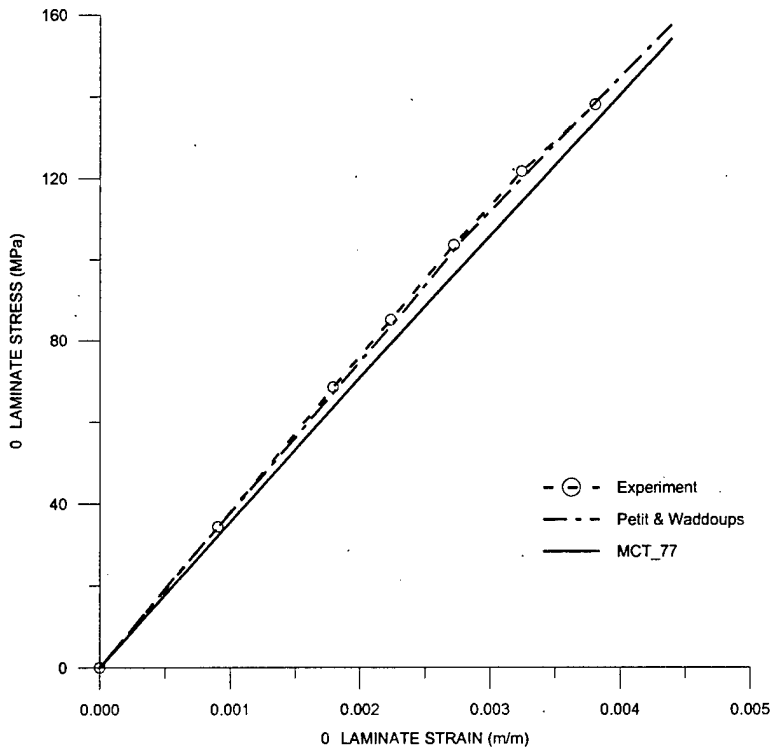


**Fig. A.16** *Boron/5505 [(90)₃/±45]ₛ laminate under uniaxial tension.*
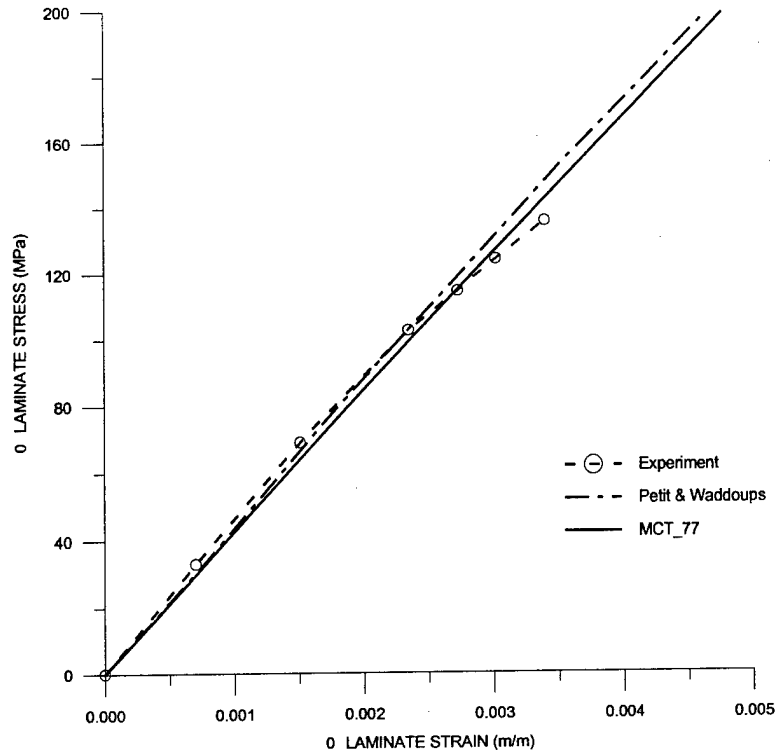
**Fig. A.17** *Boron/5505 [(65)₃/20/-70]ₛ laminate under uniaxial tension.*
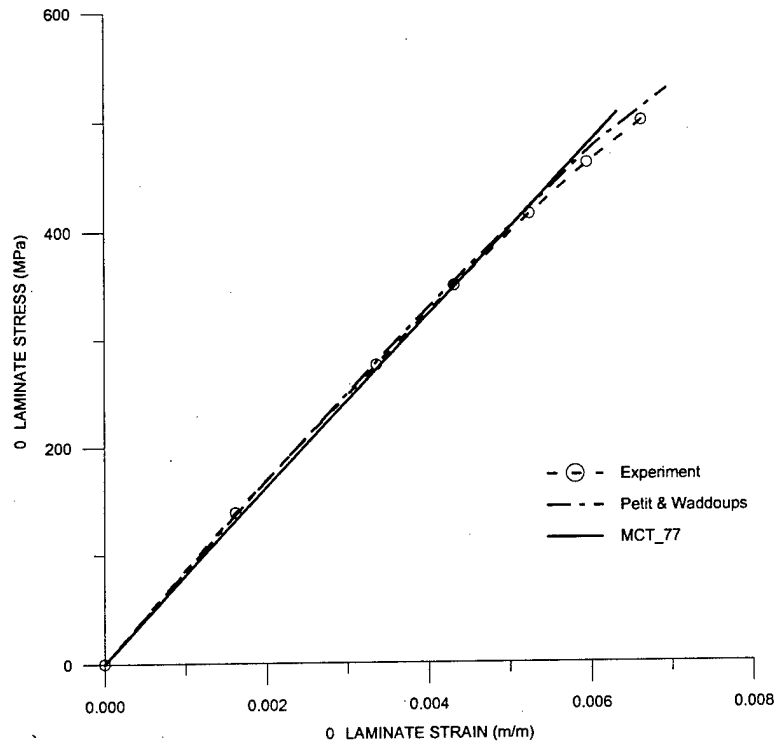


**Fig. A.18** *Boron/5505 [0/±60]ₛ laminate under uniaxial tension.*
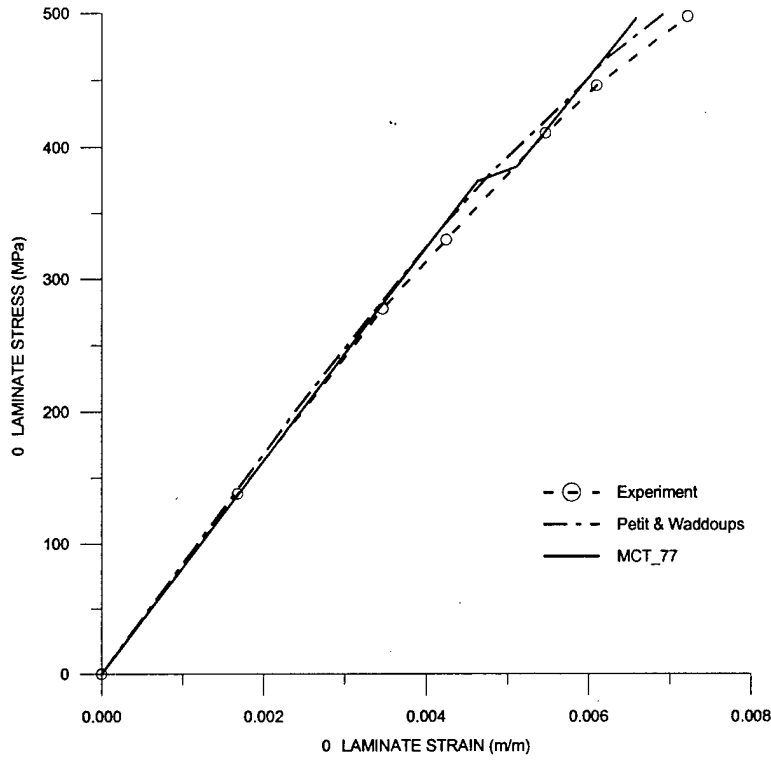
**Fig. A.19** *Boron/5505 [0/±45/90]$_S$ laminate under uniaxial tension.*
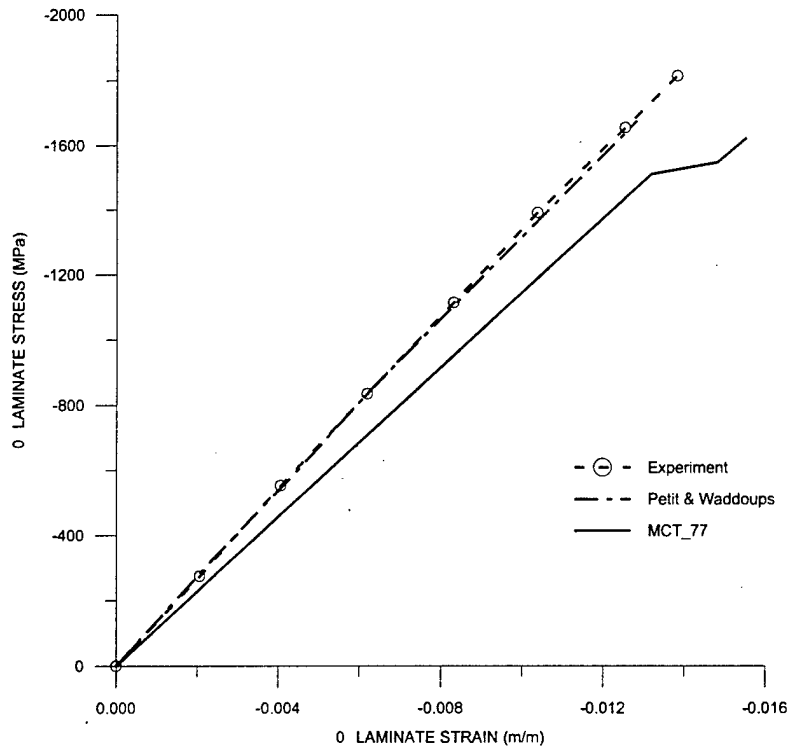


**Fig. A.20** *Boron/5505 [0/90]$_S$ laminate under uniaxial compression.*
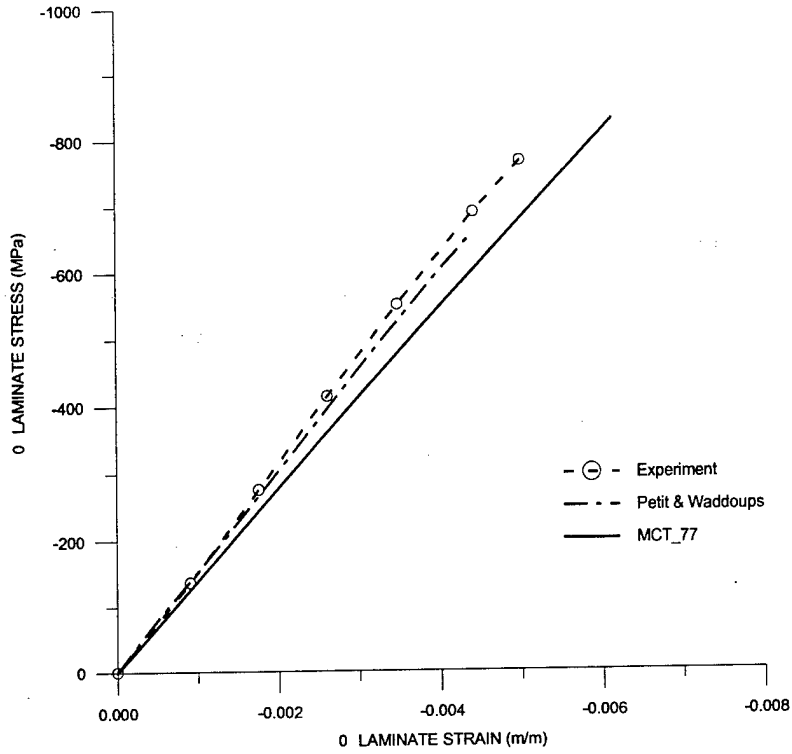
**Fig. A.21** *Boron/5505 [±20]$_S$ laminate under uniaxial compression.*
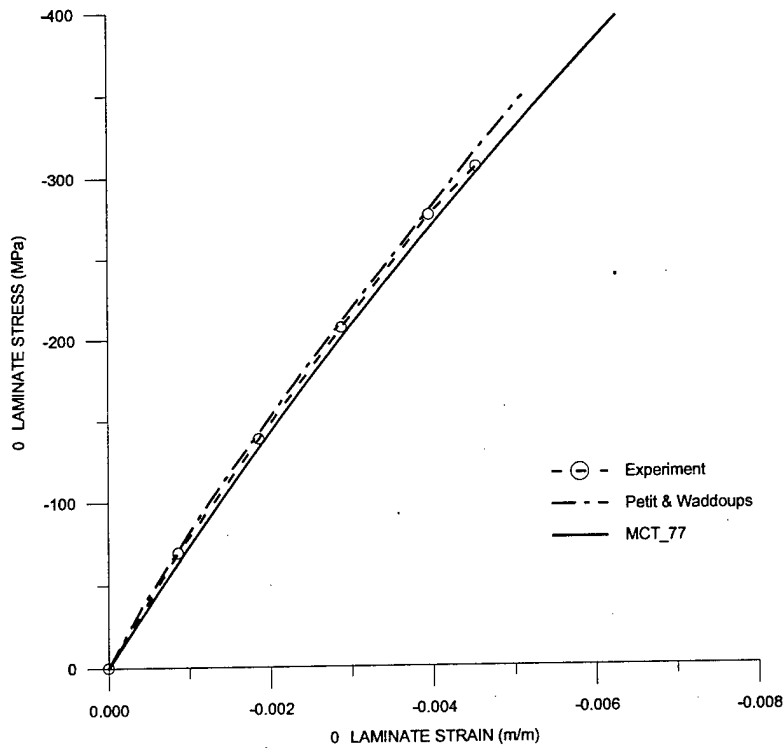


**Fig. A.22** *Boron/5505 [±30]$_S$ laminate under uniaxial compression.*
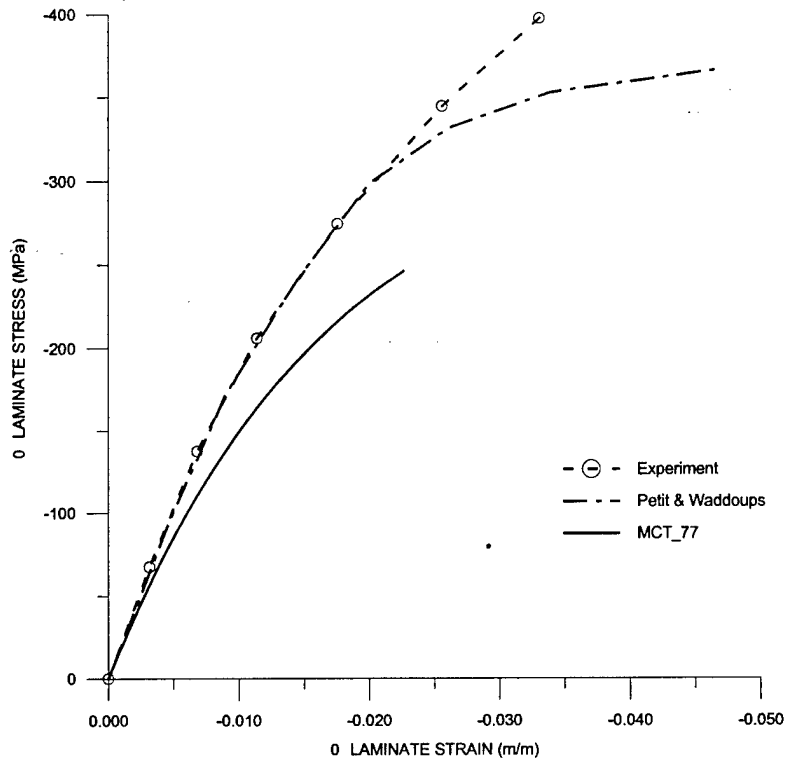
**Fig. A.23** *Boron/5505 [±60]$_S$ laminate under uniaxial compression.*
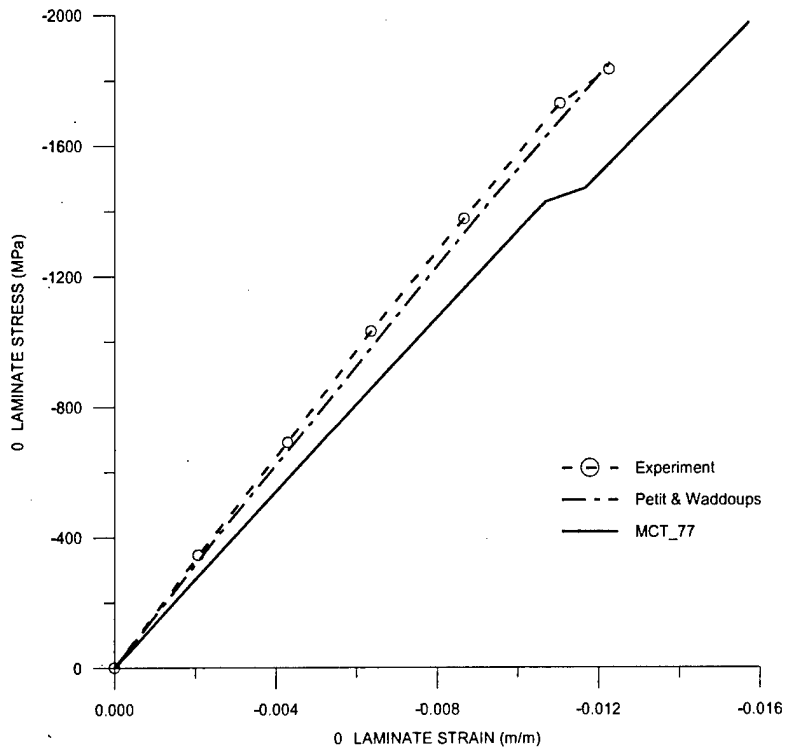


**Fig. A.24** *Boron/5505 [(0)$_3$/±45]$_S$ laminate under uniaxial compression.*

1 Pettit, P.H., M.E. Waddoups, "A Method of Prediction the Nonlinear Behavior of Laminated Composites," *Journal of Composite Materials*, Vol. 3, 1969, pp. 2-19

2 Rosen, W.B., "A Simple Procedure for Experimental Determination of the Longitudinal Shear Modulus of Unidirectional Composites," *Journal of Composite Materials*, Vol. 6, 1972, pp. 552-553

3 Petit, P.H., "A Simplified Method of Determining the Inplane Shear Stress-Strain Response of Unidirectional Composites," ASTMSTP 460, Philadelphia, PA., 1969.

# APPENDIX B

# E-GLASS/8084 LAMINA PROPERTIES

## B.1. Material Test Suite

The composite material properties presented in this appendix are from lamina composed of E-glass reinforcing fibers in a Dow Derakane 8084 rubber-toughened vinylester matrix with a proprietary modification by Seemann Composites. Average lamina fiber volume fraction is 51%. Stress-strain curves for six tests making up the material test suite (longitudinal and transverse tension and compression, and longitudinal and transverse shear) are presented in Fig. B.1 through Fig. B.6. These stress-strain curves were experimentally determined by the University of Wyoming's Composite Materials Research Group from unidirectional laminates provided by Seemann Composites, Inc. All laminates were fabricated using a proprietary vacuum assisted resin transfer mold process known as Seemann Composites Resin Infusion Process (SCRIMP©).

The E-glass/8084 results presented are based on at least five samples per test. Table B.1 presents experimentally determined initial composite elastic constants. Table B.2 presents *in situ* constituent elastic constants backed out from composite values. Table B.3 and Table B.4 presents curve fit parameters for composite nonlinear shear stress-strain curves.

**Table B.1** *E-glass/8084 composite elastic constants derived from experimental data.*

|  | $E_{11}$ (GPa) | $E_{22}$ (GPa) | $G_{12}$ (GPa) | $G_{23}$ (GPa) | $\nu_{12}$ | FVF |
|---|---|---|---|---|---|---|
| E-glass/8084 | 38.5 | 11.7 | 4.74 | 4.34 | 0.273 | 0.51 |

**Table B.2** *In situ elastic constants for E-glass/8084 constituents.*

| Constituent | E (GPa) | $\nu$ |
|---|---|---|
| E-glass | 71.0 | 0.260 |
| 8084 vinylester | 4.66 | 0.292 |

**Table B.3** *Nonlinear shear-12 curve fit parameters for E-glass/8084.*

| $C_0$ (MPa) | $C_1$ (MPa) | $C_2$ (MPa) | $a_1$ | $a_2$ |
|---|---|---|---|---|
| 60.68 | -17.68 | -43.00 | -164.7 | -42.50 |

**Table B.4** *Nonlinear shear-23 curve fit parameters for E-glass/8084.*

| $C_0$ (MPa) | $C_1$ (MPa) | $C_2$ (MPa) | $a_1$ | $a_2$ |
|---|---|---|---|---|
| 50.66 | -1320.0 | 1269.0 | -77.37 | -77.04 |
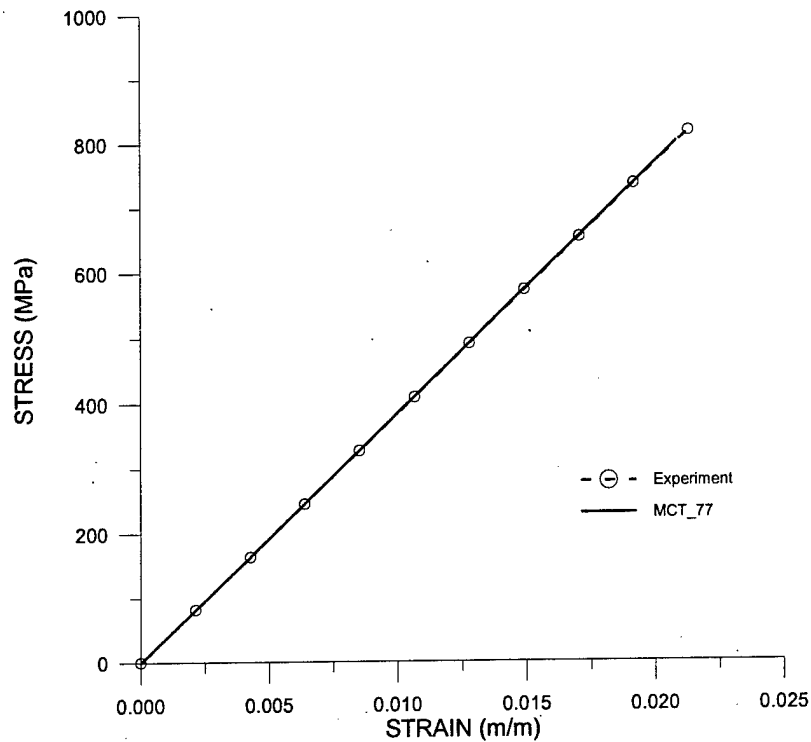


**Fig. B.1** *E-glass/8084 lamina under longitudinal tension.*
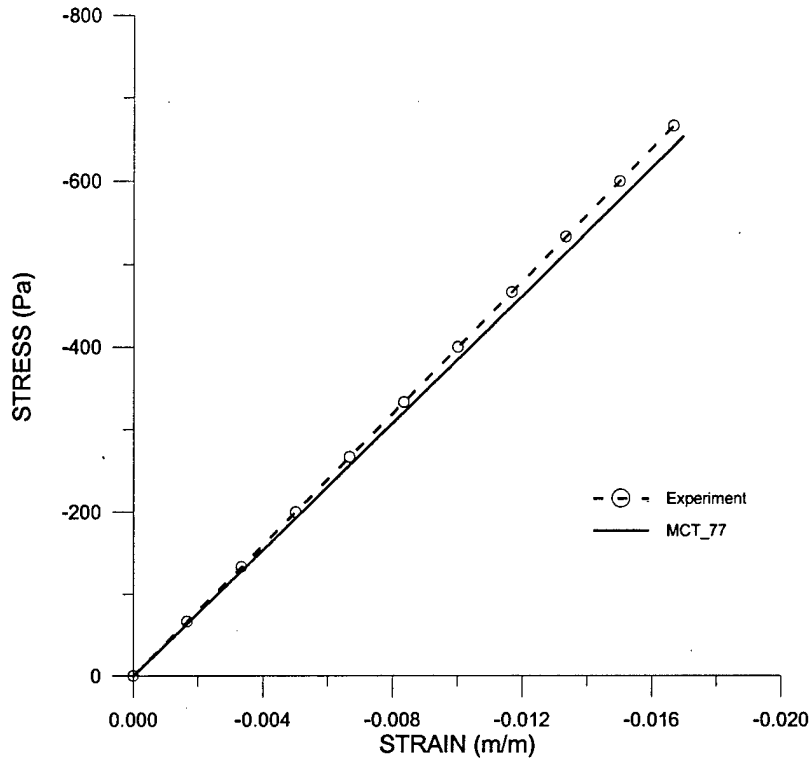
**Fig. B.2** *E-glass/8084 lamina under longitudinal compression.*
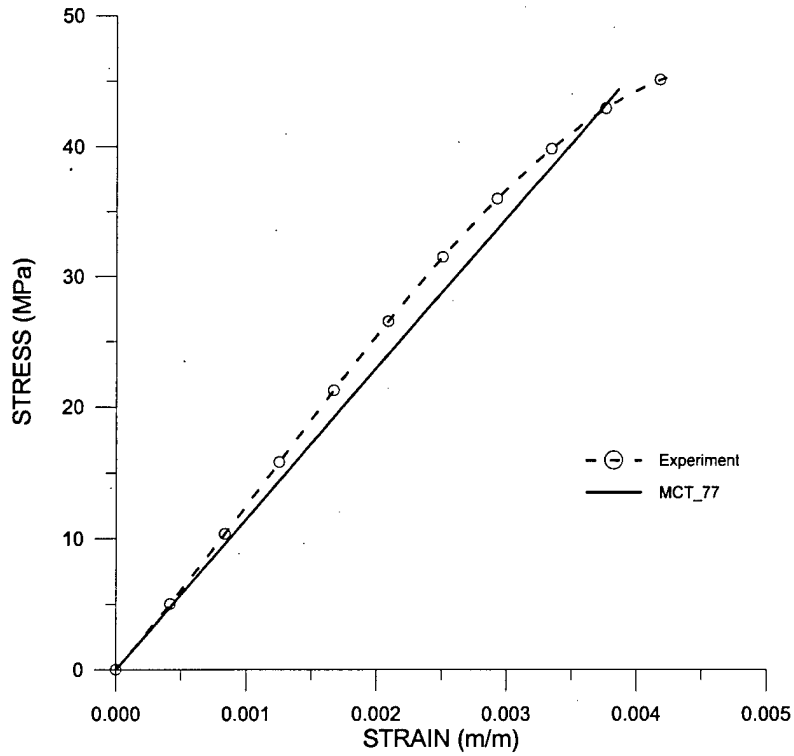


**Fig. B.3** *E-glass/8084 lamina under transverse tension.*
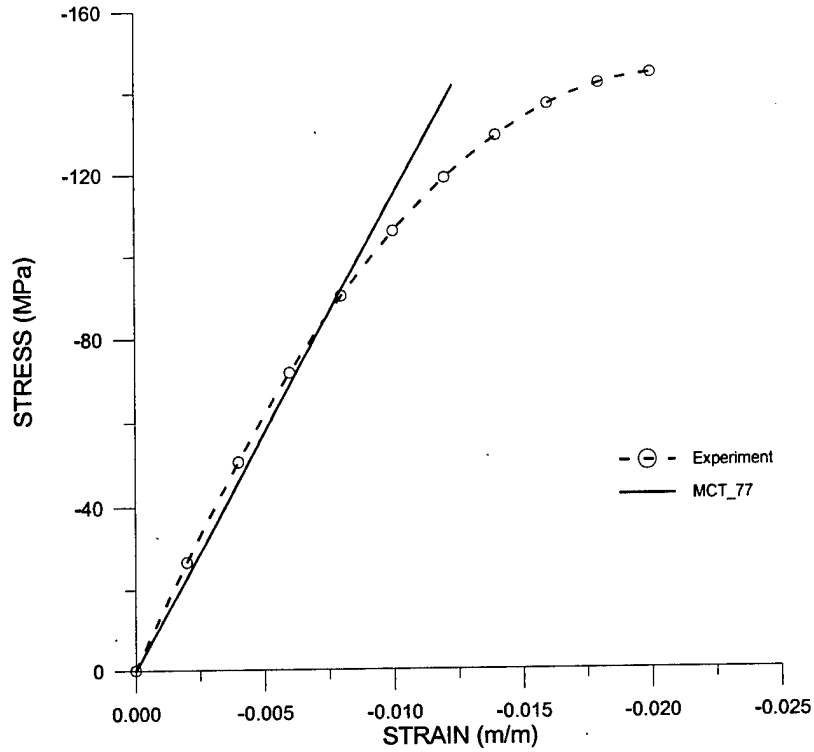
**Fig. B.4** *E-glass/8084 lamina under transverse compression.*
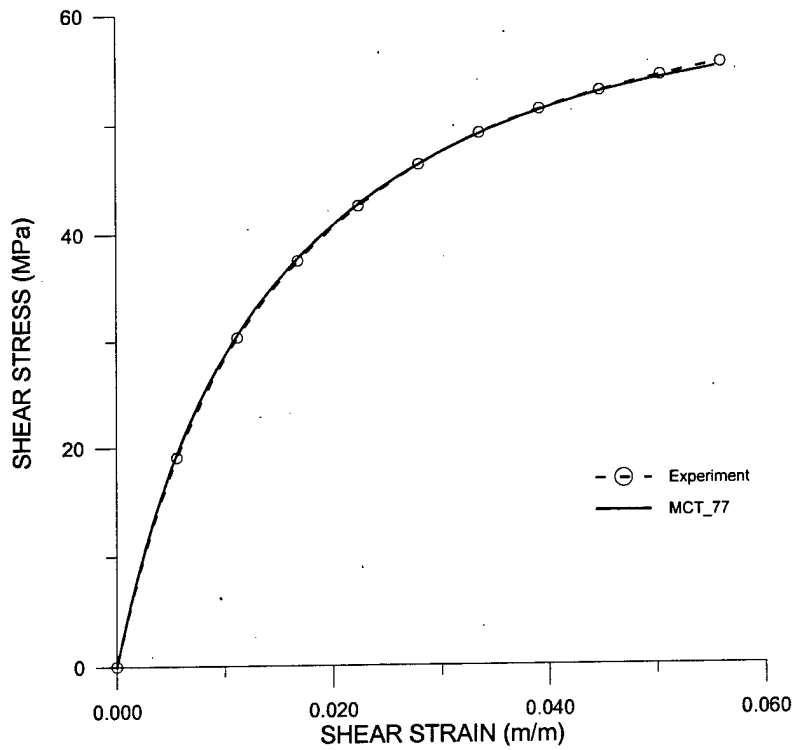


**Fig. B.5** *E-glass/8084 lamina under longitudinal shear.*
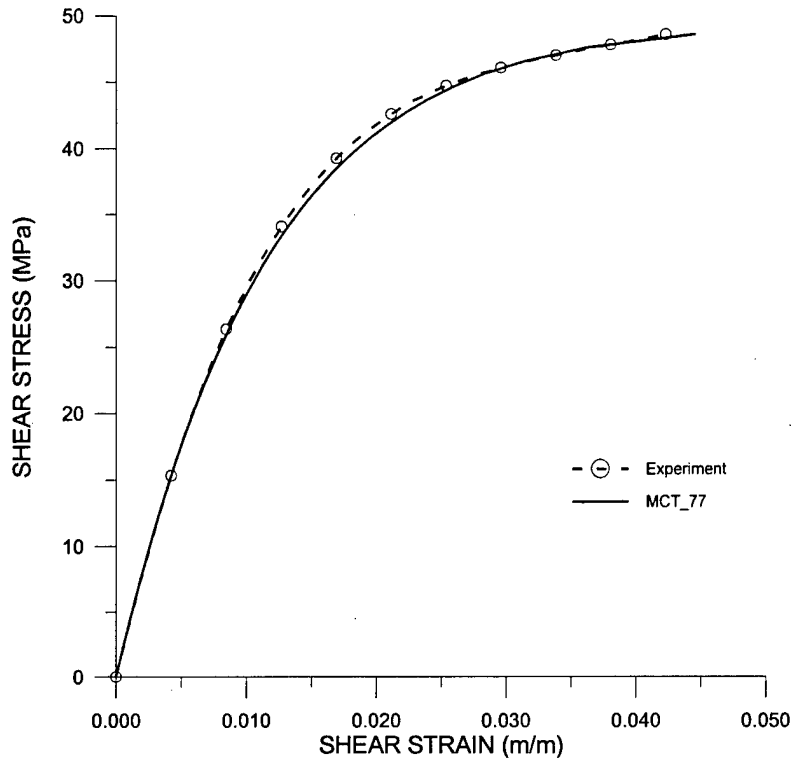
**Fig. B.6** *E-glass/8084 lamina under transverse shear.*

## B.2. Micromechanics Results: Referenced to Changing $G_{12}$

Changes in composite and matrix elastic constants with respect to change in the composite shear modulus were determined by invoking the constitutive model described in section 5.3. Although it is the composite shear strain that initiates recalculation of all material constants within the MCT_77 code, the composite-constituent relationships were developed by varying the matrix shear modulus from 0% to 100% of its initial *in situ* value and using micromechanics to derive new composite properties. Once a set of constituent-composite properties are developed, the relationships are redefined in terms of change in shear modulus. A curve, for each elastic constant normalized with respect to the tangent shear modulus, was fitted through the values determined at each data point.

Quadratic equations for four curves, $E_{22}$, $\nu_{12}$, $G_{23}$, and $G^m$, referenced to changes in composite $G_{12}$ are presented in Fig. B.7 through Fig. B.10. Numerical results are available in Table B.5.



$$y = -1.111E+00x^2 + 3.479E+00x + 5.915E-02$$
$$R^2 = 9.983E-01$$

**Fig. B.7** *E-glass/8084: $E_{22}$ as a function of change in $G_{12}$.*



$$y = 4.038E-03x^2 - 2.613E-02x + 7.975E-02$$
$$R^2 = 9.999E-01$$
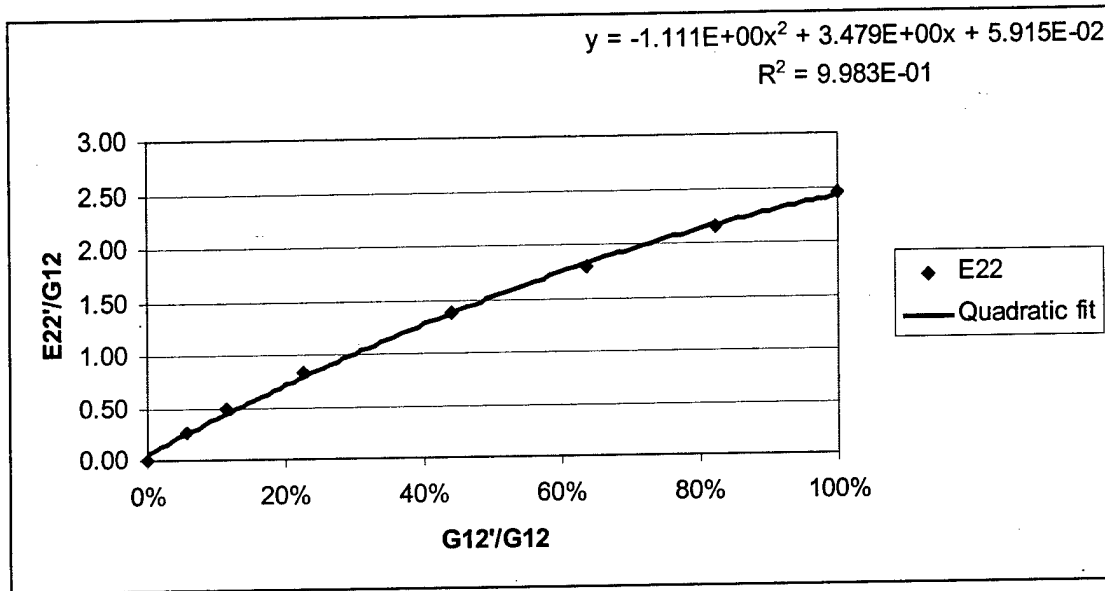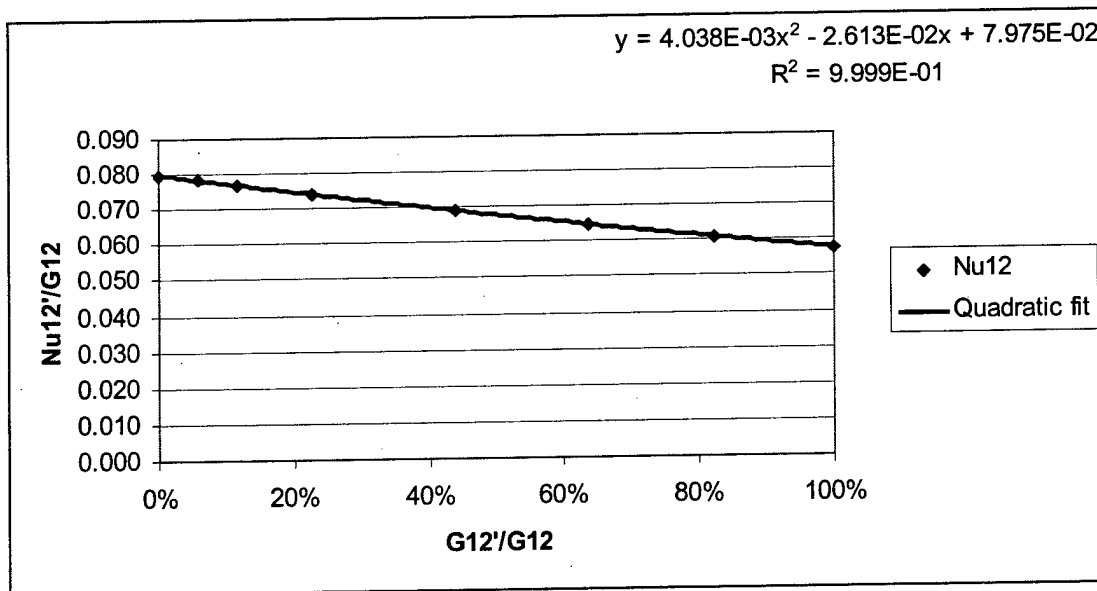
**Fig. B.8** *E-glass/8084: $\nu_{12}$ as a function of change in $G_{12}$.*
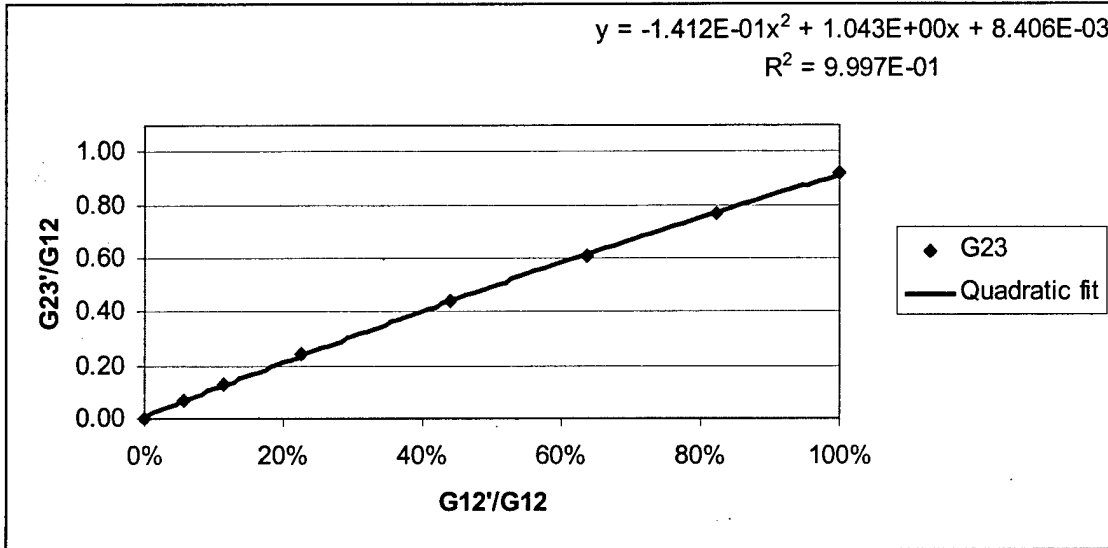
**Fig. B.9** *E-glass/8084: $G_{23}$ as a function of change in $G_{12}$.*
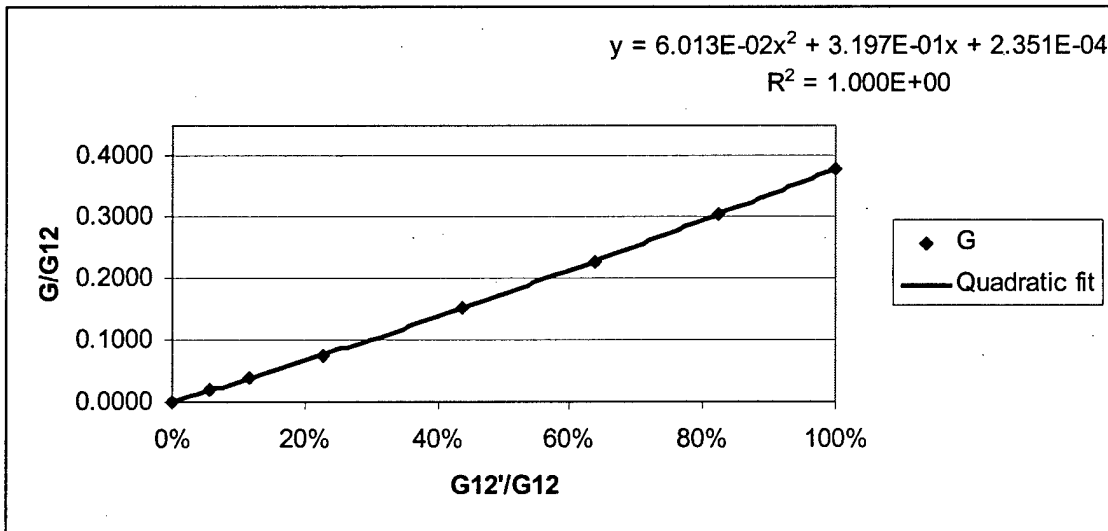


**Fig. B.10** *E-glass/8084: G as a function of change in $G_{12}$.*

**Table B.5** *Micromechanics results for E-glass/8084 lamina properties referenced to changing $G_{12}$ shear modulus.*

| Matrix | Values | Value/G12 | Composite | Values | Value/G12 |
|---|---|---|---|---|---|
| **100%** | | | | | |
| E (GPa) | 4.656 | | E11 (GPa) | 38.46 | 8.12 |
| G (GPa) | 1.802 | 0.3803 | E22 (GPa) | 11.65 | 2.459 |
| Nu | 0.292 | | G12 (GPa) | 4.738 | 1.000 |
| K (GPa) | 3.731 | | G23 (GPa) | 4.337 | 0.9154 |
| | | | Nu12 | 0.273 | 0.0576 |
| **80%** | | | | | |
| E (GPa) | 3.831 | | E11 (GPa) | 38.06 | 8.03 |
| G (GPa) | 1.441 | 0.3042 | E22 (GPa) | 10.15 | 2.142 |
| Nu | 0.329 | | G12 (GPa) | 3.904 | 0.824 |
| K (GPa) | 3.731 | | G23 (GPa) | 3.637 | 0.7676 |
| | | | Nu12 | 0.289 | 0.0610 |
| **60%** | | | | | |
| E (GPa) | 2.958 | | E11 (GPa) | 37.64 | 7.94 |
| G (GPa) | 1.081 | 0.2282 | E22 (GPa) | 8.477 | 1.789 |
| Nu | 0.368 | | G12 (GPa) | 3.019 | 0.637 |
| K (GPa) | 3.731 | | G23 (GPa) | 2.893 | 0.6106 |
| | | | Nu12 | 0.307 | 0.0648 |
| **40%** | | | | | |
| E (GPa) | 2.031 | | E11 (GPa) | 37.19 | 7.85 |
| G (GPa) | 0.721 | 0.1521 | E22 (GPa) | 6.500 | 1.372 |
| Nu | 0.409 | | G12 (GPa) | 2.078 | 0.439 |
| K (GPa) | 3.731 | | G23 (GPa) | 2.081 | 0.4392 |
| | | | Nu12 | 0.327 | 0.0690 |
| **20%** | | | | | |
| E (GPa) | 1.047 | | E11 (GPa) | 36.70 | 7.75 |
| G (GPa) | 0.360 | 0.0761 | E22 (GPa) | 3.972 | 0.8383 |
| Nu | 0.453 | | G12 (GPa) | 1.074 | 0.227 |
| K (GPa) | 3.731 | | G23 (GPa) | 1.160 | 0.2448 |
| | | | Nu12 | 0.351 | 0.0741 |
| **10%** | | | | | |
| E (GPa) | 0.5320 | | E11 (GPa) | 36.45 | 7.69 |
| G (GPa) | 0.1802 | 0.0380 | E22 (GPa) | 2.287 | 0.4827 |
| Nu | 0.476 | | G12 (GPa) | 0.5465 | 0.115 |
| K (GPa) | 3.731 | | G23 (GPa) | 0.6258 | 0.1321 |
| | | | Nu12 | 0.363 | 0.0766 |
| **5%** | | | | | |
| E (GPa) | 0.2681 | | E11 (GPa) | 36.31 | 7.66 |
| G (GPa) | 0.0901 | 0.0190 | E22 (GPa) | 1.249 | 0.2636 |
| Nu | 0.488 | | G12 (GPa) | 0.2756 | 0.058 |
| K (GPa) | 3.731 | | G23 (GPa) | 0.3279 | 0.0692 |
| | | | Nu12 | 0.371 | 0.0783 |
| **0.1000%** | | | | | |
| E (GPa) | 0.005405 | | E11 (GPa) | 36.17 | 7.63 |
| G (GPa) | 0.0018 | 0.0004 | E22 (GPa) | 0.028 | 0.0058 |
| Nu | 0.4998 | | G12 (GPa) | 0.0056 | 0.001 |
| K (GPa) | 3.731 | | G23 (GPa) | 0.0069 | 0.0015 |

### B.3. Micromechanics Results: Referenced to Changing $G_{23}$

Quadratic equations for four curves, $E_{22}$, $\nu_{12}$, $G_{12}$, and $G^m$, referenced to changes in composite $G_{23}$ are presented in Fig. B.11 through Fig. B.14. Numerical results are available in Table B.6.



$$y = -8.274E\text{-}01x^2 + 3.471E\text{+}00x + 2.591E\text{-}02$$
$$R^2 = 9.997E\text{-}01$$
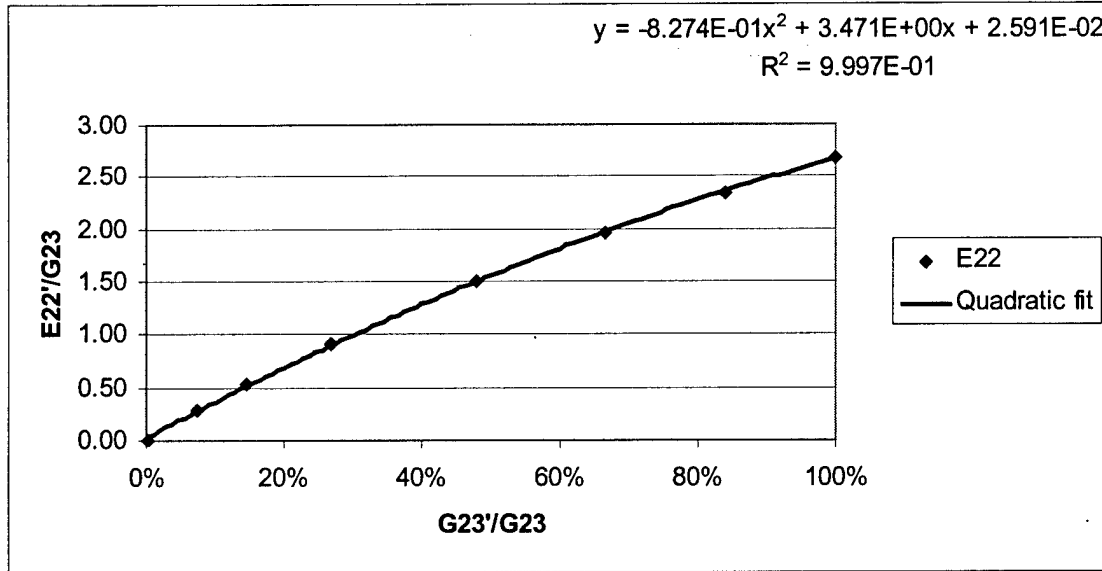
**Fig. B.11** *E-glass/8084: $E_{22}$ as a function of change in $G_{23}$.*



$$y = 5.272E\text{-}04x^2 - 2.503E\text{-}02x + 8.734E\text{-}02$$
$$R^2 = 9.998E\text{-}01$$
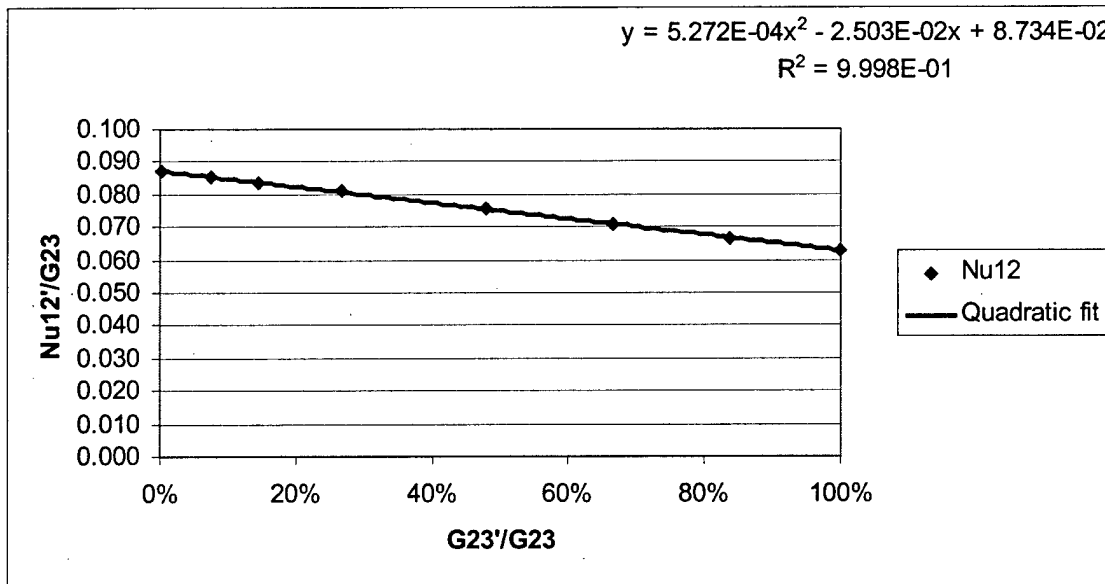
**Fig. B.12** *E-glass/8084: $\nu_{12}$ as a function of change in $G_{23}$.*

$$y = 2.001\text{E-}01x^2 + 8.991\text{E-}01x$$
$$R^2 = 9.998\text{E-}01$$
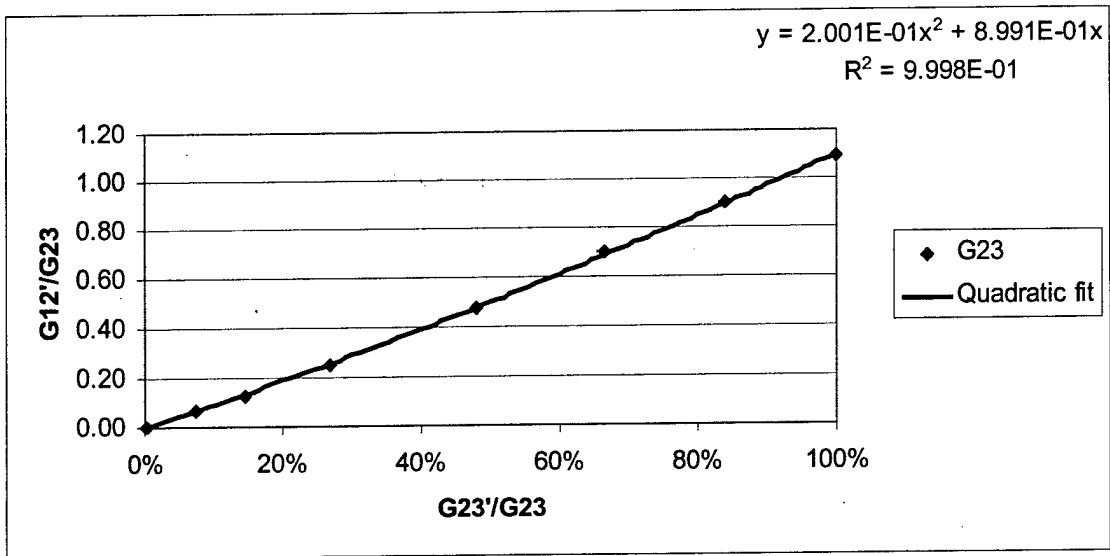
**Fig. B.13** *E-glass/8084: $G_{12}$ as a function of change in $G_{23}$.*



$$y = 1.371\text{E-}01x^2 + 2.799\text{E-}01x$$
$$R^2 = 9.999\text{E-}01$$
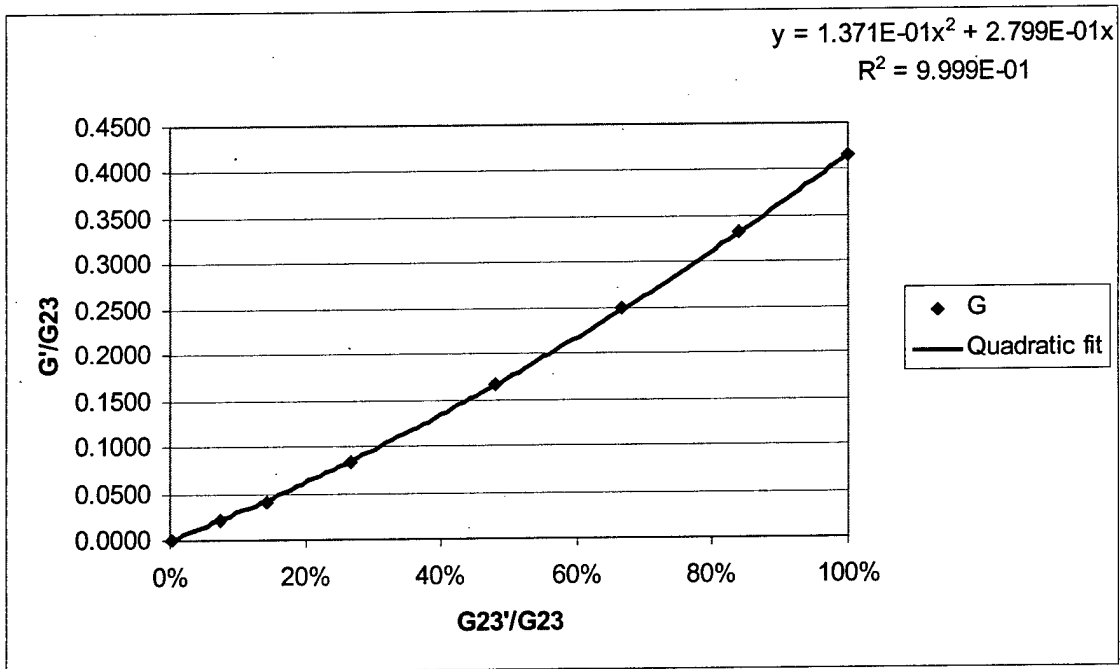
**Fig. B.14** *E-glass/8084: G as a function of change in $G_{23}$.*

**Table B.6** *Micromechanics results for E-glass/8084 lamina properties referenced to changing $G_{23}$ shear modulus.*

| Matrix | Values | Value/G23 | Composite | Values | Value/G23 |
|---|---|---|---|---|---|
| **100%** | | | | | |
| E (GPa) | 4.656 | | E11 (GPa) | 38.46 | 8.8679 |
| G (GPa) | 1.802 | 0.4155 | E22 (GPa) | 11.65 | 2.6862 |
| Nu | 0.292 | | G12 (GPa) | 4.738 | 1.0925 |
| K (GPa) | 3.731 | | G23 (GPa) | 4.337 | 1.000 |
| | | | Nu12 | 0.273 | 0.0629 |
| **80%** | | | | | |
| E (GPa) | 3.831 | | E11 (GPa) | 38.06 | 8.7757 |
| G (GPa) | 1.441 | 0.3324 | E22 (GPa) | 10.15 | 2.3403 |
| Nu | 0.329 | | G12 (GPa) | 3.904 | 0.9002 |
| K (GPa) | 3.731 | | G23 (GPa) | 3.637 | 0.839 |
| | | | Nu12 | 0.289 | 0.0666 |
| **60%** | | | | | |
| E (GPa) | 2.958 | | E11 (GPa) | 37.64 | 8.6788 |
| G (GPa) | 1.081 | 0.2493 | E22 (GPa) | 8.477 | 1.9546 |
| Nu | 0.368 | | G12 (GPa) | 3.019 | 0.6961 |
| K (GPa) | 3.731 | | G23 (GPa) | 2.893 | 0.667 |
| | | | Nu12 | 0.307 | 0.0708 |
| **40%** | | | | | |
| E (GPa) | 2.031 | | E11 (GPa) | 37.19 | 8.5751 |
| G (GPa) | 0.721 | 0.1662 | E22 (GPa) | 6.500 | 1.4987 |
| Nu | 0.409 | | G12 (GPa) | 2.078 | 0.4791 |
| K (GPa) | 3.731 | | G23 (GPa) | 2.081 | 0.4798 |
| | | | Nu12 | 0.327 | 0.0754 |
| **20%** | | | | | |
| E (GPa) | 1.047 | | E11 (GPa) | 36.70 | 8.4621 |
| G (GPa) | 0.360 | 0.0831 | E22 (GPa) | 3.972 | 0.9158 |
| Nu | 0.453 | | G12 (GPa) | 1.074 | 0.2476 |
| K (GPa) | 3.731 | | G23 (GPa) | 1.160 | 0.267 |
| | | | Nu12 | 0.351 | 0.0809 |
| **10%** | | | | | |
| E (GPa) | 0.5320 | | E11 (GPa) | 36.45 | 8.4044 |
| G (GPa) | 0.1802 | 0.0415 | E22 (GPa) | 2.287 | 0.5273 |
| Nu | 0.476 | | G12 (GPa) | 0.5465 | 0.1260 |
| K (GPa) | 3.731 | | G23 (GPa) | 0.6258 | 0.144 |
| | | | Nu12 | 0.363 | 0.0837 |
| **5%** | | | | | |
| E (GPa) | 0.2681 | | E11 (GPa) | 36.31 | 8.3721 |
| G (GPa) | 0.0901 | 0.0208 | E22 (GPa) | 1.249 | 0.2880 |
| Nu | 0.488 | | G12 (GPa) | 0.2756 | 0.0635 |
| K (GPa) | 3.731 | | G23 (GPa) | 0.3279 | 0.076 |
| | | | Nu12 | 0.371 | 0.0855 |
| **0.10%** | | | | | |
| E (GPa) | 0.005405 | | E11 (GPa) | 36.17 | 8.3399 |
| G (GPa) | 0.0018 | 0.0004 | E22 (GPa) | 0.028 | 0.0064 |
| Nu | 0.4998 | | G12 (GPa) | 0.0056 | 0.0013 |
| K (GPa) | 3.731 | | G23 (GPa) | 0.0069 | 0.002 |
| | | | Nu12 | 0.378 | 0.0872 |

## B.4. Failure Data: Elastic Constants

Failure of a constituent is assumed absolute without directionality. Moduli for failed constituents are set at near zero values, rather than zero, to avoid numerical difficulties within the MCT_77 code. As shown in Table B.7, matrix moduli are reduced to 1% of original value. Failed fiber moduli, which are initially one to two orders of magnitude larger than those of the matrix, are reduced such that their magnitudes are of the same order as that of failed matrix to avoid any artificial stiffness in failed regions. Damaged composite properties that reflect failed constituents, shown in Table B.8 and Table B.9, are calculated via the micromechanics model. A complete input file of material properties for a MCT_77 failure analysis consist of seven materials: undamaged composite, intact fiber, intact matrix, fiber-failed composite, matrix-failed composite, failed fiber, and failed matrix. A fiber-failed composite assumes simultaneous matrix failure also.

**Table B.7** *Elastic constants for E-glass/8084 constituents assuming failure.*

| Constituent | E (Gpa) | % of Original Value | $\nu$ |
|---|---|---|---|
| E-glass | 0.071 | 0.1 | 0.26 |
| 8084 vinylester | 0.047 | 1.0 | 0.292 |

**Table B.8** *E-glass/8084 composite elastic constants with failed fiber/matrix.*

| | $E_{11}$ (GPa) | $E_{22}$ (GPa) | $G_{12}$ (GPa) | $G_{23}$ (GPa) | $\nu_{12}$ | FVF |
|---|---|---|---|---|---|---|
| E-glass/8084 | 0.0590 | 0.0575 | 0.0226 | 0.224 | 0.275 | 0.51 |

**Table B.9** *E-glass/8084 composite elastic constants with failed matrix.*

| | $E_{11}$ (GPa) | $E_{22}$ (GPa) | $G_{12}$ (GPa) | $G_{23}$ (GPa) | $\nu_{12}$ | FVF |
|---|---|---|---|---|---|---|
| E-glass/8084 | 36.2 | 0.135 | 0.0555 | 0.0495 | 0.279 | 0.51 |

## B.5. Failure Data: Ultimate Strengths

Ultimate strengths of the composite are taken from material test suit results. Ultimate strengths of the fiber and matrix are backed out of composite results via a MCT_77 analysis using material constants listed in Table B.1 through Table B.3 and the composite strengths listed in Table B.10. Determination of constituent shear strengths are further refined by nonlinear regression optimization of experimental results from [±θ] tests as discussed in section 5.4. Composite ultimate strengths are not used directly in by the failure criterion implemented in MCT_77.

**Table B.10** *E-glass/8084 composite ultimate strengths.*

| $^{+}S_{11}$ (MPa) | $^{-}S_{11}$ (MPa) | $^{+}S_{22}$ (MPa) | $^{-}S_{22}$ (MPa) | $S_{12}$ (MPa) | $S_{23}$ (MPa) |
|---|---|---|---|---|---|
| 817.5 | -759.7 | 45.26 | -144.3.0 | 60.80 | 48.52 |

**Table B.11** *In situ E-glass fiber strengths.*

| $^{+}S_{11}^{11f}$ (MPa) | $^{-}S_{11}^{11f}$ (MPa) | $S_{12}^{12f}$ (MPa) |
|---|---|---|
| 1507 | -1399 | 120 |

**Table B.12** *In situ 8084 matrix strengths.*

| $^{+}S_{22}^{22m}$ (MPa) | $^{-}S_{22}^{22m}$ (MPa) | $^{+}S_{33}^{22m}$ (MPa) | $^{-}S_{33}^{22m}$ (MPa) | $S_{12}^{12m}$ (MPa) | $S_{23}^{23m}$ (MPa) |
|---|---|---|---|---|---|
| 37.10 | -118.1 | 2.20 | -7.04 | 34.39 | 25.21 |

The constituent ultimate strengths are listed in Table B.11 and Table B.12. The subscript is the component of ultimate strength and the superscript is the direction of ultimate applied load, e.g., $^{+}S_{33}^{22}$ is the strength (max stress) in the *33* direction when an ultimate *22* tensile load is applied. All constituent ultimate strengths listed are required input to the failure criterion implemented in MCT_77.

## B.6. Uniaxial Laminate Tests

Stress-strain curves for laminate specimens fabricated from E-glass/8084 (fiberglass/vinylester) composites, shown in Fig. B.14-Fig. B.21, were experimentally determined by the University of Wyoming's Composite Materials Research Group from laminates provided by Seemann Composites, Inc. All laminates were fabricated using a proprietary vacuum assisted resin transfer mold process known as Seemann Composites Resin Infusion Process (SCRIMP©).
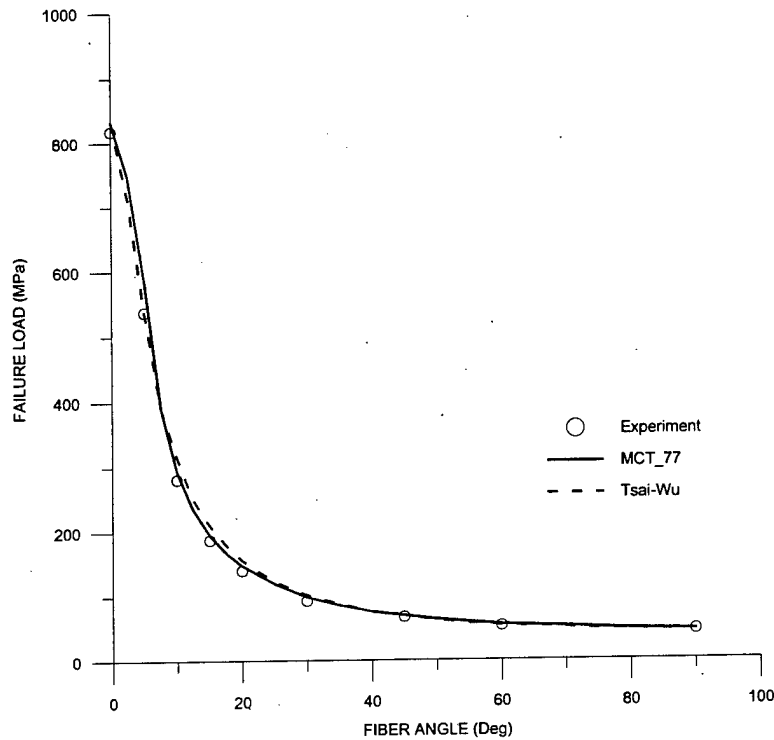


**Fig. B.15** *Off-angle E-glass/8084 lamina under uniaxial tension.*
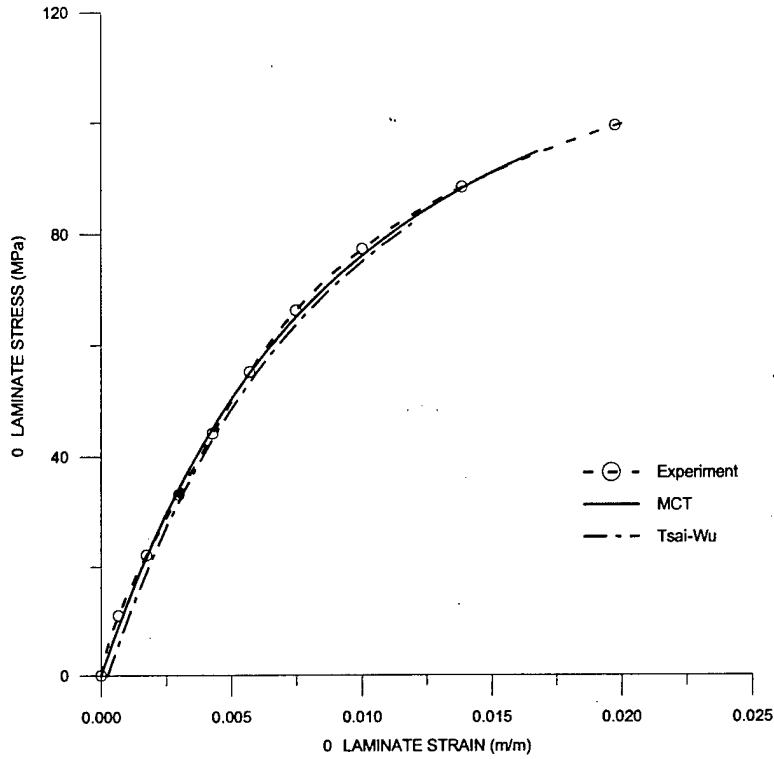
**Fig. B.16** *E-glass/8084 [±45]$_S$ laminate under uniaxial tension.*
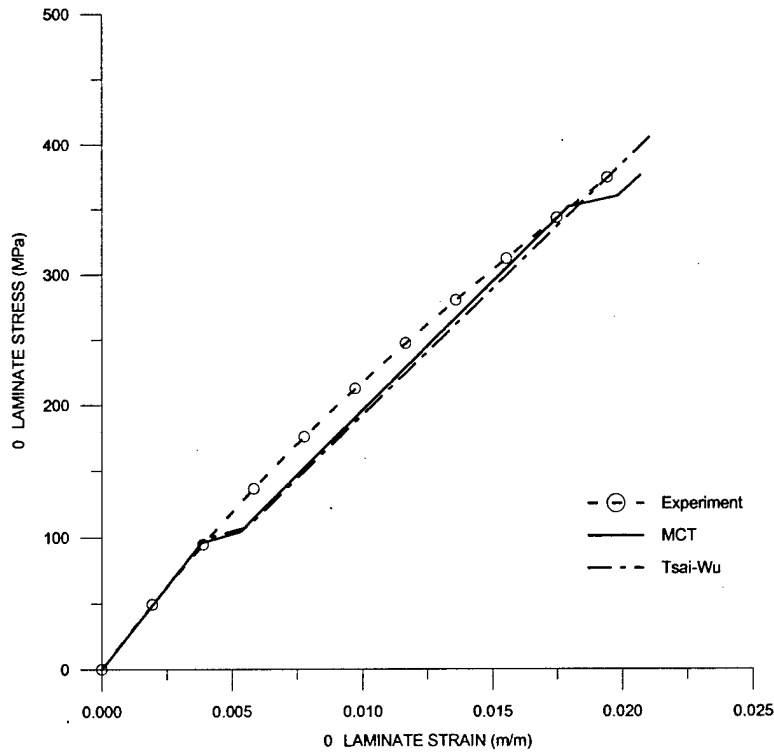


**Fig. B.17** *E-glass/8084 [0/90]$_S$ laminate under uniaxial tension.*
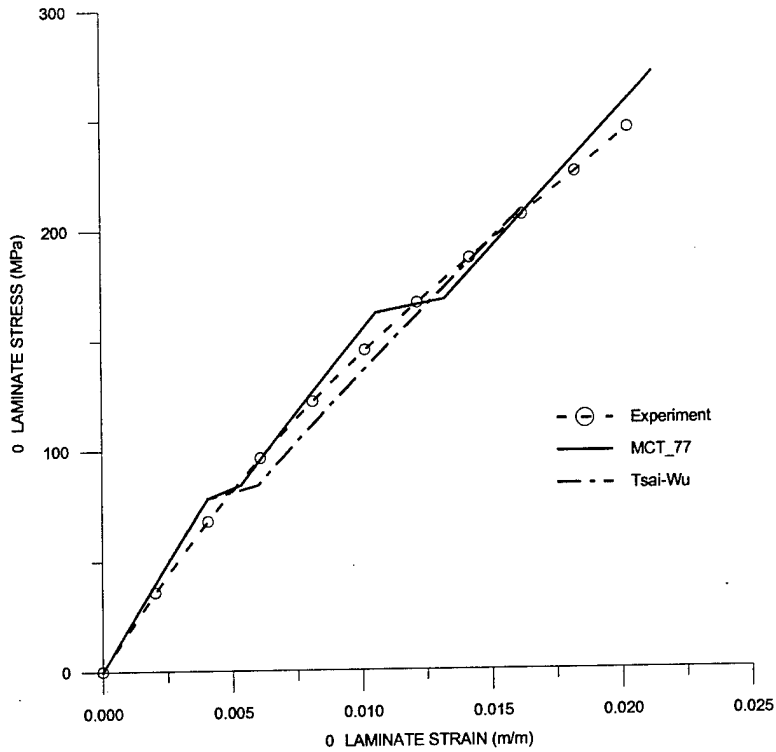
**Fig. B.18** *E-glass/8084 [0/90/±45]$_S$ laminate under uniaxial tension.*
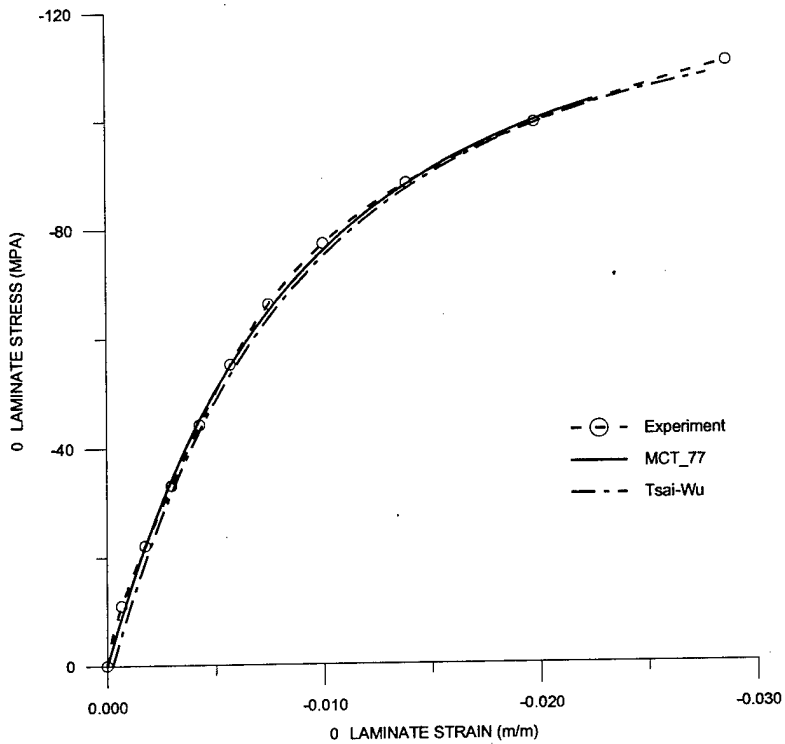


**Fig. B.19** *E-glass/8084 [±45]$_S$ laminate under uniaxial compression.*
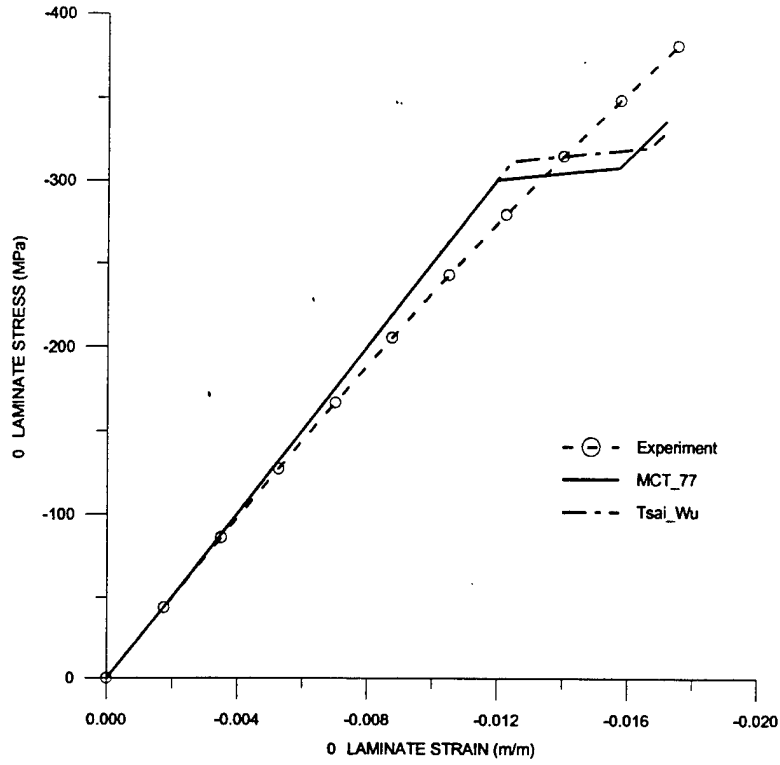
**Fig. B.20** *E-glass/8084 [0/90]ₛ laminate under uniaxial compression.*
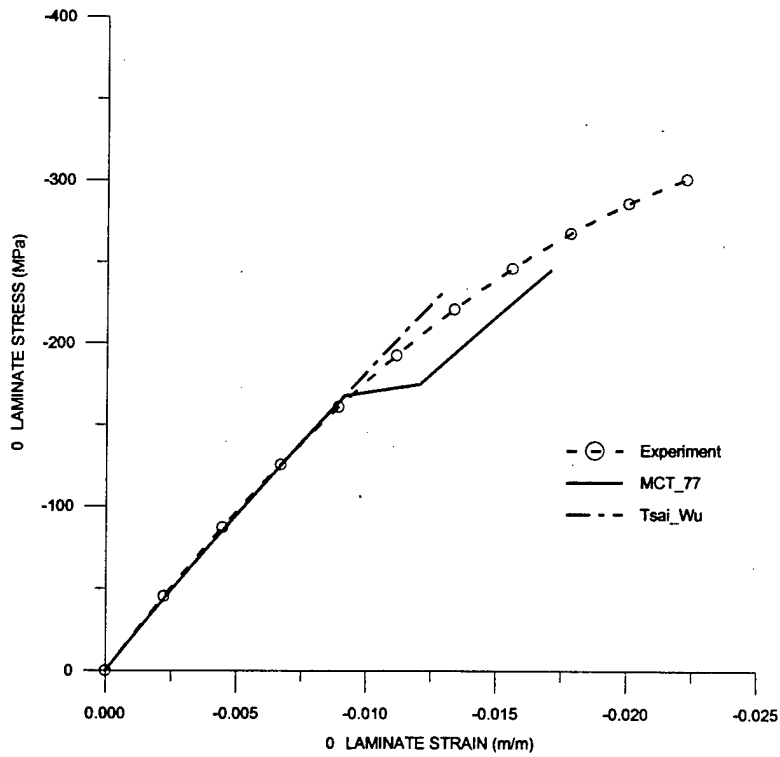


**Fig. B.21** *E-glass/8084 [0/90/±45]ₛ laminate under uniaxial compression.*

# APPENDIX C

# CARBON/3501 LAMINA PROPERTIES

### C.1. Material Test Suite

Composite material properties presented in this appendix are from lamina composed of AS4 carbon fibers in a Hercules 3501-6 epoxy matrix. Average lamina fiber volume fraction ranges from 64% to 67% depending on the data source. Stress strain curves for the six tests making up the material test suite (longitudinal and transverse tension and compression, and longitudinal and transverse shear) are presented in Fig. C.1 through Fig. C.6. These stress-strain curves were experimentally determined by the University of Wyoming's Composite Materials Research Group [1,2,3,4,5] and the Marine Composites Branch, Structures and Composite Department of the Naval Surface Warfare Center's Carderock Division [6,7]. Transverse tensile data was assumed completely linear and was taken from published values [8].

Most of the AS4/3501 results presented are based on least five samples per test. Table C.1 presents the experimentally determined initial elastic constants for the composite. Table C.2 and Table C.3 presents constituent elastic constants backed out from the composite values. Table C.4 and Table C.5 presents curve fit parameters for the nonlinear shear curves.

**Table C.1** *AS4/3501 composite elastic constants derived from experimental data.*

| | $E_{11}$ (GPa) | $E_{22}$ (GPa) | $G_{12}$ (GPa) | $G_{23}$ (Gpa) | $v_{12}$ | FVF |
|---|---|---|---|---|---|---|
| AS4/3501 | 134.0 | 9.14 | 7.29 | 3.16 | 0.261 | 0.66 |

**Table C.2** *In situ elastic constants for AS4 fiber.*

| Constituent | $E_{11}$ (GPa) | $E_{22}$ (GPa) | $G_{12}$ (GPa) | $G_{23}$ (GPa) | $\nu_{12}$ | $\nu_{23}$ |
|---|---|---|---|---|---|---|
| AS4 carbon | 201.0 | 13.5 | 95.0 | 4.90 | 0.22 | 0.25 |

**Table C.3** *In situ elastic constants for 3501 matrix.*

| Constituent | E (Gpa) | $\nu$ |
|---|---|---|
| 3501-6 epoxy | 4.30 | 0.35 |

**Table C.4** *Nonlinear shear-12 curve fit parameters for AS4/3501.*

| $C_0$ (MPa) | $C_1$ (MPa) | $C_2$ (MPa) | $a_1$ | $a_2$ |
|---|---|---|---|---|
| 95.17 | -4189. | 4093. | -32.35 | --31.32 |

**Table C.5** *Nonlinear shear-23 curve fit parameters for AS4/3501.*

| $C_0$ (MPa) | $C_1$ (MPa) | $C_2$ (MPa) | $a_1$ | $a_2$ |
|---|---|---|---|---|
| 360.7 | -4781. | 4421. | -0.2796 | 4.131 |
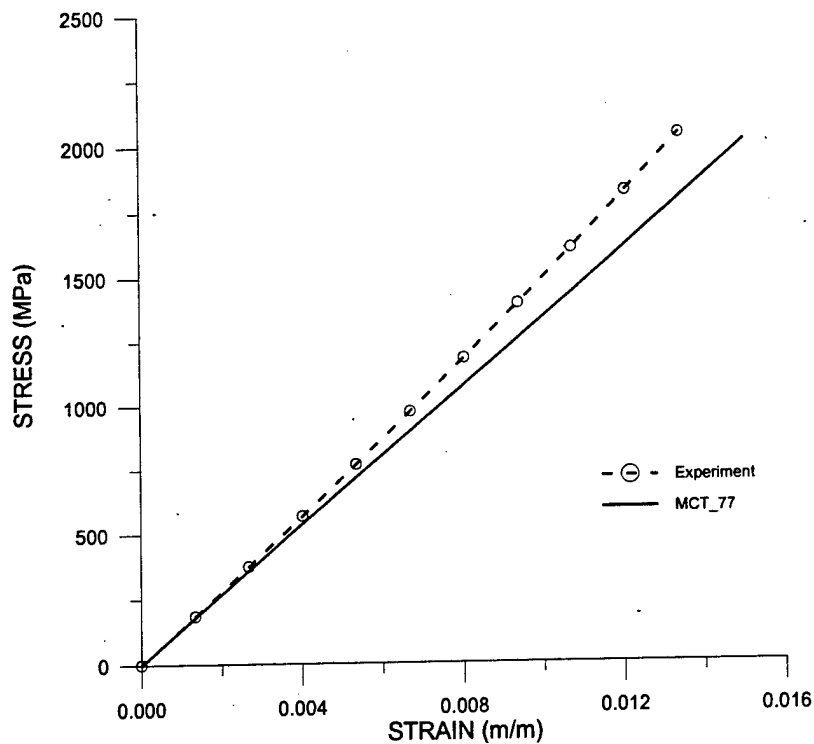


**Fig. C.1** *AS4/3501 lamina under longitudinal tension.*
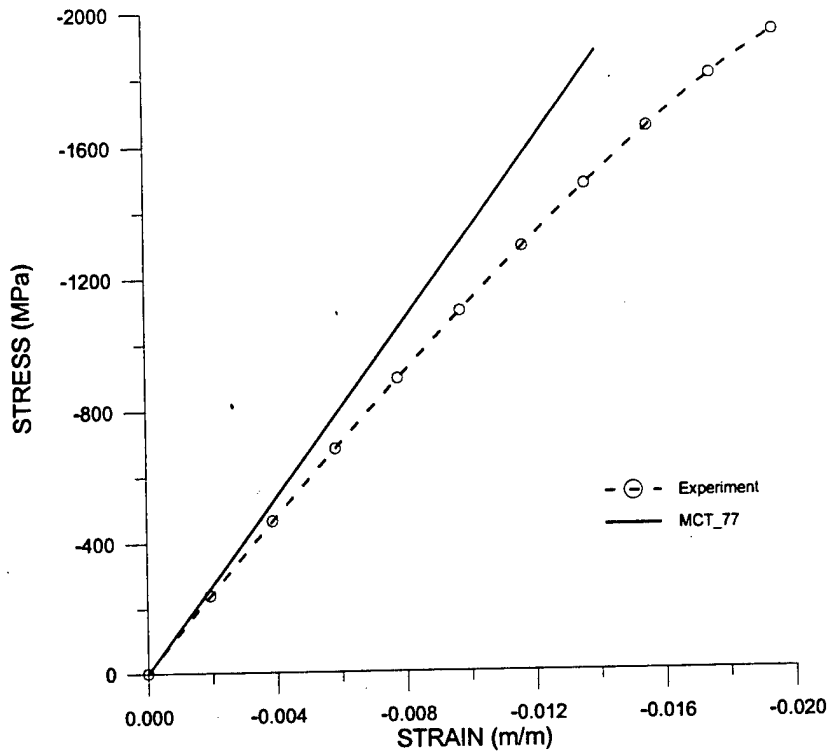
**Fig. C.2** *AS4/3501 lamina under longitudinal compression.*
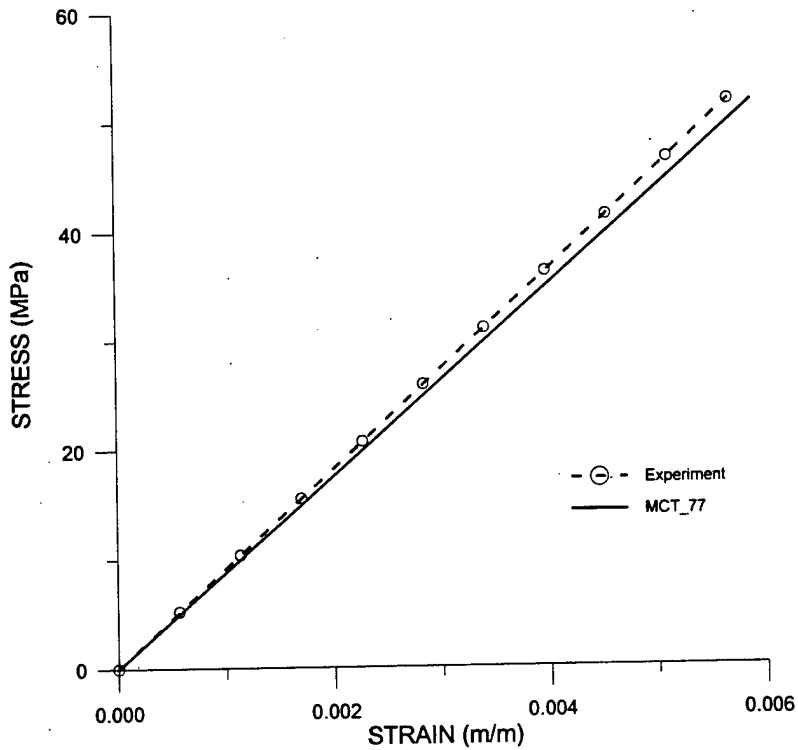


**Fig. C.3** *AS4/3501 lamina under transverse tension.*
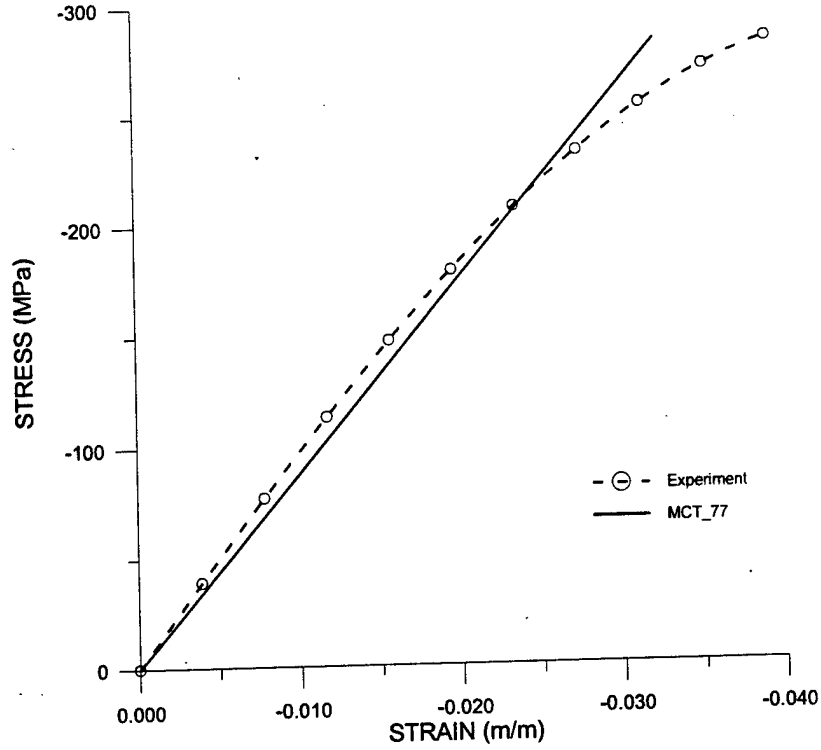
**Fig. C.4** *AS4/3501 lamina under transverse compression.*
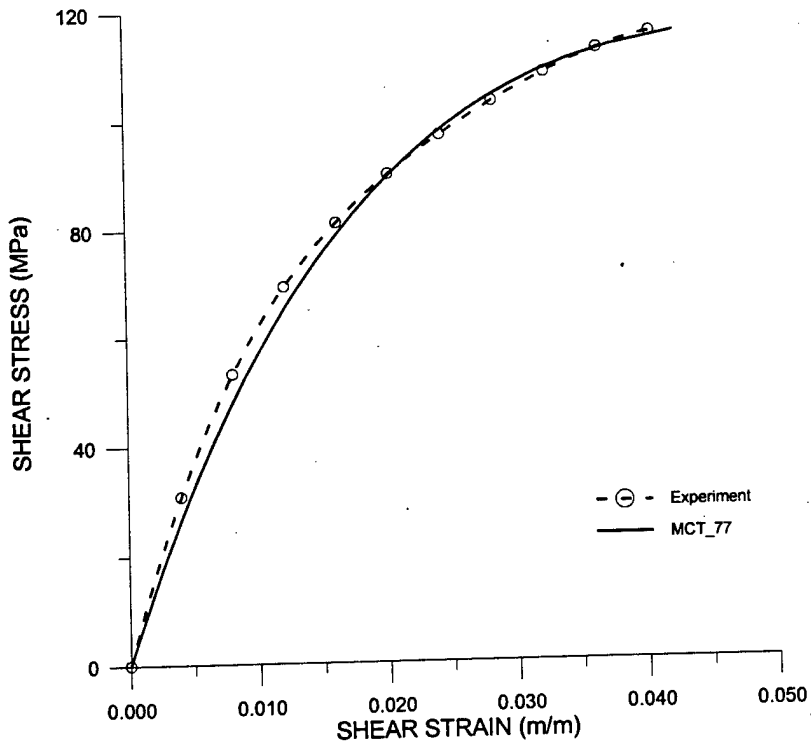


**Fig. C.5** *AS4/3501 lamina under longitudinal shear.*
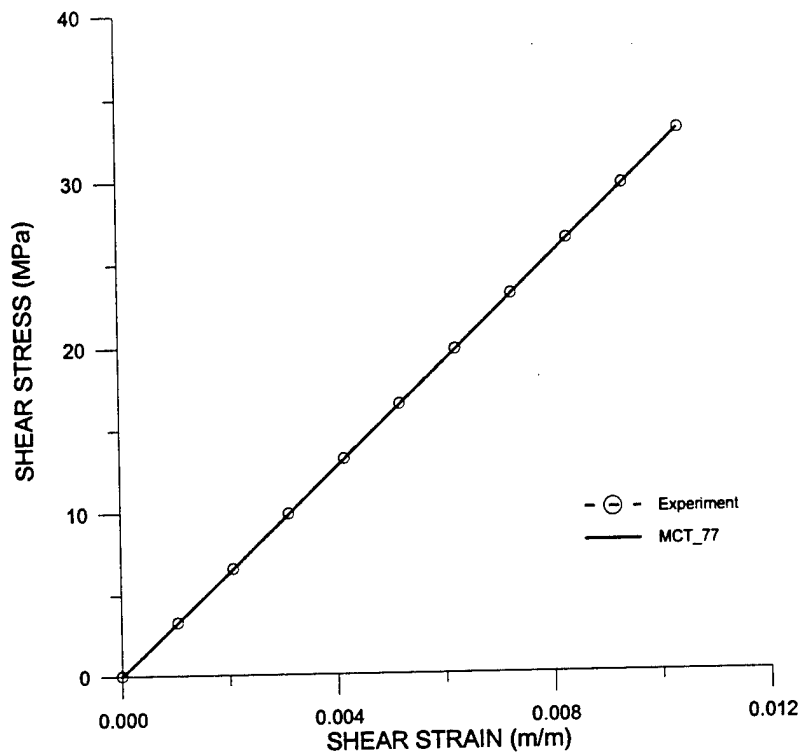
**Fig. C.6** *AS4/3501 lamina under transverse shear.*

### C.2. Micromechanics Results: Referenced to Changing $G_{12}$

Changes in composite and matrix elastic constants with respect to change in the composite shear modulus were determined by invoking the constitutive model described in section 5.3. Although it is the composite shear strain that initiates recalculation of all material constants within the MCT_77 code, the composite-constituent relationships were developed by varying the matrix shear modulus from 0% to 100% of its initial *in situ* value and using micromechanics to derive new composite properties. Once a set of constituent-composite properties are developed, the relationships are redefined in terms of change in shear modulus. A curve for each elastic constant, normalized with respect to the tangent shear modulus, was fitted through the values determined at each data point.

Quadratic equations for four curves, $E_{22}$, $v_{12}$, $G_{23}$, and $G^m$, referenced to changes in composite $G_{12}$ are presented in Fig. C.7 through Fig. C.10. Numerical results are available in Table C.6.
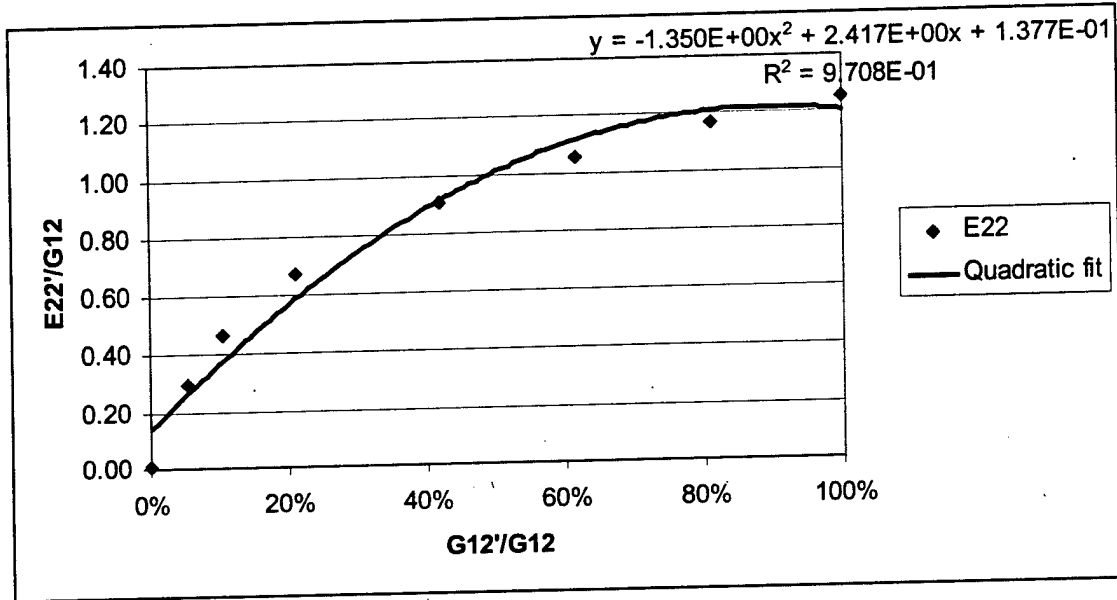


**Fig. C.7** *AS4/3501: $E_{22}$ as a function of change in $G_{12}$.*



**Fig. C.8** *AS4/3501: $v_{12}$ as a function of change in $G_{12}$.*

$$y = -3.725E-01x^2 + 7.612E-01x + 3.258E-02$$
$$R^2 = 9.861E-01$$
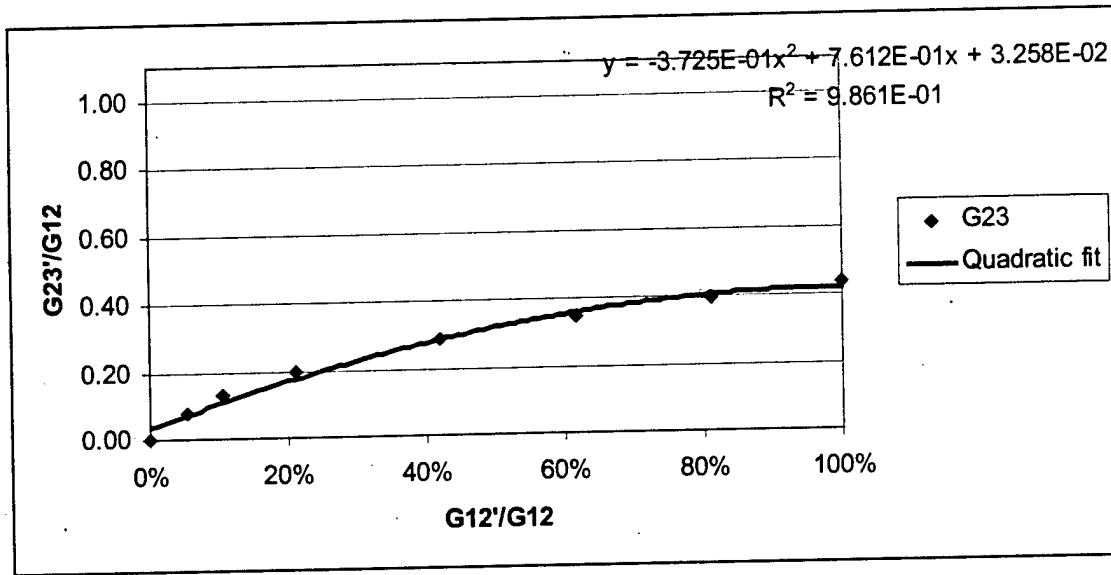
**Fig. C.9** *AS4/3501: $G_{23}$ as a function of change in $G_{12}$.*



$$y = 1.690E-02x^2 + 2.012E-01x + 3.642E-05$$
$$R^2 = 1.000E+00$$
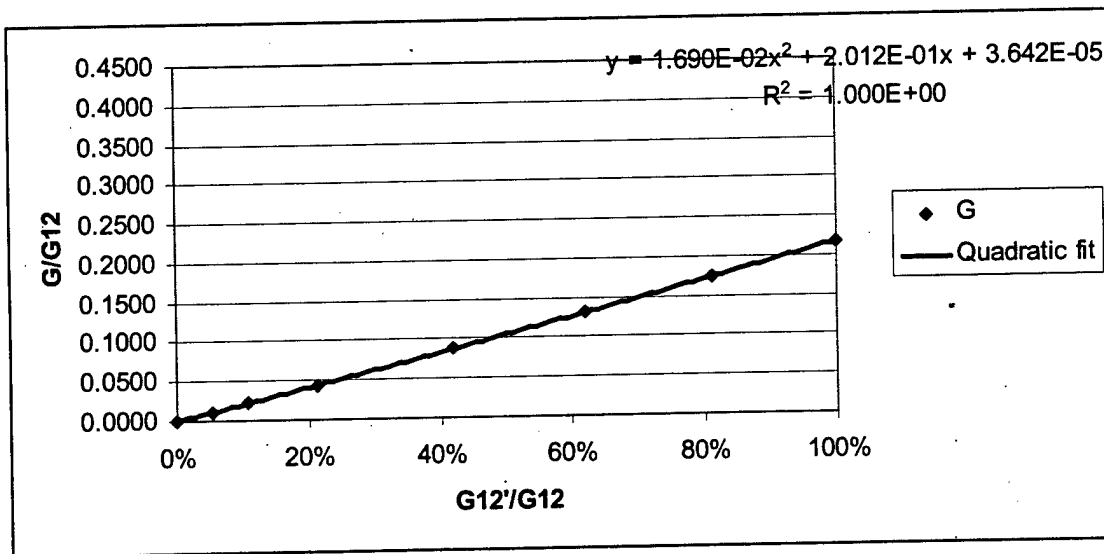
**Fig. C.10** *AS4/3501: G as a function of change in $G_{12}$.*

**Table C.6** *Micromechanics results for AS4/3501 lamina properties referenced to changing $G_{12}$ shear modulus.*

| Matrix | Values | Value/G12 | Composite | Values | Value/G12 |
|---|---|---|---|---|---|
| **100%** | | | | | |
| E (GPa) | 4.295 | | E11 (GPa) | 134.00 | 18.38 |
| G (GPa) | 1.591 | 0.2182 | E22 (GPa) | 9.140 | 1.254 |
| Nu | 0.350 | | G12 (GPa) | 7.291 | 1.000 |
| K (GPa) | 4.772 | | G23 (GPa) | 3.163 | 0.4338 |
| | | | Nu12 | 0.261 | 0.0358 |
| **80%** | | | | | |
| E (GPa) | 3.506 | | E11 (GPa) | 133.80 | 18.35 |
| G (GPa) | 1.273 | 0.1745 | E22 (GPa) | 8.497 | 1.165 |
| Nu | 0.378 | | G12 (GPa) | 5.919 | 0.8118 |
| K (GPa) | 4.772 | | G23 (GPa) | 2.869 | 0.3935 |
| | | | Nu12 | 0.271 | 0.0372 |
| **60%** | | | | | |
| E (GPa) | 2.684 | | E11 (GPa) | 133.50 | 18.31 |
| G (GPa) | 0.954 | 0.1309 | E22 (GPa) | 7.685 | 1.054 |
| Nu | 0.406 | | G12 (GPa) | 4.509 | 0.6184 |
| K (GPa) | 4.772 | | G23 (GPa) | 2.519 | 0.3455 |
| | | | Nu12 | 0.280 | 0.0384 |
| **40%** | | | | | |
| E (GPa) | 1.828 | | E11 (GPa) | 133.2 | 18.27 |
| G (GPa) | 0.636 | 0.0873 | E22 (GPa) | 6.607 | 0.906 |
| Nu | 0.436 | | G12 (GPa) | 3.053 | 0.4187 |
| K (GPa) | 4.772 | | G23 (GPa) | 2.078 | 0.2850 |
| | | | Nu12 | 0.291 | 0.0399 |
| **20%** | | | | | |
| E (GPa) | 0.9337 | | E11 (GPa) | 132.9 | 18.23 |
| G (GPa) | 0.318 | 0.0436 | E22 (GPa) | 4.895 | 0.6714 |
| Nu | 0.467 | | G12 (GPa) | 1.551 | 0.2127 |
| K (GPa) | 4.772 | | G23 (GPa) | 1.445 | 0.1982 |
| | | | Nu12 | 0.302 | 0.0414 |
| **10%** | | | | | |
| E (GPa) | 0.4720 | | E11 (GPa) | 132.7 | 18.20 |
| G (GPa) | 0.1591 | 0.0218 | E22 (GPa) | 3.397 | 0.4659 |
| Nu | 0.484 | | G12 (GPa) | 0.7811 | 0.1071 |
| K (GPa) | 4.772 | | G23 (GPa) | 0.9476 | 0.1300 |
| | | | Nu12 | 0.309 | 0.0424 |
| **5%** | | | | | |
| E (GPa) | 0.2373 | | E11 (GPa) | 132.70 | 18.20 |
| G (GPa) | 0.0795 | 0.0109 | E22 (GPa) | 2.144 | 0.2941 |
| Nu | 0.492 | | G12 (GPa) | 0.3922 | 0.0538 |
| K (GPa) | 4.772 | | G23 (GPa) | 0.5732 | 0.0786 |
| | | | Nu12 | 0.312 | 0.0428 |
| **0.1000%** | | | | | |
| E (GPa) | 0.004772 | | E11 (GPa) | 132.60 | 18.19 |
| G (GPa) | 0.0016 | 0.0002 | E22 (GPa) | 0.05909 | 0.0081 |
| Nu | 0.4998 | | G12 (GPa) | 0.00788 | 0.0011 |
| K (GPa) | 4.772 | | G23 (GPa) | 0.0148 | 0.0020 |
| | | | Nu12 | 0.315 | 0.0432 |

## C.3. Micromechanics Results: Referenced to Changing $G_{23}$

Quadratic equations for four curves, $E_{22}$, $\nu_{12}$, $G_{12}$, and $G^m$, referenced to changes in composite $G_{23}$ are presented in Fig. C.11 through Fig. C.14. Numerical results are available in Table C.7.
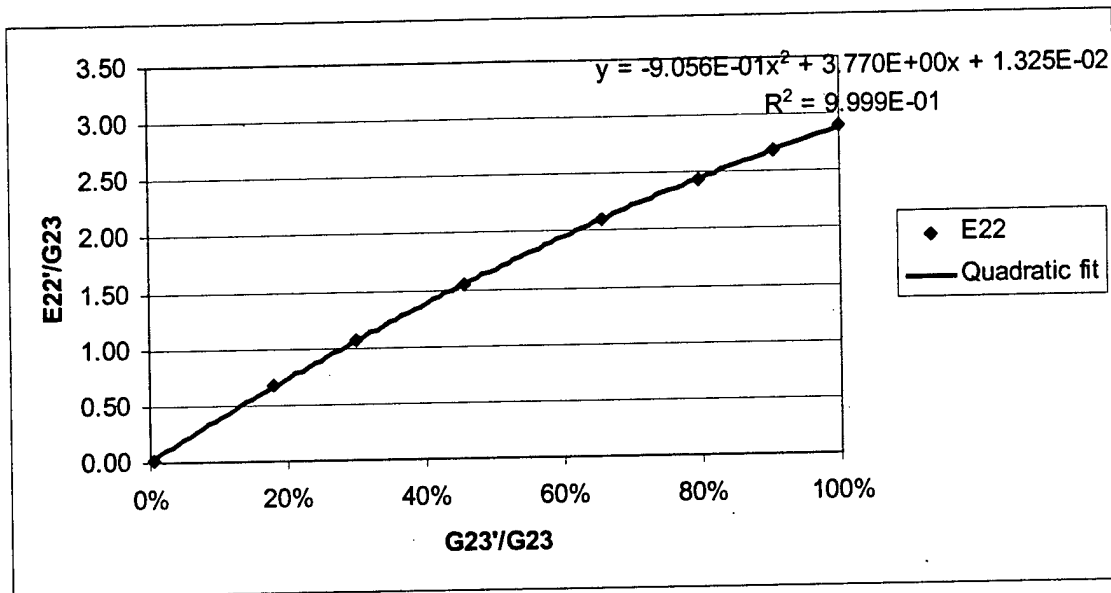


**Fig. C.11** *AS4/3501: $E_{22}$ as a function of change in $G_{23}$.*
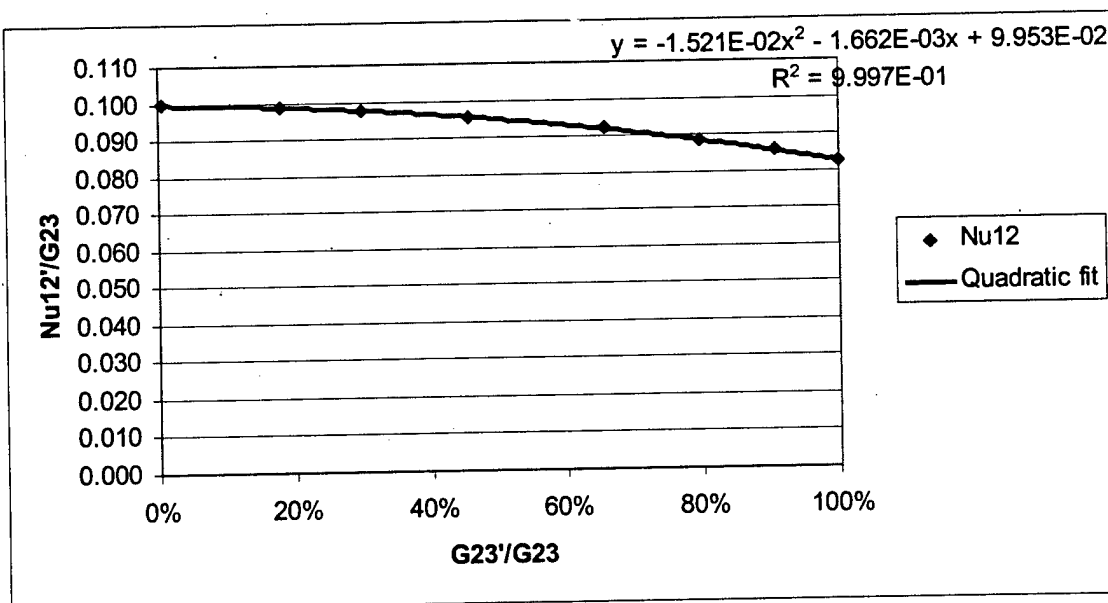


**Fig. C.12** *AS4/3501: $\nu_{12}$ as a function of change in $G_{23}$.*
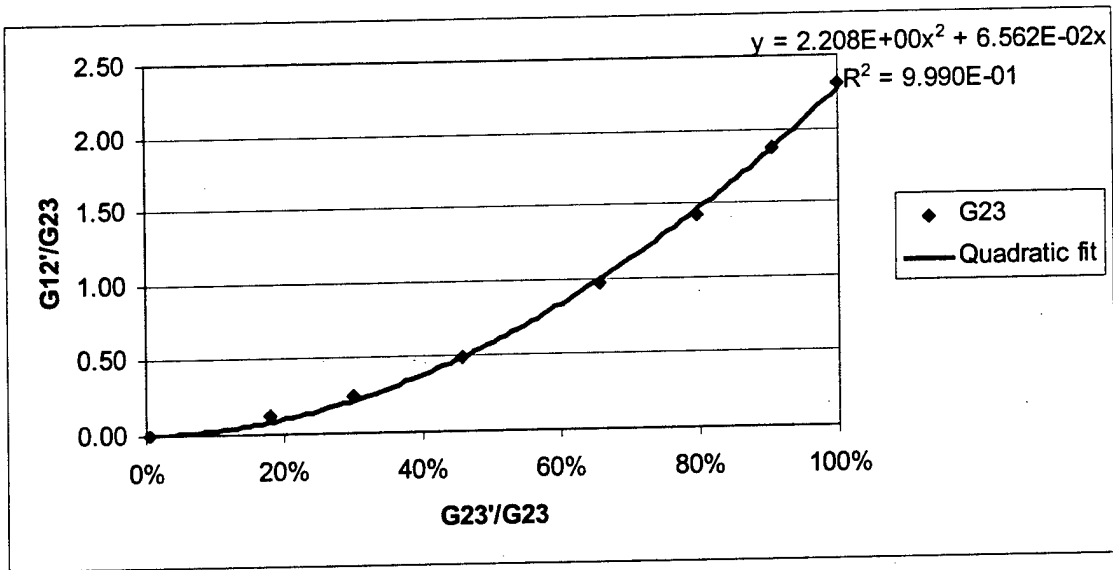
**Fig. C.13** *AS4/3501: $G_{12}$ as a function of change in $G_{23}$.*
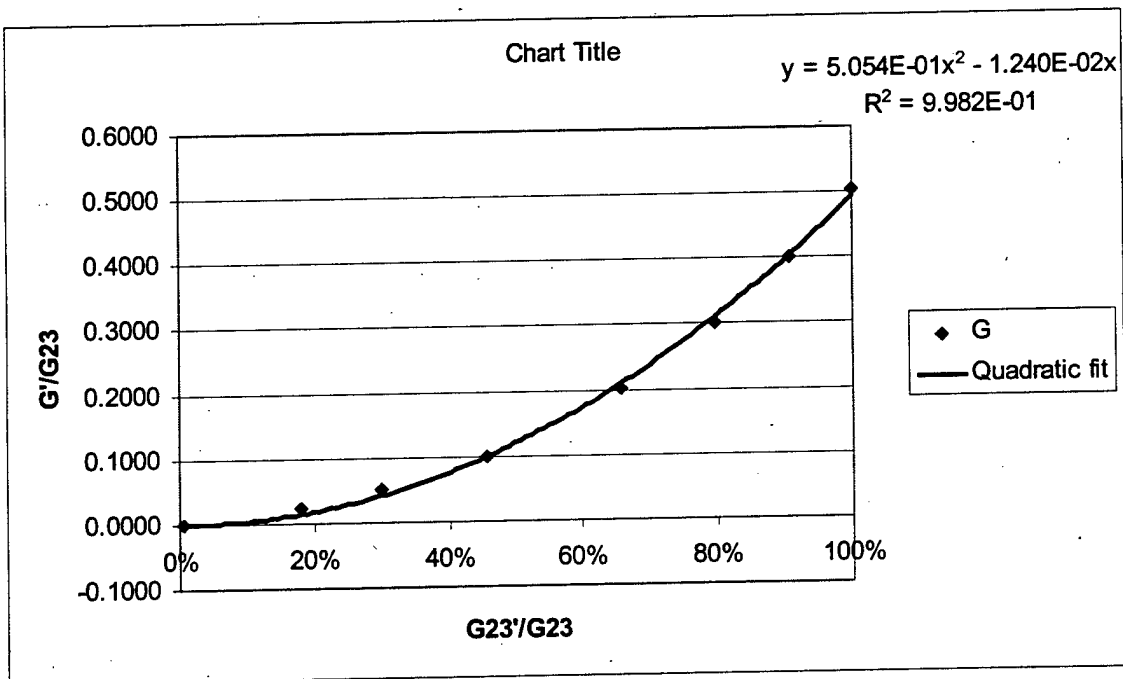


**Fig. C.14** *AS4/3501: G as a function of change in $G_{23}$.*

**Table C.7** *Micromechanics results for AS4/3501 lamina properties referenced to changing $G_{23}$ shear modulus.*

| Matrix | Values | Value/G23 | Composite | Values | Value/G23 |
|---|---|---|---|---|---|
| **100%** | | | | | |
| E (GPa) | 4.295 | | E11 (GPa) | 134.0 | 42.3648 |
| G (GPa) | 1.591 | 0.5029 | E22 (GPa) | 9.140 | 2.8897 |
| Nu | 0.350 | | G12 (GPa) | 7.291 | 2.3051 |
| K (GPa) | 4.772 | | G23 (GPa) | 3.163 | 1.0000 |
| | | | Nu12 | 0.261 | 0.0825 |
| **80%** | | | | | |
| E (GPa) | 3.506 | | E11 (GPa) | 133.8 | 42.3016 |
| G (GPa) | 1.273 | 0.4023 | E22 (GPa) | 8.497 | 2.6864 |
| Nu | 0.378 | | G12 (GPa) | 5.919 | 1.8713 |
| K (GPa) | 4.772 | | G23 (GPa) | 2.869 | 0.9071 |
| | | | Nu12 | 0.271 | 0.0857 |
| **60%** | | | | | |
| E (GPa) | 2.684 | | E11 (GPa) | 133.5 | 42.2068 |
| G (GPa) | 0.954 | 0.3018 | E22 (GPa) | 7.685 | 2.4297 |
| Nu | 0.406 | | G12 (GPa) | 4.509 | 1.4255 |
| K (GPa) | 4.772 | | G23 (GPa) | 2.519 | 0.7964 |
| | | | Nu12 | 0.280 | 0.0885 |
| **40%** | | | | | |
| E (GPa) | 1.828 | | E11 (GPa) | 133.2 | 42.1119 |
| G (GPa) | 0.636 | 0.2012 | E22 (GPa) | 6.607 | 2.0888 |
| Nu | 0.436 | | G12 (GPa) | 3.053 | 0.9652 |
| K (GPa) | 4.772 | | G23 (GPa) | 2.078 | 0.6570 |
| | | | Nu12 | 0.291 | 0.0920 |
| **20%** | | | | | |
| E (GPa) | 0.934 | | E11 (GPa) | 132.9 | 42.0171 |
| G (GPa) | 0.318 | 0.1006 | E22 (GPa) | 4.895 | 1.5476 |
| Nu | 0.467 | | G12 (GPa) | 1.551 | 0.4904 |
| K (GPa) | 4.772 | | G23 (GPa) | 1.445 | 0.4568 |
| | | | Nu12 | 0.302 | 0.0955 |
| **10%** | | | | | |
| E (GPa) | 0.4720 | | E11 (GPa) | 132.7 | 41.9538 |
| G (GPa) | 0.1591 | 0.0503 | E22 (GPa) | 3.397 | 1.0740 |
| Nu | 0.484 | | G12 (GPa) | 0.781 | 0.2469 |
| K (GPa) | 4.772 | | G23 (GPa) | 0.948 | 0.2996 |
| | | | Nu12 | 0.309 | 0.0977 |
| **5%** | | | | | |
| E (GPa) | 0.2373 | | E11 (GPa) | 132.7 | 41.9538 |
| G (GPa) | 0.0795 | 0.0251 | E22 (GPa) | 2.144 | 0.6778 |
| Nu | 0.492 | | G12 (GPa) | 0.392 | 0.1240 |
| K (GPa) | 4.772 | | G23 (GPa) | 0.573 | 0.1812 |
| | | | Nu12 | 0.312 | 0.0986 |
| **0.10%** | | | | | |
| E (GPa) | 0.004772 | | E11 (GPa) | 132.6 | 41.9222 |
| G (GPa) | 0.0016 | 0.0005 | E22 (GPa) | 0.059 | 0.0187 |
| Nu | 0.4998 | | G12 (GPa) | 0.008 | 0.0025 |
| K (GPa) | 4.772 | | G23 (GPa) | 0.015 | 0.0047 |
| | | | Nu12 | 0.315 | 0.0996 |

### C.4. Failure Data: Elastic Constants

Failure of a constituent is assumed absolute without directionality. Moduli for failed constituents are set to near zero values, rather than zero, to avoid numerical difficulties within the MCT_77 code. As shown in Table C.8, matrix moduli are reduced to 1% of the original value. Failed fiber moduli, which are initially one to two orders of magnitude larger than those of the matrix, are reduced such that their magnitudes are of the same order as that of failed matrix to avoid any artificial stiffness in failed regions. Damaged composite properties that reflect failed constituents, shown in Table C.9 and Table C.10, are calculated via the micromechanics model. A complete input file of material properties for a MCT_77 failure analysis consist of seven materials; undamaged composite, intact fiber, intact matrix, fiber failed composite, matrix failed composite, failed fiber, failed matrix. A fiber failed composite assumes simultaneous matrix failure also.

Table C.8 *Elastic constants for AS4/3501 constituents assuming failure.*

| Elastic Constant | Value (GPa) | % of Original Value |
|---|---|---|
| $E_{11}^f$ | 0.0201 | 0.01% |
| $E_{22}^f$ | 0.0135 | 0.1% |
| $G_{12}^f$ | 0.0950 | 0.1% |
| $G_{23}^f$ | 0.0490 | 1.0% |
| $E^m$ | 0.0430 | 1.0% |

Table C.9 *AS4/3501 composite elastic constants with failed fiber/matrix.*

| $E_{11}$ (GPa) | $E_{22}$ (GPa) | $G_{12}$ (GPa) | $G_{23}$ (GPa) | $\nu_{12}$ |
|---|---|---|---|---|
| 0.0280 | 0.0201 | 0.0443 | 0.0309 | 0.286 |

Table C.10 *AS4/3501 composite elastic constants with failed matrix.*

| $E_{11}$ (GPa) | $E_{22}$ (GPa) | $G_{12}$ (GPa) | $G_{23}$ (GPa) | $\nu_{12}$ |
|---|---|---|---|---|
| 132.6 | 2.205 | 0.0787 | 0.0784 | 0.257 |

## C.5. Failure Data: Ultimate Strengths

The ultimate strengths of the composite are taken from material test suit results. Ultimate strengths of the fiber and matrix are backed out of the composite results via a MCT_77 analysis using the material constants listed in Table C.1 through Table C.3 and the composite strengths listed in Table C.11. Determination of constituent shear strengths are further refined by nonlinear regression optimization of experimental results from [$\pm\theta$] tests as discussed in section 5.4. Composite ultimate strengths are not used directly in by the failure criterion implemented in MCT_77.

Table C.11 *AS4/3501 composite ultimate strengths.*

| $^{+}S_{11}$ (MPa) | $^{-}S_{11}$ (MPa) | $^{+}S_{22}$ (MPa) | $^{-}S_{22}$ (MPa) | $S_{12}$ (MPa) | $S_{23}$ (MPa) |
|---|---|---|---|---|---|
| 1335 | -1992 | 28 | -282 | 115 | 33 |

Table C.12 In situ *AS4 carbon fiber strengths.*

| $^{+}S_{11}^{11f}$ (MPa) | $^{-}S_{11}^{11f}$ (MPa) | $S_{12}^{12f}$ (MPa) |
|---|---|---|
| 2000. | -2984. | 170. |

Table C.13 In situ *3501 matrix strengths.*

| $^{+}S_{22}^{22m}$ (MPa) | $^{-}S_{22}^{22m}$ (MPa) | $^{+}S_{33}^{22m}$ (MPa) | $^{-}S_{33}^{22m}$ (MPa) | $S_{12}^{12m}$ (MPa) | $S_{23}^{23m}$ (MPa) |
|---|---|---|---|---|---|
| 22.6 | -228 | -3.63 | 36.7 | 45.1 | 25.0 |

The constituent ultimate strengths are listed in Table C.12 and Table C.13. The subscript is the component of ultimate strength and the superscript is the direction of ultimate applied load, e.g., $^{+}S_{33}^{22}$ is the strength (max stress) in the *33* direction when an ultimate *22* tensile load is applied. All constituent ultimate strengths listed are required input to the failure criterion implemented in MCT_77.

1 Welsh, J.S., and D.F. Adams, "Unidirectional Composite Compression Strengths Obtained by Testing Mini-Sandwich, Angle-, and Cross-Ply Laminates," Composite Materials Research Group Report No. UW-CMRG-R-95-106, Laramie, WY, April 1995.

2 Lewis, Q. E., "An Evaluation of Composite Material Shear Test Methods," Masters Thesis, University of Wyoming, Department of Mechanical Engineering, Laramie, WY, May 1991.

3 Kessler, J.A., and D.F. Adams, "Standardization of Test Methods for Laminated Composites – Volume II: Experimental Efforts," Composite Materials Research Group Report No. UW-CMRG-R-93-102, Laramie, WY, October 1993.

4 Finley, G.A. and D.F. Adams, "An Analytical and Experimental Study of Unidirectional Composite Thickness-Tapered Compression Specimens," Composite Materials Research Group Report No. UW-CMRG-R-95-101, Laramie, WY, January 1995.

5 Adams, D.F. and D.A. Crane, "Combined Loading Micro-Mechanical Analysis of a Unidirectional Composite", *Composites*, Vol. 15, No. 3, pp. 181-191, July 1984

6 Gipple, K.L. and D. Hoyns, "Measurement of the Out-of-Plane Shear Response of Thick Section Composite Materials Using the V-Notched Beam specimen", *Journal of Composite Materials*, Vol. 28, No. 6, pp. 543-572, 1994

7 Gipple, K.L., and D. Hoyns, Personal correspondence of unpublished experimental data, December 1998

8 Tsai, S.W., and H. T. Hahn, Introduction to Composite Materials, Technomic Publishing, Lancaster, PA, page 292, 1980

# APPENDIX D

# USING EXCEL FOR CURVE FITTING

Two types of curve fits are used by the material model within the MCT_77 finite element code. The first determines an equation defining nonlinear shear stress-strain relationships. The second defines relationships between composite and constituent properties due a varying composite shear modulus.

## D.1. Curve Fitting Nonlinear Shear Data

Three terms of an exponential series are used to determine nonlinear composite shear stress-strain relationships. The equation has the form

$$\tau = C_0 + C_1 e^{(a_1\gamma)} + C_2 e^{(a_2\gamma)},$$

(D.1)

where $C_i$ and $a_i$ are curve fit constants, $\gamma$ is engineering shear strain, and $\tau$ is shear stress. Equation (D.1) has five curve fit parameters to be determined for a best fit of shear stress-strain data points.

Microsoft® Excel, in conjunction with the Solver analysis option, offers a convenient environment for implementing a nonlinear regression approach to solve for the five curve fit constants. Microsoft® Excel Solver is an Add-in analysis package included with the standard spreadsheet routines. If Solver doesn't appear under the Tools menu on the

toolbar, then it must be installed by checking the Solver option box under Tools|Add-Ins|Available Add-Ins.

The method begins by placing stress-strain data in adjacent columns on the spreadsheet. Five cells are designated to hold the five constants to be determined. For clarity, labels identifying the constants are placed next to appropriate cells. It is also very advantageous to use the Insert|Name|Define command sequence from the toolbar to name each cell for the appropriate constant. Subsequent equations using the constants can be written in a more natural and easier to read manner. See Fig. D.1 for an example spreadsheet.
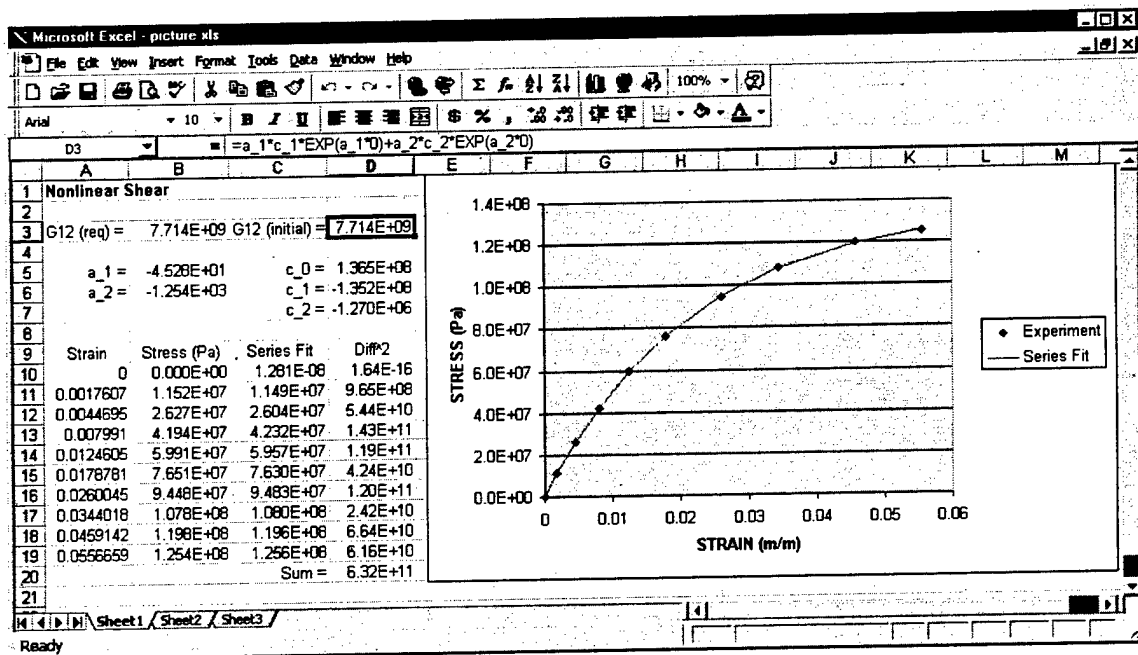


**Fig. D.1** *Nonlinear spreadsheet setup.*

Using equation (D.1), a formula for calculating predicted stress values is typed into the first cell of the column adjacent to the stress-strain data. In the formula, cell reference

notation , e.g., "A8", is used in place of the actual strain value from that data point. For example, the formula might look like

$$= c\_0 + c\_1 * EXP(a\_1 * A10) + c\_2 * EXP(a\_2 * A10). \qquad (D.2)$$

The formula defined for the first cell can then be copied and pasted to remaining cells.

The next adjacent column will contain the square-of-the-differences between predicted and actual stress values. Using cell reference notation, the formula might look like

$$= (B10 - C10)^2. \qquad (D.3)$$

Again, the formula can be written for the first cell in the column and copied to the remaining ones.

At the bottom of the column containing the square-of-the-differences, the Insert|Function|Math&Trig|Sum command sequence is used to sum the cells in the column. This cell, known as the residual, becomes the target of subsequent Solver minimization operations.

It is critical that the initial shear modulus, defined by the derivative of the stress-strain curve, is equal to the shear modulus calculated by the micromechanics model. Designate one cell on the spreadsheet to hold the shear modulus as calculated by micromechanics. In another cell, insert the derivative of the equation (D.1) evaluated at $\gamma = 0$. Equivalence

of the shear modulus determined by micromechanics and the curve equation first derivative will form a constraint on the Solver optimization.

Results of a nonlinear analysis regression are highly dependent on starting values. Generally, nonlinear composite shear curves have the same basic shape, hence, curve fit constants that work for one data set provides excellent starting values for another. Trial starting values are provided in Table D.1.

**Table D.1** *Trial starting values for nonlinear regression analysis.*

| $C_0$ (MPa) | $C_1$ (MPa) | $C_2$ (MPa) | $a_1$ | $a_2$ |
|---|---|---|---|---|
| 136.5 | -135.2 | -1.270 | -45.28 | -1254 |

Visualization of the exponential series curve fit to experimental data can be extremely helpful. Use the Chart Wizard to plot both experimental and predicted shear stress values against strain. Choose the XY (Scatter) Plot option. Format the experimental data to be displayed as symbols and the predicted data as a continuous line. (See Fig. D.2).

Nonlinear regression is accomplished by the **Tools|Solver** command sequence. Solver nonlinear optimization is accomplished via the method of Generalized Reduced Gradient. With the Solver window active make the following dialog box entries:

1. Select the sum of the difference squared cell as the S**e**t Target Cell.
2. Choose to minimize the value of that cell by setting Equal to: Mi**n**.
3. In the **B**y Changing Cells: enter (or highlight) the cells containing the five curve fit parameters.
4. In the S**u**bject to Constraints: box select **A**dd and set the cell containing the modulus calculated by the derivative of the shear stress strain curve equal to the cell containing the modulus calculated from micromechanics.
5. In the S**u**bject to Constraints: box select **A**dd and set the predicted stress value corresponding to zero strain equal to zero.

6. Select the <u>O</u>ptions button and another window will open.
7. In the Solver Options window set Tol<u>e</u>rance: to 0.1%
8. Make sure that the Use <u>A</u>utomatic Scaling option is turned on
9. Click OK to close the Solver Options window.
10. Click <u>S</u>olve to begin the Solver optimization.

See Fig. D.2 for an sample Solver window and dialog boxes.
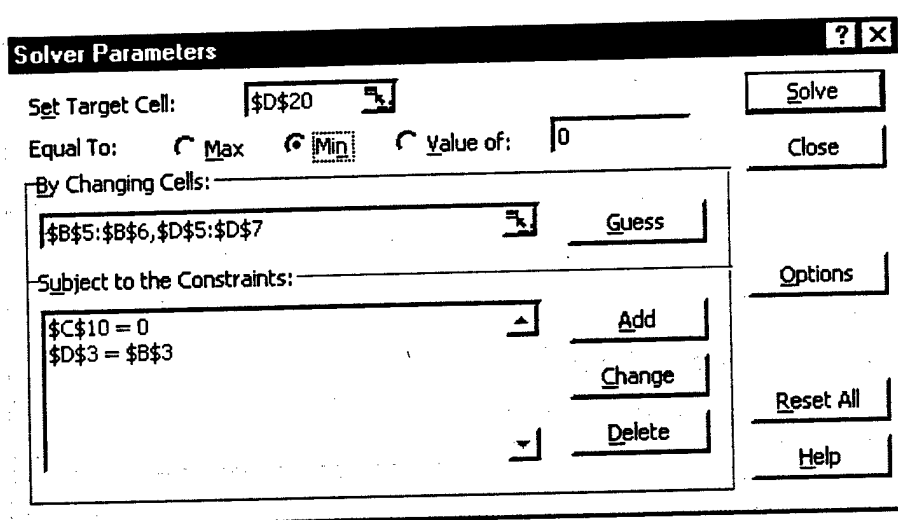


**Fig. D.2** *Sample Solver window.*

Once Solver has converged on a solution, it is recommended using the new curve fit parameters as starting values for another Solver iteration. Continue repeating until Solver no longer iterates.

Better curve fits of MCT_77 analysis results against experimental data with shear present can be achieved if the incremental modulus-strain form for predicting shear stress is used

$$= (a\_0 * c\_1 * EXP(a\_1 * A11) + a\_2 * c\_2 * EXP(a\_2 * A11)) * (A12 - A11) + C8.$$
(D.4)

Use the same Solver optimization procedure as outlined above. Note that the constant term in equation (D.2) does not appear in equation (D.4). An additional constraint must be added so that equation (D.1) produces zero stress given zero strain when optimizing equation (D.4).

Nonlinear regression can, at times, require some trial and error on the part of the user to arrive at a suitable solution. If the trial values provided in Table D.1 fail to produce a convergent solution, use the graph of actual and predicted values as a guide to manually change the curve fit parameters to find different starting values.

## D.2. Curve Fitting Composite-Constituent Relationships

The assumption of linear elasticity coupled with a nonlinear shear stress-strain curve implies that both composite and constituent material properties change when a shear load is present. MCT computes a tangent modulus from the shear stress-strain curve fit equation. In order to maintain a consistent relationship between composite and constituents, the constituents must reflect the changing composite shear modulus. Changing constituent properties, in turn, affect other composite elastic constants besides shear modulus. A set of second order polynomial (quadratic) curve fits defining the composite-constituent relationships are developed in a one-time operation outside the MCT finite element code using micromechanics and an Excel spreadsheet.

Although it is the composite shear strain that initiates recalculation of all material constants within the code, the relationships are developed by varying matrix properties in a prescribed manner and using micromechanics to derive new composite properties.

Once a set of constituent-composite properties are defined, the relationships are defined in terms of change in shear modulus.

To characterize the matrix for micromechanics analysis, it is assumed that the matrix bulk modulus is independent of stress state. The shear modulus is varied from 0%-100% (usually in increments of 10%) of its *in situ* value as determined from the material test suite and micromechanics. Note that a value near zero (~0.1%) is used instead of zero to avoid numerical difficulties. Having defined two material constants, any remaining matrix properties can be determined using standard isotropic material relationships.

The results of each discrete increment in matrix material constants provides input to the micromechanics model for calculating corresponding composite constants. The matrix and composite material constants are placed in an Excel spreadsheet. Additionally, four of the composite material constants ($E_{22}$, $G_{12}$, $G_{23}$, $v_{12}$) and the matrix shear modulus (G) must be expressed as a ratio of their current value to the initial composite shear modulus. Examples of spreadsheet layouts that effectively present the above analysis can be found in Tables A.4, B.5, B.6, C.6 and C.7.

The graphing routines within Excel have limited curve fitting capability. Use the Chart Wizard to create four plots of $E_{22}$, G, $G_{23}$, and $v_{12}$ ratios against the composite shear modulus ratio for each increment. Choose the XY (Scatter) Plot option. By default, the data points will be displayed as symbols. Within each chart, highlight the data points (left mouse click on a data point) and then right mouse click for a menu. Choose Add

Trendline. Under the Type tab, choose Polynomial. By default the Order will be set to two. Under the Options tab, check the dialog boxes for Displaying equation on chart and Display R-squared value on chart. Click OK to close the Add Trendline window. The quadratic curve fit equation for each of the four plots should be displayed. Make sure the equation's ordinate intercept has a positive or zero value. If it is negative, highlight the trendline and right mouse click for a menu. Choose Format Trendline. Under the Options tab check the dialog box for Set intercept =. The default value is zero. Click OK to close the Format Trendline window.

Coefficients of the these quadratic equations are inputs for the sdata file described in Appendix F. Examples of material ratio plots can be found in Figures A.6-A.9, B.7-B.14, and C.7-C.14.

# APPENDIX E

# USING EXCEL FOR OPTIMIZATION OF FAILURE PARAMETERS

The MCT failure criteria described in Section 4 requires determination of five failure parameters, $A_1{}^f$, $A_4{}^f$, $A_2{}^m$, $A_3{}^m$, and $A_4{}^m$. These parameters are functions of ultimate constituent strengths, $^\pm S_{11}{}^f$, $S_{12}{}^f$, $^\pm S_{22}{}^m$, $^\pm S_{33}{}^m$, $S_{12}{}^m$, and $S_{23}{}^m$. Constituent strengths are derived from experimentally determined composite lamina ultimate strengths. Determining which constituent precipitates composite failure is necessary for establishing accurate constituent failure values. Identifying which constituent precipitated failure in longitudinal and transverse lamina tension and compression tests is intuitive and straightforward. Identifying the constituent leading to shear failure is more problematic, especially in view that the ultimate constituent shear strengths are the sole contributors to failure parameters $A_3$, and $A_4$.

This appendix outlines a procedure for optimizing the failure parameters by using non-linear regression analysis in a manner similar to that used in Appendix D to characterize shear stress-strain curves.

## E.1. Failure Criterion

As shown in Section 4, the general form of the stress interactive failure criterion used here is

$$A_1 I_1^2 + A_2 I_2^2 + A_3 I_3 + A_4 I_4 = 1. \qquad (E.1)$$

Following Hashin's delineation of two failure modes, fiber influenced and matrix influenced, we develop a form of (E.1) for each constituent. The fiber failure criteria has the form

$$\pm A_1^f \left(I_1^f\right)^2 + A_4^f I_4^f = 1,$$

(E.2)

where the failure parameters were determined to be

$$\pm A_1^f = \frac{1}{\left(\pm S_{11}^f\right)^2}, \qquad \text{and} \qquad A_4^f = \frac{1}{\left(S_{12}^f\right)^2}.$$

The symbol, $\pm$, indicates that the appropriate tensile or compressive strength value be used depending on the stress state.

The matrix failure criteria has the form

$$\pm A_2^m \left(\pm I_2^m\right)^2 + A_3^m I_3^m + A_4^m I_4^m = 1,$$

(E.3)

where the failure parameters were determined to be

$$A_3^m = \frac{1}{2\left(S_{23}^m\right)^2},$$

(E.4)

$$A_4^m = \frac{1}{\left(S_{12}^m\right)^2},$$

(E.5)

and

$$\pm A_2^m = \frac{1}{\left(\pm S_{22}^{22m} + \pm S_{33}^{22m}\right)^2}\left(1 - \frac{\left(\pm S_{22}^{22m}\right)^2 + \left(\pm S_{33}^{22m}\right)^2}{2\left(S_{23}^m\right)^2}\right),$$

(E.6)

$$= \frac{1}{\left(\pm I_2^{mo}\right)^2}\left(1 - A_3^m\left(\pm I_3^{mo}\right)\right).$$

## E.2. Optimization of the Failure Parameters

Microsoft® Excel, in conjunction with the Solver analysis option, offers a convenient environment for implementing a nonlinear regression approach to solve for the failure parameters. Microsoft® Excel Solver is an Add-in analysis package included with the standard spreadsheet routines. If Solver doesn't appear under the Tools menu on the toolbar, then it must be installed by checking the Solver option box under Tools|Add-Ins|Available Add-Ins.

Data from off-angle, balanced, symmetric laminates, $[\pm\theta]_s$, provide an excellent basis for determining optimized failure parameter values. These laminates produce varying degrees of shear and normal stresses and tend to fail in modes allowing analytical identification of the constituent precipitating laminate failure. Other off-angle laminates, $[+\theta]_n$ or $[-\theta]_n$ also produce varying shear and normal stresses but should be used with caution because of non-uniform stress states caused by warping of the test specimen. It is important to generate both tension and compression results for the off-axis laminates.

From ultimate composite failure strengths for each off-angle laminate, MCT_77 is used to calculate the constituents' transversely isotropic stress invariants at the experimentally determined point of composite failure.

Next, failure modes for each laminate tested must be identified. Composite failure is generally fiber dominated at lower fiber orientation angles (approximately 20° and less) and matrix dominated at higher fiber angles. It is difficult to determine failure modes

visually, so it becomes more convenient to do so analytically. Good initial guesses for constituent ultimate shear strengths can be derived, via MCT_77, from experimentally determined ultimate composite shear strengths or taken from the literature if available. An MCT_77 failure analysis of each off-axis test, using the initial guesses, tentatively identifies the failure mode. After the first trial optimization, new derived values for $A_3$ and $A_4$ be can used to check the failure modes. If modes change, another iteration is required.

Actual optimization begins by sorting the data by failure mode and placing the transversely isotropic stress invariant data for each test in adjacent columns on separate spreadsheets. The data are further sorted by tension or compression failures. Cells are designated to hold the failure parameters to be determined. For clarity, labels identifying the parameters are placed next to the appropriate cells. It is also very advantageous to use the Insert|Name|Define command sequence from the toolbar to name each cell for the appropriate parameter. Subsequent equations using the parameters can be written in a more natural and easier to read manner. See Fig. E.1 for an example spreadsheet.

The value of $A_2$, as determined by equation (E.6), depends on the stress invariants at the ultimate transverse strength, $I_3^{mo}$ and $I_4^{mo}$. These values are also placed on the spreadsheet and named. Note that $A_2$ takes on different tensile and compressive values as do the invariants that compose it.
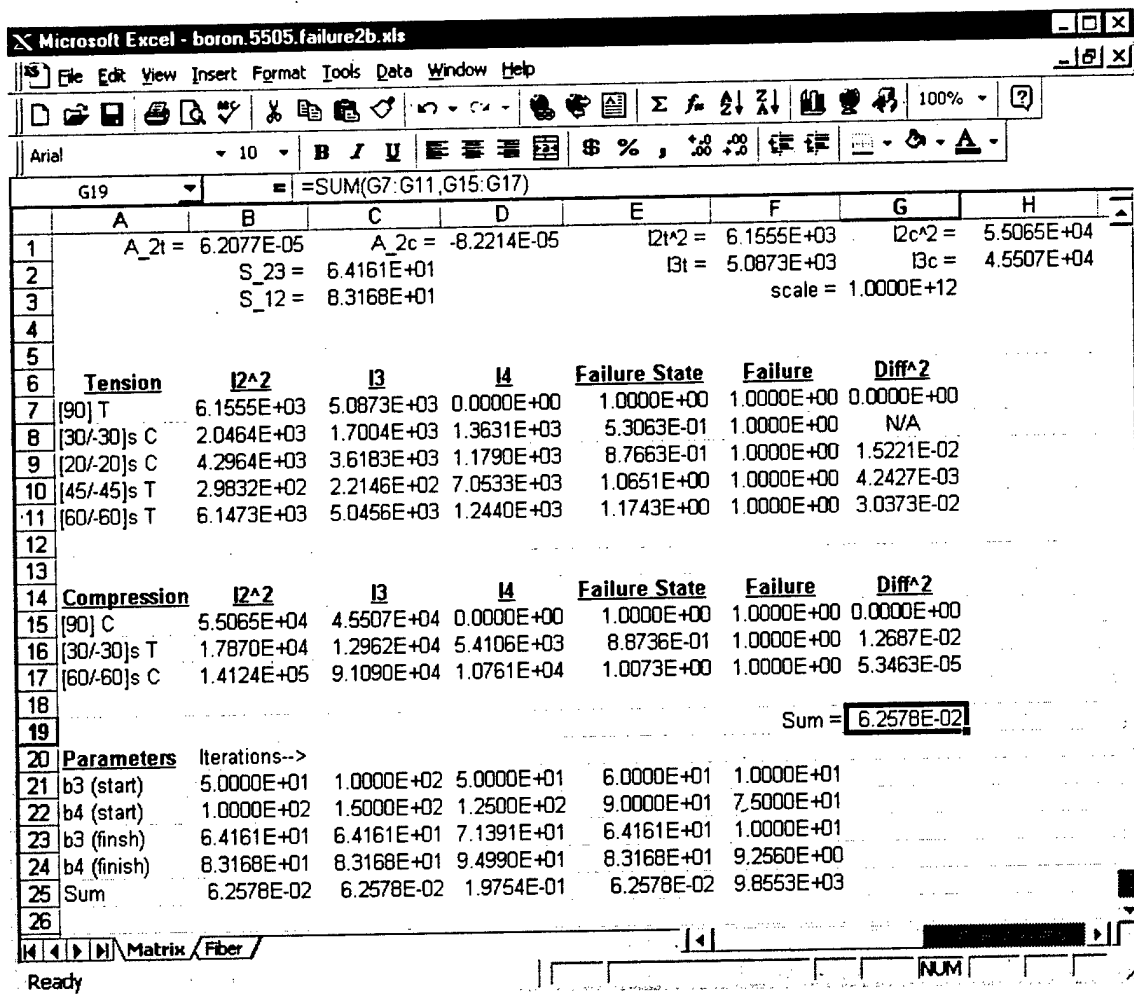
**Fig. E.1** *Excel spreadsheet setup for determining matrix failure parameters.*

For the Solver optimizer to work properly, all invariants must be scaled to a reduced magnitude. For the example shown above using SI units, the invariants are scaled by $(MPa)^2$ or $1.0 \times 10^{12}$. The failure parameters determined by the optimization will be reduced by $1.0 \times 10^6$.

Next, the failure state, as determined by the failure criterion (in this example the matrix equation (E.3)), is typed into the first cell of column adjacent to the invariant data. In the

formula, the cell reference notation , e.g., "B7", is used in place of the actual invariant value from that data point. For example, the formula might look like

$$= A\_2t * B7 + C7/S\_23^2 + D7/S\_12^2 . \qquad (E.7)$$

The formula defined for the first cell can then be copied and pasted to the remaining cells.

The next adjacent column will contain the square-of-the-differences between the predicted failure state and unity (the value designating failure). Using cell reference notation, the formula might look like

$$= (E7 - F7)^2 . \qquad (E.8)$$

Again, the formula can be written for the first cell in the column and copied and pasted to the remaining ones.

At the bottom of the column containing the square-of-the-differences, the Insert|Function|Math&Trig|Sum command sequence is used to sum both the tension and compression cells in the column. This cell, designated the residual, becomes the target of subsequent Solver optimization operations to minimize it.

It appears from the limited analysis done within this research that the more data points used in the nonlinear optimization, the better the convergence to optimized failure parameters. Convergence is further enhanced by constraining optimization to achieve

failure states of unity for the limiting cases of pure transverse tension and compression loads, and positive failure states for all other cases.

Nonlinear regression is accomplished executing the Tools|Solver command sequence. Solver nonlinear optimization is accomplished via the method of Generalized Reduced Gradient. With the Solver window active make the following dialog box entries:

1. Select the sum of the difference squared cell as the Set Target Cell.
2. Choose to minimize the value of that cell by setting Equal to: Min.
3. In the By Changing Cells: enter (or highlight) the cells containing the five curve fit parameters.
4. In the Subject to Constraints: box select Add. Set the cell containing the failure states for the transverse only loads to unity and all other failure states to greater than or equal to zero (positive definite). .
5. In the Subject to Constraints: box select Add and set the predicted stress value corresponding to zero strain equal to zero.
6. Select the Options button and another window will open.
7. In the Solver Options window set Tolerance: to 0.1%
8. Make sure that the Use Automatic Scaling option is turned on
9. Click OK to close the Solver Options window.
10. Click Solve to begin the Solver optimization.

See Fig. E.2 for an sample Solver window and dialog boxes.

The results of a nonlinear analysis regression are highly dependent on starting values. As mentioned previously, ultimate constituent shear strength values derived from experimentally determined composite results provide excellent starting values. There appear to be numerous local minima in the failure surface defined by all possible (realistic or not) failure parameters. Hence, it is important to do numerous optimizations trials using different starting points to determine the global minima. Rows 21 through 25 in the example spreadsheet show the results of five trials.
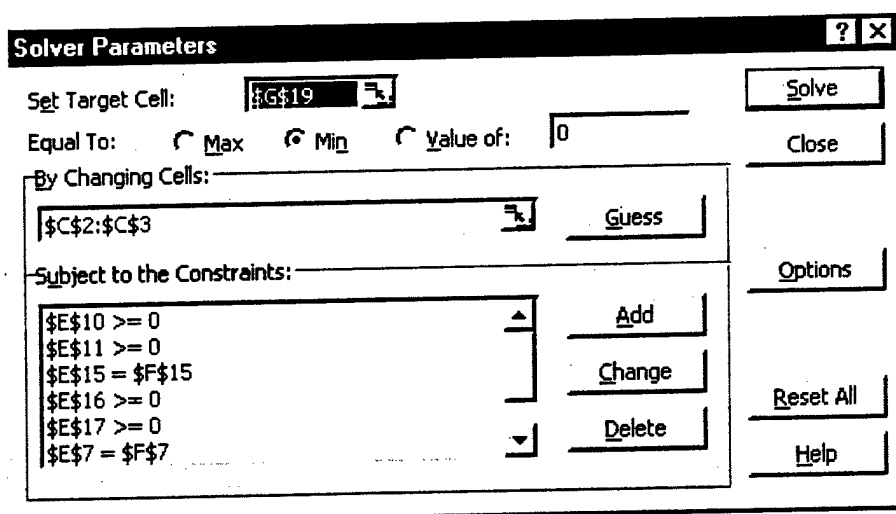
**Fig. E.2** *Sample Solver window.*

Bad data points will skew the nonlinear regression procedure and produce less than optimum failure parameters. Bad data points can be identified by their failure to converge to near unity as shown in row 8 of Fig. E.1. In this case, simply exclude the contribution of that data point's square-of-the-difference to the residual calculation.

Once the global minimum has been found, the values for the ultimate constituent shear strengths are placed in the fdata file for MCT_77 failure analysis. Note that the example shown above was an optimization for matrix parameters only. A similar procedure must be used to determine $A_4$ for the fiber.

# APPENDIX F

# MCT_77 USER'S GUIDE

## *F.1. Introduction*

MCT_77 is a traditional displacement-based, linear elastic, finite element code. What makes MCT_77 different from other finite element codes is the implementation of Multicontinuum Theory (MCT). MCT allows the user to extract constituent stress and strain fields from those of the composite during the course of a routine structural analysis.

The MCT_77 finite element software code is written in FORTRAN 77 for maximum portability. It is intended as a research code and is not optimized for speed as a commercial program might be. The code is extensively commented and written in a modular fashion for maximum readability and to facilitate changes. It contains approximately seventy subroutines and ten thousand lines of code. It has been compiled and run under DEC, IBM, and Microsoft versions of FORTRAN. The code has been tested on a DEC ALPHA workstation, an IBM workstation, and a Gateway Personal Computer.

The MVT_77 program was influenced by the following books and their example finite element codes contained within references [1, 2, 3]

In particular, Reference [1] was used as the basis for many of the finite element related formulations encoded as various subroutines in MCT_77.

A translator, ANS2MCT, has been written allowing use of the pre-processing capabilities of ANSYS to create the geometry and finite element mesh of the structure being analyzed. If requested, MCT_77 writes results files that can be read by ANSYS for post-processing.

An MCT_77 analysis is defined by three, four, or five user-generated ASCII format, input files: fdata (*failure data*), gdata (*grid data*), ldata (*load data*), mdata (*material data*), and sdata (*nonlinear shear data*). Fdata and sdata files are required only if the user requests a failure analysis and/or wants to include nonlinear shear effects.

Data in each input file is read sequentially. Order of the input lines is fixed and all input files share a common format. Each line of input is preceded by a line of descriptive text. While some lines of input may depend on the status of flags set by the user, the lines of descriptive text must always be included. Within the User's Guide, each line of input is referenced to a corresponding line of descriptive text which is designated by the LINE notation and a sequence number.

Generally, it is easier to use the ANSYS pre-processor to create new gdata and ldata files and modify existing mdata, fdata, or sdata files to fit a new case rather than create new ones from scratch.

> The user should be aware that the MCT_77 software contains virtually no capability to detect or correct contradictory or erroneous data input.

The analysis results are printed in the odata (*output data*) file. The odata file echos all input data and prints analysis results requested by the user in the ldata file.

The remainder of this appendix describes each of the five input files and the ANSYS-to-MCT_77 translator in detail. Each input file description uses the following framework:

1. **LINE #** of the descriptive text delineating a section of the file,
2. FORMAT statement (FORTRAN 77 convention) delineating the alphanumeric FIELDS defining analysis variables that form the LINE,
3. **FIELD #** provides a textual definition of each variable,
4. OPTIONS available for each FIELD, and
5. NOTES containing supplementary information for the LINE or FIELD.

## F.2. ANSYS-to-MCT_77 Translator

A translator, ANS2MCT, has been written allowing use of the pre-processing capabilities

of ANSYS to create the geometry and finite element mesh of the structure being

analyzed. The translator converts ANSYS database information to MCT_77 readable

format. ANS2MCT translates the following elements:

**Table F.1** *ANSYS to MCT element translation.*

| ANSYS Element Type | MCT Element Type |
|---|---|
| PLANE42 | QUAD4 |
| PLANE82 | QUAD8 |
| SOLID45 | BRICK8 |
| SOLID46 | BRICK8 |
| SHELL93 | SHELL8 |
| SHELL99 | SHELL8 |

Note that not every capability of the ANSYS elements listed in Table F.1 is translated to

MCT_77. The user should manually verify each translation. ANS2MCT translates the

following element attributes:

1. Nodal coordinates,
2. Nodal connectivity,
3. Plane stress/strain option,
4. Material number,
5. Non-conforming element formulation option,
6. Local coordinate system (ANSYS) ↔ Principal material direction (MCT_77),
7. Number of layers, and
8. Layer thickness.

ANS2MCT translates the following analysis options:

1. Number of load steps (always set to one),
2. Analysis type (always set to linear elastic), and
3. Failure analysis (always set to OFF).

ANS2MCT defaults to the following output options:

1. No printing of field results in odata,
2. No plot results,
3. Stress/strain values are interpolated to the nodes,
4. Stress/strain values are referenced to the principal material coordinate system (Required for ANSYS post-processing compatibility), and
5. Write ANSYS readable results files is ON.

ANS2MCT translates the following boundary conditions:

1. Prescribed homogeneous nodal displacements,
2. Prescribed non-homogeneous nodal displacements,
3. Nodal forces,
4. Uniform temperature,
5. Constraint equations, and
6. Element pressures.

MCT_77 writes ANSYS readable results files for graphical post-processing. The results files can be written for single or multi-step, linear-elastic or nonlinear-elastic, failure or non-failure, MCT_77 analyses. The following results files are created:

1. mct2ans.c (composite results),
2. mct2ans.r (reinforcement results),
3. mct2ans.m (matrix results), and
4. damage.dat (composite damage state if failure analysis).

The mct2ans files for the composite contain nodal displacements, stresses, and strains for each load step. The mct2ans files for each constituent contains stress and strain information for each load step. The damage.dat file contains material numbers corresponding to the composite damage state at each gauss point in the model.

The MCT_77 finite element program and the ANS2MCT translator can be initiated within the ANSYS graphical user interface (GUI). Five ANSYS macros that execute MCT_77 related functions have been incorporated as pushbuttons on the ANSYS toolbar.
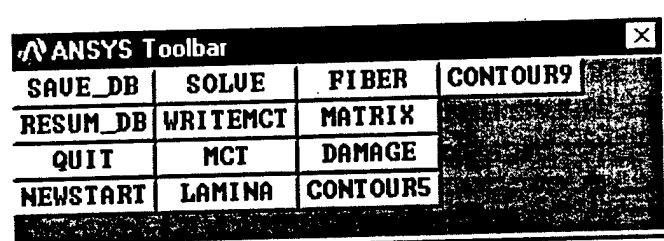
**Fig. F.1** *ANSYS toolbar with MCT_77 translator.*

The pertinent MCT toolbar buttons are:

1. WRITEMCT: Create MCT_77 input files that defining the finite element mesh (gdata) and the boundary conditions (ldata),
2. MCT: Executes the MCT_77 finite element solver,
3. LAMINA: Reads MCT_77 composite results a specified lamina for all elements,
4. FIBER: Reads MCT_77 fiber results for a specified lamina for all elements,
5. MATRIX: Reads MCT_77 matrix results for a specified lamina for all elements, and
6. DAMAGE: Reads MCT_77 material numbers for a specified lamina for all elements.

WRITEMCT macro writes the ANSYS database to a text file and executes ANS2MCT which translates the database information to gdata, and ldata files. The user is responsible for any additional files required for a MCT_77 analysis. At a minimum, the user must generate a mdata file to define material properties for the finite element model. Note that the material number assigned by ANSYS to each element must match the material number assigned by the user in the mdata file.

MCT macro runs the MCT_77 solver based on input files created by ANS2MCT and the user. WRITEMCT and MCT macros are not combined giving the user an opportunity to check ldata and gdata files and create an associated mdata file.

Currently, an ANSYS solution must be executed for the model before storage positions are created in the ANSYS database for displaying MCT_77 post-processing results. LAMINA, FIBER, MATRIX, and DAMAGE macros read MCT_77 results files into the ANSYS database. The user will be queried for a specific load step (defaults to load step 1). ANSYS does not have the capability to store stress and strain values for the composite and both constituents. Each time a macro reads an MCT_77 results file, it overwrites any existing displacement, stress, and strain values. Due to MCT-ANSYS interface difficulties, lamina results are read in one at a time. The results are read into layer 0 (zero) position in the ANSYS database. Subsequent reading of MCT_77 results overwrites data stored in this location also. DAMAGE data are read into an element table for listing or plotting.

## F.3. Fdata File

The fdata file contains ultimate strength data for the composite and its constituents (fiber, and matrix). Currently, failure in only one composite material can be modeled. Fdata and mdata files must be structured in a prescribed manner to conduct a failure analysis.

The mdata file must be have the following format:

1. Material #1 data must contain undamaged composite material constants.
2. Material #2 data must contain material #1 constants assuming damaged matrix.
3. Material #3 data must contain material #1 constants assuming damaged fiber.
4. Materials #4-#7 data contain constituent material properties corresponding to Materials #1-#3, i.e., undamaged and damaged values for the fiber and matrix.

The fdata file must have the following format:

1. Material #1 data must correspond to material #1 in the mdata file.
2. Material #2 data must correspond to the undamaged fiber material in mdata.
3. Material #3 data must correspond to the undamaged matrix material in mdata.

Changing material properties, inherent in failure analyses, requires incremental application of the load and iterations within each load step to achieve equilibrium. Two tolerances, deflection (DTOL) and load (FTOL) control equilibrium iterations. The user should monitor convergence of failure analyses carefully and modify tolerances (default values are DTOL=7.0 and FTOL=1.0E-4) as required. A sample fdata file is shown in Fig. F.2. The file contains six required LINES. A LINE-by-LINE description follows.

```
*Failure data title
 Boron/5505, 50% FVF
*Convergence tolerances, deflection, load
     1.0D0     1.0D-3
*Material Sets
  3
*Material,Composite,S11T,S22T,S33T,S12T,S13T,S23T,(repeat for compress)
   1379.0D6    86.6D6    00.0D6   125.5D6    00.0D6    00.0D6
  -2861.0D6   -262.0D6   00.0D6   125.5D6    00.0D6    00.0D6
*Material,Reinforcement,S11T,S22T,S33T,S12T,S13T,S23T,(repeat for compress)
   2708.0D6    00.0D6    00.0D6   166.5D6    00.0D6    00.0D6
  -5620.0D6    00.0D6    00.0D6   166.5D6    00.0D6    00.0D6
*Material,Matrix,S11T,S22T,S33T,S12T,S13T,S23T,(repeat for compress)
    138.0D6    69.8D6    6.68D6    84.5D6    25.9D6    28.2D6
   -345.0D6   -208.8D6  -20.0D6    84.5D6   -77.4D6    28.2D6
```

**Fig. F.2** *Sample fdata file.*

**LINE 1.** *Failure data title
Number of fields: 1
FORMAT: (A60)
FIELD 1: General description of the failure data defined in the fdata file.
OPTIONS: None
NOTE: Descriptor is printed as an identifier at the beginning of the odata file.

**LINE 2.** *Convergence tolerances, deflection, load.
Number of fields: 2
FORMAT: (1X,6G12.7)
FIELD 1: Maximum change allowed, within a load step, of the displacement $L^2$ norm
before failure of the structure is declared and program execution ends.
OPTIONS: None.
NOTE: Displacement tolerance is defined as:

$$\frac{Delta\ displacement\ for\ an\ equilibrium\ iteration}{Displacement\ for\ the\ first\ equilibrium\ iteration}$$

It is easiest to think of this tolerance as a percentage change in displacement. Except for
the first iteration in the load step, the percentage change in displacement norm is much
less than 100% and should decrease as equilibrium is achieved. When failure occurs
during equilibrium iteration, the structure can no longer support the load and
displacements grow without bound. The displacement tolerance stops the program before
numeric singularities occur. Typically, values around 6.0 work well (7.0 is default).
FIELD 2: Specifies the maximum load tolerance defined as a ratio of the $L^2$ norm of the
internal load vector norm to the $L^2$ norm of the external load vector before equilibrium is
satisfied.
OPTIONS: None.

NOTE: Changing material properties, due to failure or nonlinear shear, during an incremental analysis cause the external and internal (resisting) load vectors to be out of balance. The load tolerance controls the number of times that the delta load difference between the two load vectors is applied to the structure before equilibrium is achieved (1.0E-4 is the default).

**LINE 3.** *Material Sets
Number of fields: 1
FORMAT: (1X, 9I5)
**FIELD 1**: Number of materials for which failure data is to be read.
OPTIONS: 3 (min) to 8 (max). See Note.
NOTE: The code uses failure data for only one composite material (corresponding to the first material listed in mdata) and its associated reinforcement and matrix constituents. As such, only a value designating three materials (composite and two constituents) will produce reliable results.

**LINE 4.** *Material,Composite,S11T,S22T,S33T,S12T,S13T,S23T,(repeat for compress)
Number of fields: 12
FORMAT: (1X,6G12.7)
NOTE 1: Two lines are required, $1^{st}$ – tension, $2^{nd}$ – compression
NOTE 2: Composite values are used to calculate Tsai-Wu failure criterion.
**FIELD 1**: Ultimate composite tensile strength in the fiber ($^+S_{11}$) direction.
OPTIONS: None
**FIELD 2**: Ultimate composite tensile strength transverse to the fiber direction ($^+S_{22}$) in the plane of the lamina.
OPTIONS: None
**FIELD 3**: Ultimate composite tensile strength transverse to the fiber direction ($^+S_{33}$) out of the plane of the lamina.
OPTIONS: None
NOTE: Currently not used.
**FIELD 4**: Ultimate composite shear strength in the 12 direction ($S_{12}$).
OPTIONS: None
**FIELD 5**: Ultimate composite shear strength in the 13 direction ($S_{13}$).
OPTIONS: None
NOTE: Currently not used.
**FIELD 6**: Ultimate composite shear strength in the 23 direction ($S_{23}$).
OPTIONS: None

**FIELDS 7-12**: Repeats FIELDS 1-6 for compression values.

**LINE 5.** *Material,Reinforcement,S11T,S22T,S33T,S12T,S13T,S23T,(repeat for compress)
Number of fields: 12
FORMAT: (1X,6G12.7)
NOTE: Two lines are required, $1^{st}$ – tension, $2^{nd}$ – compression
**FIELD 1**: Ultimate reinforcement tensile strength along the fiber axis ($^+S_{11}$).

OPTIONS: None
**FIELD 2**: Ultimate reinforcement tensile strength transverse to the fiber axis ($^+S_{22}$) in the plane of the lamina.
OPTIONS: None
NOTE: Currently not used.
**FIELD 3**: Ultimate reinforcement tensile strength transverse to the fiber axis ($^+S_{33}$) out of the plane of the lamina.
OPTIONS: None
NOTE: Currently not used.
**FIELD 4**: Ultimate reinforcement shear strength in the 12 direction ($S_{12}$).
OPTIONS: None
**FIELD 5**: Ultimate reinforcement shear strength in the 13 direction ($S_{13}$).
OPTIONS: None
NOTE: Currently not used.
**FIELD 6**: Ultimate reinforcement shear strength in the 23 direction ($S_{23}$).
OPTIONS: None
NOTE: Currently not used.
**FIELDS 7-12**: Repeats FIELDS 1-6 for compression values.

**LINE 6.** *Material,Matrix,S11T,S22T,S33T,S12T,S13T,S23T,(repeat for compress)
Number of fields: 12
FORMAT: (1X,6G12.7)
NOTE: Two lines are required, $1^{st}$ – tension, $2^{nd}$ – compression.
**FIELD 1**: Matrix in-situ stress value in the 11 direction ($\sigma_{11}$) when the lamina is loaded in the 22 direction to its ultimate value ($S_{22}$).
OPTIONS: None
NOTE: Currently not used.
**FIELD 2**: Ultimate matrix in-situ tensile strength transverse to the fiber axis ($^+S_{22}$) in the plane of the lamina.
OPTIONS: None
NOTE: This is backed out of transversely loaded ($S_{22}$) lamina test.
**FIELD 3**: Matrix in-situ stress value in the 33 direction ($\sigma_{33}$) when the lamina is loaded in the 22 direction to its ultimate value ($S_{22}$).
OPTIONS: None
NOTE: This is backed out of transversely loaded ($S_{22}$) lamina test.
**FIELD 4**: Ultimate matrix in-situ shear strength in the 12 direction ($S_{12}$).
OPTIONS: None
NOTE: This is backed out of a shear loaded ($S_{12}$) lamina test.
**FIELD 5**: Ultimate matrix in-situ tensile strength along the fiber axis ($^+S_{11}$).
OPTIONS: None
NOTE: Currently not used.
**FIELD 6**: Ultimate matrix in-situ shear strength in the 23 direction ($S_{23}$).
OPTIONS: None
NOTE: This is backed out of a shear loaded ($S_{23}$) lamina test.
**FIELDS 7-12**: Repeats FIELDS 1-6 for compression values.

## F.4. Gdata File

The gdata file contains information defining elements that discretizes the structure being analyzed. A sample gdata file is shown in Fig. F.3. The gdata file contains six required LINES. A LINE-by-LINE description follows.

```
*GRID MODEL TITLE
 SINGLE ELEMENT, 8-NODE BRICK MODEL
*GRID, elem type, plain stress/strain, NCEF, #elms, #pts
   BRICK8   0   0   1   8
*LAYER, #layer/elm, thk
   4    1.D0
*COORDINATES, define global nodal coordinates.
   1   0.0000      0.0000      0.0000
   2   1.0000      0.0000      0.0000
   3   1.0000      1.0000      0.0000
   4   0.0000      1.0000      0.0000
   5   0.0000      0.0000      1.0000
   6   1.0000      0.0000      1.0000
   7   1.0000      1.0000      1.0000
   8   0.0000      1.0000      1.0000
*CONNECTIVITY, define element connectivity.
   1   1   2   3   4   5   6   7   8
*ORIENTATION, define element material, layer principal material direction.
   1   1  30. -30. -30.  30.
```

**Fig. F.3** *Sample gdata file.*

**LINE 1.** *GRID MODEL TITLE
Number of fields: 1
FORMAT: (A60)
FIELD 1:General description of the mesh defined in the gdata file.
OPTIONS: None
NOTE: Descriptor is printed as an identifier at the beginning of the odata file.

**LINE 2.** *GRID, elem type, plain stress/strain, NCEF, #elms, #pts
Number of fields: 5
FORMAT: (1X,A10,4I5)

**FIELD 1**: Type of element used.
OPTIONS:
 a) QUAD4 (4 node quadrilateral),
 b) QUAD8 (8 node quadrilateral),
 c) BRICK8 (8 node brick),
 d) SHELL8 (8 node shell).
NOTE: Currently only one type of element can be use within an analysis.
**FIELD 2**: Element kinematic assumptions.
OPTIONS:
 a) QUAD4 – (1) = plane stress or (2) = plane strain,
 b) QUAD8 – (1) = plane stress or (2) = plane strain,
 c) BRICK8 – (0) only (fully three dimensional),
 d) SHELL8 – (1) only (plane stress).
**FIELD 3**: Request that a non-conforming element formulation be used.
OPTIONS:
 a) QUAD4 – Off (0) or On (1),
 b) QUAD8 – Off (0) only,
 c) BRICK8 – Off (0) or On (1),
 d) SHELL8 – Off (0) only.
NOTE: This option is only applicable to linear elements.
**FIELD 4**: Number of elements in the model.
OPTIONS: None
**FIELD 5**: Number of nodes in the model.
OPTIONS: None


**LINE 3.** *LAYER, #layer/elm, thk
Number of fields: 2
FORMAT: (1X,I5,G10.5)
**FIELD 1**: Number of layers per element,
OPTIONS: 1 (min) to 26 (max) layers.
**FIELD 2**: Element thickness in the $\zeta$ direction as determined by element connectivity.
OPTIONS:
 a) QUAD4 – constant thickness,
 b) QUAD8 – constant thickness,
 c) BRICK8 – constant thickness. Note that this value must agree with the thickness as determined by distance between the nodes in $\zeta$ direction.
 d) SHELL8 – constant thickness.


**LINE 4.** *COORDINATES, define global nodal coordinates.
Number of fields: Variable 3 to 4 depending on element type.
FORMAT: (1X,I5,10G15.8)
**FIELD 1**: Node's numeric label.
OPTIONS: None
NOTE: Nodes must be numbered sequentially starting with 1 having no gaps or duplicates.
**FIELD 2**: Value of x coordinate in global Cartesian coordinate system.

OPTIONS: None
**FIELD 3**: Value of y coordinate in global Cartesian coordinate system.
OPTIONS: None
**FIELD 4**: Value of z coordinate in global Cartesian coordinate system.
OPTIONS:
  a) QUAD4 – elements must be in the x-y plane, z coordinate set to zero,
  b) QUAD8 – elements must be in the x-y plane, z coordinate set to zero,
  c) BRICK8 – three dimensional nodal coordinates,
  d) SHELL8 – three dimensional nodal coordinates.
NOTE: Number of lines must equal number of nodes specified in LINE 2.


**LINE 5.** CONNECTIVITY, define element connectivity.
Number of fields: Variable 4-8 depending on element type.
FORMAT: (1X,9I5)
**FIELD 1**: Node's numeric label.
OPTIONS: None
NOTE: Nodes must be numbered sequentially starting with 1 having no gaps or duplicates.
**FIELDS 2-9**: Element connectivity.  Order is counterclockwise, corner nodes first, midside nodes next (if any).
OPTIONS: None
NOTE: Number of lines must equal number of elements specified in LINE 2.


**LINE 6.** *ORIENTATION, define element material, layer principal material direction.
Number of fields: Variable 3-16 depending on number of layers in element.
FORMAT: (1X,2I5,14G5.1)
**FIELD 1**: Element number.
OPTIONS: None
NOTE: Elements must be numbered sequentially starting with 1 having no gaps or duplicates.
**FIELD 2**: Material type for this element.
OPTIONS: None
NOTE: Only one material type per element is allowed regardless of the number of layers. Must correspond to one of eight possible material types defined in mdata.
**FIELDS 3-16**: Principal material direction in each layer as an angle of rotation about positive z axis (positive counterclockwise) of the <u>element coordinate system</u>. See Notes 2 and 3.
OPTIONS: None
NOTE 1: Number of lines must equal number of elements specified in LINE 2.
NOTE 2: Number of fields must equal number of layers specified in LINE 3.
NOTE 3: Each element has an associated coordinate system.  This system is the frame of reference for determining principal (fiber) material direction.  The element coordinate system is determined by a projection of the global coordinate system (referred to as the "shadow" axis) onto the element surface using the following rules:

a) Element normal (z' direction) is computed using the cross product of the positive $\xi$ and $\eta$ vectors originating at the first node. Note that these vectors are generally not orthogonal in xyz space.

b) If the normal has an absolute z component (global reference) greater than 1 degree, the shadow coordinate system coincides with the global coordinate system, i.e., no rotation is necessary for projection.

c) If the normal is within one degree of the global x-y plane and has a POSITIVE y component, rotate the shadow coordinate system -90 degrees about the global x-axis and project (positive shadow z axis coincides with positive global y axis).

d) If the normal is within one degree of the x-y plane and has a NEGATIVE y component, rotate shadow coordinate system +90 degrees about the global x-axis and project (positive shadow z axis coincides with negative global y axis)

e) If the normal is within one degree of the global x-y plane and within one degree of the POSITIVE x-axis, rotate the shadow coordinate system +90 degrees about the global y-axis and project (positive shadow z axis coincides with positive global x axis).

f) If the normal is within one degree of the global x-y plane and within one degree of the NEGATIVE x-axis, rotate the shadow coordinate system -90 degrees about the global y-axis and project (positive shadow z axis coincides with the negative global x axis).

## F.5. Ldata File

The ldata file contains information defining boundary conditions of the structure being analyzed. A sample ldata file is shown in Fig. F.4. The ldata file contains thirteen required LINES. A LINE-by-LINE description follows.

```
*LOAD CASE TITLE
 Combined boundary conditions, single brick8 element.
*LOAD CONTROL, # steps total, #steps to execute, analysis type
    1   1   0
*LOAD INDEX, #BCs, #N-forces, #N-displ, #MPCs, #E-Press, B-force, T-loads
    7   4   1   4   1   0   1
*FIXED BC, define homogenous nodal dof displacements.
    1 111
    2 011
    3 001
    4 101
    5 110
    6 010
    8 100
*NODAL FORCES, define nodal dof forces.
    5      00.00D0   00.00D0  100.00D6
    6      00.00D0   00.00D0  100.00D6
    7      00.00D0   00.00D0  100.00D6
    8      00.00D0   00.00D0  100.00D6
*NODAL DISPS, define nonzero nodal dof displacements.
    3 021    0.0000   1.0D-3   0.0000
*MPC, define multi-point dof contraints.
    2 0.00000E+00   3 2 1.0000     4 2 -1.0000
    2 0.00000E+00   3 2 1.0000     7 2 -1.0000
    2 0.00000E+00   3 2 1.0000     8 2 -1.0000
*ELM PRESSURES, define element edge or face pressures.
    1   3  -100.0D6   -100.0D6   -100.0D6   -100.0D6
*BODY FORCE, define forces due to accelerations.
*TEMPERATURE LOAD, define uniform or nodal temperatures
    10.0     0.0
*OUTPUT CONTROL,Maxprn,prnsteps,Local,Gauss,Lay,Fail,ANSYS,Plot
    1   1   0   0   0   1   1
*PRINT CONTROL,Inc,Displs,Nsts,Nstn,Asts,Astn,Ests,Estn,Psts,Ists,Rfor
    1 YNNYYNNNYN
*PLOT CONTROL,{force id,force#,blank,blank} or {field id,node,lay,elem}
    23   1   0   0   3   2   1   1
```

**Fig. F.4** *Sample ldata file.*

**LINE 1.** *LOAD CASE TITLE
Number of fields: 1
FORMAT: (A60)
**FIELD 1**:General description of the boundary conditions defined in the ldata file.
OPTIONS: None
NOTE: Descriptor is printed as an identifier at the beginning of the odata file.


**LINE 2.** *LOAD CONTROL, # steps total, #steps to execute, analysis type
Number of fields: 3
FORMAT: (1X, 7I5)
**FIELD 1**: Number of load steps in the analysis.
OPTIONS: If FIELD value is negative, RAMP function is flagged ON.
NOTE: If value is positive, loads (nodal, pressure, thermal, etc.) must be defined below
for each load step. If value is negative, only the total of each load type is read and
uniform load steps are automatically generated.
**FIELD 2**: Number of load steps to be executed.
OPTIONS: None
NOTE: Situations may arise where a number of load steps are defined but the user only
wants an initial portion of those executed to check the progress of the analysis.
**FIELD 3**: Type of analysis.
OPTIONS:
  a)  0 = Linear elastic analysis,
  b)  1 = Reserved for future use,
  c)  2 = Data check.
NOTE: Option c) echos all user's input files to odata file in an easy to read and verify
form.


**LINE 3.** *LOAD INDEX, #BCs, #N-force, #N-displ, #MPCs, #E-Press, B-force, T-loads
Number of fields: 7
FORMAT: (1X, 7I5)
**FIELD 1**: Number of lines of homogeneous nodal displacement data to be read below
LINE 4.
OPTIONS: Value can be zero.
**FIELD 2**: Number of lines of nodal force data to be read below LINE 5.
OPTIONS: Value can be zero.
**FIELD 3**: Number of lines of nonhomogeneous nodal displacement data to be read
below LINE 6.
OPTIONS: Value can be zero.
**FIELD 4**: Number of lines of multi-point constraint data to be read below LINE 6.
OPTIONS: Value can be zero.
**FIELD 5**: Number of lines of element pressure data to be read below LINE 7.
OPTIONS: Value can be zero.
**FIELD 6**: Number of lines of body force data to be read below LINE 8.
OPTIONS: Value can be zero.
**FIELD 7**: Number of lines of thermal load data to be read below LINE 9.
OPTIONS:

a) 0 = No thermal load,
b) 1 = Uniform temperature,
c) 2 = Prescribed nodal temperatures,

**LINE 4.** *FIXED BC, define homogenous nodal dof displacements.
Number of fields: 2-5 depending on element type.
FORMAT: (1X, I5, 1X, 5I1)
NOTE: Number of lines defining nodes with prescribed homogeneous displacements must agree with FIELD 1 in LINE 3.
**FIELD 1**: Node number.
OPTIONS: None
**FIELD 2**: Constraint code for translation in global x direction.
OPTIONS:
  a) 0 = unconstrained,
  b) 1 = fixed (zero displacement).
**FIELD 3**: Constraint code for translation in global y direction.
OPTIONS:
  a) 0 = unconstrained,
  b) 1 = fixed (zero displacement).
**FIELD 4**: Constraint code for translation in global z direction.
OPTIONS:
  a) 0 = unconstrained,
  b) 1 = fixed (zero displacement).
NOTE: Not required for two dimensional elements (QUAD4 and QUAD8)
**FIELD 5**: Constraint code for rotation about global x-axis.
OPTIONS:
  a) 0 = unconstrained,
  b) 1 = fixed (zero rotation).
NOTE: Currently only used with SHELL8 elements, not required otherwise.
**FIELD 6**: Constraint code for rotation about global y axis.
OPTIONS:
  a) 0 = unconstrained,
  b) 1 = fixed (zero rotation).
NOTE: Currently only used with SHELL8 elements, not required otherwise.

**LINE 5.** *NODAL FORCES, define nodal dof forces.
Number of fields: 2-5 depending on element type.
FORMAT: (1X, I5, 5X, 5(G10.4))
NOTE 1: Number of lines defining nodes with prescribed loads must agree with FIELD 2 in LINE 3.
NOTE 2: Number of lines defining nodal loads, specified by FIELD 2 in LINE 3, must be listed for each load step specified in FIELD 1 in LINE 2 unless RAMP option is ON.
**FIELD 1**: Node number.
OPTIONS: None
**FIELD 2**: Force in global x direction.
OPTIONS: Can have zero value.

**FIELD 3**: Force in global y direction.
OPTIONS: Can have zero value.
**FIELD 4**: Force in global z direction.
OPTIONS: Can have zero value.
NOTE: Not required for two dimensional elements (QUAD4 and QUAD8).
**FIELD 5**: Moment about global x-axis.
OPTIONS: Can have zero value.
NOTE: Currently only used with SHELL8 elements, not required otherwise.
**FIELD 6**: Moment about global y-axis.
OPTIONS: Can have zero value.
NOTE: Currently only used with SHELL8 elements, not required otherwise.


**LINE 6.** *NODAL DISPS, define nonzero nodal displacements.
Number of fields: 4-11 depending on element type.
FORMAT: (1X, I5, 1X, A5, 5(G10.4))
NOTE 1: Number of lines defining nodes with prescribed nonzero displacements must agree with FIELD 3 in LINE 3 unless RAMP function is flagged ON.
NOTE 2: The same number of lines defining nodal displacements, specified by FIELD 3 in LINE 3, must be listed for each load step specified in FIELD 1 in LINE 2 unless RAMP option is ON.
NOTE 3: Prescribed displacement, both zero and nonzero, defined here override any defined for the same node number in LINE 4.
NOTE 4: FIELDS 2-6 are read as a single word and converted to integers internally.
**FIELD 1**: Node number.
OPTIONS: None
**FIELD 2**: Constraint code for translation in global x direction.
OPTIONS:
  a)  0 = unconstrained,
  b)  1 = fixed (zero displacement),
  c)  2 = nonzero displacement.
**FIELD 3**: Constraint code for translation in global y direction.
OPTIONS:
  a)  0 = unconstrained,
  b)  1 = fixed (zero displacement),
  c)  2 = nonzero displacement.
**FIELD 4**: Constraint code for translation in global z direction.
OPTIONS:
  a)  0 = unconstrained
  b)  1 = fixed (zero displacement)
  c)  2 = nonzero displacement
NOTE: Not applicable for two dimensional elements (QUAD4 and QUAD8)
**FIELD 5**: Constraint code for rotation about global x-axis.
OPTIONS:
  a)  0 = unconstrained
  b)  1 = fixed (zero rotation)
  c)  2 = nonzero rotation

NOTE: Currently only used with SHELL8 elements, not required otherwise.
**FIELD 6**: Constraint code for rotation about global y-axis.
OPTIONS:
   a) 0 = unconstrained,
   b) 1 = fixed (zero rotation),
   c) 2 = nonzero rotation.
NOTE: Currently only used with SHELL8 elements, not required otherwise.
**FIELD 7**: Translation in global x direction.
OPTIONS: Can have zero value.
**FIELD 8**: Translation in global y direction.
OPTIONS: Can have zero value.
**FIELD 9**: Translation in global z direction.
OPTIONS: Can have zero value.
NOTE: Not applicable for two dimensional elements (QUAD4 and QUAD8)
**FIELD 10**: Rotation about global x axis.
OPTIONS: Can have zero value.
NOTE: Currently only used with SHELL8 elements, not required otherwise.
**FIELD 11**: Rotation about global y axis.
OPTIONS: Can have zero value.
NOTE: Currently only used with SHELL8 elements, not required otherwise.


**LINE 7.** *MPC, define multi-point dof constraints.
Number of fields: 8-29 depending on the constraint equation formulated.
FORMAT: (1X, I5, G12.5,3(I5,I2,G12.5),:,2(/,18X,3(I5,I2,G12.5))
NOTE 1: Number of lines defining multi-nodal degree-of-freedom constraint relationships must agree with FIELD 4 in LINE 3.
NOTE 2: Up to three lines may be required to define a single constraint equation.
NOTE 3: Constraint equations allow the user to define complex relationships between degrees-of-freedom of different nodes. For example, constrain equations are useful in applying boundary conditions representing a plane of symmetry of a model. Constraint equations have the form:

$$C_1 * DOF_i^1 + C_2 * DOF_j^2 + ... + C_n * DOF_k^n = C$$

*where* :

$C_i$ = Constants

$DOF_i^n$ = Displacement in degree of freedom $i$ of node $n$

A simple constraint equation coupling the degrees-of-freedom, in the x direction of nodes 1 and 2, so they move together (same magnitude), would look like:

$$(1) * DOF_1^1 + (-1) * DOF_1^2 = 0$$

**FIELD 1**: Number of terms in constraint equation.
OPTIONS: 2 (min) – 9 (max)
**FIELD 2**: Right hand value (constant) of constraint equation.

OPTIONS: None.
**FIELD 3**: Node number of first term in constraint equation.
OPTIONS: None
**FIELD 4**: Degree-of-freedom constrained.
OPTIONS: 1-5 depending on element type.
**FIELD 5**: Coefficient of first term in constraint equation.
OPTIONS: None
**FIELDS 6-11**:Repeat FIELDS 3-5 for the next two terms in the constraint equation.
OPTIONS: None
NOTE 1: FIELDS 6-11 are on the same line as FIELDS 1-5.
NOTE 2: Number of terms must agree with FIELD 1
**FIELDS 12-20**: Repeat FIELDS 3-5 for the next three terms in the constraint equation.
OPTIONS: None
NOTE 1: FIELDS 12-20 are all on a second line below FIELDS 1-11.
NOTE 2: Number of terms must agree with FIELD 1
**FIELDS 21-29**: Repeat FIELDS 3-5 for the next three terms in the constraint equation.
OPTIONS: None
NOTE 1: FIELDS 21-29 are all on a third line below FIELDS 12-20.
NOTE 2: Number of terms must agree with FIELD 1


**LINE 8.** *ELM PRESSURES, define element edge or face pressures.
Number of fields: 4-7 depending on element type.
FORMAT: (1X, 2I5, 4G12.4)
NOTE 1: Number of lines defining applied element pressures must agree with FIELD 5 in LINE 3.
NOTE 2: Number of lines defining element pressures, specified by FIELD 5 in LINE 3, must be listed for each load step specified in FIELD 1 in LINE 2 unless RAMP option is ON.
NOTE 3: Element pressure are defined as positive acting into an element face or edge.
NOTE 4: Element faces or edges are defined by node number sequence determined by element connectivity. Apply right-hand rule to node sequences listed in Table F.2 through Table F.4 to determine the NEGATIVE normal (positive pressure) to edge or face.
NOTE 5: Pressures can only be specified at corner nodes. Pressures at midside nodes (if any) are interpolated internally. Pressures can vary linearly over an element face or edge.
NOTE 6: For plane elements (QUAD4, QUAD8,) node numbering is shown in Fig. F.5.
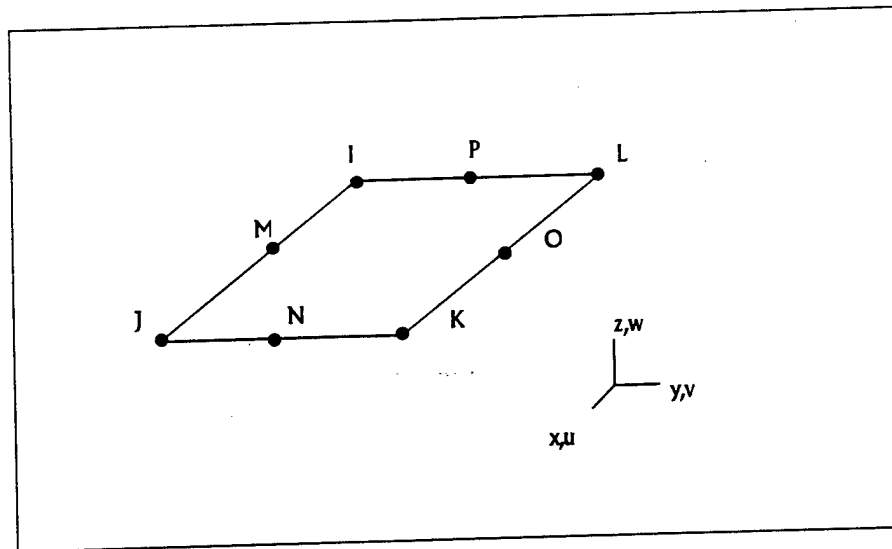
**Fig. F.5** *Node numbering for generic plane element.*

The element edges for plane elements are defined in Table F.2

**Table F.2** *Edge numbering for QUAD4 and QUAD8 elements.*

| Edge | Corner Nodes |
|------|--------------|
| 1 | I,J |
| 2 | J,K |
| 3 | K,L |
| 4 | L,I |

Element edges and faces for SHELL8 element (Fig. F.5) are defined in Table F.3.

**Table F.3** *Edge and face numbering for SHELL8 element.*

| Edge or Face | Corner Nodes |
|--------------|--------------|
| 1 | I,J,K,L |
| 2 | I,J |
| 3 | J,K |
| 4 | K,L |
| 5 | L,I |
| 6 | I,L,K,J |

For BRICK8 element node sequence is shown in Fig. F.6.
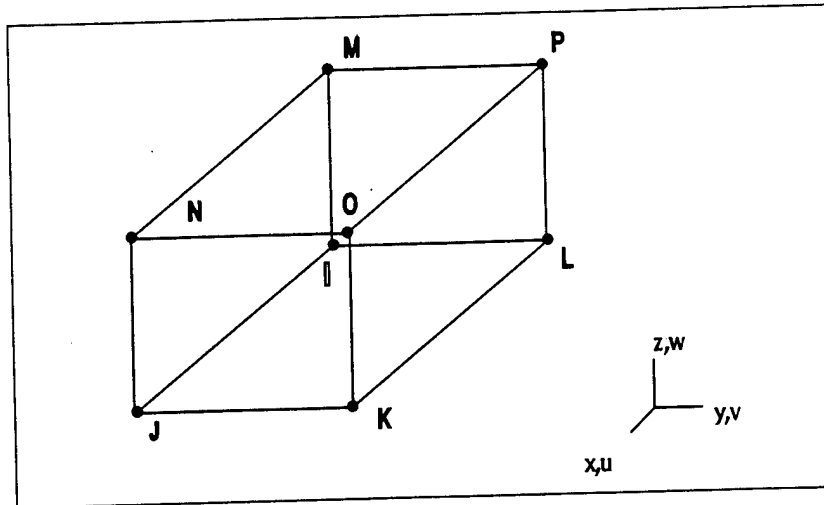
**Fig. F.6** *Node numbering for BRICK8 element.*

The element faces for BRICK8 element are defined in Table F.4.

**Table F.4** *Face numbering for BRICK8 element.*

| Edge or Face | Corner Nodes |
|:---:|:---:|
| 1 | I,J,K,L |
| 2 | I,M,N,J |
| 3 | J,N,O,K |
| 4 | K,O,P,L |
| 5 | I,L,P,M |
| 6 | M,P,O,N |

**FIELD 1**: Element number.
OPTIONS: None
**FIELD 2**: Face or edge number.
OPTIONS: None.
NOTE: See NOTE 6 for face and edge numbering.
**FIELD 3**: Element number.
OPTIONS: None
**FIELD 4**: Pressure at first node defining face or edge.
OPTIONS: None.
**FIELD 5**: Pressure at second node defining face or edge.
OPTIONS: None.
Note: Only required for specifying face pressures.
**FIELD 6**: Pressure at third node defining face.
OPTIONS: None.
Note: Only required for specifying face pressures.
**FIELD 7**: Pressure at fourth node defining face or edge.
OPTIONS: None.
NOTE: Only required for specifying face pressures.

**LINE 9.** *BODY FORCE, define forces due to accelerations.

Number of fields: 5-11 depending on acceleration type.

FORMAT: (1X, 3G10.4)

NOTE 1: The existence of lines defining body forces must agree with FIELD 6 in LINE 3.

NOTE 2: If both rotational and translational body forces are defined, FIELDS 3-8 are used to define rotation vectors and FIELDS 9-11 are used to define direction vector.

NOTE 3: Body forces can only be applied in an analyses using a single load step.

NOTE 4: A density must be defined for each material in mdata.

**FIELD 1**: Rotational acceleration.

OPTIONS: Can have zero value.

**FIELD 2**: Translational acceleration.

OPTIONS: Can have zero value.

NOTE 1: This value is generally gravity or some multiple of it.

NOTE 2: FIELDS 1-2 form the first of 2-4 lines of input defining body forces.

**FIELD 3**: Global x-coordinate of a vector.

OPTIONS:

   a) Free vector tail if defining axis of rotation,

   b) Bound vector head if defining direction of translation.

NOTE: OPTION b) is used if only translational acceleration exists.

**FIELD 4**: Global y-coordinate of vector.

OPTIONS

   a) Free vector tail if defining axis of rotation,

   b) Bound vector head if defining direction of translation.

NOTE: OPTION b) is used if only translational acceleration exists.

**FIELD 5**: Global z-coordinate of vector.

OPTIONS:

   a) Free vector tail if defining axis of rotation,

   b) Bound vector head if defining direction of translation.

NOTE: OPTION b) is used if only translational acceleration exists.

NOTE: FIELDS 3-5 form the second group of 2-4 lines of input defining body forces.

**FIELD 6**: Global x-coordinate of free vector head that defining axis of rotation.

OPTIONS: None.

NOTE: Required for rotational body force only.

**FIELD 7**: Global y-coordinate of free vector head defining axis of rotation.

OPTIONS: None.

NOTE: Required for rotational body force only.

**FIELD 8**: Global z-coordinate of free vector head defining axis of rotation.

OPTIONS: None.

NOTE: Required for rotational body force only.

NOTE: FIELDS 6-8 form the third group of 2-4 lines of input defining body forces.

**FIELD 9**: Global x-coordinate of bound vector defining direction of translation.

OPTIONS: None.

NOTE: Required only if both rotational and translational body forces exist.

**FIELD 10**: global y-coordinate of bound vector defining direction of translation.

OPTIONS: None.
NOTE: Required only if both rotational and translational body forces exist.
FIELD 11: Global z-coordinate of bound vector defining direction of translation.
OPTIONS: None.
NOTE 1: Required only if both rotational and translational body forces exist.
NOTE 2: FIELDS 9-11 form the fourth group of 2-4 lines of input defining body forces.


**LINE 10.** *TEMPERATURE LOAD, define uniform or nodal temperatures
Number of fields: 2-3 depending on option requested.
FORMAT: Either (1X, 5G10.4) (uniform temperature option) or (1X, I5, 2G10.5)
(prescribed nodal temperatures option)
NOTE 1: Number of lines defining thermal loads must agree with FIELD 6 in LINE 3.
See NOTE 2.
NOTE 2: If uniform temperature option is requested, only one line of input required. If
nodal temperature option is requested, temperature at every node must be specified.
NOTE 3: Number of lines defining thermal loads, specified by FIELD 6 in LINE 3, must
be listed for each load step specified in FIELD 1 in LINE 2 unless RAMP option is ON.
NOTE 4: Analysis requiring iterations for load equilibrium (failure or nonlinear shear),
all thermal loads are applied in the first load step.
FIELD 1: Either temperature (uniform option) or node number (nodal option).
OPTIONS: None.
FIELD 2: Either reference temperature (uniform option) or nodal temperature (nodal
option).
OPTIONS: None.
FIELD 3: Reference temperature (nodal option).
OPTIONS: None.
NOTE: Not required under the uniform temperature option.


**LINE 11.** *OUTPUT CONTROL, Maxprn, prnsteps, Local, Gauss, Lay, Fail, ANSYS,
Plot
Number of fields: 8.
FORMAT: (1X, 9I5)
NOTE 1: First of two LINES controlling form and quantity of analysis results printed in
odata.
NOTE 2: Generally, descriptors of stress and strain values, based on flags set in LINE
11, are printed in odata.
FIELD 1: Request gross printing of results.
OPTIONS:
  a) 0 = Gross print flag is OFF,
  b) 1 = All load steps are printed using print control pattern requested in LINE 12,
  c) >1 = Load steps that are multiples of this value will be printed using print control
    pattern requested in LINE 12.
FIELD 2: Number of load steps specifically flagged to be printed using print control
patterns requested for each load step listed in LINE 12.
OPTIONS:
  a) 0 = Load step print flag is OFF,

b) ≥1 = Number of load steps to be printed. Load step print flag is ON.
NOTE: FIELD 2 is over-ridden by FIELD 1 if gross print flag is ON.
**FIELD 3**: Coordinate system reference for stress and strain output.
OPTIONS:
  a) 0 = Global coordinate system,
  b) 1 = Principal material (fiber direction) coordinate system.
**FIELD 4**: Location within an element for stress and strain output.
OPTIONS:
  a) 0 = Nodes,
  b) 1 = Gauss points.
**FIELD 5**: Location within a layer for stress and strain output.
OPTIONS:
  a) -1 = Bottom of a layer,
  b) 0 = Midplane,
  c) 1 = Top of a layer.
**FIELD 6**: Request failure analysis.
OPTIONS:
  a) 0 = Failure analysis flagged OFF.
  b) 1 = Predict an ultimate failure load for each element. See NOTES 1 & 2.
  c) 2 = Fail fiber and matrix according to criteria set in fdata. See NOTE 3.
  d) 3 = Predict composite failure according to 3D Tsai-Wu criterion. See NOTE 3.
NOTE 1: OPTION b) requires:
  a) Single load step,
  b) One load type per analysis, e.g., nodal forces,
  c) Magnitude of applied load must equal 1 (unit load),
  d) QUAD4 or QUAD8 elements only,
  e) ANSYS output flag must be set ON (see FIELD 7).
NOTE 2: Ultimate failure loads are output as ETABLE entries in the ANSYS readable output files. See FIELD 7.
NOTE 3: OPTION b) requires fdata file and incremental (multiple load steps) analysis. Can be used with any element type.

**FIELD 7**: Request output files of stress, strain and displacement results in an ANSYS readable format.
OPTIONS:
  a) 0 = ANSYS output flagged OFF.
  b) >0 = ANSYS output flagged ON. See NOTES 1 and 2.
NOTE 1: OPTION b) causes three or four output files to be created:
  1.mct2ans.c (composite displacements, strains and stresses),
  2.mct2ans.r (reinforcement displacements, strains and stresses),
  3.mct2ans.m (matrix displacements, strains and stresses).
  4.damage.dat (material number corresponding to composite damage state).
If ultimate failure loads are requested (FIELD 6 OPTION C) they are output as ETABLE entries in each of the three files.
NOTE 2: In a multi-step analysis MCT_77 writes ANSYS readable out put starting at the load step specified, e.g., a value of 3 will output all results from load step 3 onward.

**FIELD 8**: Request output file of results specified in LINE 13 in a format suitable to be read by graphing program or spreadsheet.

OPTIONS:

a) 0 = Plot output flagged OFF.

b) 1 = Plot output flagged ON. If stress or strain are requested, composite values will be used.

c) 2 = Plot output flagged ON. If stress or strain are requested, reinforcement values will be used.

d) 3 = Plot output flagged ON. If stress or strain are requested, matrix values will be used.

NOTE : OPTIONS b)-d) create an ASCII format file, plot.dat.

**LINE 12.** *PRINT CONTROL, Inc, Displs, Nsts, Nstn, Asts, Astn, Ests, Estn, Psts, Ists, Rfor

Number of fields: 11.

FORMAT: (1X, I5, 1X, A10)

NOTE 1: Second of two LINES controlling form and quantity of analysis results printed in odata.

NOTE 2: Input under LINE 13 is required only if either FIELD 1 or 2 in LINE 11 is flagged ON.

NOTE 3: Number of lines defining print control patterns must agree with FIELDS 1-2 in LINE 11.

NOTE 4: In most cases, setting flags specified in LINE 12 to OFF causes program to skip execution of associated subroutines, significantly decreasing overall execution times for large models.

**FIELD 1**: Load step to be printed

OPTIONS: None.

NOTE 1: Ignored if gross print flag is set ON in FIELD 1 of LINE 11.

**FIELD 2**: Print request - displacements.

OPTIONS:

a) N = Print request is OFF (No),

b) Y = Print request is ON (Yes).

**FIELD 3**: Print request – nodal stresses.

OPTIONS:

a) N = Print request is OFF (No),

b) Y = Print request is ON (Yes).

**FIELD 4**: Print request – nodal strains.

OPTIONS:

a) N = Print request is OFF (No),

b) Y = Print request is ON (Yes).

**FIELD 5**: Print request – stresses averaged at nodes.

OPTIONS:

a) N = Print request is OFF (No),

b) Y = Print request is ON (Yes).

**FIELD 6**: Print request – strains averaged at nodes.

OPTIONS:

a) N = Print request is OFF (No),
b) Y = Print request is ON (Yes).

**FIELD 7**: Print request – stresses calculated at element centroid.
OPTIONS:
a) N = Print request is OFF (No),
b) Y = Print request is ON (Yes).

**FIELD 8**: Print request – strains calculated at element centroid.
OPTIONS:
a) N = Print request is OFF (No),
b) Y = Print request is ON (Yes).

**FIELD 9**: Print request – principal stresses.
OPTIONS:
a) N = Print request is OFF (No),
b) Y = Print request is ON (Yes).

**FIELD 10**: Print request – transversely isotropic stress invariants.
OPTIONS:
a) N = Print request is OFF (No),
b) Y = Print request is ON (Yes).

**FIELD 11**: Print request – reaction forces at nodes.
OPTIONS:
a) N = Print request is OFF (No),
b) Y = Print request is ON (Yes).

**LINE 13.** *PLOT CONTROL,{load id, load#, blank, blank} or {field id, node, lay, elem}

Number of fields: 8.
FORMAT: (1X, 2(4I5))
NOTE 1: Input under LINE 13 is required only if FIELD 8 in LINE 11 is flagged ON.
NOTE 2: Typically two corresponding quantities are output, e.g., stress and strain.
NOTE 3: LINE 13 specifies incremental quantities to be written. Quantities that can be written are:
a) Field variables LINE 12 using FIELDS: {field identifier, node number, layer, element}
b) Loads in LINE 3 using FIELDS: {load identifier, load number, BLANK, BLANK}

The field identifiers are:
a) 1 = Nodal displacements,
b) 2 = Nodal stresses,
c) 3 = Nodal strains,
d) 4 = Stresses averaged at nodes,
e) 5 = Strains averaged at nodes,
f) 6 = Stresses at element centroid,
g) 7 = Strains at element centroid,
h) 8 = Principal stresses,
i) 9 = Transversely isotropic stress invariants.

All field variables of that type and at that point are printed, e.g. displacements in the x, y, and z direction.

The load identifiers are:
  a) 21 = Nodal loads,
  b) 22 = Prescribed (nonzero) nodal displacements,
  c) 23 = Element pressures,
  d) 24 = Nodal temperature.
Load number corresponds to position, within loads of that type, as specified in ldata file, e.g., first element pressure, second element pressure, tenth element pressure, etc.

**FIELD 1**: Quantity identifier.
OPTIONS:
  a) Field identifier,
  b) Load identifier.
NOTE: See NOTE 3 under LINE 13.
**FIELD 2**: Sub-identification.
OPTIONS:
  a) Node number (field option),
  b) Load number (load option).
**FIELD 3**: Sub-identification.
OPTIONS:
  a) Layer number (field option),
  b) Blank (load option).
**FIELD 4**: Sub-identification.
OPTIONS:
  a) Element number (field option),
  b) Blank (load option).
**FIELDS 5-8**: Repeat FIELDS 1-4 for a corresponding quantity.
OPTIONS: Same as for FIELDS 1-4.
NOTE: Fields and loads can be listed as corresponding quantities.

## F.6. Mdata File

The mdata file contains information defining elastic material constants for up to eight orthotropic materials. A sample mdata file is shown in Fig. F.7. The mdata file requires a minimum of three LINES to define a single homogeneous material, a minimum of 5 LINES to define a composite material and its two constituents, and a minimum of 9 lines to define a single composite material and its two constituents in damaged and undamaged states. All materials are assumed to be transversely isotropic. A LINE-by-LINE description follows.

**LINE 1.** *Material Title
Number of fields: 1
FORMAT: (A60)
**FIELD 1**: General description of the materials defined in the mdata file.
OPTIONS: None
NOTE: Descriptor is printed as an identifier at the beginning of the odata file.

**LINE 2.** *Material Sets
Number of fields: 2
FORMAT: (1X, 9I5)
**FIELD 1**: Number of material constant sets to be read.
OPTIONS: 1 (min) – 8 (max).
**FIELD 2**: Request analysis with nonlinear shear effects.
OPTIONS:
  a) 0 = Nonlinear shear analysis flagged OFF,
  b) 1 = Nonlinear shear analysis flagged ON. See NOTE.
NOTE: OPTION b) requires an sdata file and incremental (multiple load step) analysis.

```
*Material Title
 Boron/5505, 50% FVF, Order important for failure analysis
*Material Sets
   7   1
*Material,1,Undamaged composite
   4   5   0.50
    207.0D+9   20.98D+9   20.98D+9
    0.29369    0.29369    0.45140
    7.715D+9   7.715D+9   7.229D+9
    0.1012D-4  0.2803D-4  0.2803D-4
    2.000D+3   0.000D+0   0.000D+0
*Material,2,Composite with damaged matrix
   4   7   0.50
    203.3D+9   0.2201D+9  0.2201D+9
    0.29349    0.29349    0.46414
    0.8050D+8  0.8050D+8  0.7515D+8
    0.9526D-5  0.2812D-4  0.2812D-4
    2.000D+3   0.000D-0   0.000D-0
*Material,3,Composite with damaged fiber
   6   5   0.50
    3.644D+9   1.733D+9   1.733D+9
    0.34846    0.34846    0.38027
    0.9089D+9  0.9089D+9  0.6282D+9
    0.4109D-4  0.4063D-4  0.4063D-4
    2.000D+3   0.000D-0   0.000D-0
*Material,4,Undamaged fiber
   4   4   0.00
    407.0D+9   407.0D+9   407.0D+9
    0.25000    0.25000    0.25000
    162.8D+9   162.8D+9   162.8D+9
    0.9520D-5  0.9520D-5  0.9520D-5
    2.600D+3   0.000D-0   0.000D-0
*Material,5,Undamaged matrix
   5   5   0.00
    7.239D+9   7.239D+9   7.239D+9
    0.35000    0.35000    0.35000
    2.681D+9   2.681D+9   2.681D+9
    0.4120D-4  0.4120D-4  0.4120D-4
    1.200D+3   0.000D-0   0.000D-0
*Material,6,Damaged fiber
   6   6   0.00
    407.0D+5   407.0D+5   407.0D+5
    0.25000    0.25000    0.25000
    162.8D+5   162.8D+5   162.8D+5
    0.9520D-5  0.9520D-5  0.9520D-5
    2.600D+3   0.000D-0   0.000D-0
*Material,7,Damaged matrix
   7   7   0.00
    7.239D+7   7.239D+7   7.239D+7
    0.35000    0.35000    0.35000
    2.681D+7   2.681D+7   2.681D+7
    0.4120D-4  0.4120D-4  0.4120D-4
    1.200D+3   0.000D-0   0.000D-0
```

**Fig. F.7** *Sample mdata file.*

**LINE 3.** *Material #
Number of fields: 18
FORMAT: (1X, 2I5, 14G5.1) for FIELDS 1-3 and (1X,6G12.7) for FIELDS 4-18.
NOTE 1: Six lines of input follow LINE 3.
NOTE 2: Material number is determined by its sequential position within ldata file.
NOTE 3: The existence of LINES 3-10 must agree with FIELD 1 in LINE 2.
**FIELD 1:** Material number of corresponding reinforcement constituent.
OPTION: None.
NOTE : All materials are assumed to be composites. FIELD 1 specifies which material,
listed sequentially within ldata file, defines reinforcement material constants for this

composite. Homogeneous materials are defined by specifying constituent material numbers (FIELDS 1 and 2) to be the same as the "composite".

**FIELD 2**: Material number of corresponding matrix constituent.

OPTION: None.

NOTE : All materials are assumed to be composites. FIELD 2 specifies which material, listed sequentially within ldata file, defines matrix material constants for this composite.. Homogeneous materials are defined by setting constituent material numbers (FIELDS 1 and 2) to be the same as the "composite".

**FIELD 3**: Reinforcement volume fraction.

OPTION: None.

NOTE 1: FIELD 3 for homogenous material defaults internally to 0.50.

NOTE 2: FIELDS 1-3 form the first of 6 lines of input under LINE 3.

**FIELD 4**: Young's modulus along longitudinal axis of fiber ($E_{11}$).

OPTION: None.

**FIELD 5**: Young's modulus transverse to longitudinal axis of fiber ($E_{22}$).

OPTION: None.

**FIELD 6**: Young's modulus transverse to longitudinal axis of fiber ($E_{33}$).

OPTION: None.

NOTE 1: Under the assumption of transverse isotropy, $E_{33} = E_{22}$.

NOTE 2: FIELDS 4-6 form the second of 6 lines of input under LINE 3.

**FIELD 7**: Major Poisson's ratio ($v_{12}$).

OPTION: None.

NOTE: Defined as:

$$\upsilon_{12} = -\frac{\varepsilon_2}{\varepsilon_1}$$

**FIELD 8**: Major Poisson's ratio ($v_{13}$).

OPTION: None.

NOTE: Under the assumption of transverse isotropy, $v_{13} = v_{12}$.

**FIELD 9**: Transverse Poisson's ratio ($v_{23}$).

OPTION: None.

NOTE: Defined as:

$$\upsilon_{23} = -\frac{\varepsilon_3}{\varepsilon_2}$$

NOTE: FIELDS 7-9 form the third of 6 lines of input under LINE 3.

**FIELD 10**: Longitudinal shear modulus ($G_{12}$).

OPTION: None.

**FIELD 11**: Longitudinal shear modulus ($G_{13}$).

OPTION: None.

NOTE 1: Under the assumption of transverse isotropy, $G_{13} = G_{12}$.

**FIELD 12**: Transverse shear modulus ($G_{23}$).

OPTION: None.

NOTE: FIELDS 10-12 form the fourth of 6 lines of input under LINE 3.

**FIELD 13**: Coefficient of thermal expansion along fiber axis ($\alpha_1$).

OPTION: None.

**FIELD 14** Coefficient of thermal expansion transverse to fiber axis ($\alpha_2$).

OPTION: None.

NOTE 1: Under the assumption of transverse isotropy, $G_{13}=G_{12}$.

FIELD 15: Coefficient of thermal expansion transverse to fiber axis ($\alpha_3$).

OPTION: None.

NOTE 1: Under the assumption of transverse isotropy, $\alpha_3=\alpha_2$.

NOTE 2: FIELDS 13-15 form the fifth of 6 lines of input under LINE 3.

FIELD 16: Material density ($\rho$)

OPTION: None.

FIELD 17 BLANK

OPTION: None.

FIELD 18: BLANK

OPTION: None.

NOTE: FIELDS 16-18 form the sixth of 6 lines of input under LINE 3.


## LINE 4. *Material #

Number of fields: 18

FORMAT: (1X, 2I5, 14G5.1) for FIELDS 1-3 and (1X,6G12.7) for FIELDS 4-18.

NOTE 1: LINES 4-10 are identical to LINE 3, each defining another material.

NOTE 2: The existence of LINES 4-10 must agree with FIELD 1 in LINE 2.

## F.7. Sdata File

The sdata file contains parameters of curve fit equations that form constitutive relationships among elastic material constants for a composite and its constituents under nonlinear shear effects. In MCT_77, only one material can have nonlinear shear behavior. The parameters in this file correspond to material #1 in the mdata file.

A changing composite shear modulus requires incremental application of the load and iterations within each load step to achieve equilibrium. Two tolerances, deflection (DTOL) and load (FTOL) control equilibrium iterations. Default values (DTOL=7.0 and FTOL=1.0E-5) are used in a non-failure MCT_77 analysis with nonlinear shear. The user can change the tolerances in a non-failure analysis by setting the failure analysis flag to ON in ldata and the number of materials to 0 in fdata. MCT_77 will open fdata and read user defined tolerance values.

A sample sdata file is shown in Fig. F.8. The sdata file requires eleven LINES. A LINE-by-LINE description follows.

**LINE 1.** *Curve Fit Title
Number of fields: 1
FORMAT: (A60)
**FIELD 1**: General description of material defined in sdata file.
OPTIONS: None
NOTE: Descriptor is printed as an identifier at the beginning of odata file.

```
*Curve Fit Title
 Boron/5505, 50% FVF
*Max strain, shear_12, shear_23
    0.0462D0   0.0462D0
*Shear 12 stress/strain parameters: a_0,a_1,a_2,c_0,c_1,c_2
    0.000D+0  -5.757D+1  -5.755D+1
    1.340D+8  -1.327D+8  -1.253D+6
*E22/G12 parameters: p_0,p_1,p_2
    4.270D-2   3.853D+0  -1.201D+0
*V12/G12 parameters: p_0,p_1,p_2
    4.861D-2  -1.290D-2   2.374D-3
*G23/G12 parameters: p_0,p_1,p_2
    5.497D-3   1.095D+0  -1.674D-1
*G/G12 parameters: p_0,p_1,p_2
    1.234D-5   3.327D-1   1.474D-2
*Shear 23 stress/strain parameters: a_0,a_1,a_2,c_0,c_1,c_2
    0.000D+0  -4.523D+1  -8.818D+2
    1.386D+8  -1.369D+8  -1.726D+6
*E22/G23 parameters: p_0,p_1,p_2
    4.270D-2   3.853D+0  -1.201D+0
*V12/G23 parameters: p_0,p_1,p_2
    4.861D-2  -1.290D-2   2.374D-3
*G12/G23 parameters: p_0,p_1,p_2
    5.497D-3   1.095D+0  -1.674D-1
*G/G23 parameters: p_0,p_1,p_2
    1.234D-5   3.327D-1   1.474D-2
```

**Fig. F.8** *Sample sdata file.*

**LINE 2.** *Max strain, shear_12, shear_23.
Number of fields: 2
FORMAT: (1X,6G12.7)
**FIELD 1**: Maximum shear strain to be used in nonlinear composite shear 12 stress-strain curve-fit equation.  See NOTE
OPTIONS: None.
**FIELD 2**: Maximum shear strain to be used in nonlinear composite shear 23 stress-strain curve-fit equation.  See NOTE.
OPTIONS: None.
NOTE: Shear strain in a general lamina can exceed the domain of shear stress-strain equations resulting in poor equilibrium convergence.  Shear moduli calculated at the maximum defined shear strain is used when lamina shear strains exceed maximum value.

**LINE 3.** *Shear 12 stress/strain parameters: a_0,a_1,a_2,c_0,c_1,c_2
Number of fields: 6
FORMAT: (1X,6G12.7)
NOTE: Defines nonlinear shear 12 stress/strain curve.
**FIELD 1**: BLANK.
OPTIONS: None
**FIELD 2**: Curve fit parameter in first exponent ($a_1$).

OPTIONS: None.

**FIELD 3**: Curve fit parameter in second exponent ($a_2$).

OPTIONS: None.

NOTE 2: FIELDS 1-3 form the first of 2 lines of input under LINE 3.

**FIELD 4**: Curve fit constant forming first term of equation ($c_0$).

OPTIONS: None.

**FIELD 5**: Curve fit constant coefficient in second term of equation ($c_1$).

OPTIONS: None.

**FIELD 6**: Curve fit constant coefficient in third term of equation ($c_2$).

OPTIONS: None.

NOTE 1: Three term shear stress/strain curve fit equation has the form:

$$\tau = C_0 + C_1 e^{(a_1 \gamma)} + C_2 e^{(a_2 \gamma)}$$

where $C_i$ and $a_i$ are curve fit parameters and $\gamma$ is engineering shear strain.

NOTE 2: FIELDS 4-6 form the second of 2 lines of input under LINE 3.

**LINE 4.** *E22/G12 parameters: p_0,p_1,p_2

Number of fields: 3

FORMAT: (1X,6G12.7)

NOTE: Defines relationship between $E_{22}$ and nonlinear $G_{12}$.

**FIELD 1**: Curve fit constant forming first term of equation ($p_0$).

OPTIONS: None.

**FIELD 2**: Curve fit constant coefficient in second term of equation ($p_1$).

OPTIONS: None.

**FIELD 3**: Curve fit constant coefficient in third term of equation ($p_2$).

OPTIONS: None.

NOTE 1: Second order polynomial curve fit equation has the form:

$$Value = p_0 + p_1 * ratio + p_2 * ratio^2$$

**LINE 5.** *V12/G12 parameters: p_0,p_1,p_2

Number of fields: 3

FORMAT: (1X,6G12.7)

NOTE: Defines relationship between $v_{12}$ and nonlinear $G_{12}$.

**FIELD 1**: Curve fit constant forming first term of equation ($p_0$).

OPTIONS: None.

**FIELD 2**: Curve fit constant coefficient in second term of equation ($p_1$).

OPTIONS: None.

**FIELD 3**: Curve fit constant coefficient in third term of equation ($p_2$).

OPTIONS: None.

**LINE 6.** *G23/G12 parameters: p_0,p_1,p_2

Number of fields: 3

FORMAT: (1X,6G12.7)

NOTE: Defines relationship between $G_{23}$ and nonlinear $G_{12}$.

**FIELD 1**: Curve fit constant forming first term of equation ($p_0$).
OPTIONS: None.
**FIELD 2**: Curve fit constant coefficient in second term of equation ($p_1$).
OPTIONS: None.
**FIELD 3**: Curve fit constant coefficient in third term of equation ($p_2$).
OPTIONS: None.

**LINE 7.** *G/G12 parameters: p_0,p_1,p_2
Number of fields: 3
FORMAT: (1X,6G12.7)
NOTE: Defines relationship between G (matrix shear modulus) and nonlinear $G_{12}$.
**FIELD 1**: Curve fit constant forming first term of equation ($p_0$).
OPTIONS: None.
**FIELD 2**: Curve fit constant coefficient in second term of equation ($p_1$).
OPTIONS: None.
**FIELD 3**: Curve fit constant coefficient in third term of the equation ($p_2$).
OPTIONS: None.

**LINE 8.** *Shear 23 stress/strain parameters: a_0,a_1,a_2,c_0,c_1,c_2
Number of fields: 6
FORMAT: (1X,6G12.7)
NOTE: Defines nonlinear shear 23 stress/strain curve.
**FIELD 1**: BLANK.
OPTIONS: None
**FIELD 2**: Curve fit parameter in first exponent ($a_1$).
OPTIONS: None.
**FIELD 3**: Curve fit parameter in second exponent ($a_2$).
OPTIONS: None.
NOTE 2: FIELDS 1-3 form the first of 2 lines of input under LINE 8.
**FIELD 4**: Curve fit constant forming first term of equation ($c_0$).
OPTIONS: None.
**FIELD 5**: Curve fit constant coefficient in second term of equation ($c_1$).
OPTIONS: None.
**FIELD 6**: Curve fit constant coefficient in third term of equation ($c_2$).
OPTIONS: None.
NOTE 1: The three term shear stress/strain curve fit equation has the form:

$$\tau = C_0 + C_1 e^{(a_1 \gamma)} + C_2 e^{(a_2 \gamma)}$$

where $C_i$ and $a_i$ are curve fit parameters and $\gamma$ is engineering shear strain.

NOTE 2: FIELDS 4-6 form the second of 2 lines of input under LINE 8.
NOTE 3: If shear 23 data is unavailable, shear 12 data can be used as an approximation.

**LINE 9.** *E22/G23 parameters: p_0,p_1,p_2
Number of fields: 3

FORMAT: (1X,6G12.7)

NOTE: Defines relationship between $E_{22}$ and nonlinear $G_{23}$.

**FIELD 1**: Curve fit constant forming first term of equation ($p_0$).

OPTIONS: None.

**FIELD 2**: Curve fit constant coefficient in second term of equation ($p_1$).

OPTIONS: None.

**FIELD 3**: Curve fit constant coefficient in third term of equation ($p_2$).

OPTIONS: None.

NOTE : Second order polynomial curve fit equation has the form:

$$Value = p_0 + p_1 * ratio + p_2 * ratio^2$$

**LINE 10.** *V12/G23 parameters: p_0,p_1,p_2

Number of fields: 3

FORMAT: (1X,6G12.7)

NOTE: Defines relationship between $v_{12}$ and nonlinear $G_{23}$.

**FIELD 1**: Curve fit constant forming first term of equation ($p_0$).

OPTIONS: None.

**FIELD 2**: Curve fit constant coefficient in second term of equation ($p_1$).

OPTIONS: None.

**FIELD 3**: Curve fit constant coefficient in third term of equation ($p_2$).

OPTIONS: None.

**LINE 11.** *G12/G23 parameters: p_0,p_1,p_2

Number of fields: 3

FORMAT: (1X,6G12.7)

NOTE: Defines relationship between $G_{12}$ and nonlinear $G_{23}$.

**FIELD 1**: Curve fit constant forming first term of equation ($p_0$).

OPTIONS: None.

**FIELD 2**: Curve fit constant coefficient in second term of equation ($p_1$).

OPTIONS: None.

**FIELD 3**: Curve fit constant coefficient in third term of equation ($p_2$).

OPTIONS: None.

**LINE 12.** *G/G23 parameters: p_0,p_1,p_2

Number of fields: 3

FORMAT: (1X,6G12.7)

NOTE: Defines relationship between G (matrix shear modulus) and nonlinear $G_{23}$.

**FIELD 1**: Curve fit constant forming first term of equation ($p_0$).

OPTIONS: None.

**FIELD 2**: Curve fit constant coefficient in second term of equation ($p_1$).

OPTIONS: None.

**FIELD 3**: Curve fit constant coefficient in third term of equation ($p_2$).

OPTIONS: None.

1 Cook, R.D., Malkus, D.S, Plesha M.E., "Concepts and Applications of Finite Element Analysis", 3rd Ed., John Wiley & Sons (1989)

2 Hinton, E., Owen, D.R.J., "Finite Element Programming", Academic Press, (1977)

3 Hughes, T.J.R., "The Finite Element Method: Linear Static and Dynamic Analysis", Prentice-Hall. (1987).

# APPENDIX G

# OVERVIEW OF MATERIAL FAILURE THEORIES

## *G.1. Categorizing Failure Analysis*

Failure of a material can be classified by yield (ductile material failure), or fracture (brittle material failure). These failure modes can occur in combinations making them sometimes difficult to identify. Furthermore, a material can, depending on temperature, stress state, or rate of loading, act in either a brittle or ductile manner [1]. But over a wide range of conditions, a particular material typically behaves in either a ductile or brittle manner. Within this paper, only failure under quasi-static load conditions is considered.

## *G.2. Brittle Material Failure Criteria*

### G.2.1. Linear Elastic Fracture Mechanics

For brittle failure, the most commonly used failure criteria are maximum stress or strain, and linear elastic fracture mechanics (LEFM). LEFM attempts to determine the stress necessary to cause a pre-existing through-thickness crack in a primarily brittle material to grow in an unstable (self-propagating or catastrophic) manner. The three most common approaches to LEFM are [2] : classical, stress intensity factor, and strain energy release rate. It is important to note that compressive failure of a material is not addressed by LEFM.

Classical (Griffith type) LEFM approach to a mode I (opening) crack propagation defines only the critical applied stress and has the form

$$\sigma\sqrt{\pi a} = \sqrt{2E\gamma} ,$$ 

(G.1)

where

$\sigma$ = applied stress,
a = half-crack length,
E = Young's modulus,
$\gamma$ = surface energy per unit area,

with the critical stress defining the mode I fracture toughness as

$$K_{Ic} = \sigma_c \sqrt{\pi a}$$

(G.2)

The stress intensity factor LEFM approach develops stress values about the crack tip and has the form:

$$\sigma_x = \frac{K_I}{\sqrt{2\pi r}} f_1(\theta),$$

$$\sigma_y = \frac{K_I}{\sqrt{2\pi r}} f_2(\theta),$$

(G.3)

$$\tau_{xy} = \frac{K_I}{\sqrt{2\pi r}} f_3(\theta),$$

where

$f_i$ = trigonometric functions of the angle $\theta$,
$K_I = \sigma\sqrt{\pi a}$ = stress intensity factor (mode I).

In application, these approaches are similar in that the classical critical fracture toughness (or the critical stress intensity factor which is identical) is a material property that can be determined experimentally. In application, once the fracture toughness is known, the critical applied stress can be determined based on an experimentally determined critical crack size.

Both of the above approaches can be difficult to implement for complex loading, geometry, and anisotropic materials. The strain energy release rate, as is typical of energy approaches, is generally easier to apply to a broader range of problems and proven to be a powerful tool in crack growth studies [2]. The strain energy release rate approach to LEFM has the form:

$$G_I = \frac{P^2}{2t}\frac{\partial s}{\partial a}$$ (G.4)

where

$P$ = load
$t$ = through crack thickness,
$s = \dfrac{u}{P}$, the system compliance,
$u$ = change in displacement at the point of load application due to crack growth,

and the critical strain energy release rate for mode one defined as:

$$G_{IC} = \frac{P_C^2}{2t}\left(\frac{\partial s}{\partial a}\right)_C$$

The advantage of the strain energy release rate approach is that knowledge of material properties or crack tip stresses is not required. Simply plotting system compliance verses crack length and computing the slope at critical load determines critical strain energy release rate. It has been shown [3] that:

$$K_{IC}^2 = G_{IC}E$$ (G.5)

Hence, the critical applied stress can be determined based on a known critical crack size.

There are analogous $K_{IC}$ developments for crack propagation caused by mode II (sliding) and mode III (tearing) loads. Load and boundary conditions can produce crack propagation that is a combination of cracking modes requiring a "mixed" mode analysis.

### G.2.2. Maximum Stress (or Strain) Failure Criteria

The maximum stress (strain) criteria can be stated as follows:

"The material at a point in a structure fails when the maximum stress (strain) exceeds the tensile stress (strain) or the minimum stress (strain) exceeds the maximum compressive stress (strain) as determined in a simple uni-axial specimen of the same material when it failed" [4].

The maximum and minimum stresses (strains) stated above can refer to principal (coordinate invariant) stresses but can also refer to local stresses in principal material directions (coordinate dependent) typical of fiber reinforced composites.

In general, a material will not fail if:

$$\begin{aligned} {}^{-}S \leq \sigma_1 \leq {}^{+}S \\ {}^{-}S \leq \sigma_2 \leq {}^{+}S \\ {}^{-}S \leq \sigma_3 \leq {}^{+}S \end{aligned} \tag{G.6}$$

where

$\quad {}^{+}S$ = ultimate unidirectional tensile stress (strain),
$\quad {}^{-}S$ = ultimate unidirectional compressive stress (strain),
$\quad \sigma$ = principal or local stress (strain).

In stress (strain) space, a general maximum stress (strain) failure criteria is uncoupled, i.e., failure is unaffected by interaction of the stresses; see Fig. G.1.
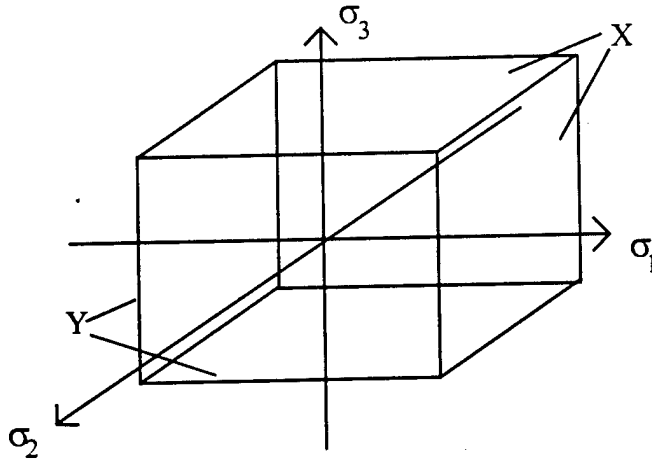
**Fig. G.1** *Stress (strain) space.*

In actuality, global stresses are coupled during principal stress or local stress calculations. When maximum stresses (strains) are examined in strain (stress) space, the strains (stresses) are coupled by Hook's law:

$$\varepsilon_1 = \frac{1}{E}\left(\sigma_1 - \upsilon\sigma_2 - \upsilon\sigma_3\right)$$

$$\varepsilon_2 = \frac{1}{E}\left(\sigma_2 - \upsilon\sigma_1 - \upsilon\sigma_3\right)$$

$$\varepsilon_3 = \frac{1}{E}\left(\sigma_3 - \upsilon\sigma_1 - \upsilon\sigma_2\right)$$

### G.3. Ductile Material Failure

Failure of ductile materials involves predicting transition from elastic to plastic behavior and the concept of a yield surface. Tresca and von Mises are two widely used ductile failure criteria.

### G.3.1. Maximum Shear Stress Failure Criterion

Tresca, or maximum shear stress, criterion states that yielding begins in a material point under a multi-axial stress state when maximum shear stress equals maximum shear stress

of a point at yield in a uni-axial tension or compression test of the same material. The material fails if:

$$\tau_{max} \geq S_S,$$ (G.7)

where

$$S_S = \frac{\sigma_{uniaxial}}{2},$$

and $\tau_{max}$ is the largest of

$$\tau_1 = \frac{|\sigma_2 - \sigma_3|}{2} \quad \tau_2 = \frac{|\sigma_3 - \sigma_1|}{2} \quad \tau_3 = \frac{|\sigma_1 - \sigma_2|}{2}.$$

$$\sigma_i = \text{principle stress}$$

## G.3.2. Distortional Energy Density (von Mises)

The von Mises criterion, also known as distortional energy density or maximum octahedral shear-stress criterion, uses the concept that strain energy at a point can be broken into two components. Part of the energy is used for volumetric change and the remainder in element distortion. The von Mises criterion states that yielding begins in a material point under a multi-axial stress state when distortional strain energy density equals distortional strain energy density of a point at yield in a uni-axial tension or compression test of the same material. The von Mises criterion can be stated in several forms. Failure occurs when:

$$U_D \geq U_{Dy}$$ (G.8)

where

$$U_D = \frac{(\sigma_1 - \sigma_2)^2 + (\sigma_2 - \sigma_3)^2 + (\sigma_3 - \sigma_1)^2}{12G},$$

$$U_{Dy} = \frac{\sigma_{uniaxial}}{2G},$$

$$G = \text{Shear modulus}$$

also

$$U_D = \frac{1}{2G} J_2 \, U_D = \frac{3}{4G} \tau^2_{octahedral} \quad ,$$

with the octahedral shear stress and second deviatoric stress invariant defined as

$$\tau^2_{octahedral} = \frac{(\sigma_1 - \sigma_2)^2 + (\sigma_2 - \sigma_3)^2 + (\sigma_3 - \sigma_1)^2}{9}$$

$$J_2 = \frac{(\sigma_1 - \sigma_2)^2 + (\sigma_2 - \sigma_3)^2 + (\sigma_3 - \sigma_1)^2}{6}$$

Implied in both von Mises and Tresca failure criterion is that hydrostatic stress,

$$\sigma_m = (\sigma_1 + \sigma_2 + \sigma_3)/3,$$

has no effect on yielding.

G.3.3. General Quadratic Interaction Criteria

The isotropic von Mises failure criterion is a special case of a general form called Quadratic Interaction Criteria. So named because they include terms to account for interaction between the stress components. Hill [5] generalized the von Mises criterion to include the effects of anisotropic behavior. The Hill criterion is given by:

$$U_D \geq 1 \tag{G.9}$$

where

$$U_D = F_1(\sigma_1 - \sigma_2)^2 + F_2(\sigma_2 - \sigma_3)^2 + F_3(\sigma_3 - \sigma_1)^2$$
$$+ F_{23}(\sigma_{23} + \sigma_{32})^2 + F_{13}(\sigma_{13} + \sigma_{31})^2 + F_{12}(\sigma_{12} + \sigma_{21})^2$$

and

$$2F_1 = \frac{1}{S_{11}^2} + \frac{1}{S_{22}^2} - \frac{1}{S_{33}^2}, \quad 2F_2 = \frac{1}{S_{22}^2} + \frac{1}{S_{33}^2} - \frac{1}{S_{11}^2}, \quad 2F_3 = \frac{1}{S_{33}^2} + \frac{1}{S_{11}^2} - \frac{1}{S_{22}^2},$$

$$2F_{12} = \frac{1}{S_{12}^2}, \quad 2F_{13} = \frac{1}{S_{13}^2}, \quad 2F_{23} = \frac{1}{S_{23}^2},$$

$S_{ii}$ ~ uniaxial yield strengths in the 1,2,3 directions,

$S_{ij}$ ~ Shear yield strengths in the ij direction.

Stresses are referenced to the principal axes of anisotropy (principal material directions), i.e., this criterion cannot be used in principal (coordinate invariant) stress space. As presented, Hill's criterion assumes no difference between tensile and compressive yield strengths.

The most general form of quadratic interaction criteria [2] as suggested by Gol'denblat and Kopnov [18] and proposed by Tsai and Wu [19] is of the form:

$$F_i \sigma_i + F_{ij} \sigma_i \sigma_j \geq 1 \qquad (G.10)$$

where contracted notation is used ($i,j$ = 1 to 6) and $F_i$ and $F_{ij}$ are experimentally determined strength tensors. Hoffman [20] has suggested keeping the linear terms in the normal stresses as a way to account for differences in tensile and compressive strengths.

### G.3.4. Strain Energy Density Criterion

In elastic non-linear materials, both volumetric and distortional changes may have an effect on failure hence the strain energy density failure criterion may be appropriate. The strain energy density criterion states that yielding begins in a material point under a multi-axial stress state when total strain energy density equals total strain energy density

of a point at yield in a uni-axial tension or compression test of the same material. Failure under the strain energy density criterion occurs when:

$$U_O = U_{Oy},$$ 

(G.11)

where

$$U_O = \frac{(\sigma_1 + \sigma_2 + \sigma_3)^2}{18K} + \frac{(\sigma_1 - \sigma_2)^2 + (\sigma_2 - \sigma_3)^2 + (\sigma_3 - \sigma_1)^2}{12G},$$

$$U_{Oy} = \frac{\sigma_{uniaxial}^2}{2E},$$

$K \sim$ Bulk Modulus.

Noting that the first term in the expression for $U_O$ is strain energy density associated with pure volume change and the second term is distortional strain energy density.

### G.4. Discussion

At this time there appears to be little to no advantage in using, in a general manner, one failure criteria over another. The accuracy of a particular criteria is likely to be case dependent. Arguments for such a statement begin with an observation that none of the available failure theories have been shown to accurately predict failure for all materials and loading conditions. Furthermore, there is no consensus within the engineering community as to which theory is best [2].

Ultimately the goal of a failure prediction methodology is to extrapolate results of an easy-to-conduct laboratory experiment, simple test specimen geometry and uniaxial loading, to real-world applications with complex structural geometry and multiaxial loading. All failure criteria mentioned above are semi-empirical, phenomenological attempts to develop analytical models to describe experimental observations.

Phenomenological, because only the occurrence of failure is predicted, not mode of failure. Failure details such as fiber pullout, fiber breakage, fiber micro-buckling, matrix cracking, delamination, etc., are not discerned. Wu [2,6] states that a large experimental data base alone could form the basis for an empirical failure criterion, but semi-empirical mathematical models are preferable because they can reduce the number of required experiments and provide a more systematic approach to design [2].

1 Boresi, A.P., R. Schmidt, and O. Sidebottom, <u>Advanced Mechanics of Materials</u>, 5th Ed., Wiley & Sons, New York (1993)

2 Gibson, R.F., <u>Principals of Composite Material Mechanics</u>, McGraw-Hill, New York (1994)

3 Irwin, G.R., *Fracturing of Metals*, 147-166, American Society of Metals, Cleveland, OH (1949)

4 Hyer, M.W., Mechanics of Composites Materials Class Notes, Engineering Science Course 233, Virginia Polytechnical Institute and State University (1988)

5 Hill, R., <u>The Mathematical Theory of Plasticity</u>, New York, Oxford University Press (1950)

6 Wu, E.M., "Phenomenological Anisotropic Failure Criterion," in G.P. Sendeckyj (ed.), *Composite Materials Volume 2*: pp. 353-431 *Mechanics of Composite Materials*, Academic Press, New York (1974)